The EURODELTA III exercise – Model evaluation with observations issued from the 2009 EMEP intensive period and standard measurements in Feb/Mar 2009

TFMM & MSC-W
Technical Report 1 /2014

The EURODELTA III exercise – Model evaluation with observations issued from the 2009 EMEP intensive period and standard measurements in Feb/Mar 2009

By:

B. Bessagnet, A. Colette, F. Meleux, L. Rouïl, A. Ung, O. Favez
INERIS, National Institute for Industrial Environment and Risks, Parc technologique ALATA, F-60550 Verneuil-en-Halatte, France.

C. Cuvelier
Ex European Commission, Joint Research Centre JRC Institute for Environment and Sustainability I-21020 Ispra (Va), Italy.

P. Thunis
European Commission, Joint Research Centre JRC Institute for Environment and Sustainability I-21020 Ispra (Va), Italy.

S. Tsyro
Climate Modelling and Air Pollution Division, Research and Development Department, Norwegian Meteorological Institute (MET Norway) P.O. Box 43, Blindern, N-0313 Oslo, Norway.

R. Stern
Freie Universität Berlin, Institut für Meteorologie Troposphärische Umweltforschung Carl-Heinrich-Becker Weg 6-10, D-12165 Berlin, Germany.

A. Manders, R. Kranenburg
TNO, Dept. Climate, Air and Sustainability, P.O. Box 80015, 3508 TA Utrecht, The Netherlands.

A. Aulinger, J. Bieser
HZG, Helmholtz-Zentrum Geesthacht, Institute for Coastal Research, Max-Planck-Straße 1, 21502 Geesthacht, Germany.

M. Mircea, G. Briganti, A. Cappelletti
ENEA, Italian National Agency for New Technologies, Energy and Sustainable Economic Development (ENEA), Via Martiri di Monte Sole 4, 40129 Bologna, Italy.

G. Calori, S. Finardi, C. Silibello
ARIANET Srl, Via Gilino n.9 20128, Milano, Italy.

G. Ciarelli, S. Aksoyoglu, A. Prévot
PSI, Paul Scherrer Institute, OFLA/007 5232 Villigen, Switzerland.

M.-T. Pay, J. M. Baldasano
BSC, Barcelona Supercomputing Center, Centro Nacional de Supercomputación, Nexus II Building, Jordi Girona, 29, 08034 Barcelona, Spain.

M. García Vivanco, J. L. Garrido, I. Palomino and F. Martín
CIEMAT, Atmospheric Pollution Unit, Avda. Complutense, 22, 28040 Madrid, Spain.

G. Pirovano
RSE S.p.A., via Rubattino 54, 20134 Milano, Italy.

P. Roberts, L. Gonzalez
CONCAWE, Boulevard du Souverain 165, B-1160 Brussels, Belgium.

L. White

AERIS EUROPE Ltd., Strouds Church Lane West Sussex RH17 7AY, United Kingdom.

L. Menut

Laboratoire de Météorologie Dynamique, École Polytechnique, ENS, UPMC, CNRS, Institut Pierre-Simon Laplace, 91128 Palaiseau, France.

J.-C. Dupont

Institut Pierre-Simon Laplace, CNRS-Ecole Polytechnique, 91128 Palaiseau, Paris, France.

C. Carnevale, A. Pederzoli

Department of Electronics for the Automation, University of Brescia, via Branze 38, I 25123 Brescia, Italy

Table of content

Glossary

ACE-FTS	Atmospheric Chemistry Experiment Fourier Transform Spectrometer
AirBase	The European Air quality database
AMS	Aerosol Mass Spectrometer
APINEN	Alpha-pinene
AQMEII	Air Quality Model Evaluation International Initiative
ASOA-xx	Anthropogenic Secondary Organic Aerosols with diameter below xx µm
BC	Black Carbon
BC	Boundary conditions
BEIS	Biogenic Emission Inventory System
BVOC	Biogenic Volatile Organic Carbon
BSC	Barcelona Supercomputing Center
BSOA-xx	Biogenic Secondary Organic Aerosols with diameter below xx µm
Ca	Calcium
CAMx	USA CTM
CHIMERE	French CTM
CH_4	Methane
CIEMAT	Centro de Investigaciones Energéticas, Medioambientales y Tecnológicas
CMAQ	US CTM
CLRTAP	Convention on Long-range Transboundary Air Pollution
CONCAWE	Conservation of clean Air and Water in Europe
CO_2	Carbon Dioxide
COSMO	COnsortium for SMall scale MOdeling
CRMSE	Centred Root Mean Square Error
CTM	Chemistry Transport Model
DUST-xx	Dust for particles with diameter below xx µm
EBAS	Database hosting observation data of atmospheric chemical composition
EC	European Commission
EC	Elemental Carbon
EC-xx	Elemental Carbon for particles with diameter below xx µm
ECMWF	European Centre for Medium-Range Weather Forecasts
EC4MACS	European Consortium for Modelling of Air Pollution and Climate Strategies (EU LIFE project)
ED	EURODELTA
EEA	European Environment Agency
EMEP	European Monitoring and Evaluation Programme / Norwegian CTM
ENEA	Ente per le Nuove tecnologie, l'Energia e l'Ambiente
EPA	Environmental Protection Agency
EPER	European Pollutant Emission Register
EU	European Union
FAIRMODE	Forum for Air quality Modelling (EEA/EC project)
FUB	Freie Universität Berlin
GAINS	Greenhouse Gas and Air Pollution Interactions and Synergies
GOME	Global Ozone Monitoring Experiment
HC	Hydrocarbon
HCHO	Formaldehyde
HNO3	Nitric Acid
HZG	Helmholtz-Zentrum Geesthacht

IA	Integrated Assessment
IFS	Integrated Forecast System
IIASA	International Institute for Applied Systems Analysis
INERIS	Institut National de l'Environnement Industriel et des Risques
IPSL	Institut Pierre-Simon Laplace
ISOP	Isoprene
JRC	Joint Research Centre
LIDAR	LIght Detection And Ranging
LMD	Laboratoire de Météorologie Dynamique
LOTOS-EUROS	Dutch CTM
LPS	Large Point Source
MACC	Monitoring Atmospheric Composition and Climate (EU FP7 project)
MB	Mean Bias
MEGAN	Model of Emissions of Gases and Aerosols from Nature
Met.NO	Norwegian Meteorological Institute
MGE	Mean Gross Error
MINNI	Italian CTM
MIPAS	Michaelson Interferometer for Passive Atmospheric Sounding
MLS	Microwave Limb Sounder
MSC-W	Meteorological Synthesizing Centre – West
NA-xx	Sodium for particles with diameter below xx µm
NH3	Ammonia
NH4-xx	Ammonium for particles with diameter below xx µm
NMB	Normalized Mean Bias
NMVOC	Non Methane VOC
NO	Nitrogen monoxide
NOx	Nitrogen oxides
NOy	Collective name for oxidized forms of nitrogen in the atmosphere
NO_2	Nitrogen dioxide
NO3-xx	Nitrate for particles with diameter below xx µm
OC	Organic Carbon
OM	Organic Matter
OMI	Ozone Monitoring Instrument
OOA	Oxidized Organic Aerosol
OPOM	Other primary particulate matter
O_3	Ozone
PAN	Peroxyacyl nitrates
PBL	Planetary Boundary Layer
PM	Particulate Matter
PM_{10}	Particulate Matter with particle diameters < 10 µm
$PM_{2.5}$	Particulate Matter with particle diameters < 2.5 µm
POA	Primary Organic Aerosol
POMS2-xx	Primary Organic Material from SNAP2 for particles with diameter below xx µm
PSI	Paul Scherrer Institute
RAIN	Total precipitation
REM Calgrid	German CTM
RMSE	Root Mean Square Error
RMSU	Root Mean Square Error including Uncertainties
RSE	Ricerca sul Sistema Energetico
SD	Standard Deviation
SIRTA	Site Instrumental de Recherche par Télédétection Atmosphérique
SMOKE	Sparse Matrix Operational Kernel Emissions

SNAP	Selected Nomenclature for Air Pollutants
SOA	Secondary Organic Aerosol
SOA-xx	Total Secondary Organic Aerosols with diameter below xx µm
SO_2	Sulphur dioxide
SO4-xx	Sulphate for particles with diameter below xx µm
SOx	Sulphur oxides
SVOC	Semi-Volatile Organic Compounds
TFMM	Task Force on Measurements and Modelling
TKE	Turbulent Kinetic Energy
TNH4	Total ammonium
TNO	Toegepast Natuurwetenschappelijk Onderzoek
TNO3	Total nitrate
TOM-xx	Total Organic Material for particles with diameter below xx µm
TPOM-xx	Total Primary Organic Material for particles with diameter below xx µm
T2M	2m temperature
VBS	Volatility Basis set
VOC	Volatile Organic Compounds
UNECE	United Nations Economic Commission for Europe
USGS	United States Geological Survey
USTAR	Friction velocity
U10	10 meter wind speed
WOUDC	World Ozone and Ultraviolet Radiation Data Centre
WRF	USA Mesoscale meteorological model
WNHx	wet deposition of reduced nitrogen species
WNOx	wet deposition of oxidized nitrogen species
WSOx	wet deposition of oxidized sulphur species

EXECUTIVE SUMMARY

Over time EURODELTA (ED) has very successfully extended the European Air Quality Modelling capability by providing a forum in which modelling teams could share experiences in simulating technically interesting and policy relevant problems. The joint exercises contribute to further improve modelling techniques, as well as to quantify and understand the sources of calculation uncertainty. EURODELTA is now an activity contributing to the scientific work of the UNECE[1] Task Force on Measurement and Modelling (TFMM) under the Convention on Long-range Transboundary Air Pollution (CLRTAP). The Task Force on Measurements and Modelling was established in 2000 to offer a forum to the Parties, the EMEP[2] centres and other international organizations for scientific discussions to evaluate measurements and modelling and to further develop working methods and tools. In that context, the Gothenburg Protocol[3] signed in 1999 is a multi-pollutant protocol of the Convention designed to reduce acidification, eutrophication and ground-level ozone by setting emissions ceilings for sulphur dioxide, nitrogen oxides, volatile organic compounds, fine particulate matter and ammonia.

The objective of this report is to analyse the models behaviour during the **EMEP intensive period 2009 (25 Feb - 26 Mar),** particularly the EMEP model that is the official model of the LRTAP Convention which also involved in the EU air quality policy making process. Such a short time period is appropriate to make use of valuable intensive measurements for more in-depth analysis of models' skills, and to take advantage of contemporarily hourly measurements at several sites, which facilitates explaining particulate daily/annual biases.
The results are presented in terms of model performance for regulatory pollutants and also for Particulate Matter (PM) components and their precursors. To better assess the ability of models to simulate the physical and chemical processes, the results were analyzed on hourly and daily bases. The meteorology was also assessed. In this first phase, seven models were run over the 2009 campaign. The institutes/laboratories participating in the ED III with their models are **PSI/RSE, INERIS, HZG, Met.NO/MSC-West, TNO, ENEA, and FUB**, respectively with **CAMx, CHIMERE, CMAQ, EMEP, LOTOS-EUROS, MINNI and RCG** air quality models. The other participants **JRC, BSC, CIEMAT, CONCAWE, AERIS EUROPE, LMD/IPSL and University of Brescia** contributed to the project bringing their expertise in air quality modelling and management of observational data.

Although most of inputs were harmonized, we can clearly observe a rather large variability of model outputs and related performance statistics for all modelled species. A different implementation of chemical and physical processes into the models as well as pre-processing of input data can explain this variability. For instance, the comparison of meteorological data actually used by the models displays differences on diagnosed variable like the PBL. The same can happen even with directly used data like wind speed or temperature because of some differences in interpolation processes. For the wind speed some discrepancies between model and observations can be observed even on native IFS meteorological data. The comparison of modelled concentrations against wind speed and PBL heights confirmed that meteorology strongly influences CTMs performance. Particularly the temporal evolution of wind speed is most responsible of model skilfulness in reproducing the daily variability of pollutant concentrations (e.g. the development of peak episodes). The reconstruction of the PBL diurnal cycle seems more influential in driving the corresponding diurnal profile of pollutants and hence the presence of systematic positive and negative bias detectable on daily basis.

[1] United Nations Economic Commission for Europe
[2] The European Monitoring and Evaluation Programme (EMEP) is a scientifically based and policy driven programme under the Convention on Long-range Transboundary Air Pollution (CLRTAP) for international co-operation to solve transboundary air pollution problems.
[3] Protocol to the 1979 Convention on Long-Range Transboundary Air Pollution to abate acidification, euthrophication and ground-level ozone.

For each group of species, we draw some general conclusions for the studied period that cannot be extrapolated to a full year.

Ozone and nitrogen dioxide

The models (with some exceptions) are found to underestimate observed ozone concentrations. EMEP, CHIMERE and CMAQ display the highest ozone concentration particularly over water surfaces but still below the observations. This negative bias is partly explained by a systematic underestimation of the ozone provided by the boundary conditions, provided by MACC reanalysis fields. MINNI and RCG show the highest negative biases which can totally be explained at Mace Head by the corresponding bias on boundary conditions. The spatial correlations are rather different among the models: 0.35 for CMAQ; 0.59 for CHIMERE, EMEP and LOTOS-EUROS; 0.64 for CAMx and 0.66 for MINNI and up to 0.67 for RCG. Regarding the ozone vertical profiles, the models skills in reproducing the O_3 mixing ratio within the PBL are in the range of values obtained in other studies, showing a relative bias of 3%, RMSE of 17% and correlation of 0.75. The evaluation of MACC analysis data shows a better agreement with measurement in the middle than in the lower troposphere. In the troposphere the reanalysis shows bias of -5% to 10% with respect to O_3 sondes. In short, the regional models perform better than the global MACC analysis within the planetary boundary layer.

The performances for NO_2 are similar for all models (with five models underestimating and two overestimating the observations); the highest positive bias is given for CMAQ. For all models the correlations in time and space are close to 0.6.

PM_{10} and $PM_{2.5}$

For PM_{10} concentration the differences between models are significant and are partly associated to the models treatment of natural PM (dust and sea salts). The main PM hotspots in Poland and Po valley are simulated by all models. MINNI and CHIMERE results are found to be closer to the PM_{10} and $PM_{2.5}$ observations in term of bias than the other models; EMEP has the best correlation coefficient. Usually, all models underestimate the highest values, MINNI and CHIMERE can overestimate some low values. For most of stations the error on PM_{10} is dominated by a wrong reconstruction of the temporal correlation. Differently, for LOTOS the error is related to both correlation and standard deviation.

Though the main features of observed PM spatial distribution are reproduced fairly well, the modelled regional gradients are smaller than the measured ones. For this campaign, most models tend to underestimate the PM concentrations except MINNI and CHIMERE which show a slight overestimation somehow counterbalanced by an overestimation of some chemical compounds.

Deposition

Regarding wet deposition most of the models show a better agreement with observations at sites with relatively low and medium measured accumulated wet deposition values. For WNHx most of the models underestimate the highest observed values, with EMEP presenting the lowest mean bias. The lowest mean RMSE is obtained by LOTOS-EUROS, also showing the best spatial correlation. In the case of WNOx there is a general tendency to underpredict the highest accumulated wet depositions, with some differences between the models: CHIMERE, EMEP and LOTOS-EUROS calculate higher values than the other models for this period, being closer to observations. In the case of WSOx, CMAQ is providing the best performance for the highest observed values, most of them registered in the Atlantic area. This fact seems to be related to the natural sulphate emissions associated to sea salt processes that this model considers (note that measurements of SO4 in precipitations used here include for sea salt sulphate). Unfortunately, the uneven distribution of monitoring sites makes it difficult to decide on model performance in some areas of Europe characterized by strong differences among the models.

Regarding dry deposition, CMAQ estimates the highest DNOx deposition over the Mediterranean area and the eastern part of the domain. Strong differences are found between this model and the rest, with CHIMERE/RCG/EMEP group presenting the lowest values. CMAQ is also estimating the

highest values of DSOx, while EMEP and MINNI produced the lowest ones. As for DNHx, differences between models are not as strong as in case of DSOx and DNOx, with all the models presenting a quite similar spatial pattern. In the light of the obtained results, the importance of having any kind of methodology to evaluate dry deposition is clear, especially for SOx and NOx.

Sulphur compounds

On average EMEP, CHIMERE and LOTOS-EUROS present the lowest bias for SO_2 concentrations. In this exercise CAMX has too high concentrations because all SO_2 was injected at the ground level; high concentrations are also displayed by RCG. The correlation coefficients between calculated and measured SO_2 are quite similar among the models. EMEP, CMAQ and MINNI behave the best for sulphate concentrations when looking at the RMSE. CHIMERE exhibits the highest overestimation of sulphate concentrations. The results from all models have to some extent been affected by overestimated MACC Analysis boundary conditions at the eastern boarders. Even if the sulphur chemistry is well known, the co-analysis of sulphur depositions and concentrations suggest that some improvements can be done yet on this topic, which has a direct influence on SIA chemistry.

Nitrate and ammonium

Nitrate and ammonium are the species showing the best performance in this exercise; the main regional footprint is coherent between models with some discrepancies over the Benelux and the Po valley. For nitrates, LOTOS-EUROS and EMEP simulate the lowest concentration values, while CHIMERE simulates low values mainly in the south of Europe. For the total nitrate (TNO3), there is a clear difference between one group of models, including MINNI, RCG, CMAQ and CAMX, which strongly overestimate the concentrations and the other group, including CHIMERE, EMEP and LOTOS-EUROS, which slightly underestimate the total nitrate concentrations.

CHIMERE, EMEP and LOTOS-EUROS underestimate the highest values of nitrate concentrations. The models behaviour for nitrates shows a clear difference between the group LOTOS-EUROS/EMEP/CHIMERE which underestimate the high nitrate concentrations (-30 to -40%) whereas the other models slightly overestimate the observed values.

Carbonaceous species

EC-10 concentrations are on average overestimated by the models, with biases up to 50-60% for CHIMERE, RCG and MINNI; EMEP is the only model showing a null bias.

A first comparison against Oxydized Organic Aerosol (OOA) measurements tends to support the fact that models underestimate SOA concentrations. CHIMERE exhibits the lowest underestimations particularly in ES78 but with a low correlation. In Melpitz and Vavihill the amplitude of OOA peaks are not reproduced by the models with SOA. At this stage, it is difficult to say more on this comparison because a part of OOA can have a primary origin. Indeed, the observed OOA and Biomass Burning Organic Aerosol (BBOA) concentrations peaks seem correlated particularly in Vavihill (SE11). The implementation of more sophisticated modules including more knowledge of processes and a work on the harmonization of POA emissions are pressing issues. Finally, all models underestimate the observd peak of organic matter by a factor from 2 to 6.

Natural aerosols

All the models simulate high concentrations of sea salt sodium over the oceans and seas with some differences because of the parameterisation. On average the spatial correlation is very good in the range 0.90 – 0.95 for all models. CHIMERE and MINNI simulate the highest concentrations over lands that are clearly overestimated with respect to the observations.

EMEP and LOTOS-EUROS simulate the lowest dust concentrations values, whereas RCG and MINNI the highest ones. The correlations in time and space for dust concentrations in the PM_{10} fraction are close to zero for all models, the spatial correlations are better for LOTOS-EUROS and RCGC (0.50) and EMEP (0.62) and near zero for all other models. This large difference in the computed correlation between EMEP, LOTOS-EUROS and RCG with respect to the other models shows that the dust

parameterisations used in former group were rather suitable in reproducing dust events during the considered period.

1 Introduction

EURODELTA (ED) has very successfully extended the European Air Quality Modelling capability by providing a forum in which modelling teams could share experiences in simulating technically interesting and policy relevant problems. The joint exercises contribute to further improve modelling, techniques as well as to quantify and understand the sources of calculation uncertainty. EURODELTA is now an activity contributing to the scientific work of the UNECE[4] Task Force on Measurement and Modelling (TFMM) under the Convention on Long-range Transboundary Air Pollution (CLRTAP). The Task Force on Measurements and Modelling was established in 2000 to offer a forum to the Parties, the EMEP[5] centres and other international organizations for scientific discussions to evaluate measurements and modelling and to further develop working methods and tools. In that context, the Gothenburg Protocol[6] signed in 1999 is a multi-pollutant protocol of the Convention designed to reduce acidification, eutrophication and ground-level ozone by setting emissions ceilings for sulphur dioxide, nitrogen oxides, volatile organic compounds, fine particulate matter and ammonia.

In 2004, **EDI** examined the common performance of the models in predicting recent (2000) and future (2020) air quality in Europe using the concept of a model ensemble to measure robustness of predictions. The spread of predictions about the ensemble gave a measure of uncertainty for each predicted value. In a 2020 world the effect of making emission reductions for key pollutants of NOx, SO_2, VOC and NH_3 independently in France, Germany and Italy, and of NOx and SOx in sea areas, was investigated. Source-receptor relationships used in integrated assessment (IA) modelling were derived for all the models and compared to assess how model choice might affect this key input.
ED II built on this project by taking a closer look at how the different models represent the effect on pollutant impacts on a European scale of applying emission reductions to individual emission sectors (Thunis *et al*., 2008).

In the recent literature, several intercomparison and evaluation exercises are reported for PM models : McKeen *et al*. (2007), van Loon *et al*., (2007), Vautard *et al*. (2007), Hayami *et al*. (2008), Stern *et al*. (2008), Smyth *et al*. (2009), Vautard *et al*. (2009), Solazzo *et al*. (2012), Pernigotti, *et al*. (2013). Most of these model intercomparison exercises were performed at the regional scale with chemistry transport models. In one of the most recent exercise, AQMEII (Solazzo *et al*., 2012), models clearly tend to underestimate PM_{10} background concentrations in US and EU regions. Model results for $PM_{2.5}$ concentrations showed better performances but large uncertainty remains in the devoted to the simulation of secondary organic aerosols.

The new **ED III** exercise is to use and interpret the EMEP intensive measurements by making a retrospective analysis of the campaigns and informing on the contribution of some emission sources to the pollutant concetrations. Four EMEP campaign will be used to evaluate the model:

- 1 Jun - 30 Jun 2006
- 8 Jan - 4 Feb 2007
- 17 Sep - 15 Oct 2008
- **25 Feb - 26 Mar 2009**

Differently to the previous intercomparison exercises, almost all models have now been run with the same input data (emissions, meteorology, boundary conditions) and over the same domain (domain extension and resolution). Moreover, vertical profiles, depositions and meteorology were included in the evaluation to better understand the behaviour of models.

[4] United Nations Economic Commission for Europe
[5] The European Monitoring and Evaluation Programme (EMEP) is a scientifically based and policy driven programme under the Convention on Long-range Transboundary Air Pollution (CLRTAP) for international co-operation to solve transboundary air pollution problems.
[6] Protocol to the 1979 Convention on Long-Range Transboundary Air Pollution to abate acidification, euthrophication and ground-level ozone.

To conduct a retrospective analysis of air quality over the policy horizon of the Convention on Long Range Transport **1990** will be takes as the starting point. This was the reference year for the first accounting of a multi-pollutant, multi-effect approach to European Air Quality assessment. Over this time our ability to model (both transport and effects) has increased enormously. A retrospective view will illuminate the progress made in pollution levels using a multi model approach with state-of-the-art models. **1999** will be taken as an intermediary year (signature of the Gothenburg protocol), and **2008** will be a recent year. This **retrospective analysis** over three years will set the bases of a full trend analysis of the pollution over the last two decades (1) to assess the ability of models to reproduce such a large decrease of pollutant emissions and (2) to evaluate the impact on air quality of emission reduction strategies in force for twenty years.

The objective of this report is to analyse the behaviour of models on the **EMEP intensive period 2009 (25 Feb - 26 Mar)** with a focus on the EMEP model, the official model of the LRTAP Convention which is also involved in the EU air quality assessment processes. The results are presented in terms of model performance for regulatory pollutants as well as for Particulate Matter (PM) components and their precursors. To better assess the ability of models to simulate the physical and chemical processes, the results are analyzed on hourly and daily bases. The meteorology is also assessed. In this first phase, seven models were run over the 2009 campaign. The institutes/laboratories participating in the ED III with their models are reported in Table 1.1. The colour codes for the plots referring to models are the same through the report and mentioned in Table 1.1. The other participants JRC, BSC, CIEMAT, CONCAWE, AERIS EUROPE, LMD/IPSL and University of Brescia contributed to the project bringing their expertise in air quality modelling and management of observational data.

Table 1.1: Models involved in the study

Teams	Models	Model acronym in this report	Colour codes
PSI/RSE	CAMx	CAMX	
INERIS	CHIMERE	CHIM	
HZG	CMAQ	CMAQ	
MSC-W - Met.NO	EMEP MSC-W	EMEP	
TNO	LOTOS-EUROS	LOTO	
ENEA	MINNI	MINNI	
FUB	REM Calgrid	RCGC	

2 Input data

2.1 Anthropogenic emissions

Development of the emission inventory for the reference year 2007

The first step in the emission preparation was to calculate the spatial pattern of emissions for the reference year 2007, that was selected because it was a key year for the TNO-MACC inventory (Kuenen *et al*., 2011). The anthropogenic emission input was harmonized. The total emissions were then scaled to year 2009. Models used their own speciation factors for NOx, SOx and NMVOC emissions.

Gridding

The gridded distribution of anthropogenic emissions was provided by INERIS and it was based on a merging of databases from:

- *TNO 0.125°×0.0625° emissions for 2007 from MACC (Kuenen et al., 2011)*
- *EMEP 0.5°×0.5° emission inventory for 2009 (Vestreng et al., 2007)*
- *Emission data from the GAINS[7] database*
- *INERIS expertise on re-gridding with various proxies (population[8], landuse[9], Large Point Source (LPS) data)*

The TNO-MACC dataset provides two distinct datasets (i) large point sources (LPS) with the coordinates of stacks and (ii) surface emissions on a fine grid (0.125°×0.0625°). In the gridding process, the first step consisted in summing up LPS emissions from the TNO-MACC emissions inventory for 2007 with surface emissions to obtain only one type of emissions as in the EMEP inventory. For the various activity sectors (SNAP[10]) the processing steps were the following:

- **The emissions were scaled with 2009 annual totals as reported on the EMEP web site**
- SNAP 2: The country emissions were re-gridded with coefficients based on population density and French bottom-up data, the methodology (Bessagnet *et al*., 2012, Terrenoire *et al.*, 2013) was extrapolated to the whole Europe. For $PM_{2.5}$ emissions, the annual EMEP totals were kept except for the countries CZ, BA,BE, BY, ES, FR, HR, IE, LT, LU, MD, MK, NL, CS, TR. For these countries, $PM_{2.5}$ emissions from GAINS were used. Additional factors were applied on two Polish regions (×4 or ×8) for $PM_{2.5}$ and PM_{10} emissions (Personal communication from IIASA[11]). The former activity in coal mine regions still leads to high emissions of PM due to domestic uses of coal.
- SNAP 3,7,8,9,10: TNO-MACC emissions spatial distribution was used as proxy to regrid EMEP 0.5°x0.5° annual totals into the finer modelling grid.

[7] The Greenhouse Gas and Air Pollution Interactions and Synergies (GAINS)-Model provides a consistent framework for the analysis of co-benefits reduction strategies from air pollution and greenhouse gas sources (*http://*gains.iiasa.ac.at/gains)

[8] The population data come from EEA database (http://www.eea.europa.eu/data-and-maps/data/population-density-disaggregated-with-corine-land-cover-2000-2) merged with global data (from SEDAC http://sedac.ciesin.columbia.edu) to fill gaps in Europe.

[9] US Geophysical Survey landuse data are used at 1 km resolution (http://www.usgs.gov/)

[10] SNAP : Selected Nomenclature for Air Pollutants: (1) Public Power stations, (2) Comm./inst. Combustion, (3) Industrial combustion, (4) Production processes, (5) Extraction fossil fuel, (6) Solvents, (7) Road traffic, (8) Other mobile sources (trains, shipping, aircrafts, ...), (9) Waste treatment, (10) Agriculture, (11) Natural.

[11] International Institute for Applied Systems Analysis

- SNAP 1,4,5,6: EMEP 0.5°x0.5° emissions were regridded by adequate proxies ("artificial landuse", EPER[12] data for industries).

For countries where TNO-MACC emissions were not available, the EMEP 0.5°×0.5° emissions were used (Iceland, Liechtenstein, Malta and Asian countries) and regridded with adequate proxies ("artificial landuse", EPER data for industries).
The spatial pattern of $PM_{2.5}$ emission from residential emissions is presented in Figure 2.1. Residential emissions are dominant in wintertime in most of countries; they come from wood burning or coal uses. Germany, Sweden, Spain clearly have the lowest levels of emissions. Romania, Poland and France have the highest levels of emissions.

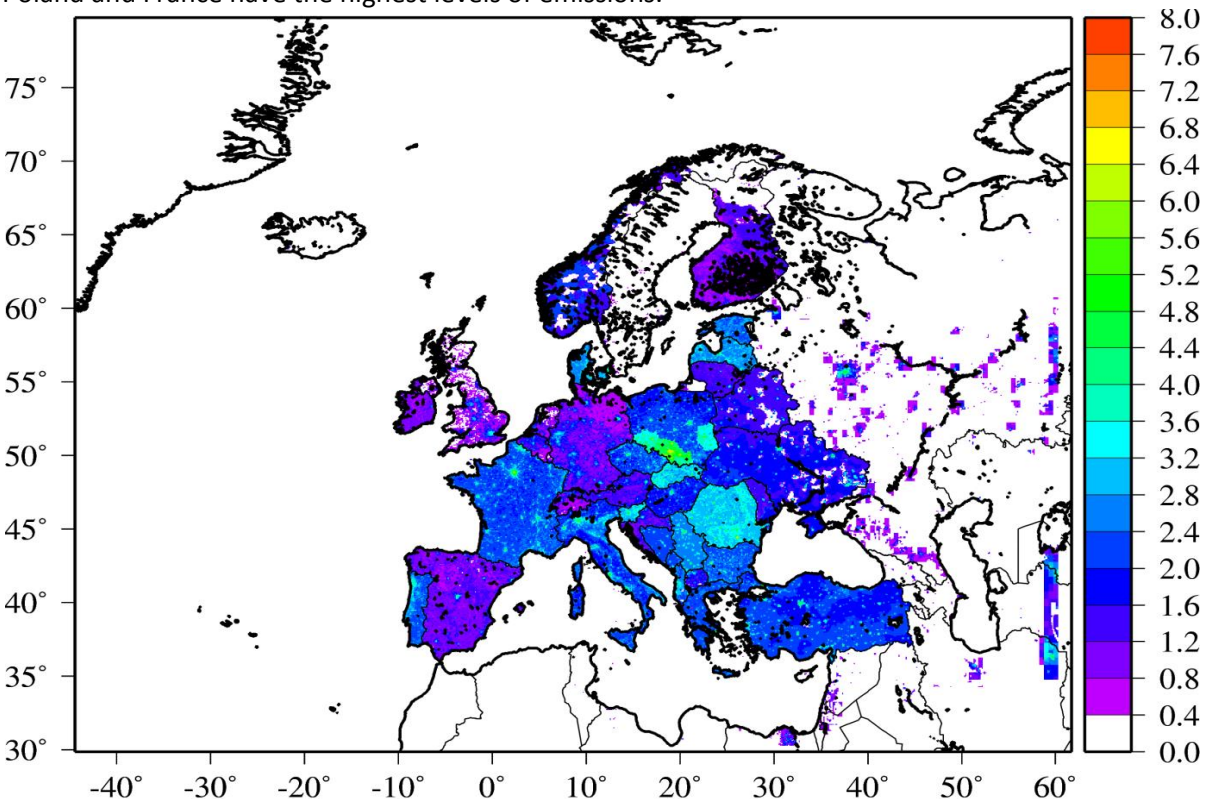

Figure 2.1: Emission patterns of $PM_{2.5}$ emissions from the residential sector (SNAP2), units are in logarithm for clarity.

The time profiles are those used in the frame of the **EDII** exercise (Thunis *et al.*, 2008). Three types of profiles are provided:

- Seasonal factors : one value per species, month, activity sector and country
- Weekly factors : one value per species, day type (Monday – Sunday), activity sector and country
- Hourly factors : one value per hour (local time), species and activity sector

Since only $PM_{2.5}$ and PM_{coarse} emissions were provided by the EMEP, we used a PM split provided by IIASA (Personal Communication from IIASA) to estimate the fraction of Elemental Carbon and Organic Matter per activity sectors, per country. Models used their own split for NOx, SOx and NMVOC emissions.

The following emitted species have been used in the models:

[12] The EPER Decision is based on Article 15(3) of Council Directive 96/61/EC concerning integrated pollution prevention and control. EPER is a web-based register, which enables the public to view data on emissions to water and air of 50 key pollutants from large and medium-sized industrial point sources in the European Union. The register is hosted by the European Environment Agency. http://www.eea.europa.eu/data-and-maps/data/eper-the-european-pollutant-emission-register-4

CH_4	: Methane (this species comes from the TNO-MACC inventory)
CO	: Carbon monoxide
NH3	: Ammonia
SOx	: Sulfur oxides
NMVOC	: Non methane volatile organic compounds
NOx	: Nitrogen oxides
EC_25	: Elemental carbon $\phi < 2.5$ µm
EC_Co	: Elemental carbon $2.5\mu m < \phi < 10$ µm
POMS2_25	: Primary organic matter from SNAP2 $\phi < 2.5$ µm
POMS2_Co	: Primary organic matter from SNAP2 $2.5\mu m < \phi < 10$ µm
OPOM_25	: Other primary organic material (non SNAP2 POM) $\phi < 2.5$ µm
OPOM_Co	: Other primary organic material (non SNAP2 POM) $2.5\mu m < \phi < 10$ µm
OPPM_25	: Other primary particulate matter (non carbonaceous, all SNAP) $\phi<2.5\mu m$
OPPM_Co	: Other primary particulate matter (non carbonaceous, all SNAP) $2.5\mu m< \phi <10$ µm

2.2 Biogenic emissions of reactive species

BVOC emissions from vegetation

CHIM and MINNI used the version 2.04 of the MEGAN model (Guenther *et al*., 2006, 2012). The Model of Emissions of Gases and Aerosols from Nature (MEGAN[13]) is a modelling framework for estimating fluxes of biogenic compounds between terrestrial ecosystems and the atmosphere using simple mechanistic algorithms to account for the major known processes controlling biogenic emissions. It is available as an offline code and has also been coupled into land surface and atmospheric chemistry models.

EMEP, LOTO and RCGC used parameterizations derived from Simpson *et al*. (1999) for the temporal variations according temperature and light, with maps of tree species from Koeble and Seufert (2001).

CAMX used a specific module detailed in Oderbolz *et al*. (2013). A specific study was performed in this exercise to improve the seasonality of BVOC emissions. The concentrations of biogenic species simulated by CAMX were compared against measurements of isoprene and monoterpenes in Hohenpeissenberg (Germany) for both summer and winter. The agreement between observed and modelled concentrations was better in summer than in winter. This was partly attributed to the difficulty of the model to simulate accurately weather conditions in winter, but also to the increased anthropogenic influence on the concentrations of BVOC compounds in winter. This suggests that land-cover inventories used to derive tree-cover must be chosen with care. Also, uncertainties in the classification of land-cover pixels must be taken into account and remain high.

CMAQ used the BEIS (Biogenic Emission Inventory System) module developed by the US EPA. BEIS estimates volatile organic compound (VOC) emissions from vegetation and nitric oxide (NO) and carbon monoxide (CO) emissions from soils. Because of resource limitations, recent BEIS development has been incorporated into the Sparse Matrix Operational Kernel Emissions (SMOKE) system, so that the native version of BEIS is built within the SMOKE architecture.

NO soil emissions

CHIM and MINNI used the version 2.04 of the MEGAN model to calculate the NO emissions.

[13] The offline version of MEGAN source code and driving variables is available from http://bai.acd.ucar.edu/MEGAN/

EMEP and RCGC used a parameterization of NO emissions described in Simpson *et al*. (1999).

CAMX and LOTO did not include NO emissions in this simulation.

CMAQ used the BEIS (Biogenic Emission Inventory System) module developed by the US EPA.

Sea salt emissions

All models host very different schemes based on Monahan (1986) for CHIM and updates from Martensson *et al*. (2003) for LOTO and EMEP or Gong *et al*. (1997) for RCGC. CMAQ and MINNI use the Zhang *et al*. (2005) parameterization and CAMX sea salt emissions are based on Gong (2003).
CMAQ emits also sea salts sulphate using a fraction of 7.76% of emitted sea salts split into the accumulation and coarse modes.

NO emissions from lightning

Climatologies of NO emissions from lightning is based on Köhler *et al*. (1995) in EMEP. The other models do not account for this kind of emissions.

Emissions from fires were not taken into account for this wintertime campaign.

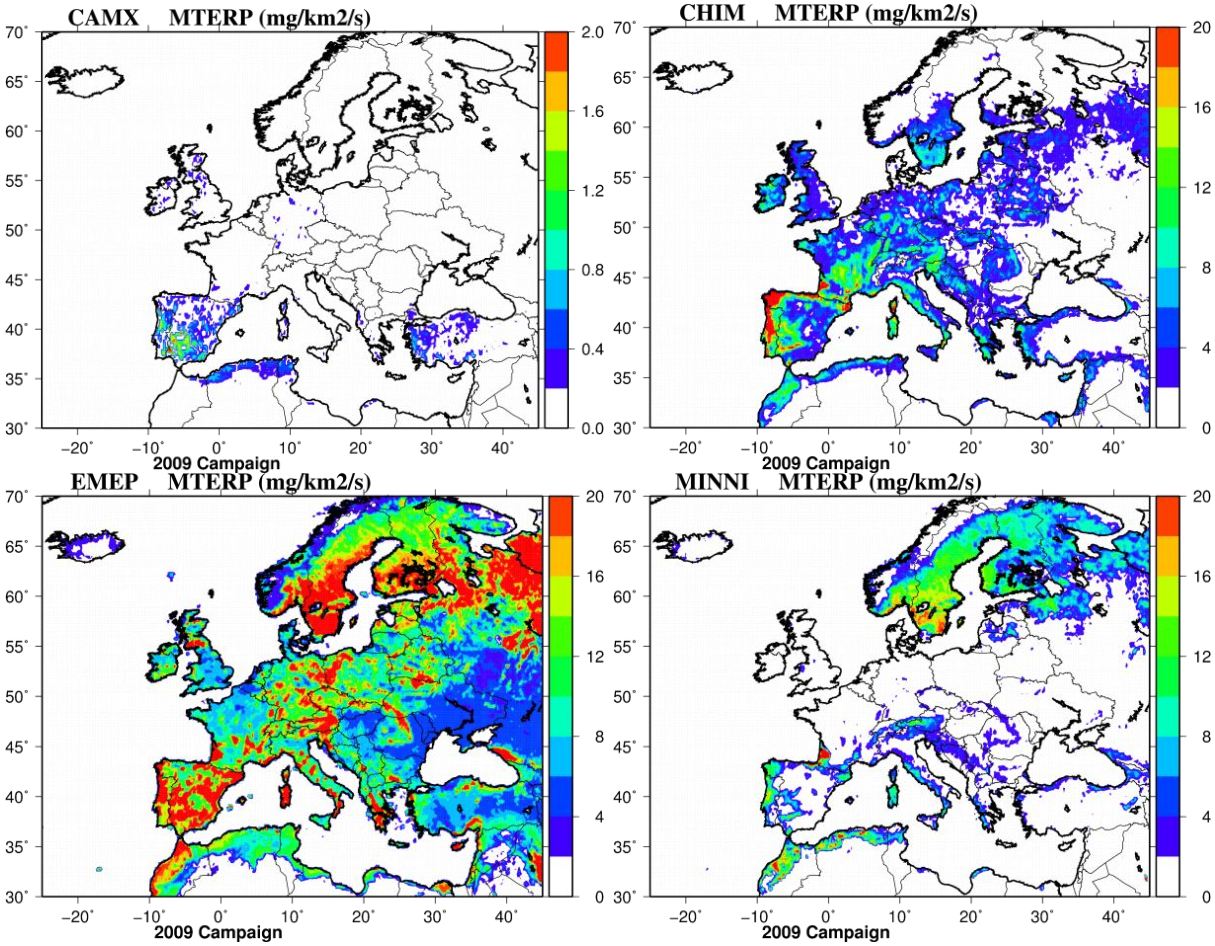

Figure 2.2: Average monoterpene emissions for CAMX, CHIM, EMEP and MINNI. Note that CAMX has a different colour scale with lower emission intensities.

Figure 2.2 displays the average emission flux of monoterpene for several models is very different from model to model. CHIM and MINNI are supposed to use the same emission module (MEGAN) but the spatial distribution and the order of magnitude is very different particularly in Scandinavia. CAMX simulates lower emission fluxes compared to the other models. By extrapolating data reported in

Lindfors and Laurila (2000), one can expect monoterpene emission fluxes in early spring lower than 0.5 mg km^{-2} s^{-1} in Scandinavian forests. MINNI and EMEP monoterpene emissions could then be largely overestimated over this region.

2.3 Meteorology

All models except CMAQ and RCGC shared the same meteorological dataset at 0.2° resolution based on ECMWF IFS (Integrated Forecast System) calculations. A full documentation is available on-line at : http://www.ecmwf.int/research/ifsdocs/CY25r1/Physics/Physics-01-1.html

For RCGC, a different meteorological data set was used. The 3-D-data for wind, temperature, humidity and density were produced employing a diagnostic meteorological analysis system based on an optimum interpolation procedure on isentropic surfaces developed at Freie Universität Berlin. The system takes into account all available observed synoptic surface and upper air data as well as topographical and land use information (Reimer and Scherer, 1992). Rain data, cloud data and boundary layer heights were retrieved from the IFS data set. Boundary layer parameters as friction velocity and Monin-Obukhov-lenghth were calculated on-the-fly applying standard boundary layer theory.

The CMAQ model operated by HZG used meteorological variables calculated with the COSMO model in CLimate Mode (COSMO-CLM) version 4.8 clm 11. The COSMO model is the non-hydrostatic operational weather prediction model applied and further developed by the national weather services joined in the COnsortium for SMall scale MOdeling (COSMO). The boundary layer height in COSMO is calculated with the turbulent kinetik energy (TKE) method (Doms *et al*. 2011).

PBL in IFS
Because of its importance for applications (*e.g.* in air pollution modelling), the boundary layer height was diagnosed and made available for post-processing. The parameterization of the mixed layer (and entrainment) uses a boundary layer height from an entraining parcel model. But in order to get a continuous field, also in neutral and stable situations the bulk Richardson method proposed by Troen and Mahrt (1986) is used as a diagnostic, independent of the turbulence parameterization. Boundary layer height is defined as the level where the bulk Richardson number, based on the difference between quantities of energy at that level and the lowest model level, reaches the critical value Ri_{cr} = *0.25*.

2.4 Boundary conditions

In this study, the MACC[14] reanalysis were used as input data for the boundary conditions (Inness *et al*., 2013; Benedetti *et al*., 2009). The reanalysis production stream provides analyses and 1-day forecasts of global fields of O_3, CO, NO_2, SO_2, HCHO, CO_2, CH_4, and aerosols. Other reactive gases are available from the coupled chemistry transport model. The reanalysis was started on 17 March 2010 with a 1-month spin-up and will cover the period 2003 - 2011. It runs at approximately 78 km by 78 km over 60 levels. The coupled chemistry transport model has the same 60 vertical levels and a horizontal resolution of 1.125 degrees x 1.125 degrees. For aerosols only elemental carbon, organic carbon, dust and sulphate were used.

[14] The MACC II (Modelling Atmospheric Composition and Climate, www.gmes---atmosphere.eu) project is establishing the core global and regional atmospheric environmental service delivered as a component of Europe's GMES (Global Monitoring for Environment and Security) initiative.

Stratospheric ozone fields from the MACC reanalysis agree with ozone sondes and ACE-FTS data (Atmospheric Chemistry Experiment Fourier Transform Spectrometer) within ±10% in most seasons and regions. In the troposphere the reanalysis shows biases of −5% to +10% with respect to ozone sondes and aircraft data in the extratropics, while larger negative biases are shown in the tropics. Area-averaged total column ozone agrees with ozone fields from a multi-sensor reanalysis data set within a few percent. For aerosols, the observed Aerosol Optical Depth (AOD) is assimilated in the model with a feedback on individual PM species (sea salts, dust, elemental carbon, organic carbon and sulphate). When available, the MACC reanalysis is compared with observations, the model acronym in the report is MACCA.

3 Simulation with Chemistry transport models

3.1 Methodology

Domain and resolutions

All the models have been run on the same domain at 0.25°x0.25° resolution in longitude and latitude as presented in Figure 3.1, except CMAQ. CMAQ simulations have been carried out on a lambert-conformal conic grid with the standard parallels at 30 and 60 degrees and a grid of 112 by 106 cells of size 24km x 24km. The results of the CMAQ simulations were interpolated to the prescribed EURODELTA grid (Byun and Schere, 2006; Matthias *et al*. 2011).

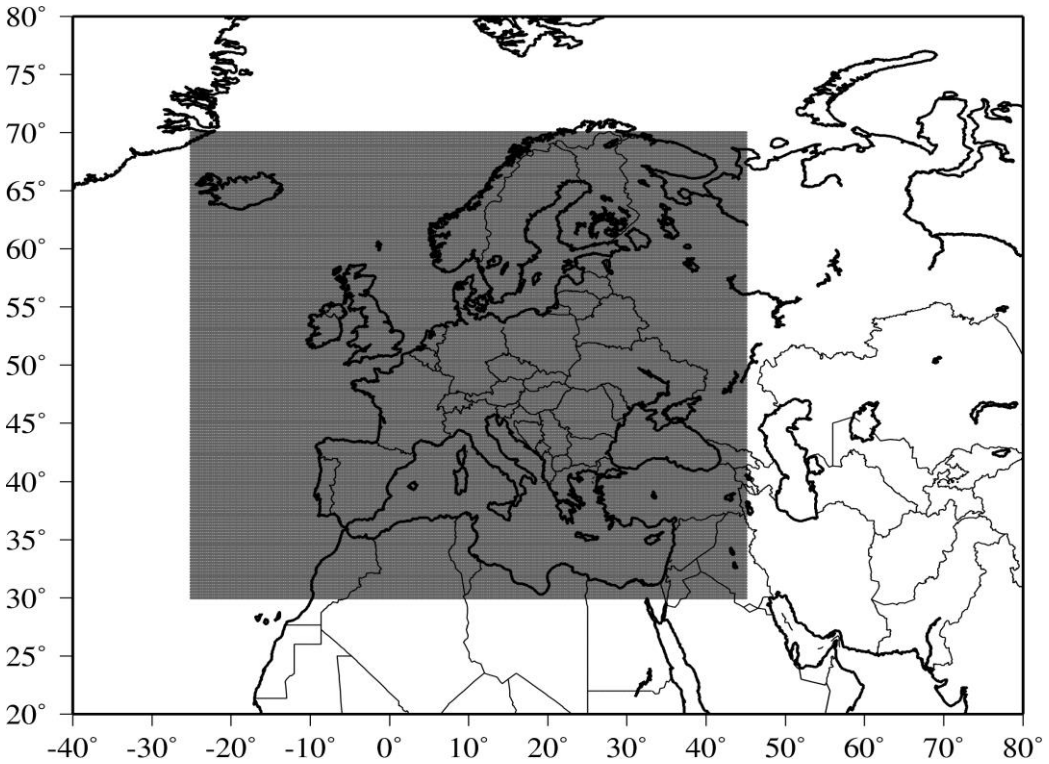

Figure 3.1: The grey zone corresponds to the EDIII domain. All model simulations have been performed over this domain except CMAQ.

Output species

All air concentrations and meteorological parameters are delivered by the participants, most of variables are delivered on a hourly basis, dry and wet depositions are provided on a daily basis. The output species include the Secondary Inorganic Aerosols (SIA : ammonium, sulphate and nitrate), all other PM components relevant for the analysis, and the total PM mass in both 2.5 and 10 µm fractions (PM_{10} and $PM_{2.5}$). **The delivered air concentrations correspond to the standard measurement height (typically 3 m) and were derived from the values of the lowest layer; LOTO and EMEP correct the concentrations from the first layer to be representative of 3-m concentrations, the other models directly extract the data from the calculated first level.** Here below, the required modelled output species (xx = 2.5, 10 µm) are listed:

- Air concentrations (saved on hourly basis)
  - PM_{10} : Particulate matter for particles with diameter below 10 µm
  - $PM_{2.5}$: Particulate matter for particles with diameter below 2.5 µm
  - NO3-xx : Nitrate for particles with diameter below xx µm

- NH4-xx : Ammonium for particles with diameter below xx µm
- SO4-xx : Sulphate for particles with diameter below xx µm
- NA-xx : Sodium for particles with diameter below xx µm
- DUST-xx : Dust for particles with diameter below xx µm
- TOM-xx: Total Organic Material for particles with diameter below xx µm
- TPOM-xx: Total Primary Organic Material for particles with diameter below xx µm
- POMS2-xx: Primary Organic Material from SNAP2 for particles with diameter below xx µm
- ASOA-xx: Anthropogenic Secondary Organic Aerosols with diameter below xx µm
- BSOA-xx: Biogenic Secondary Organic Aerosols with diameter below xx µm
- SOA-xx: Total Secondary Organic Aerosols with diameter below xx µm
- EC-xx: Elemental Carbon for particles with diameter below xx µm
- O3 : Ozone
- NO2 : Nitrogen dioxide
- SO_2 : Sulphur dioxide
- APINEN : Alpha-pinene
- HNO3 : Nitric acid
- NH3 : Ammonia
- TNO3 : Total nitrate (TNO3 = NO3-10 + $HNO3_{eq.\ Nitrate}$)
- TNH4 : Total ammonium (TNH4 = NH4-10 + $NH3_{eq.\ Ammonium}$)

- Depositions (saved on a daily basis) in mg(S or N)/m^2 according deposited species reported in Table 3.1:
  - WSOx : wet deposition of oxidized sulphur species
  - WNOx: wet deposition of oxidized nitrogen species
  - WNHx :wet deposition of reduced nitrogen species
  - DSOx : dry deposition of oxidized sulphur species
  - DNOx: dry deposition of oxidized nitrogen species
  - DNHx : dry deposition of reduced nitrogen species

Table 3.1: Composition of wet (W) and dry (D) scavenged species

Name of scavenged species	Name of deposited species
W or DSOx	SO_2, SO_4^{2-}
W or DNOx	HNO_3, NO_3^-, NO, NO_2 (and minor species like N_2O_5, PAN for some models)
W or DNHx	NH_3, NH_4^+

- Meteorological variables were also required (saved on hourly basis):
  - T2M : 2m temperature (K)
  - PBL : Planetary Boundary Layer height (m)
  - U10 : 10 meter wind speed (m/s)
  - USTAR : Friction velocity (m/s)
  - RAIN : total precipitation (mm/h)

All models did not save all output species, for instance the POMS2 species were only tracked by CHIM and RCGC.
The participating models differ in the availability of PM components and formation routes. For instance, EMEP, LOTO and RCGC contain coarse mode nitrate formation, whereas the others do not. Also, CHIM, CAMX, CMAQ, EMEP, MINNI and RCGC compute secondary organic aerosol, whereas the LOTO modelling team considers their SOA model formulations too uncertain for use in policy support. The PM_{10} concentration is calculated as follows in each model:

CAMX	PM_{10} = PPM + SO_4^{2-}+NO_3^-+NH_4^+ + SOA + Dust
CHIM	PM_{10} = PPM + SO_4^{2-}+NO_3^-+NH_4^++ Sea Salt + SOA + Dust
CMAQ	PM_{10} = PPM + SO_4^{2-}+NO_3^-+NH_4^++ Sea Salt + SOA + Dust
EMEP	PM_{10} = PPM + SO_4^{2-}+NO_3^-+NH_4^++ Sea Salt + SOA + Dust
MINNI	PM_{10} = PPM + SO_4^{2-}+NO_3^-+NH_4^++ Sea Salt + SOA + Dust
LOTO	PM_{10} = PPM + SO_4^{2-}+NO_3^-+NH_4^++ Sea Salt + Dust
RCGC	PM_{10} = PPM + SO_4^{2-}+NO_3^-+NH_4^++ Sea Salt + SOA + Dust

where PPM stands for Primary Particulate Matter and includes EC and POM.
In CMAQ additional anthropogenic dust is calculated as 90% of unspecified PM coarse emissions and attributed to fugitive dust (Binkowsky and Roselle, 2003).

Additional outputs for EMEP and LOTO
EMEP and LOTO delivered two additional outputs corresponding to their lowest model levels before correction with profiles. In the EMEP model, correction of species' concentrations from the lowest model layer (about 90 m) to 3-m height (a standard height for air pollution measurements) is performed based on the assumption of constant fluxes in the surface layer, using their respective dry deposition velocities. EMEP surface concentrations have been used for comparisons within the ED III exercise.

The LOTO model contains the option to diagnose the concentration (c_g) at measuring height (z_{ref}). To diagnose the concentration at measuring height we supposed that the deposition flux is constant over height. The concentration at measuring height is than computed as follows:

$$c_g = c_1 \cdot \left(1 - \frac{Ra_{zref}}{R_{tot}}\right) = c_1 \cdot (1 - V_d \cdot Ra_{zref})$$

Where c_1 is the concentration in layer 1, Ra_{zref}, the atmospheric resistance at measuring height and V_d, the deposition velocity in the first layer.

These extra outputs are referred to as **EMEPa** and **LOTOa** in this report.

3.2 Synthetic model description

Table 3.2: Model description part 1

MODEL	EMEP	CHIM	LOTO	RCGC	CMAQ	MINNI	CAMx
version	rv4.1.3	Chimere2013	v1.8	v2.1	V4.7.1	V3.1.12	V5.40
operator	met.no	INERIS	TNO	FU Berlin	HZG	ENEA/Arianet S.r.l.	PSI-LAC
contact	Svetlana Tsyro	Bertrand Bessagnet	Astrid Manders	Rainer Stern	Armin Aulinger	Mihaela Mircea Camillo Silibello Giuseppe Calori	Sebnem Aksoyoglu
email	svetlana.tsyro@met.no	bertrand.bessagnet@ineris.fr	astrid.manders@tno.nl	rstern@zedat-fu-berlin.de	Armin.aulinger@hzg.de	mihaela.mircea@enea.it c.silibello@aria-net.it g.calori@aria-net.it	sebnem.aksoyoglu@psi.ch
VERTICAL MODEL STRUCTURE							
Vertical layers	20 sigma	9 sigma	4 (3 dynamic layers and a surface layer)	6 fixed terrain following layers	30 sigma	16 fixed terrain-following layers	33 sigma
Vertical extent	100 hPa	500 hPa	3500 m	3000 m	100 hPa	10000 m	8000 m
Depth first layer	90 m	20 m	25 m	25 m	42 m	40 m	20 m
Correction of first level	Yes	No	Yes	No	No	No	No
NATURAL EMISSIONS							
Biogenic VOC	Based upon maps of 115 species from Koeble and Seufert (2001), and hourly temperature and light. See Simpson *et al*. (2012)	MEGAN model v2.04	Based upon maps of 115 species from Koeble and Seufert (2001), and hourly temperature and light. See Beltman et al (2013)	Based upon maps of 115 species from Koeble and Seufert (2001), and hourly temperature and light.using emissions factors of Simpson *et al.* (1999)	BEIS 3.14	MEGAN v2.04	PSI model (Oderbolz *et al.*, 2013)
Forest fires	None	None	None	None	None	None	None
Soil-NO	See in Simpson *et al.* (2012)	MEGAN model v2.04	Not used here	From Simpson *et al.* (1999)	BEIS 3.1.4	MEGAN v2.04	Not used here
Lightning	Climatological fields, Köhler *et al.* (1995)	None	None	None	None	None	None
Sea salt	Monahan (1986) and Martensson (2003), see Tsyro *et al.* (2011).	Monahan *et al.* (1986)	Martensson *et al.* (2003) and Monahan *et al.* (1986)	Gong *et al.* (1997) and Monahan *et al.* (1986)	Zhang *et al.* (2005) and Clarke *et al.* (2006)	Zhang *et al.* (2005)	Gong (2003), not used for the 2009 simulation
Windblown Dust	See Simpson *et al.* (2012)	Vautard *et al.* (2005), not used here	Denier van der Gon *et al.* (2009).	Loosemore and Hunt (2000), Claiborn *et al.* (1998)	None	Vautard *et al.* (2005)	None
Agricultural land management	None	None	None	None	None	None	None
Dust traffic suspension	Denier van der Gon *et al.* (2009).	None	None	None	None	None	None
LANDUSE							
Landuse database	CCE/SEI for Europe, elsewhere GLC2000	GLOBCOVER (24 classes)	Corine Land Cover 2000 (13 classes)	Corine Land Cover 2000 (13 classes)	Corine Land Cover 2006 (44 classes)	Corine Land Cover 2006 (22 classes)	GLOBCOVERv2.2
Resolution	Flexible, CCE/SEI ~ 5 km	About 300 m	1/60 x 1/60 degrees	1/60 x 1/60 degrees	100m x 100m	About 250 m	About 300 m
BOUNDARY CONDITIONS							
Ozone and oxidants	MACC	MACC	MACC	MACC	MACC	MACC	MACC
Aerosols	MACC	MACC	MACC	MACC	MACC	MACC	MACC

Table 3.3: Model description part 2

MODEL	EMEP	CHIM	LOTO	RCGC	CMAQ	MINNI	CAMx
METEOROLOGY							
Description	ECMWF	ECMWF IFS + urban mixing	ECMWF	ECMWF + Observations	CCLM	ECMWF	ECMWF IFS
Resolution	0.22 deg x 0.22 deg	0.22 deg x 0.22 deg	0.22 deg x 0.22 deg	0.22 deg x 0.22 deg	24 km x 24 km (Lambert Conformal Conic Projection)	0.22 deg x 0.22 deg	0.22 deg x 0.22 deg
PROCESSES							
Advection scheme	Bott (1989a,b)	Van Leer (1984)	Walcek (2000)	Walcek (2000) modified by Yamartino (2003).	Blackman cubic polynomials (Yamartino, 1993	Blackman cubic polynomials (Yamartino, 1993)	Bott (1989a,b)
Vertical diffusion	Kz approach following O'Brien (1970	Kz approach following Troen and Mart (1986)	Kz approach	Kz-approach	ACM2 PBL scheme (Pleim, 2007)	Kz approach following hybrid semi-implicit Crank-Nicolson / fully implicit scheme (Yamartino *et al.*, 1992)	Kz approach following O'Brien (1970)
Dry deposition	resistance approach for gases, Venkatram and Pleim (1999) for aerosols, Simpson *et al.* (2012)	resistance approach Emberson (2000a,b)	Resistance approach,DEPAC3.11 for gases, Van Zanten *et al.* (2010) and Zhang et al (2001) for aerosols	resistance approach, DEPAC-module	Resistant approach, Venkatram and Pleim (1999)	Resistance model (Walcek and Taylor, 1986; Wesely, 1989)	Resistance model for gases (Zhang *et al.*,2003) and aerosols (Zhang *et al.*, 2001)
Compensation points	No, but zero NH_3 deposition over growing crops	No	Only for NH_3 (for stomatal, external leaf surface and soil (= 0))	No	No	No	No
Stomatal resistance	DO3SE-EMEP: Emberson *et al.* (2000a,b), Tuovinen *et al.* (2004), Simpson *et al.* (2012)	Emberson (2000a,b)	Emberson (2000a,b)	Wesely (1989)	Wesely (1989)	Wesely (1989)	Wesely (1989)
Wet deposition gases	In-cloud and sub-cloud scavenging coefficients	In-cloud and sub-cloud scavenging coefficients	sub-cloud scavenging coefficient	pH dependent scavenging coefficients	In-cloud and sub-cloud scavenging which depends on Henry's law constants, dissociation constants and cloud water pH. Chang *et al.* (1987)	In-cloud and sub-cloud scavenging coefficients (EMEP, 2003)	Scavenging model for gases and aerosols (Seinfeld and Pandis, 1998)
Wet deposition particles	In-cloud and sub-cloud scavenging	In-cloud and sub-cloud scavenging	sub-cloud scavenging coefficient	sub-cloud scavenging coefficients	In-cloud and sub-cloud scavenging	In-cloud and sub-cloud scavenging coefficients	Scavenging model for gases and aerosols (Seinfeld and Pandis, 1998)
Gas phase chemistry	EmChem09	MELCHIOR	TNO-CBM-IV	CBM-IV	CB-05 with chlorine chemistry extensions (Yarwood *et al.*, 2005)	SAPRC99 (Carter, 2000a,b)	Carbon Bond 2005 (Yarwood *et al.*, 2005)
Cloud chemistry	Aqueous SO_2 chemistry	Aqueous SO_2 chemistry and ph dependent SO_2 chemistry	Banzhaf *et al.* (2011) (not used for 2009 campaitn)	Simplified aqueous SO_2 chemistry	Aqueous SO_2 chemistry (Walcek and Taylor, 1986)	Aqueous SO_2 chemistry (Seinfeld and Pandis, 1998)	Aqueous SO_2 chemistry RADM-AQ (Chang *et al.*, 1987)
Coarse nitrate	Yes	No reaction with Ca or Na but coarse might exists with transfer from smaller particles	Yes	Yes	No	No	No
Ammonium nitrate equilibrium	MARS (Binkowski and Shankar,1995)	ISORROPIA (Nenes *et al.*, 1999)	ISORROPIA v.2	ISORROPIA	ISORROPIAv1.7	ISORROPIA v1.7 (Nenes *et al.*, 1998)	ISORROPIA (Nenes *et al.*, 1998)
SOA formation	VBS-NPAS –Simpson *et al.* (2012)	After Bessagnet *et al.* (2009)	not used	SORGAM module (Schell et al., 2001)	SORGAM module (Schell et al., 2001)	SORGAM module (Schell et al., 2001)	SOAP (Strader *et al.*, 1999) and oligomerization
VBS	Yes, Bergström *et al* (2012), Simpson *et al.* (2012)	None	Based on Bergström et al (2012), Not used for 2009 campaing	None	None	None	no
Aerosol model	Bulk- approach (2 modes)	8 bins (40 nm to 10 µm)	Bulk- approach (2 modes)	Bulk approach (2 modes)	AERO5 (Carlton *et al.*, 2010) Log-normal approach (3 modes)	AERO3 (Binkowski, 1999); 3 modes: Aitken, accumulation, coarse	Bulk- approach (2 modes)
Aerosol physics	Not used	coagulation/condensation/nucleation	Not used	None	Coagulation/condensation/nucleation	Coagulation/condensation/nucleation	Not used

3.3 Dust emissions

CAMX, CHIM and CMAQ
No dust module is activated for this exercise for these three models. Natural dust only comes from the boundary conditions.

EMEP
Windblown dust parameterisation is documented in Simpson *et al*. (2012). Road dust calculations are included in the calculations from Denier van der Gon *et al*. (2009).

LOTO
LOTO contains emission parameterizations for several sources of mineral dust (Schaap *et al* 2009). Only wind-blown dust, resulting from wind erosion of bare soil, was taken into account here, together with dust from boundary conditions. Other sources (agricultural activities, road dust resuspension) were not activated in EDIII.

MINNI
Dust emission from local erosion and particle resuspension (Vautard *et al*., 2005) with attenuation in the presence of vegetation from Zender *et al*. (2003).

RGCC
RCGC considers resuspension of mineral aerosol as a function of friction velocity and the nature of soil. Two mechanisms are treated: direct release of small dust particles by the wind (Loosmore and Hunt, 2000), and indirect release by collisions with bigger soil grains, that are lifted by the wind but return to the surface because of their weight (saltation process, Claiborn *et al*., 1998). Road dust resuspension was not considered in this exercise.

3.4 PBL and mixing in models

CAMX
In EDIII the Planetary Boundary Layer is directly taken from the IFS ECMWF data. The PBL height is then used by CAMX pre-processor to derive *K(z)* profiles. For EDIII the O'Brien scheme (1970) has been used to derive *K(z)* profiles as:

$$K(z) = K_A + \frac{(z - z_A)^2}{\Delta z^2}\left\{K_B - K_A + (z - z_B)\left(K'_B + 2\frac{K_B - K_A}{\Delta z}\right)\right\}$$

Where K_A is a value of $K(z_A)$ at the height of the atmospheric boundary layer, z_A, and K_B is $K(z_B)$ at the height of the surface layer z_B, the so-called constant-flux layer. Minimum *K(z)* values have been set to 1. Any values of *K(z)* calculated below, will be set to this value. By default, CAMX employs a standard "K-theory" approach for vertical diffusion to account for sub-grid scale mixing layer-to-layer.

CHIM
Horizontal turbulent fluxes are not considered. Vertical turbulent mixing takes place only in the boundary layer. The formulation uses K-diffusion following the parameterization of (Troen and Mahrt, 1986), without counter-gradient term. In each model column, diffusivity K_z is calculated as:

$$K_z = \mathrm{k}\,\mathrm{w_s}\,\mathrm{z}\left(1 - \frac{\mathrm{z}}{\mathrm{h}}\right)^{1/3}$$

where w_s is a vertical scale given by similarity formulae.

- In the stable case (surface sensible heat flux < 0): $w_s = u_*/(1 + 4.7\,z/L)$

- In the unstable case: $w_s = ({u_*}^3 + 2.8e{w_*}^3)^{1/3}$

where *e = max(0.1,z/h)*, *L* is the Monin-Obukhov Length, w_* is the convective velocity scale, u_* the friction velocity and *h* the boundary layer height. A minimal K_z is assumed, with a value of 0.01 m^2/s.
Kz and the wind speed are corrected in urban zones according Terrenoire *et al.* (2013) by applying a correction factor to limit the diffusion within the urban canopy, but this correction has very little effect at this resolution.
In CHIM, the boundary layer height *h* can be either directly provided by the meteorological model (as it is the case for EDIII) or recalculated in the meteorological diagnostic model. In the latter case the boundary layer height is considered as the maximum of the (Troen and Mahrt, 1986) boundary layer height calculated from the Richardson number profile, as the lowest altitude where Ri = 0.5, and a more convectively-based boundary layer height calculation. The latter is based on a simplified and diagnostic version of the approach of (Cheinet, 2002). It consists in the resolution of the (dry) thermal plume equation with diffusion. The in-plume vertical velocity and buoyancy equations are solved and the boundary layer is taken as the height where vertical velocity stops. Thermals are initiated with a non-vanishing vertical velocity and potential temperature departure, depending on the turbulence similarity parameters in the surface layer. **In EDIII the Planetary Boundary Layer is directly taken from the IFS ECMWF data.**

EMEP
The mixing height is calculated using a slightly modified Richardson number (Ri_B) following Jeričevič *et al*. (2010) and defined as the lowest height at which the Ri_B>0.25. Finally, the PBL is smoothed with a second order Shapiro filter in space. The PBL height is not allowed to be less than 100 m or exceed 3000 m.

The initial calculation of the vertical exchange coefficients is done using the Ri number and wind speed vertical gradient for the whole domain. Then, K_z values within the PBL are recalculated based on Jeričevič *et al*. (2010) for stable and neutral conditions. For unstable situations K_z is calculated based on the similarity theory of Monin-Obukhov for the surface layer, whereas K_z profiles from O'Brian (1970) are used for the PBL above the surface layer. For more detail see Simpson *et al*. (2012).

LOTO
The first model layer is by definition the mixing layer, with height equal to the boundary layer height as given by ECMWF. Horizontal diffusion is not used, but for vertical mixing the vertical diffusion coefficient is calculated according to

$$K_v = \frac{\kappa u^*}{\Phi(z/L)}$$

With *k* the von Karman constant, *u** the friction velocity, *Φ* the functions proposed by Businger (1971) for stable, neutral or unstable atmosphere, z the height and L the Monin-Obhukov length. The friction velocity is calculated depending on the wind at reference height (10 m), the Businger functions and the roughness length per land use class.

MINNI
Friction velocity, scale temperature and Monin-Obukhov length are determined by using:-Holtslag and van Ulden (1983) iterative scheme for unstable conditions (sensible heat flux greater than zero and Venkatram (1980) iterative method for stable conditions. Convective velocity scale (set to zero for stable conditions) is subsequently determined by starting from mixing height, sensible heat flux and scale temperature. Micro-meteorological parameters over water are derived with the Profile method, using air-sea temperature difference (Hanna *et al*., 1985), with the needed roughness length, depending on wind speed, supplied by the Hosker (1974) parameterization.

During daytime both convective and mechanical heights have been determined, keeping then the maximum value between the two parameters. The convective height is calculated following the Maul (1980) version of Carson (1973) algorithm, essentially based on heat conservation equation; mechanical mixing height is instead estimated by using Venkatram (1980) algorithm. During nighttime, Bulk Richardson number method (Sorensen, 1998), in which the height of the boundary layer is given by the smallest height at which the bulk Richardson number reaches a prescribed critical value, depending on Brunt-Väisälä frequency: 0.25 is the advised value that can be modified by the user. The linear regression approximation suggested by Zilitinkevich and Baklanov (2002) can be chosen alternatively to compute automatically the critical value as a function of Brunt-Väisälä frequency and Coriolis parameter in stable conditions.

RCGC

The mixing layer depth in the model is the height of the layer closest to the input boundary layer height taken from the IFS ECMWF data. Vertical diffusion parameters for stable and unstable conditions are derived using the Monin-Obukhov similarity theory for the description of the structure of the diabatic surface layer. The friction velocity and Monin-Obukhov-length are calculated iteratively depending on the 10 m wind, the stability corrections factors and the land use dependent roughness length.

4 Observation dataset and statistics

4.1 Observational datasets

Air concentrations and deposition (Particles and gases)

The evaluation is carried out on the available EMEP standard monitoring and intensive period observations for 2009 on hourly and daily bases (see Annex 1 and 2 for the characteristics of stations). The measurements were downloaded from the EBAS database[15], all information regarding the stations is accessible on the EBAS web site, coordinates and altitudes of stations can be found at http://www.nilu.no/projects/ccc/network/index.html. All available data were used, the list of stations is reported in Annex 1 but some altitude sites have been removed for this study. Data from AirBase[16] (Mol and de Leeuw, 2005) are also included in the analyses in section 5 for $PM_{2.5}$ and PM_{10} concentrations.

In this report, dust observations are estimated from Calcium concentrations as $DUST = 8 \times \mathrm{Ca}$. The ratio of 8 is chosen as an average value for dust from "local" soils (Guinot *et al.*, 2007) and from desert areas (Putaud *et al.*, 2004). When Organic Carbon concentrations were available, observed TOM concentrations were estimated as $TOM = 1.6 \times \mathrm{OC}$ (OC as Organic Carbon). POMS2-25 is compared to observed Biomass Burning Organic Aerosol (BBOA), SOA-25 is compared to observed OOA (Oxidized Organic Aerosol) for several stations as described in Crippa *et al.* (2013).

In some supersites like Melpitz (DE44) and Payerne (CH02), AMS instrument (Aerosol Mass Spectrometer) provides hourly measurements for aerosol components in particles with diameter below 1 µm. **These observed concentrations are compared with modelled $PM_{2.5}$ concentrations in this report**, explaining a potential bias in the comparison, however the differences are expected to be small according Aksoyoglu *et al*. (2011).

It is important to note that daily measurements for a day N is the averaged (or accumulation for deposition) value between day N HH:00 and day N+1 HH:00, with HH usually varying in the range [00, 09].

For most of species, measurements on daily and hourly bases are not necessarily performed for the same set of stations.

Meteorology

Temperature, wind speed and precipitation

The temperature, wind speed and precipitation measurements come from 2016 synoptic stations in Europe reported by the European meteorological centres. The data are provided on an hourly basis. The temperature is measured at 2 m and the wind speed at 10 m.

Some meteorological data are also reported at some EMEP stations like the precipitation amounts that are reported on a daily basis. For these EMEP sites, as for deposition, **daily measurements for a day N is the accumulation of precipitation between day N HH:00 to day N+1 HH:00, with HH usually varying in the range [00, 09].**

Planetary Boundary Layer

The soundings data were extracted from the University of Wyoming database (http://weather.uwyo.edu/cgi-bin/sounding). For each site and for each day, two soundings are

[15] EBAS is a database hosting observation data of atmospheric chemical composition and physical properties. EBAS hosts data submitted by data originators in support of a number of national and international programs ranging from monitoring activities to research projects. EBAS is developed and operated by the Norwegian Institute for Air Research (NILU). For a complete list of programmes and projects for which EBAS serves as a database, please consult the information box in the Framework filter of the web interface (http://ebas.nilu.no/)

[16] AirBase is the public air quality database system of the EEA. It contains air quality monitoring data and information submitted by the participating countries throughout Europe.

available at 00:00 and 12:00. The provided meteorological parameters are the pressure (hPa), the corresponding height above ground level (m), the dew point (C), the relative humidity (%), the mixing ratio (g/kg), the wind direction (degrees) and the wind speed (expressed in knot and converted in m/s by applying the conversion factor 0.514), the potential and virtual potential temperature (in Kelvin). For the present study, data were extracted over 77 stations in Europe. Looking for the boundary layer height, the profiles are analyzed only for the first 25 vertical points, roughly corresponding to an altitude of 5000m above ground level. The boundary layer height is estimated using the calculation of the Bulk Richardson number profile and searching for the altitude where the critical value of $Ri_{cr}=0.25$ is reached. **The boundary layer height being a concept only valid for convective periods, only the sounding of 12Z were analyzed and used for the models validation.** In addition to the previous PBL data, hourly heights of the atmospheric boundary layer were calculated from LIDAR measurements in a background site near Paris (SIRTA in Palaiseau). A new objective method for the determination of the atmospheric boundary layer depths using routine LIDAR measurements have been used (Pal *et al*., 2013). A geophysical process-based analysis is introduced to improve the attribution of the LIDAR derived aerosol gradients for a robust detection of the PBL depths which is so far the most challenging part in any gradient-based technique. LIDAR-derived aerosol backscatter signal intensity at different altitudes are used to determine the hourly averaged vertical profiles of variance yielding the location of maximum turbulent mixing within the PBL, hence mean PBL depth. On the other hand, using micrometeorological measurements of Obukhov length scale both early morning transition and evening transition periods are determined and a first-order approximation on the boundary layer growth rates is obtained. To this end, the variance-based results guide the attribution by searching the appropriate minimum of the gradient closest to the mean PBL depth while two transition periods of a day are used to separate the turbulence regimes during the well-mixed convective PBL and nocturnal/stable PBL. An empirical classification of the PBL stratification patterns into three different types is proposed in terms of the variability of the PBL depths and near surface stability scenarios.

Ozone soundings

The vertical ozone sounding are taken from the World Ozone and Ultraviolet Data Center (WOUDC) (http://www.woudc.org). There are 9 available sounding sites for the period campaign (from 2009-02-25 to 2009-03-26). Table 4.1 and Figure 4.1 indicate the geographical characteristics of the available profiles. The frequency of the measurements is irregular. There are stations (STN053, STN156 and STN242) with around three soundings per week, but most of the stations have only one measurement per week.

Table 4.1. Characteristics of the O_3 sounding sites over the EuroDelta domain for the study period.

ID	Station	Country	Latitude	Longitude	Height (m)	Profiles
STN043	LERWICK	Great Britain	60.14	-1.19	80	5
STN053	UCCLE	Belgium	50.8	4.35	100	12
STN156	PAYERNE	Switzerland	46.49	6.57	491	12
STN221	LEGIONOWO	Poland	52.4	20.97	96	4
STN242	PRAHA	Czech Republic	50	14.44	304	10
STN308	BARAJAS	Spain	40.47	-3.58	631	4
STN316	DE BILT	The Netherlands	52.1	5.18	4	4
STN318	VALENTIA OBSERVATORY	Ireland	51.93	-10.25	14	4
STN348	ANKARA	Turkey	39.97	32.86	890	3

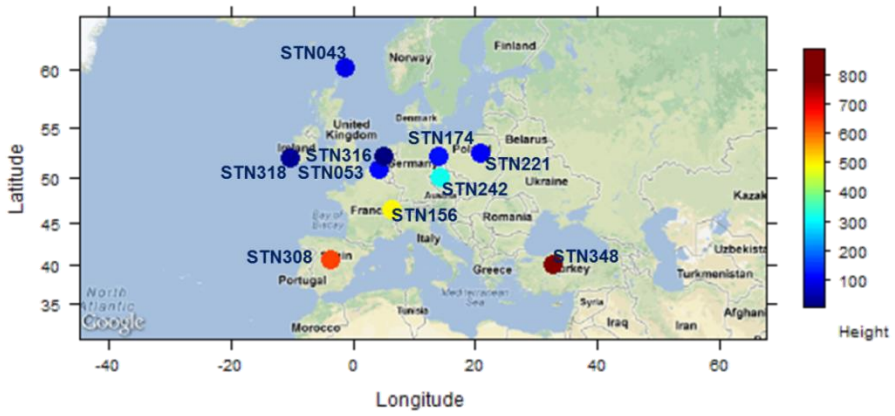

Figure 4.1. Location of the measurement sites of O_3 profiles available at WOUDC over Europe during the study campaign.

4.2 Error statistics for the model performance evaluation

The errors statistics considered in this report are presented in Table 4.2.

Table 4.2: Error statistics used to evaluate model performance (M and O refers respectively with Model and observations data, and N is the number of observations)

Mean Bias	$(\bar{M} - \bar{O})$ with $\bar{M} = \frac{1}{N}\sum_{i=1}^{N} M_i$ and $\bar{O} = \frac{1}{N}\sum_{i=1}^{N} O_i$
Normalised Mean Bias	$NMB = (\bar{M} - \bar{O})/\bar{O}$
Mean Bias	$MB = (\bar{M} - \bar{O})$
Mean Gross Error	$MGE = \frac{1}{N}\sum_{i=1}^{N} \lvert M_i - O_i \rvert$
Standard Deviation	$SD_X = \sqrt{\frac{1}{N}\sum_{i=1}^{N}(X_i - \bar{X})^2}$ with X=O or M
Root Mean Square Error	$RMSE = \sqrt{\frac{1}{N}\sum_{i=1}^{N}(M_i - O_i)^2}$
Correlation Coefficient	$R = \left(\sum_{i=1}^{N}(M_i - \bar{M})(O_i - \bar{O})\right) \Big/ \left(\sqrt{\sum_{i=1}^{N}(M_i - \bar{M})^2 \times \sum_{i=1}^{N}(O_i - \bar{O})^2}\right)$
Centred Root Mean Square Error	$CRMSE = \sqrt{\frac{1}{N}\sum_{i=1}^{N}\left((M_i - \bar{M}) - (O_i - \bar{O})\right)}$
Normalised Mean Standard Deviation	$NMSD = (SD_M - SD_O)/SD_O$
Mean Fractional Bias	$MFB = \frac{1}{N}\sum_{i=1}^{N}\frac{M_i - O_i}{(M_i + O_i)/2}$
Mean Fractional Error	$MFE = \frac{1}{N}\sum_{i=1}^{N}\frac{\lvert M_i - O_i \rvert}{(M_i + O_i)/2}$

5 Overall model performance evaluation on criteria pollutants

5.1 Evaluation at EMEP background sites

Table 5.1 presents the main model performance statistics for O_3, NO_2, SO_2, PM_{10}, $PM_{2.5}$ for the period of 25 February-26 March 2009 with all available measurement data from stations in Europe. **An important notice is that hourly and daily statistical analysis is performed over different sets of stations**. However, for a given pollutant, the model performance statistics are computed for a common set of stations (over the same common geographic area).

The models underestimate daily and hourly O_3 concentrations between 5 and 20% (in the case of MINNI) on average. The correlation coefficients are between 0.42 and 0.64 for daily and 0.43 and 0.59 for hourly concentrations. CHIM, CAMX and EMEP obtain for ozone the best performances in terms the RMSE. For NO_2, the models achieve quite similar correlations (usually between 0.57 and 0.70) both on daily and hourly bases. CAMX and RCGC show the largest underestimation of measured NO_2 concentrations, whereas CMAQ overestimates the concentrations the most. **It should be pointed out that the observed NO_2 concentrations can be slightly overestimated because of sampling artefact (evaporation of nitric acid).** For SO_2, EMEP results are close to the observations, the models RCGC, MINNI and CAMX overestimate the concentrations on average, while CHIM underestimates the observed values. The correlation for SO_2 is lower compared to NO_2 and O_3 for all the models (about 0.50), and especially in case of the hourly concentrations (0.27-0.39). For O_3, a part of the models' bias can be explain by the too low boundary conditions (from MACC), as pointed out from the statistics in Mace Head (IE31). The smallest negative bias is found for CHIM and CMAQ (-8 µg m^{-3}) as shown in Figure 5.1. On average the MACC analysis has a very strong negative bias (about 20 µg m^{-3}), this clearly affects the results of RCGC and MINNI, at Mace Head whereas the effect is less pronounced in the simulation for EMEP, CHIM and CMAQ.

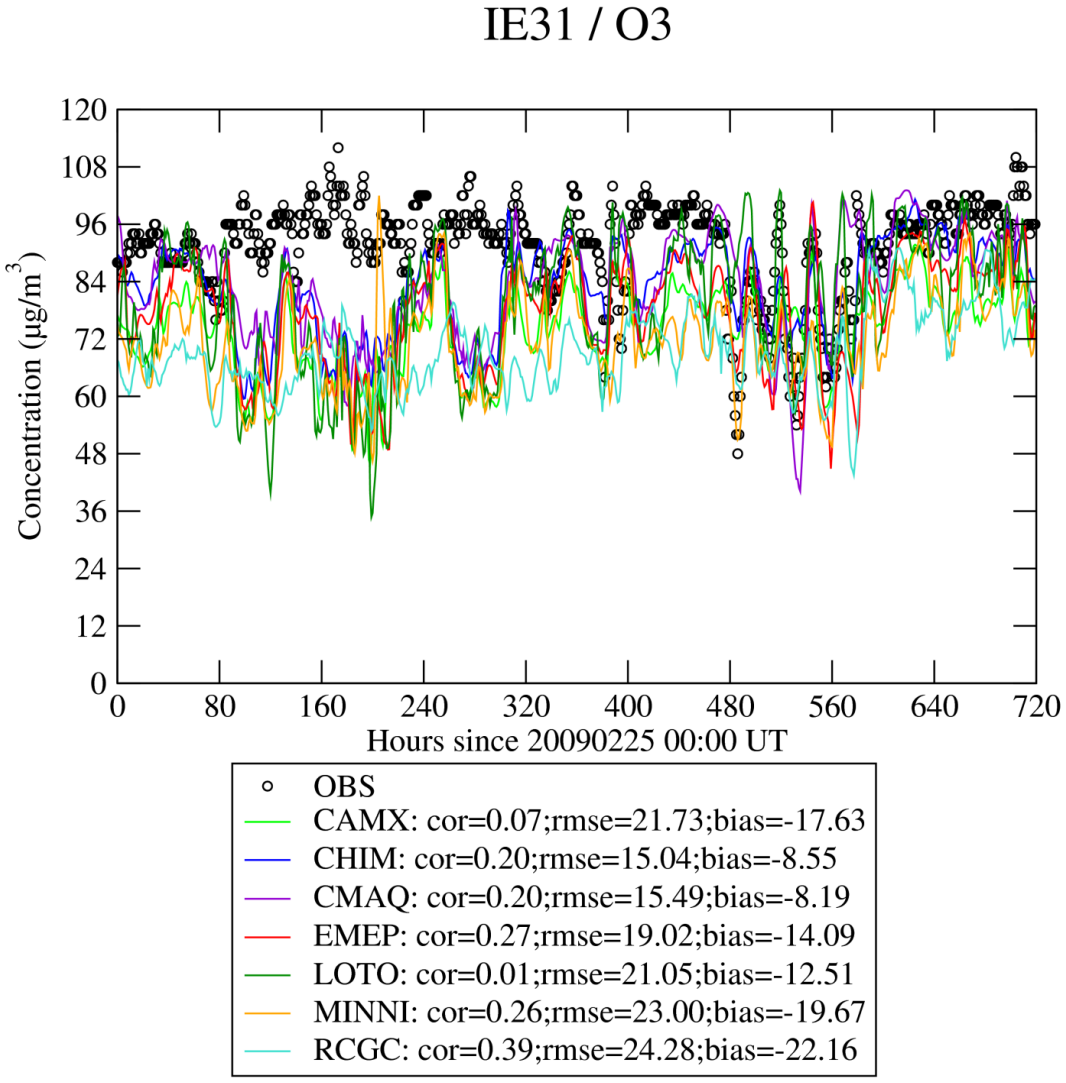

Figure 5.1: Time series of hourly ozone concentrations at Mace Head (Ireland)

For PM_{10}, all the models underestimate the observed concentrations, with the only exception of MINNI which slightly overestimates the measured PM_{10}. The correlations are spread over a large range between 0.32 and 0.62. EMEP, CHIM and MINNI obtain the best performances for RMSE. For $PM_{2.5}$, only CHIM and MINNI show a small overestimation of concentrations while the other models underestimate the observed values. The correlation for $PM_{2.5}$ is generally better than PM_{10}, also showing a narrower spread.

These performance statistics will be explained later in this report by looking at individual aerosol components and analysing the effect of input data like meteorology and boundary conditions.

Table 5.1: Model evaluation for O_3, NO_2, SO_2, PM_{10} and $PM_{2.5}$ concentrations (µg m^{-3}) for the campaign period of 25 February-26 March 2009. Correlations in time and space (*Cor.*), Biases (in µg m^{-3}) and Root Mean Square Errors in (*RMSE in* µg m^{-3}) are computed based on daily values (left table) and hourly values (right table). Observation values (*Obs.* in µg m^{-3}) and model values (in µg m^{-3}) are the average concentrations. *Nb* is the number of available observations for a given pollutant. The best model performance for the RMSE is displayed in bold character.

Daily basis

Pollutant	Obs.	Model name	Model val.	Bias	Cor.	RMSE	Nb.
O3	69.86	CAMX	61.16	-8.70	0.61	17.48	3410
		CHIM	65.28	-4.58	0.57	**15.96**	
		CMAQ	61.90	-7.96	0.42	21.82	
		EMEP	62.21	-7.65	0.55	17.52	
		LOTO	61.45	-8.41	0.52	18.15	
		MINNI	53.92	-15.94	0.61	21.78	
		RCGC	57.61	-12.26	0.64	18.61	
NO2	7.64	CAMX	6.21	-1.42	0.66	**6.28**	2366
		CHIM	6.93	-0.70	0.65	6.53	
		CMAQ	10.71	3.08	0.57	10.01	
		EMEP	7.34	-0.29	0.64	6.50	
		LOTO	7.58	-0.06	0.64	6.53	
		MINNI	8.10	0.47	0.66	6.61	
		RCGC	6.54	-1.09	0.62	6.58	
SO2	1.10	CAMX	2.73	1.63	0.49	2.85	1618
		CHIM	0.89	-0.21	0.48	**1.33**	
		CMAQ	1.47	0.36	0.49	1.60	
		EMEP	1.09	-0.01	0.50	1.37	
		LOTO	1.19	0.08	0.48	1.33	
		MINNI	2.35	1.25	0.49	2.23	
		RCGC	2.49	1.39	0.49	2.50	
PM10	17.16	CAMX	12.37	-4.79	0.35	15.70	1449
		CHIM	16.56	-0.60	0.43	14.07	
		CMAQ	12.24	-4.92	0.32	15.71	
		EMEP	12.69	-4.48	0.62	**13.03**	
		LOTO	10.92	-6.24	0.52	15.02	
		MINNI	18.23	1.07	0.42	14.18	
		RCGC	15.17	-1.99	0.41	14.35	
PM25	12.83	CAMX	11.16	-1.67	0.59	8.95	964
		CHIM	13.07	0.24	0.65	**8.02**	
		CMAQ	9.25	-3.58	0.55	9.67	
		EMEP	8.67	-4.16	0.69	8.81	
		LOTO	7.65	-5.18	0.63	10.01	
		MINNI	13.45	0.62	0.64	8.19	
		RCGC	11.25	-1.58	0.54	9.04	

Hourly basis

Pollutant	Obs.	Model name	Model val.	Bias	Cor.	RMSE	Nb.
O3	69.81	CAMX	61.20	-8.60	0.59	20.41	81502
		CHIM	65.34	-4.47	0.57	**19.42**	
		CMAQ	61.98	-7.82	0.43	25.61	
		EMEP	62.26	-7.55	0.55	20.68	
		LOTO	61.55	-8.26	0.51	22.64	
		MINNI	54.01	-15.80	0.59	24.35	
		RCGC	57.67	-12.13	0.58	22.54	
NO2	8.87	CAMX	7.21	-1.66	0.70	**7.66**	30382
		CHIM	8.44	-0.43	0.66	8.91	
		CMAQ	11.80	2.93	0.55	13.56	
		EMEP	8.34	-0.53	0.67	8.22	
		LOTO	9.04	0.17	0.63	9.12	
		MINNI	9.57	0.70	0.69	8.40	
		RCGC	7.67	-1.20	0.65	8.21	
SO2	1.24	CAMX	3.26	2.01	0.27	3.98	20403
		CHIM	1.00	-0.24	0.37	**1.73**	
		CMAQ	1.58	0.34	0.31	2.19	
		EMEP	1.24	0.00	0.39	1.89	
		LOTO	1.33	0.08	0.31	1.83	
		MINNI	2.54	1.30	0.36	2.68	
		RCGC	2.93	1.69	0.28	3.30	
PM10	20.05	CAMX	11.39	-8.66	0.65	15.15	9485
		CHIM	19.35	-0.70	0.59	13.27	
		CMAQ	13.05	-7.00	0.52	15.62	
		EMEP	14.75	-5.29	0.61	13.93	
		LOTO	11.97	-8.07	0.63	15.56	
		MINNI	20.62	0.57	0.61	**12.89**	
		RCGC	15.52	-4.53	0.56	14.29	
PM25	9.38	CAMX	8.66	-0.73	0.64	7.41	4323
		CHIM	12.57	3.18	0.60	8.42	
		CMAQ	7.68	-1.71	0.56	8.19	
		EMEP	7.70	-1.69	0.65	**6.89**	
		LOTO	6.59	-2.79	0.66	6.92	
		MINNI	11.98	2.60	0.65	8.42	
		RCGC	9.55	0.16	0.59	7.39	

The spatial patterns of modelled NO_2 concentrations are quite similar and are very close to those of NO_2 emissions (Figure 5.2), the spatial correlation is close to 0.70 for all models. For Ozone, MINNI has lower concentrations over land coherent with slightly higher NO_2 concentrations in these areas. CMAQ, followed by CAMX, displays the highest O_3 concentrations in Spain, which is in a better agreement with observations. The diurnal cycle for NO_2 reveals the systematic overestimation at night by all the models except for RCGC and CAMX and the underestimation during the afternoon.

The RCGC model gives the O_3 pattern similar to the MACC analysis (MACCA in Figure 5.2). Over the sea, EMEP and CHIM give the highest O_3 concentrations values. The spatial correlations are rather different among the models: 0.35 for CMAQ; 0.59 for CHIM, EMEP and LOTO; 0.64 for CAMX and 0.66 for MINNI and up to 0.67 for RCGC. All models are able to catch the mean features of the observed diurnal cycle of ozone, with lower values during night-time, higher values during daytime and a daily maximum in the afternoon (Figure 5.2), though they all underestimate the measured ozone concentrations both at night and day time hours. This result is quite different of the ones presented in van Loon *et al*. (2007) particularly for CHIM, the period of interest in van Loon *et al*. (2007) was an entire year, but for the winter period alone CHIM and other models displayed overestimates in wintertime.

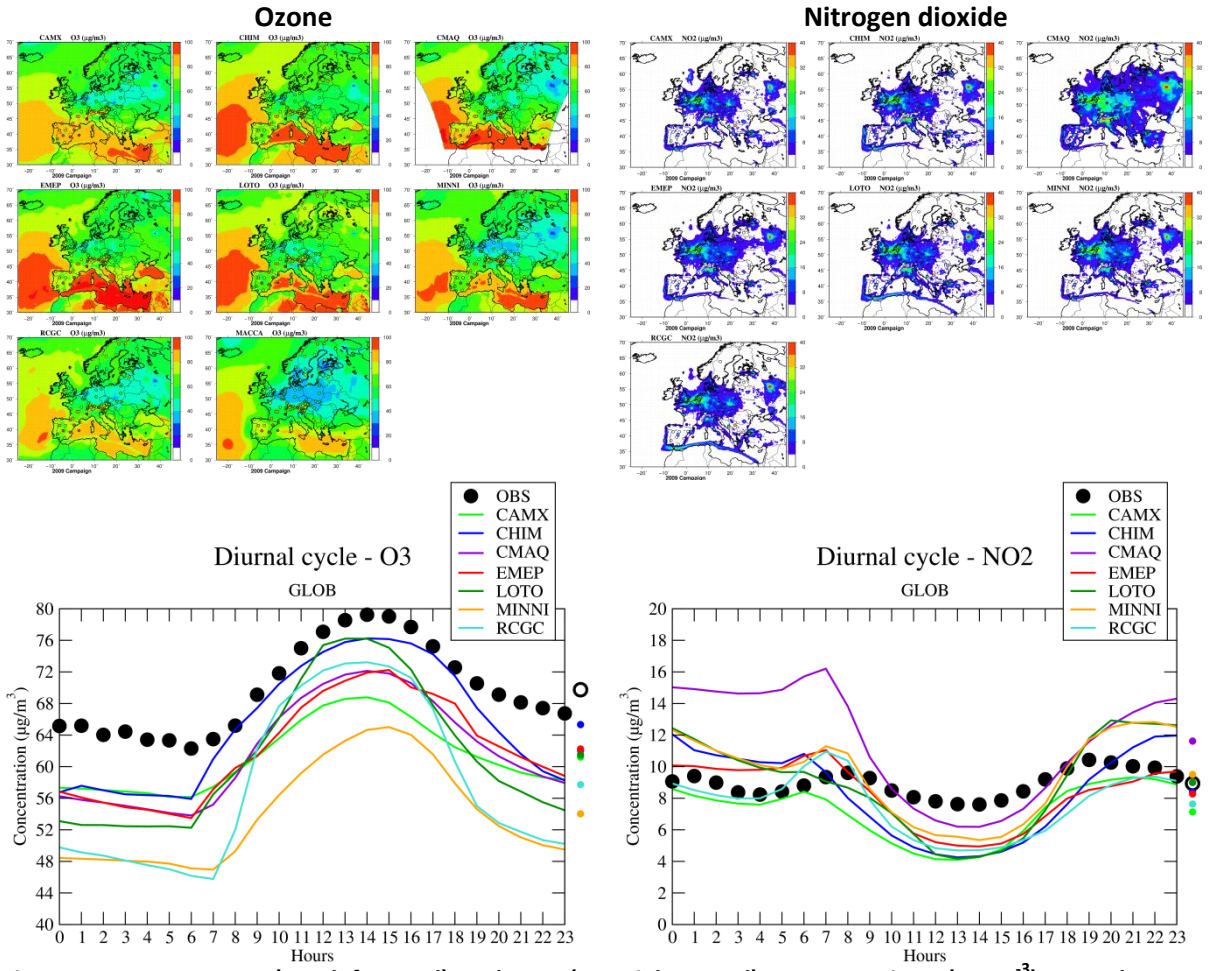

Figure 5.2: Average O_3 (top left panel) and NO_2 (top right panel) concentrations (µg m^{-3}) over the 2009 campaign period for all the models. The colour circles are the observed values at EMEP sites. Mean diurnal cycles are display for O_3 (bottom left panel) and NO_2 (bottom right panel) for the 2009 campaign period.

5.2 Focus on PM_{10}

Figure 5.3 displays the mean PM_{10} concentrations for the 2009 campaign. It is noticeable that spatial patterns are rather different from model to model; this feature will be explained when looking at individual PM components; the spatial correlation ranges from near 0 for CAMX and CMAQ to 0.68 for EMEP. Some differences in the PM composition can be attributed to natural particles that are accounted for in different ways with the models (for instance CAMX has not included sea salt). EMEP exhibits higher concentrations in the south of the domain because the model includes windblown dust production from dry soils. All the models show high concentrations over the south of Poland due to high primary emissions in this area.

The averaged diurnal cycle over all sites is rather flat in the observations with a slight decrease in the afternoon. All the models simulate a maximum value in the morning with a decrease in the afternoon, though sharper than observed. The shape of the diurnal cycle for MINNI is quite good.

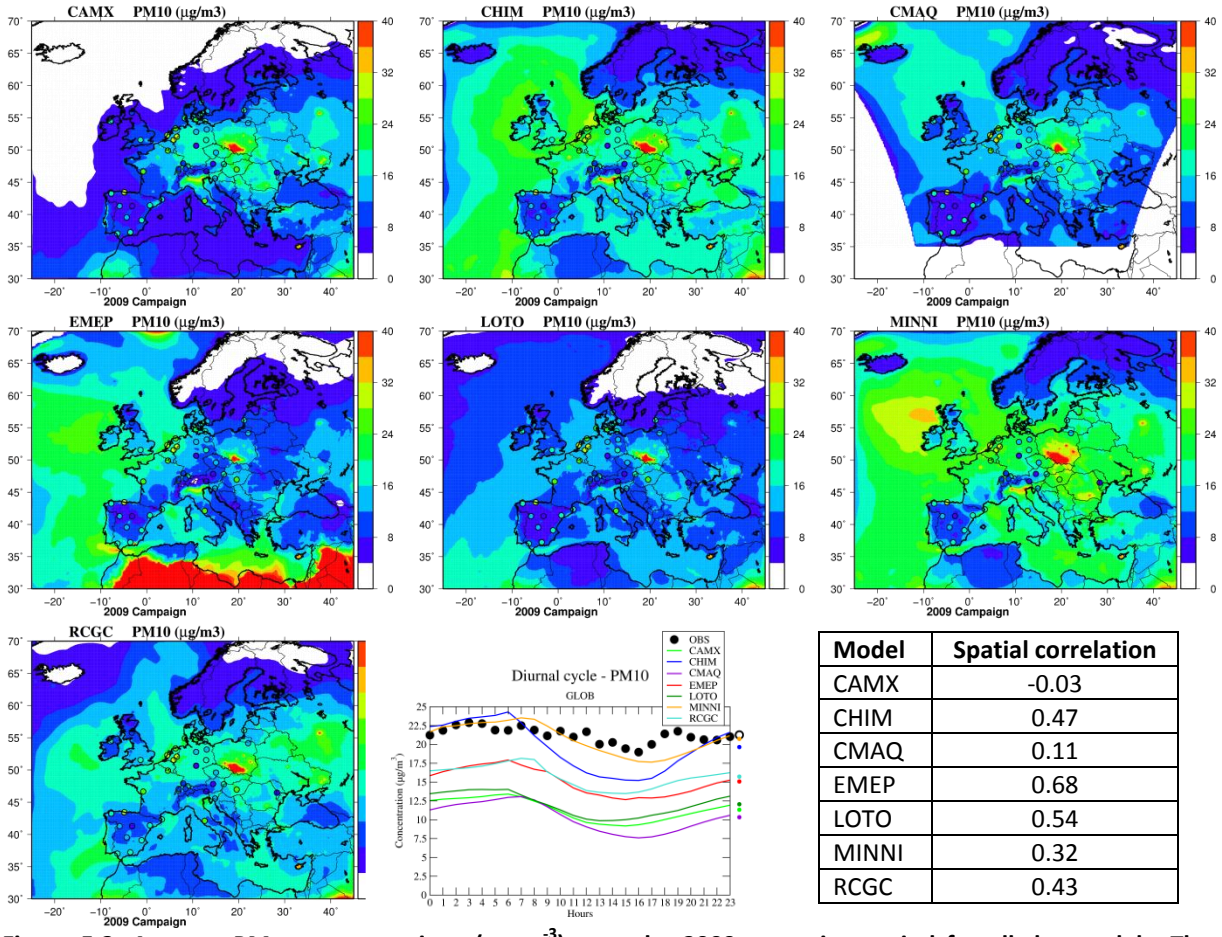

Model	Spatial correlation
CAMX	-0.03
CHIM	0.47
CMAQ	0.11
EMEP	0.68
LOTO	0.54
MINNI	0.32
RCGC	0.43

Figure 5.3: Average PM_{10} concentrations (µg m^{-3}) over the 2009 campaign period for all the models. The colour circles are the observed values at EMEP sites. Spatial correlations are reported in the table. The mean diurnal cycle is displayed at the bottom center.

Evaluation of the PM_{10} concentrations has been performed using the observational data available from the EMEP intensive and routine measurements. For PM_{10} the analysis was based on 51 stations. For all details of the stations, including geographical position, altitude, country, station type, and pollutants measured, we refer to Annex 3 of this report. In the analysis we considered 15 PM_{10} stations grouped by City (*i.e.* stations within a radius of 30 km of the city centre), 51 stations grouped by Country, and 36 remote stations. It is important to be informed that the number of stations included in each of the City groups or the Country groups is different, ranging from 1 to 11 stations as seen from the following specifications.

PM_{10} Country stations:	AT=3, CH=5, CY=1, CZ=1, DE=7, DK=1, ES=11, FR=4, GB=4, GR=1, IT=1, LV=2, MD=1, NL=4, PL=1, SE=3, SI=1 (see Annex 4 for the EU countries abbreviation)
PM_{10} City stations:	Bar=2, Ber=2, Ham=1, Lon=1, Mad=2, Pra=1, Rom=1, Sev=2, Sto=1, Val=1, Vie=1 (see Annex 4 for the cities abbreviation)
PM_{10} station topography	Plain=34, Valley=16, Mountain=1

All graphical results in this chapter were produces using the DeltaTool developed in the frame of the FAIRMODE activity (http://aqm.jrc.ec.europa.eu/delta/)

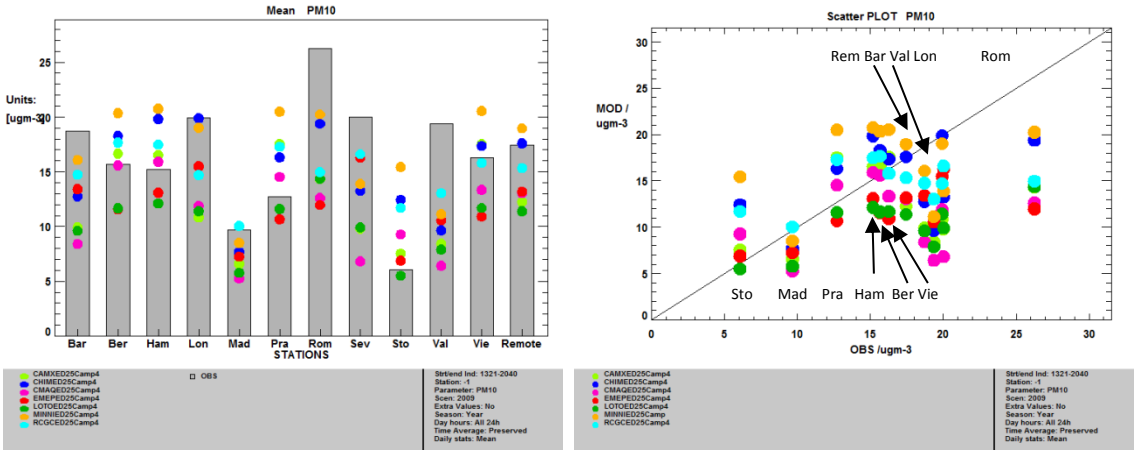

Figure 5.4: PM_{10}, City groups, Bar plot, Scatter plot

Figure 5.4 (left panel) shows the mean values of PM_{10} for all the models at the City groups. The first point we notice is the relatively large spread of the model results around the observed values. All models underestimate in Barcelona, Madrid, Rome, Sevilla, Valencia (Mediterranean cities), and London. On the other hand, PM_{10} levels are over-estimated by almost all the models in Stockholm and Prague. For the other agglomerations we find an overestimation by CHIM, MINNI, and RCGC, an under-estimation by EMEP and LOTO, and a mixed behaviour of CAMX and CMAQ. Figure 5.4 (right panel) shows the same results in a scatter plot. It can be noted that the variability among the cities in the observed PM_{10} levels is not well captured by the models. For example higher observed values in London compared to Prague and Hamburg are not always captured by the model results. Comparing Rome to Stockholm, we see that the measured values are approximately 5 times higher, while the model results show a factor of 1.5 to 3.

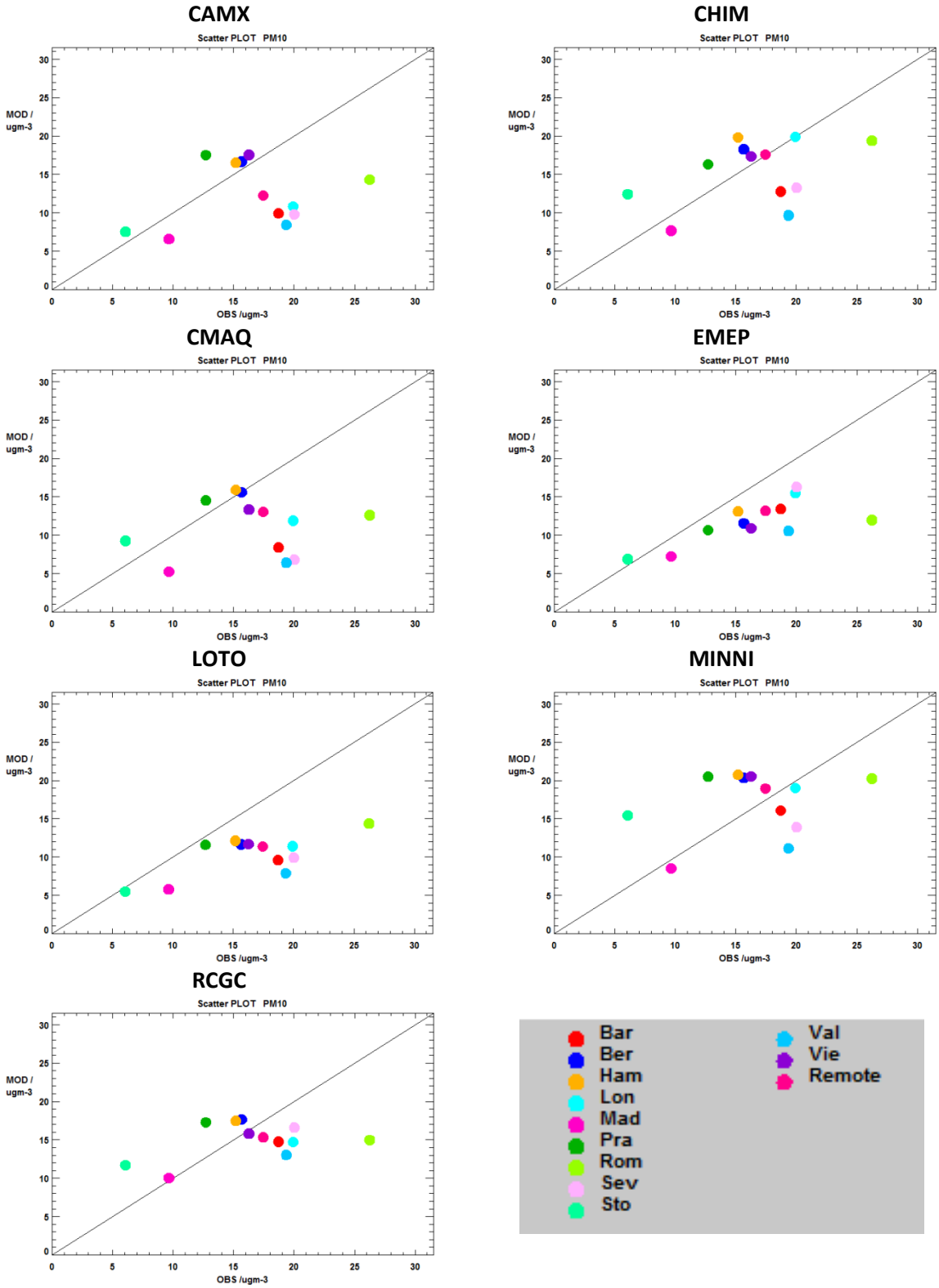

Figure 5.5: PM_{10}, City groups, Scatter plot for each model

Figure 5.5 shows model by model the results presented in Figure 5.4. Most of the models performs pretty well for the cities with low PM_{10} levels (*i.e.* Stockholm and Madrid). EMEP and LOTO results are similar, although the slope coefficients of the linear regression between Observed and modelled values are too small. EMEP and LOTO manage to reproduce observed PM_{10} spatial variation for the City Groups, though they flatten out the gradients. The RCGC model calculates a very flat PM_{10} distribution, meaning insensitive for higher PM_{10} concentrations values. The results from CAMX,

MINNI, and CMAQ are quite similar and show quite large disagreement with observed PM_{10} spatial distribution for the City groups.

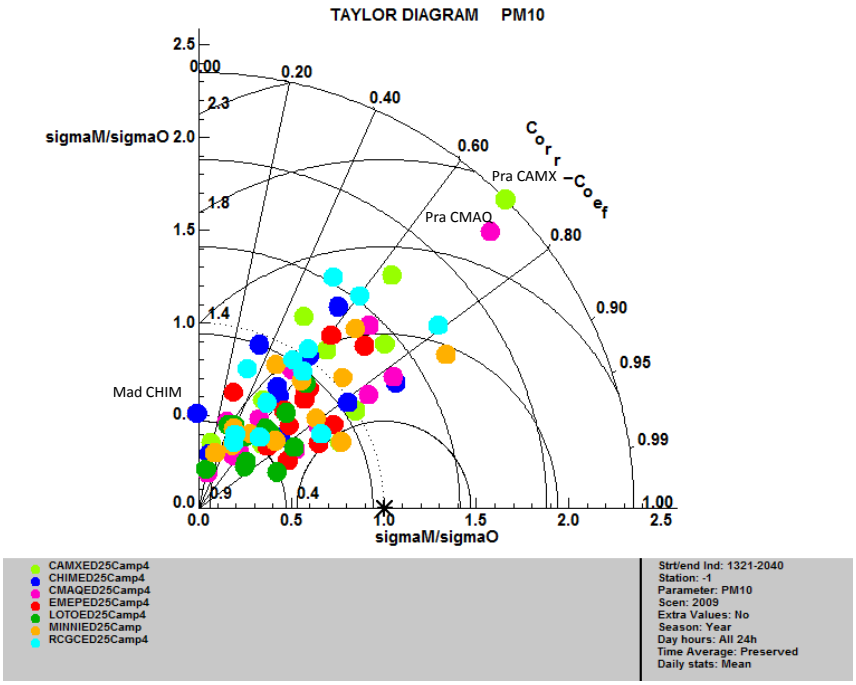

Figure 5.6: Daily PM_{10}, City groups, Taylor plot

Figure 5.6 shows a Taylor plot for all models (different colours) for all the City groups. The correlation coefficient is within the range of 0.25 to 0.85, with the exception of 0-correlation between CHIM calculations and measurements in Madrid. The normalized standard deviation has a large spread ranging from 0.2 to 2.3, with extreme values in Prague for CAMX and CMAQ.

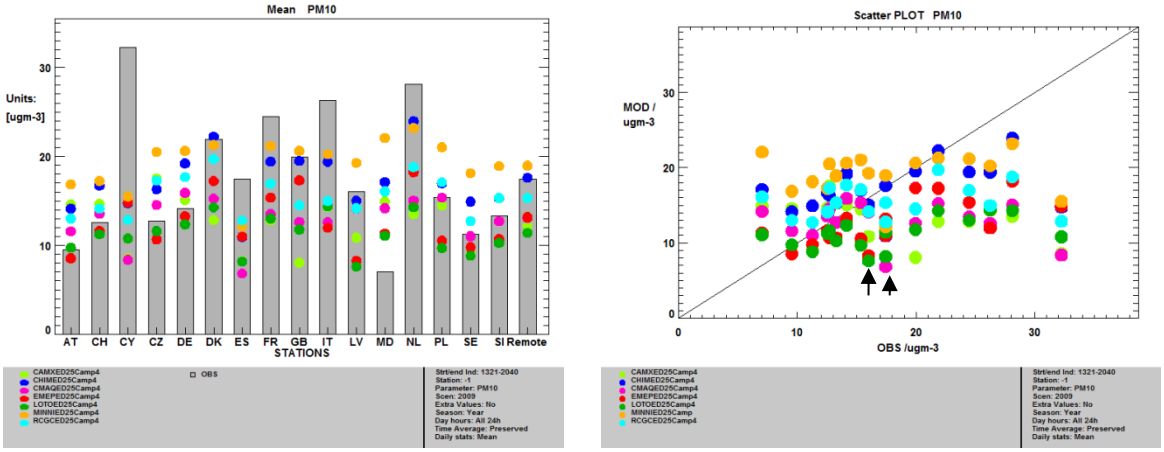

Figure 5.7: PM_{10}, Country groups, Bar plot, Scatter plot

Figure 5.7 (left panel) shows the mean values of PM_{10} for all the models at the country groups. The first point we notice is the relatively large spread of the model results around the observational values. All models underestimate in Cyprus, Spain, France, Italy, and the Netherlands. In general we notice that MINNI, CHIM always produce the largest values, and CMAQ, EMEP and LOTO the lowest values. Like for City groups, individual models fail to reproduce the observed regional PM_{10} gradients (see right panel). Remarkable is the model performance at Cyprus, where all modelled PM_{10} concentrations models are below 50% of the observational values. Cyprus observed PM

concentrations are driven by a dust outbreak that occurred during the 2009 campaign (see section 11.2).

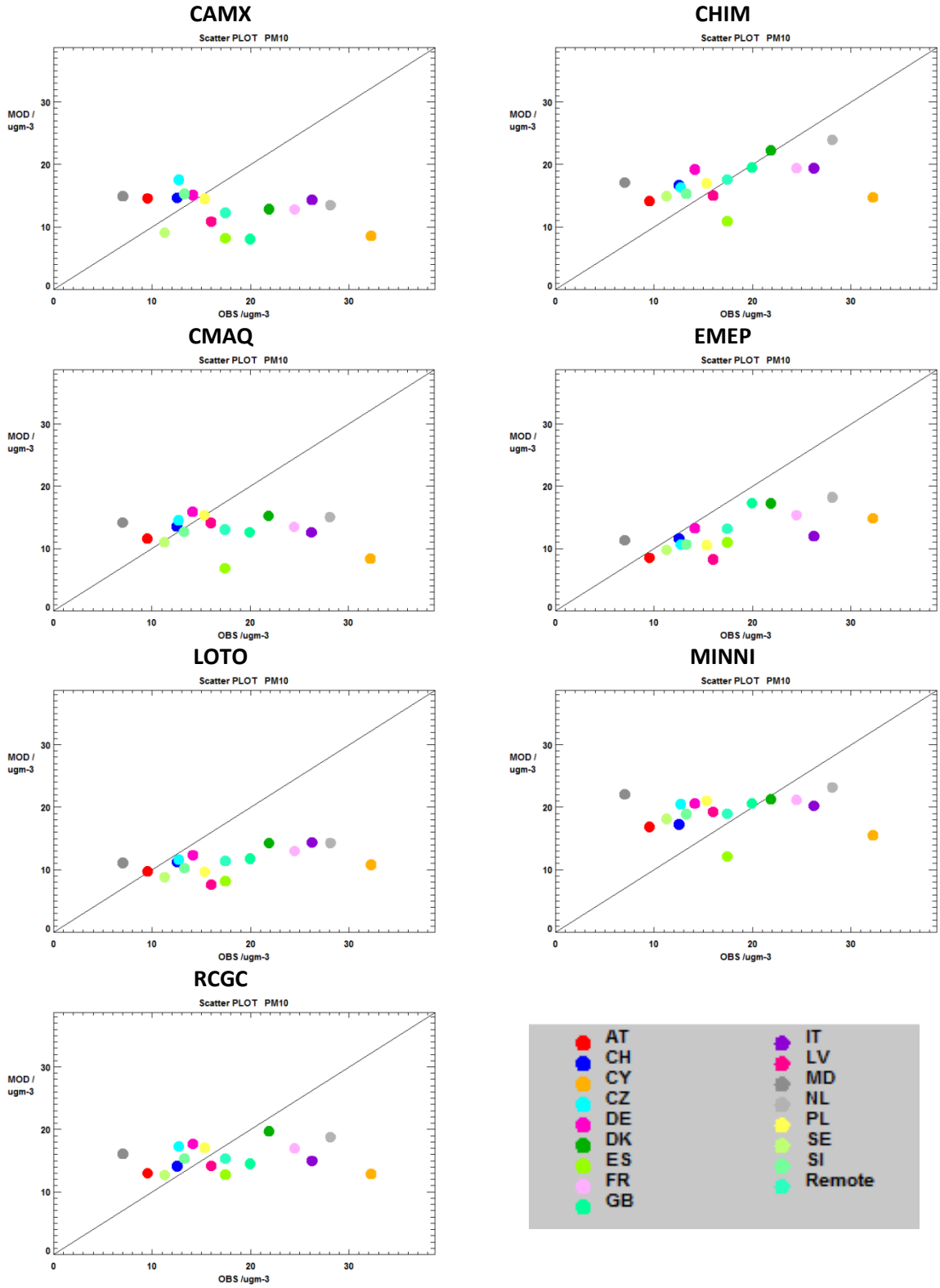

Figure 5.8: PM_{10}, Country groups, Scatter plot for each model

Figure 5.8 shows for the individual models the results presented in Figure 5.7. All models show fairly good agreement with observations for the countries with low PM_{10} levels (*i.e.* Austria, Sweden, Czech

Republic, and Switzerland). EMEP and LOTO produce quite similar results, with somewhat flat PM_{10} gradients. Similar behaviour is found for the CHIM and MINNI models if we consider Cyprus and Spain as outliers. The PM_{10} dots from the RCGC model show a flat slope of the linear regression, meaning the model is not able to reproduce higher PM_{10} values. The results from CAMX and CMAQ show the same behaviour, even with negative slope.

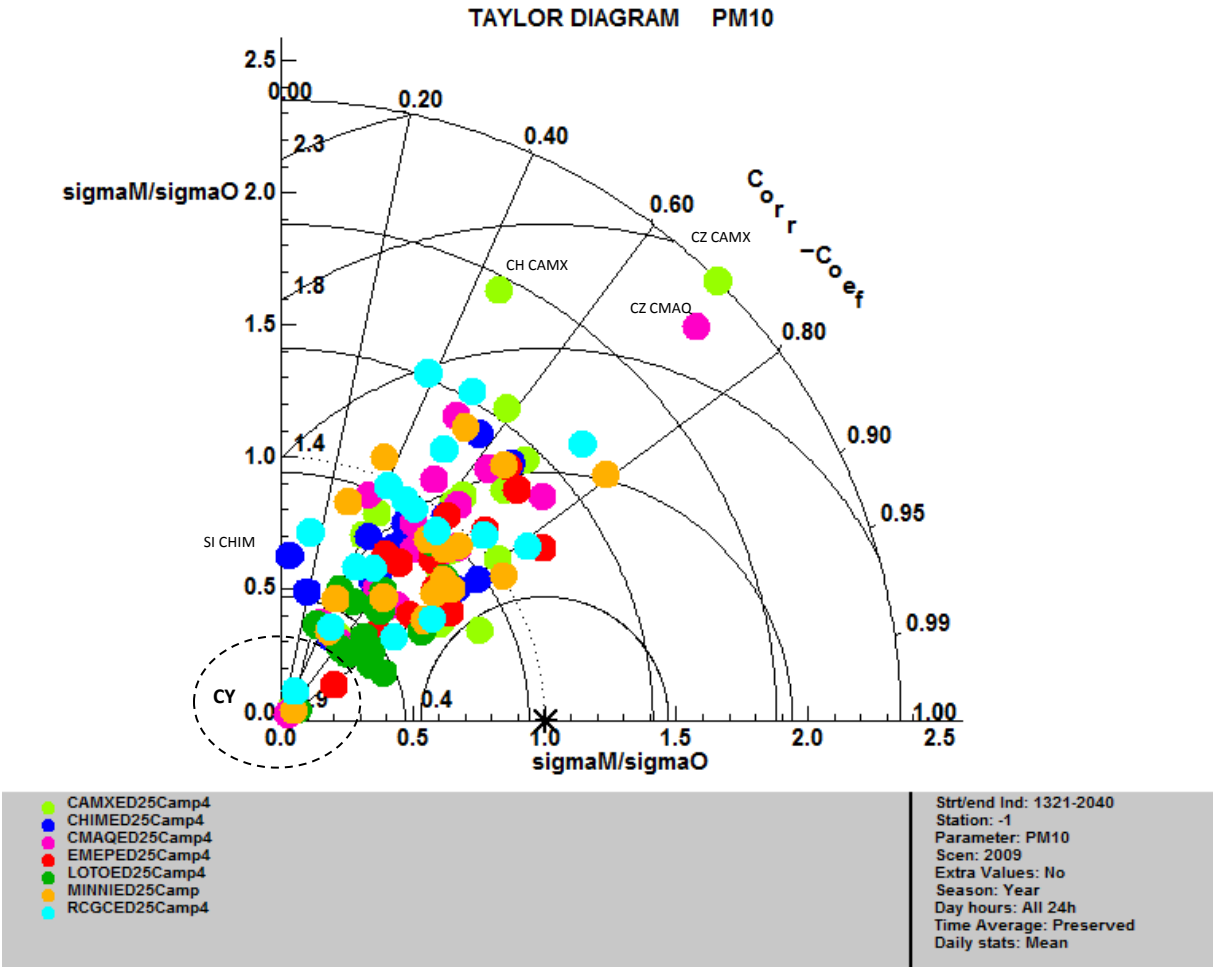

Figure 5.9: Daily PM_{10}, Country groups, Taylor plot

Figure 5.9 shows a Taylor plot for all models (different colours) for all the country groups. The correlation coefficient is within the range of 0.2 to 0.85, with the exception of 0-correlation in Slovenia for CHIM. The normalized standard deviation has a large spread ranging from 0 to 2.3, with extreme values in Czech Republic for CAMX and CMAQ and in Switzerland for CAMX. We also notice here the particular behaviour at Cyprus, with the model's dots clustering near the graph's origin.

CAMX

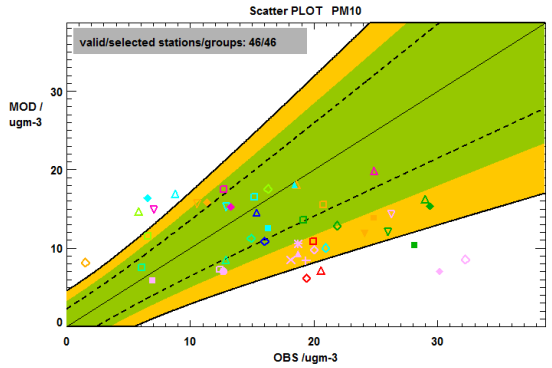

CHIM

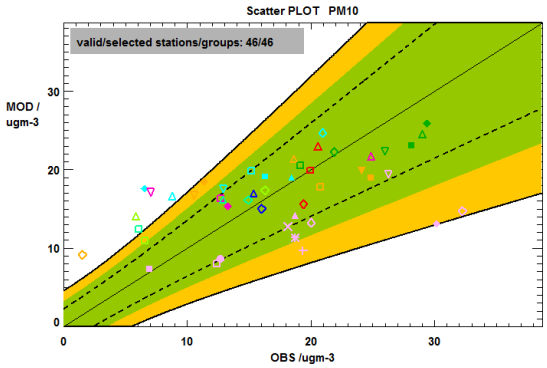

CMAQ

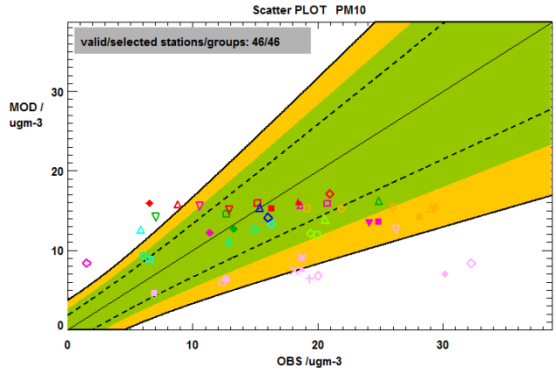

EMEP

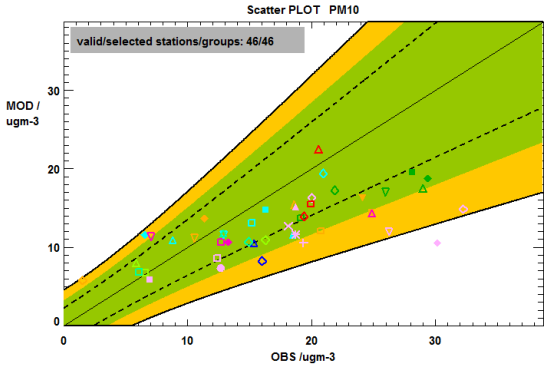

LOTO

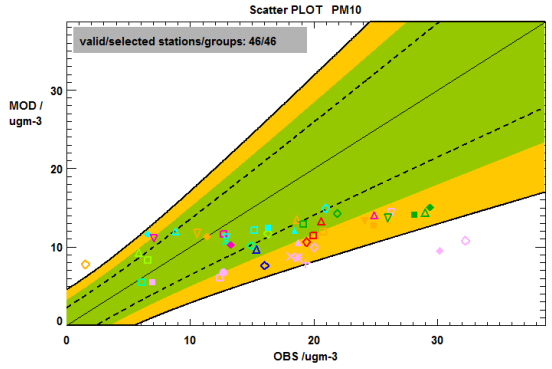

MINNI

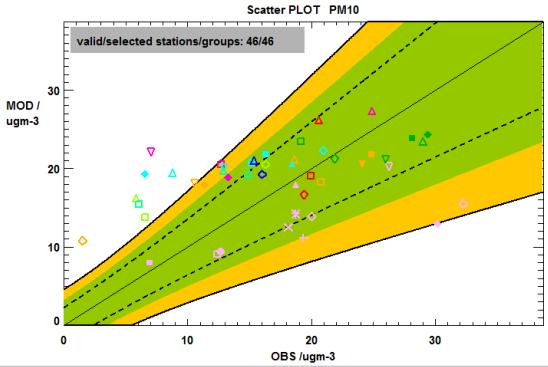

RGCG

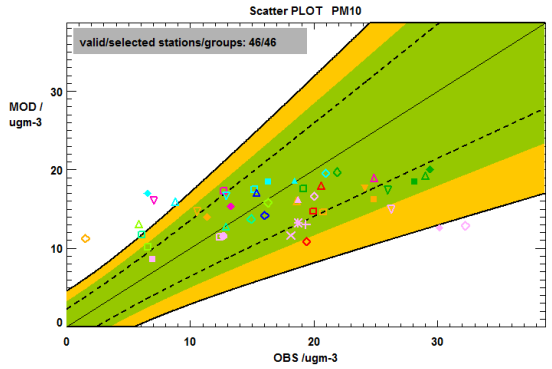

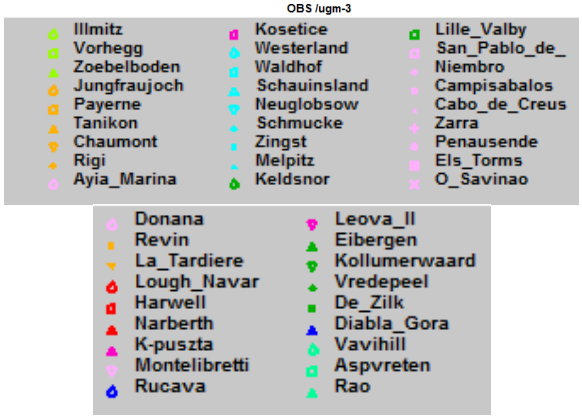

Figure 5.10: Scatter plot with confidence zone for PM_{10} concentrations (all models)

Figure 5.10 shows, for all models, a PM_{10} scatter plot for all the individual stations. The green/orange shaded area is defined by $|Obsi - Modi| < 2*RMS_U$[17], where RMS_U is the quadratic mean of the expanded measured uncertainty U_i. This green/orange shaded area takes into account the absolute measurement uncertainty for PM_{10} observations. For details we refer to Thunis *et al.* (2012). Dashed and solid lines indicate $NMB/2RMS_U$ ratios of 0.5 and 1, respectively., where NMB stands for Normalized Mean Bias. The orange region is delimited by ratio $\sqrt{0.5} = 0.71$. This is considered to be a more "fair" way of comparing calculated and observed data. The plot indicates that the calculated PM_{10} concentrations represent the observations quite well if measurement uncertainties are taken into account.

The only station that falls out of the confidence zone is Niembro for EMEP. The closer look reveals that this is mainly because neither the EMEP nor all other models have managed to reproduce a few pollution episodes at Niembro, especially the large one in the end of February 2009. For CHIM, CAMX, CMAQ MINNI and RCGC, a group of stations with low observed concentrations fall out of this confidence zone, these stations are mainly elevated sites. A group of stations (in Spain and UK) is outside this zone for CMAQ and CAMX which underestimate high observed concentrations.

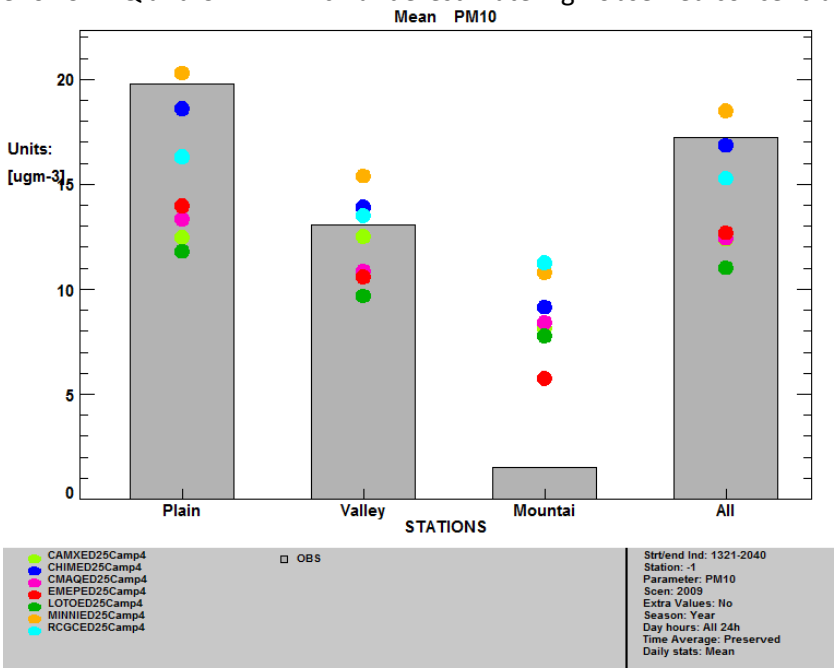

Figure 5.11: Daily PM_{10}, Station topography, Bar plot

Figure 5.11 shows the model behaviour according to station topography. We distinguish the following types: Mountain, Plain and Valley stations. The last bar shows the results for all the sites. Most of the models significantly underestimate at Plain stations, and show a mixed picture for stations in the Valley. In the model ranking for Plain and Valley stations, MINNI and CHIM are always at the upper end; CMAQ and LOTO always at the lower end of PM_{10} range, while the others are more or less in the middle. For Mountain stations all models overestimate PM_{10} concentrations. Here the observations are compared with calculated concentrations from the lowest models' layers. Though

[17] The quadratic mean of the uncertainty is used as main normalization factor. This quantity is calculated as: $RMS_U = ku_r^{RV}\sqrt{(1-\alpha)(\overline{O}^2) + \alpha * RV^2}$

where:

- $\mathbf{u_r^{RV}}$ represents the estimated relative measurement uncertainty around a reference value (RV) for a reference time averaging, e.g. the daily/hourly Limit Values (LV) of the AQD.
- **α** is the fraction of the uncertainty which is non-proportional to the concentration level around the Limit Value.
- **k** is the coverage factor. Each value of k gives a particular confidence level that the true value lays within the interval of confidence consisting in $O_i \pm U$. Most commonly, the expanded uncertainty is scaled by using the coverage factor k = 2, to give a level of confidence of approximately 95 percents. Levels of confidence of 90% and 99% would lead to coverage factors around k=1.40 and k=2.6, respectively.

the lowest layers follow the topography, relatively coarse models resolution does not allow to accurately describe the highest tops (or the lowest valleys). In other words, the elevation of some mountain sites can be larger than the grid mean topography in the models, thus leading to a model overestimation.

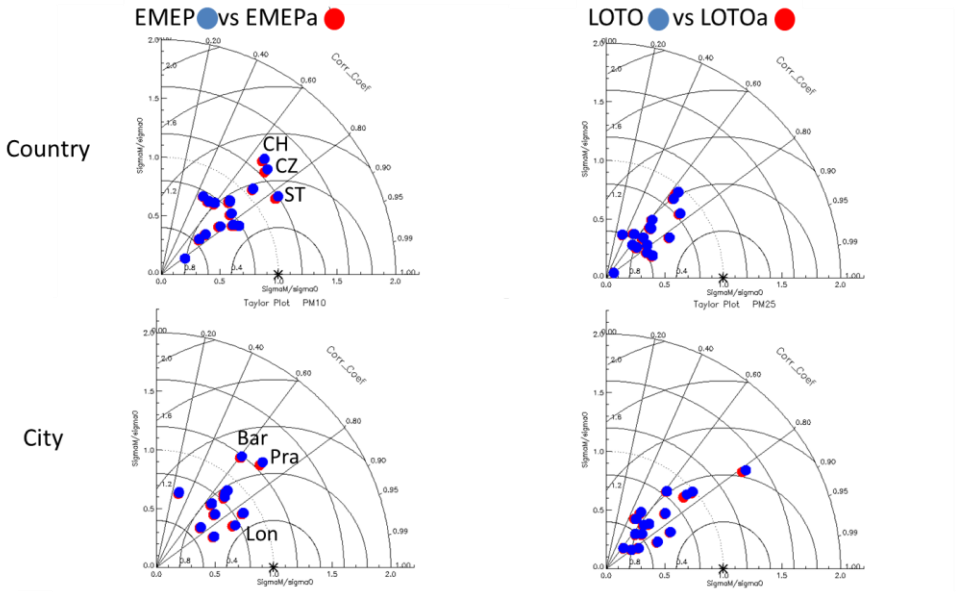

Figure 5.12: PM_{10}, The effect of using concentrations at 3m: EMEP *vs* EMEPa, LOTO *vs* LOTOa

As documented in section 3.1, differently from the other models in the exercise, in comparisons with observations EMEP and LOTO use concentrations at 3m heights which are derived from the model values in the lowest layers. Figure 5.12 compares EMEP (left column) and LOTO (right column) results for PM_{10} concentrations corresponding to the lowest models layer which are respectively 90m and 25m thick (EMEPa and LOTOa) and for PM_{10} corrected to 3-m height. Since dry deposition of most of calculated PM_{10} components is rather slow, the differences between PM_{10} at the lowest ca. 90m and at the measurement height are rather small. For EMEP the difference in the model results for Country groups is less than 2-4%, being largest in Switzerland, Czech Republic and Slovenia, and very small in the other countries. For the City groups the effect of PM_{10} retrieval height on EMEP results is at most 3%. The same behaviour is seen for LOTO (differences less than 2%).

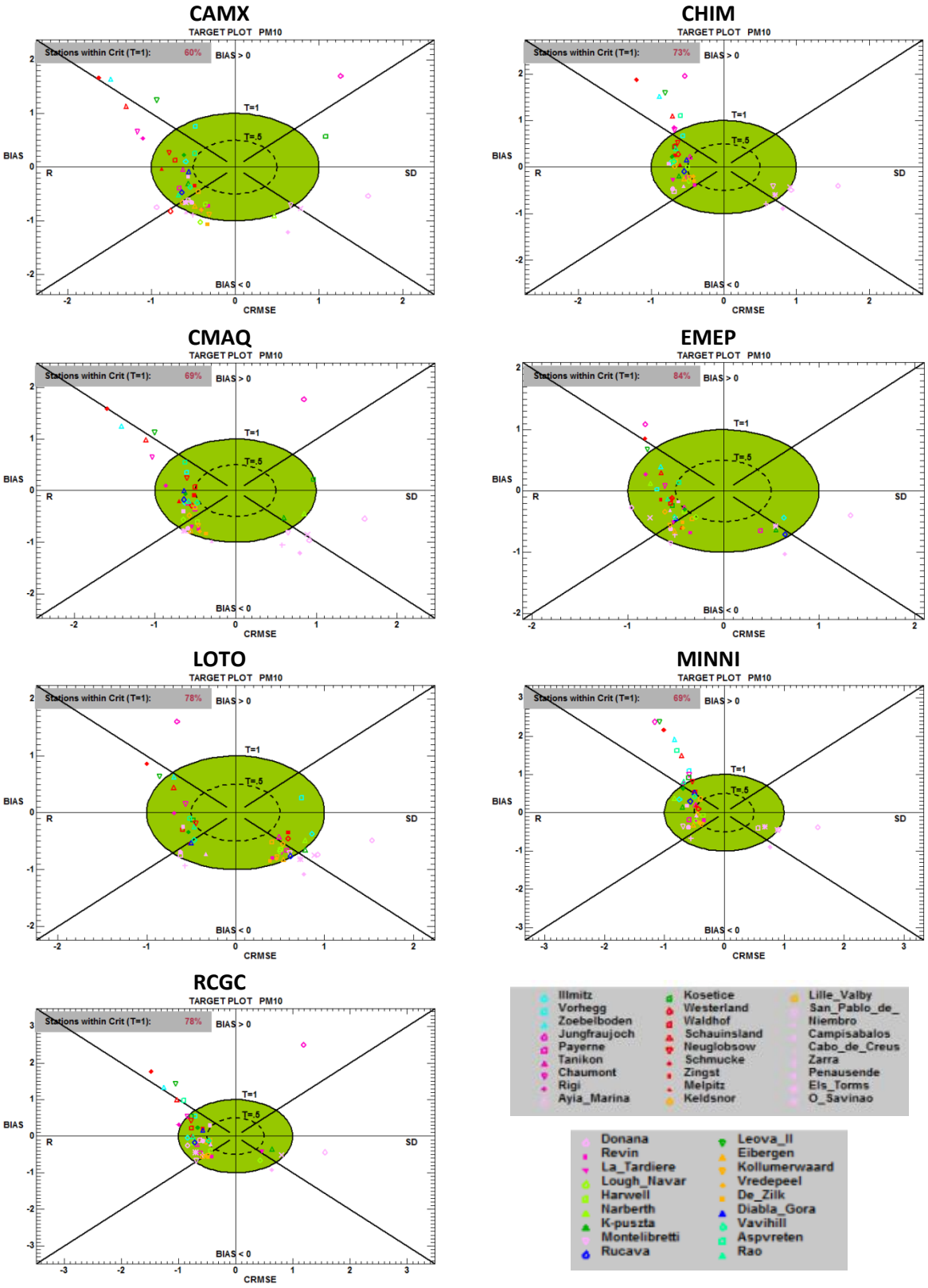

Figure 5.13: PM_{10}, Target plot, individual stations, all models

PM_{10} results for individual stations are shown in a Target plot, model by model (Figure 5.13), with the Bias as vertical axis and the CRMSE as horizontal axis, both normalized by $2*RMS_U$. In this way the distance to the origin gives the normalized RMSE. Since the CRMSE is a positive value we put the station symbol on the right hand side or left hand side of the diagram according to whether the error

at the station is dominated by correlation (left) or standard deviation (right). In order to satisfy the Model Quality Objective (RMSE <= 2*RMS_U), station symbols should be within the Green shaded area. From the diagrams in Figure 5.13 we conclude that systematic problems (*i.e.* for most of the models) occur in the following stations: Jungfraujoch-CH (high altitude site), Schmucke-DE, Niembro-ES, AiyaMarina-CY, Zoebelboden-AT, Aspvreten-SE, Schauinsland-DE, Donana-ES. The percentage of stations that fall within the Criteria zone differs from model to model: EMEP 84%, CHIM 73 %, LOTO 78 %, RCGC 78%, CAMX 60%, MINNI 69%, CMAQ 69%.

5.3 Focus on $PM_{2.5}$

The $PM_{2.5}$ concentration maps calculated by the models (Figure 5.14) show more similarity than the PM_{10} spatial patterns,, however, the spatial correlations range is larger, spreading from 0.37 (CMAQ and RCGC) to 0.62 (CHIM). EMEP and LOTO give lower mean concentrations over land than the other models for the considered period. Two main hot spots can be identified in Southern Poland and Northern Italy. Again, EMEP displays high concentrations over the southern border of the domain due to calculated windblown dust from North Africa. The diurnal cycle is rather flat in the observations, with somewhat elevated concentrations in the morning and a slight decrease in the afternoon. The models calculate the morning's maximum, but occurring 2-3 hours earlier. A possible reason could be that the models are too sensitive to the development of the boundary layer, which dilutes the calculated concentrations, and in addition they may lack the secondary PM production. It may also be a consequence of the diurnal cycle of the emissions.

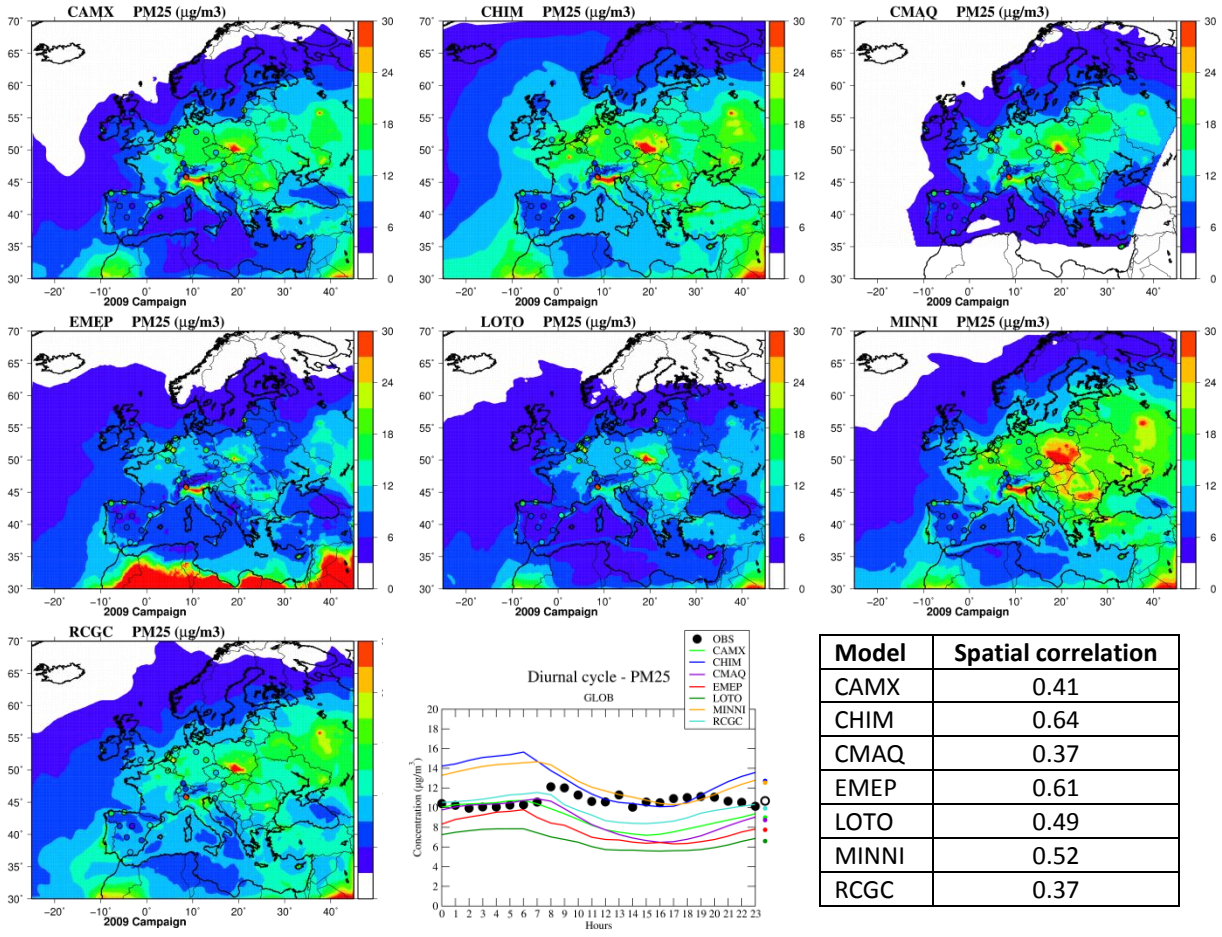

Model	Spatial correlation
CAMX	0.41
CHIM	0.64
CMAQ	0.37
EMEP	0.61
LOTO	0.49
MINNI	0.52
RCGC	0.37

Figure 5.14: Average $PM_{2.5}$ concentrations (µg m^{-3}) over the 2009 campaign period for all the models. The colour circles are the observed values at EMEP sites. Spatial correlations are reported in the table. The mean diurnal cycle is displayed at the bottom centre.

Evaluation of the $PM_{2.5}$ model performance has been based on the observational data available from the EMEP field campaigns. For $PM_{2.5}$ the analysis is based on 38 stations. For all details of the stations, including geographical position, altitude, country, station type, and pollutants measured, we refer to Annex 3 of this report. In the analysis we considered 14 $PM_{2.5}$ stations grouped by City (*i.e.* stations within a radius of 30 km of the city centre), 38 stations grouped by Country, and 24 remote stations. It is important to point out that the number of stations included in each of the City groups or the Country groups is different, ranging from 1 to 11 stations as seen from the following specifications.

$PM_{2.5}$ Country stations: AT=1, CH=2, CY=1, CZ=1, DE=3, ES=11, FR=4, GB=2, IE=1, IT=1, LV=2, NL=4, PL=1, SE=3, SI=1 (see Annex 4 for the EU countries abbreviations)

$PM_{2.5}$ City stations: Bar=3, Ber=1, Ham=1, Lon=1, Mad=2, Mil=1, Pra=1, Sev=1, Sto=1, Val=1, Vie=1 (see Annex 4 for the cities abbreviations)

$PM_{2.5}$ station topography: Plain=26, Valley=12

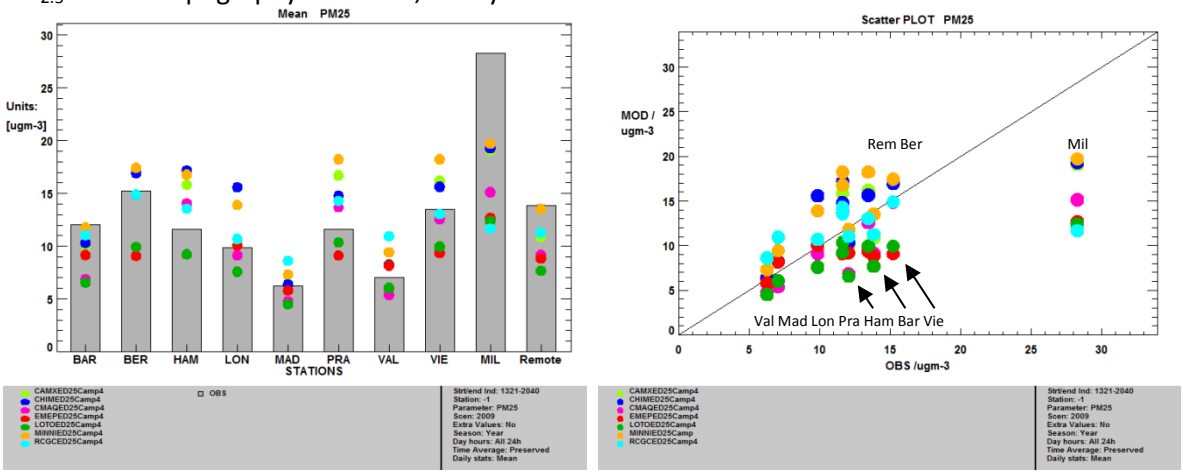

Figure 5.15: $PM_{2.5}$, City groups, Bar plot, Scatter plot

Figure 5.15 (left panel) shows the mean values of $PM_{2.5}$ concentration for all models according to the city groups. The first point we notice is the relatively large spread of the model results around the observational values. Most models underestimate in Barcelona, Madrid (except RCGC, MINNI and CHIM), and all of them in Milan. At the other cities there is a mixed spread in the model results, with LOTO and EMEP at the lower side of the spread and CAMX, CHIM and MINNI at the higher side. Figure 5.15 (right panel) shows the same results in a scatter plot. From here it is seen that the models have difficulties in reproducing observations in pollution hotspots like Milan.

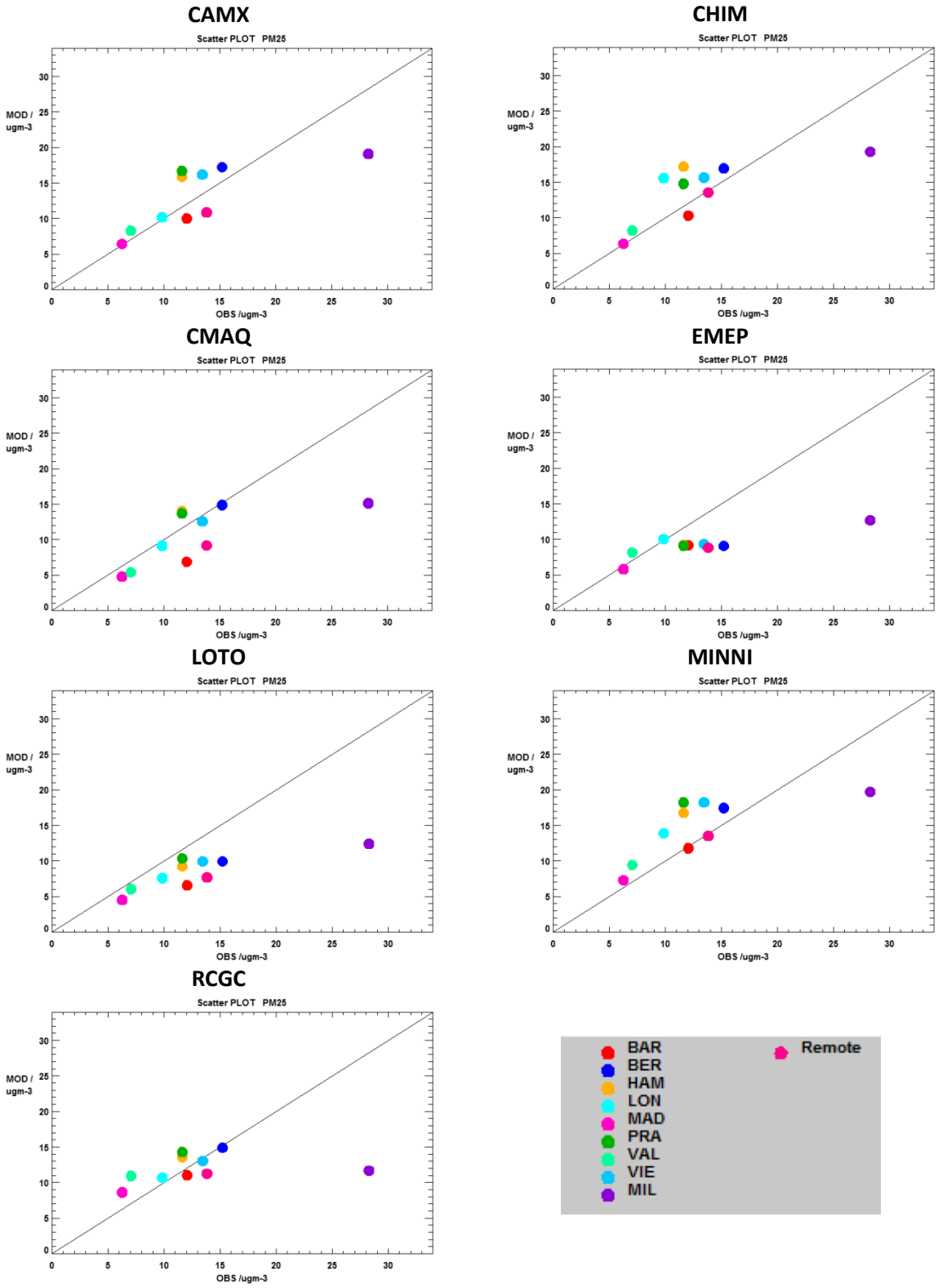

Figure 5.16: Daily $PM_{2.5}$, City groups, Scatter plot for each model

In Figure 5.16 the results shown in Figure 5.15 are split out per model. All models behave rather well for the cities with low $PM_{2.5}$ levels. For EMEP, LOTO and RCGC the results are similar, with slope values which are too flat. The results from CHIM, CAMX, MINNI, and CMAQ show the same type of behaviour with better slopes. All models significantly under-estimate $PM_{2.5}$ in Milan.

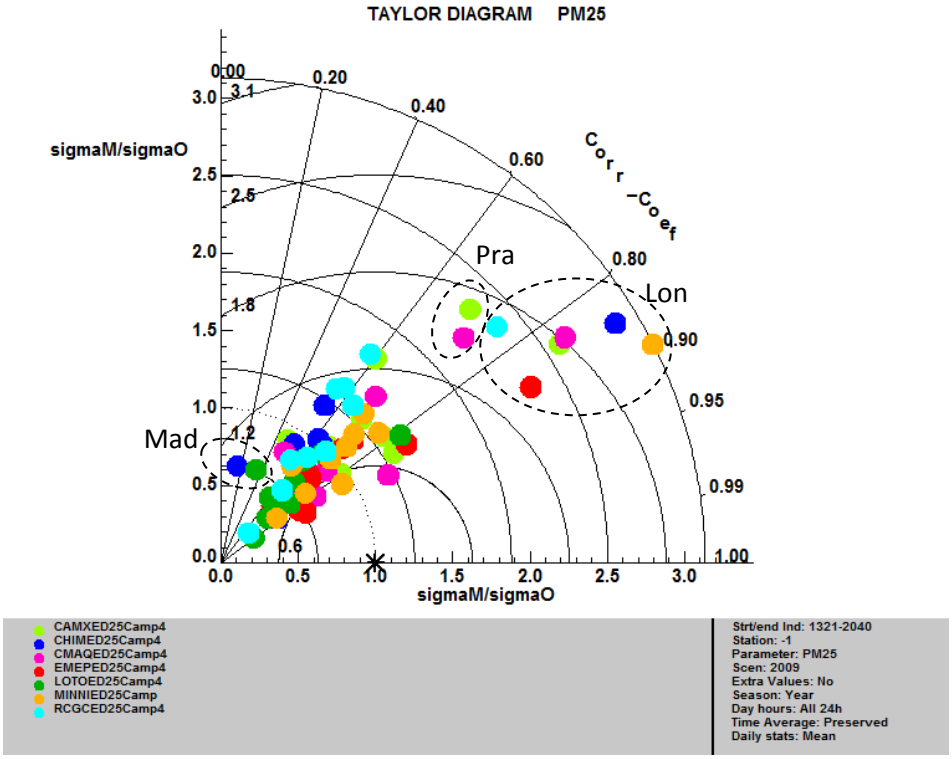

Figure 5.17: $PM_{2.5}$, City groups, Taylor plot

Figure 5.17 shows a Taylor plot for all models (different colours) for all the City groups. The correlation coefficient is within the range of 0.4 to 0.9, with the exception of 0.2 correlation in Madrid for CHIM and LOTO. The normalized standard deviation has a large spread ranging from 0.2 to 3.1, with extreme values in London for all models (except LOTO), and in Prague for CAMX and CMAQ.

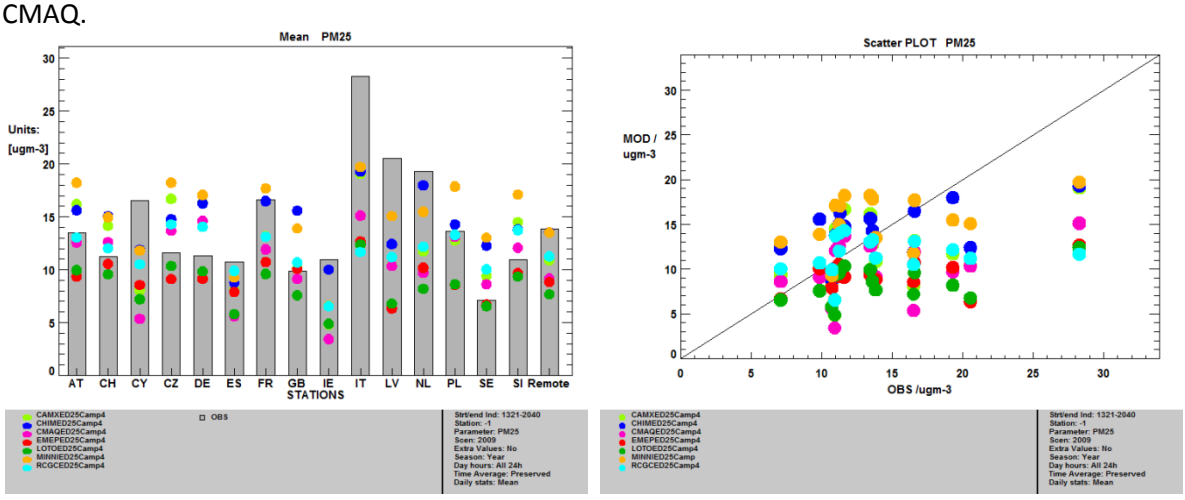

Figure 5.18: $PM_{2.5}$, Country groups, Bar plot, Scatter plot

Figure 5.18 (left panel) shows the mean values of $PM_{2.5}$ for all the models at the Country groups. The first point we notice is the relatively large spread of the model results around the observational values. All models under-estimate in Cyprus, Spain, Ireland, Italy, Latvia and the Netherlands and a mixed under/over-estimation in the other countries. In general we notice that LOTO and EMEP always produce low values, whereas CHIM, MINNI and CAMX are at the higher side of the models spread. RCGC is in the middle of the modelled values range.

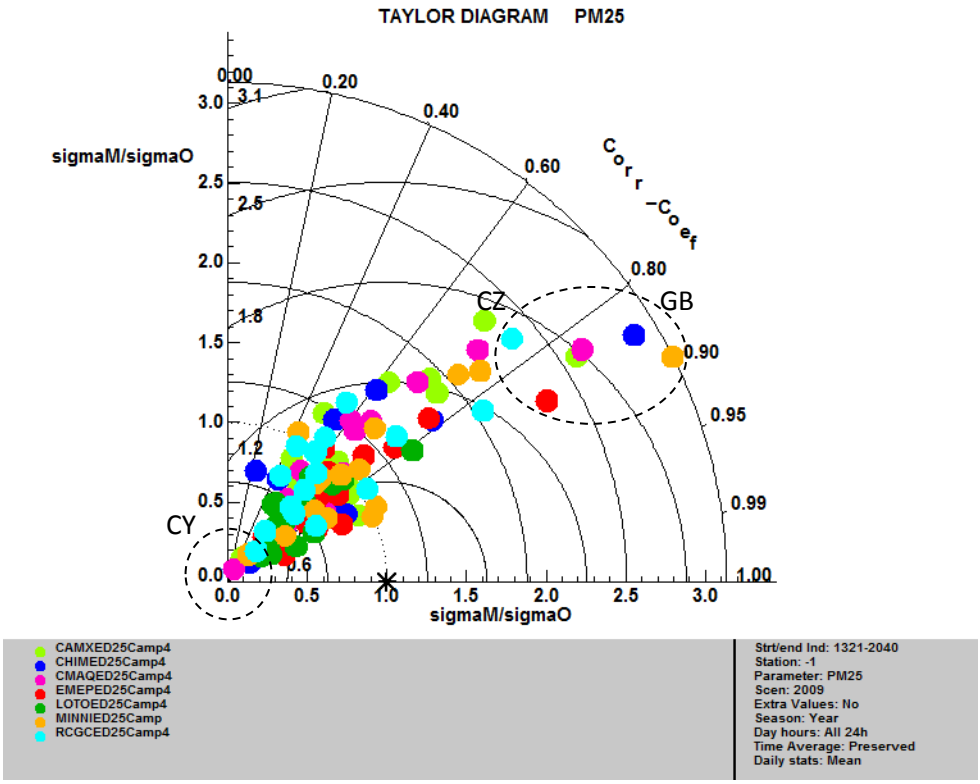

Figure 5.19: $PM_{2.5}$, Country groups, Taylor plot

Figure 5.19 shows a Taylor plot for all models (different colours) for all the Country groups. The correlation coefficient is within the range of 0.3 to 0.9, with the exception of 0.2 correlation in Slovenia for CHIM. The normalized standard deviation has a large spread ranging from 0 to 3.1, with extreme values in UK and Czech Republic. We also notice here the particular behaviour at Cyprus with a cluster of models near the origin indicating a low variability of models compared to observed values.

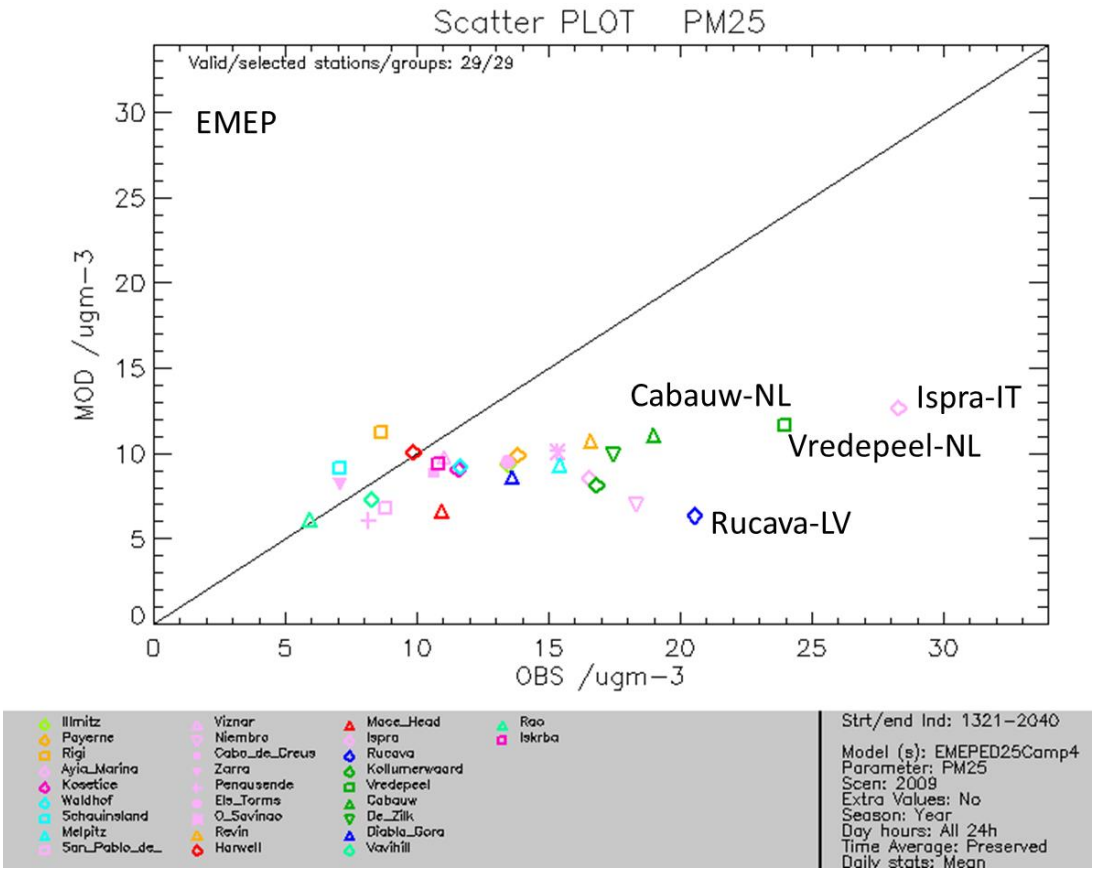

Figure 5.20: Scatter plot of $PM_{2.5}$ averaged concentrations for all stations, EMEP model

Figure 5.20 shows, for the EMEP model, a $PM_{2.5}$ scatter plot for all the individual stations. We notice the flat slope of the linear regression line through the station symbols, indicating that the higher $PM_{2.5}$ values are not well reproduced by the model.

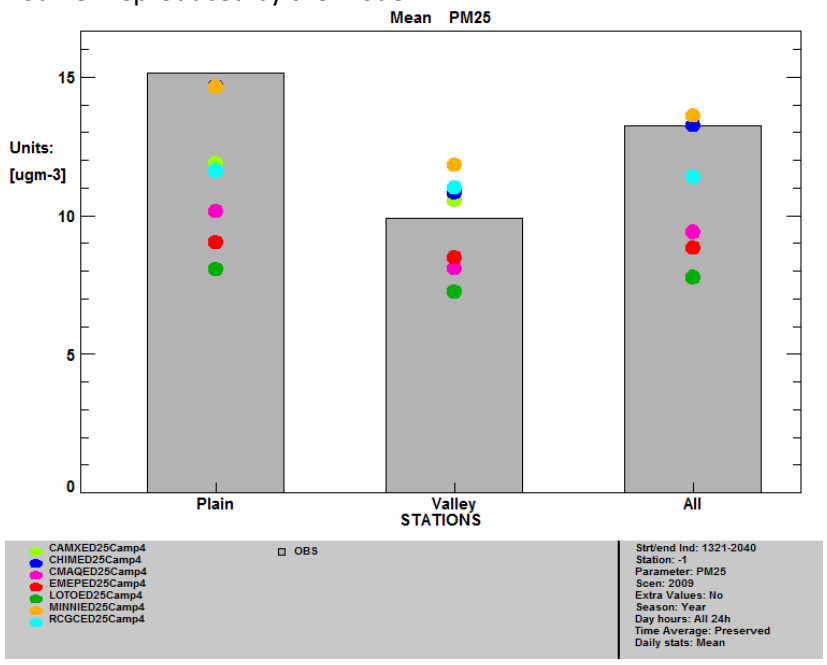

Figure 5.21: $PM_{2.5}$, Station topography, Bar plot

Figure 5.21 shows the models' behaviour according to the station types. We distinguish "Plain" and "Valley" stations. An additional bar is added with all the stations. All models under-estimate $PM_{2.5}$

mean values at Plain stations, and show a mixed picture for stations in the Valley. In the model ranking for Plain and Valley stations, MINNI and CHIM are always high, EMEP and LOTO always low, while the others are more or less in the middle.

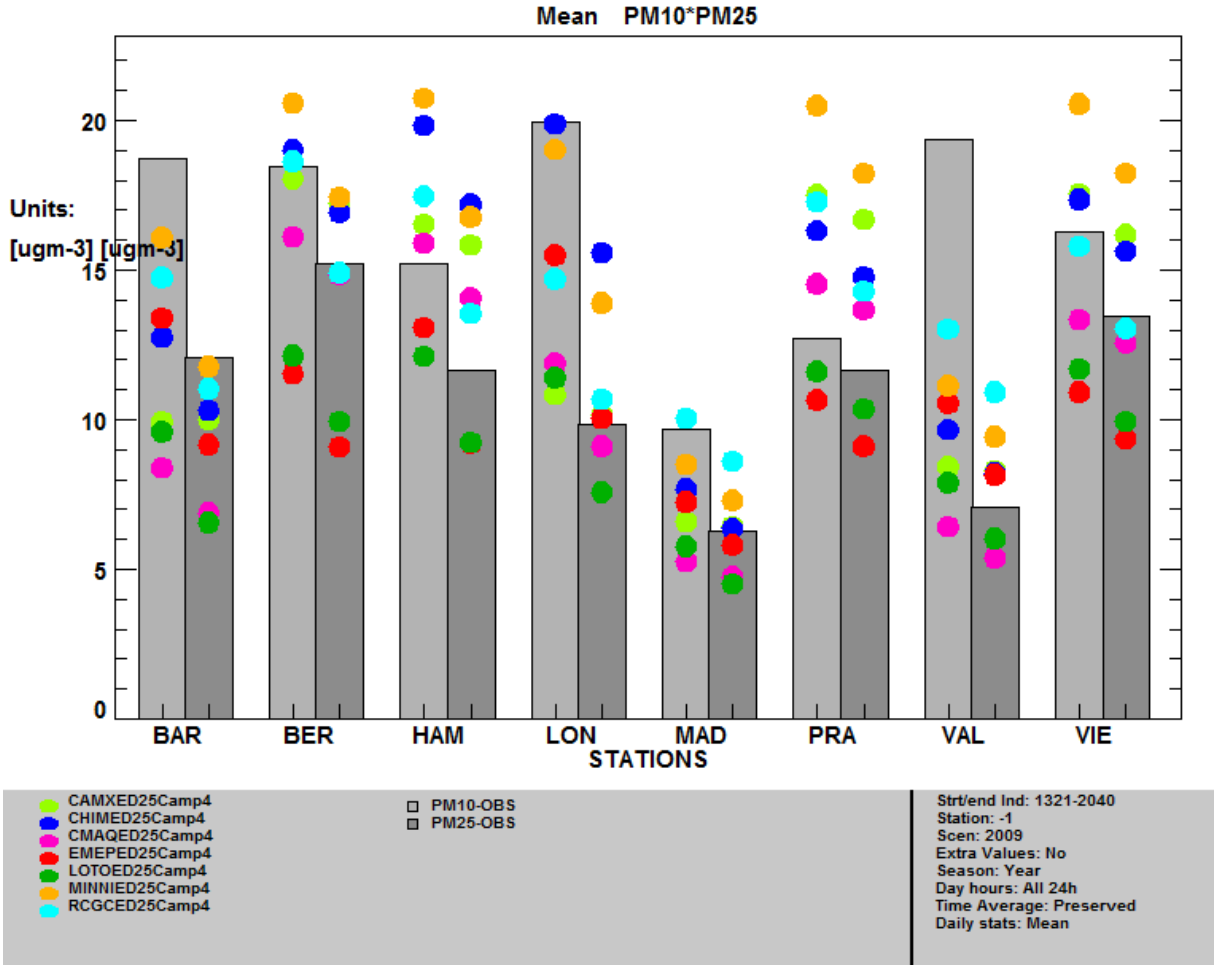

Figure 5.22: $PM_{2.5}$ and PM_{10} direct comparison, City groups, Bar plot

Figure 5.22 shows, for City groups, a comparison of observations and model results for PM_{10} and $PM_{2.5}$. First we notice the considerable contribution of coarse particles in measured PM_{10} in London, Valencia and also Barcelona. The coarse fraction in PM_{10} is found to be underestimated by the models in those and also other cities (*e.g.* Madrid). The ranking of the models with respect to calculated PM_{10} and $PM_{2.5}$ levels remains more or less the same for the cities, with LOTO always low and MINNI always high.

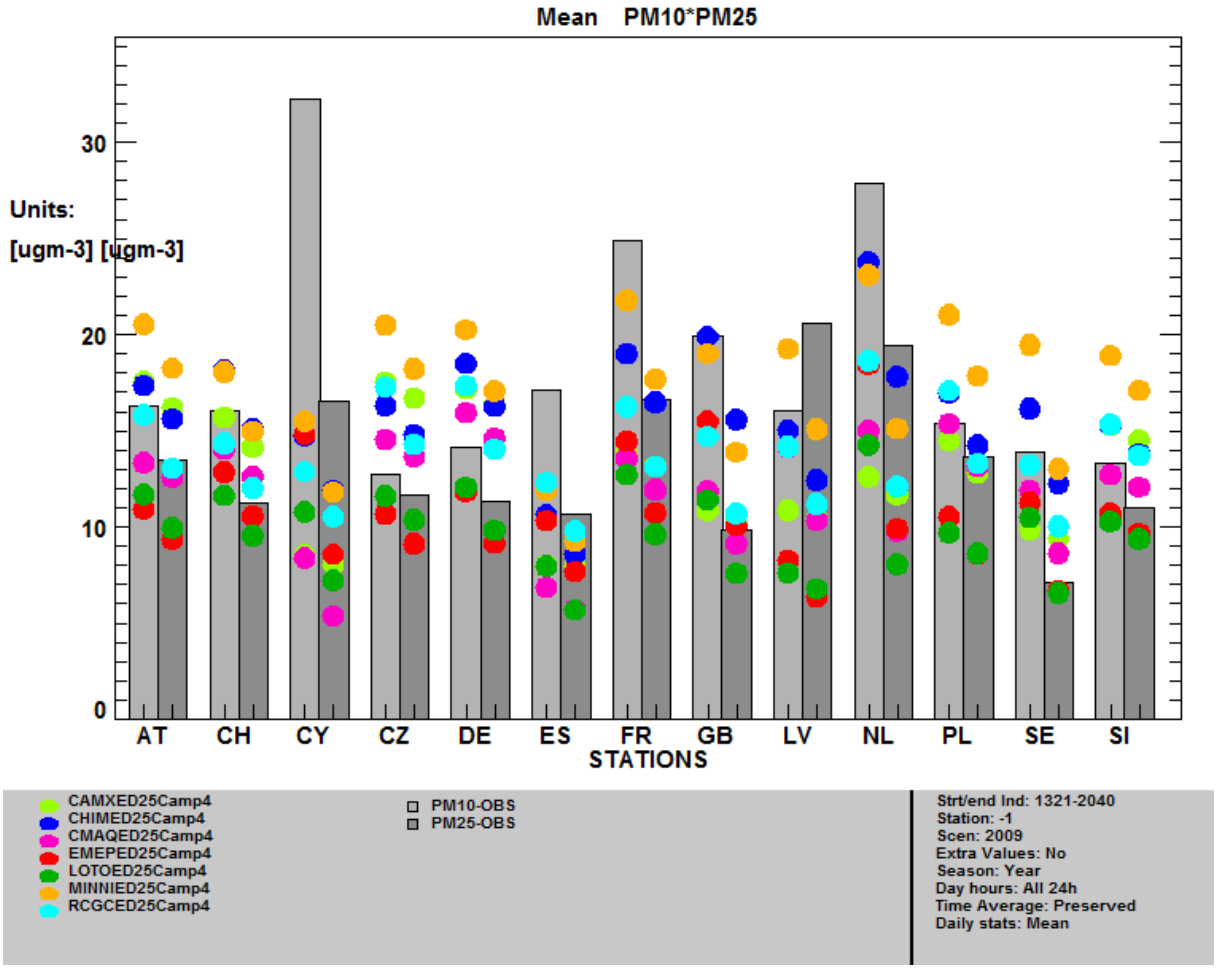

Figure 5.23: $PM_{2.5}$ and PM_{10} direct comparison, Country groups, Bar plot

Figure 5.23 shows, a comparison of observed and model results for PM_{10} and $PM_{2.5}$ according to the Country group. For Latvia, PM10 < PM2.5 indicating a problem in the observation dataset. First, we notice the large difference in the observed levels of $PM_{2.5}$ and PM_{10} in Cyprus, GB, and to a lesser extent in Spain and Sweden. This relatively large fraction of coarse PM in PM_{10} is not reproduced by the models. The coarse PM, typically dominated by dust particles of natural and anthropogenic origin, is probably lacking in the models. The ranking of the models for PM_{10} and $PM_{2.5}$ is more or less preserved for each country, with LOTO and EMEP always low and MINNI always high.

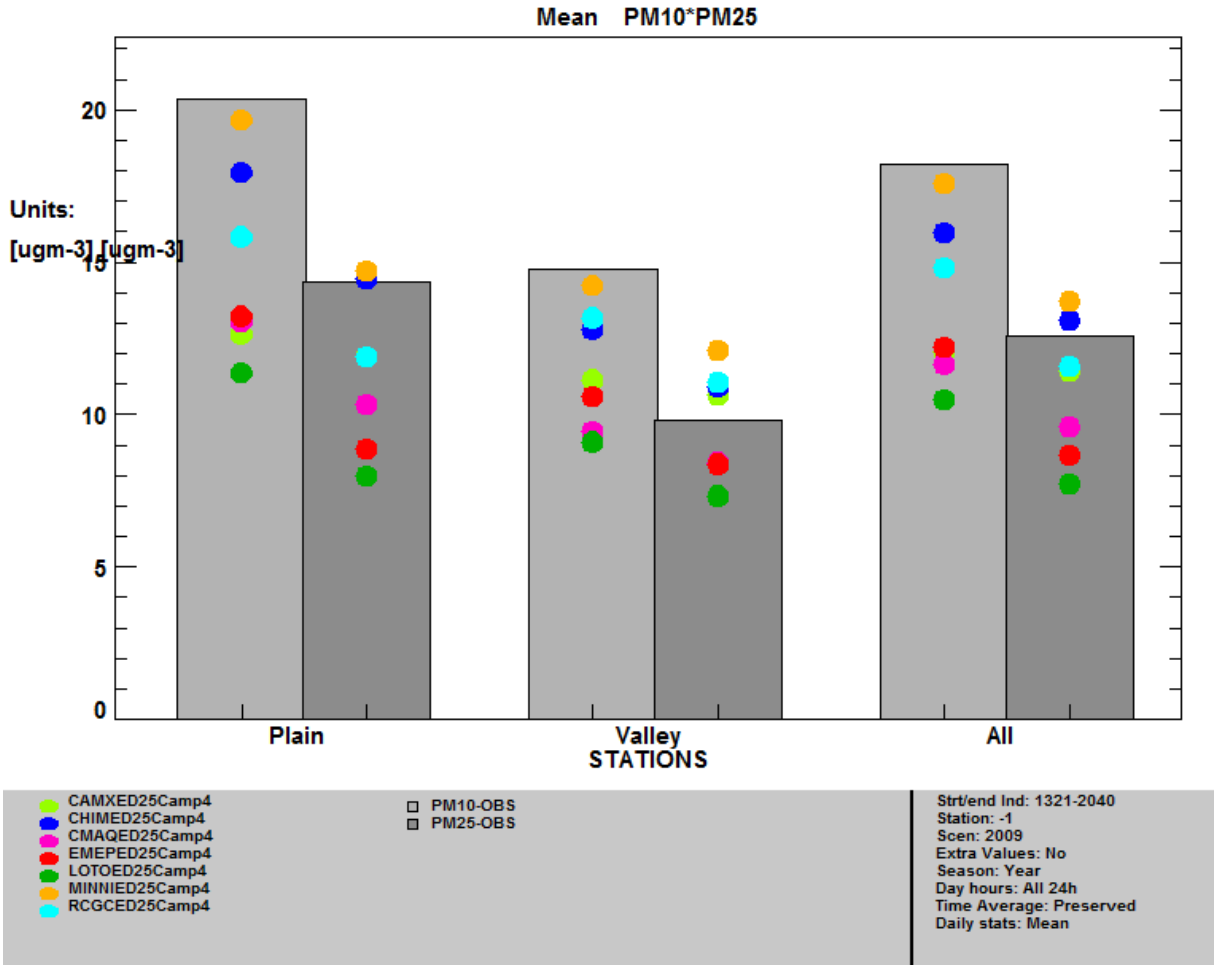

Figure 5.24: $PM_{2.5}$ and PM_{10} direct comparison, Station topography, Bar plot

A comparison of model results according to station topography in given in Figure 5.24. For PM_{10} all models under-estimate with low values for LOTO and EMEP. At $PM_{2.5}$ plain stations models underestimate, except MINNI and CHIM. Same behaviour is noticed for $PM_{2.5}$ valley stations with MINNI, CHIM, CAMX and RCGC over-estimating, and CMAQ, EMEP and LOTO under-estimating.

6 Evaluation of meteorology

We remind here that only CMAQ and RCGC use different sources of meteorological fields. CMAQ uses COSMO meteorology. RCGC use 2D data from IFS and 3D data from observations. The other models uses the same meteorological data set but some additional parameters have been diagnosed by each modelling system before feeding the CTM (PBL for instance).

6.1 Wind speed & Temperature

Table 6.1: Model evaluation for T2M and U10 (respectively in K and m s^{-1}). Correlations in time and space (*Cor*.), Biases (in K and m s^{-1}) and Root Mean Square Errors in (*RMSE in* K and m s^{-1}) are computed for the whole 2009 campaign based on hourly values. Observation values (*Obs*. in K and m s^{-1}) and model values (in K and m s^{-1}) are averaged over the whole 2009 campaign. *Nb* is the number of available observations for a given variable. The best model performance for the RMSE is displayed in bold characters.

Pollutant	Obs.	Model name	Model val.	Bias	Cor.	RMSE	Nb.
T2M	276.21	CAMX	275.54	-0.71	0.94	2.23	977899
		CHIM	275.59	-0.66	0.94	2.21	
		CMAQ	274.57	-1.57	0.89	3.13	
		EMEP	275.44	-0.84	0.93	2.35	
		LOTO	275.55	-0.70	0.94	2.19	
		MINNI	ND	ND	ND	ND	
		RCGC	276.32	0.04	0.94	**2.10**	
U10	4.01	CAMX	4.52	0.51	0.75	2.08	894872
		CHIM	4.50	0.49	0.76	2.06	
		CMAQ	3.99	-0.02	0.68	2.26	
		EMEP	4.50	0.49	0.74	2.11	
		LOTO	4.56	0.55	0.75	2.08	
		MINNI	ND	ND	ND	ND	
		RCGC	4.04	0.03	0.76	**1.95**	

Temperature

As summarized in Table 6.1, the models showed comparable high temporal correlation coefficients over the whole domain (0.89 < R < 0.94) with highest R values in northern Germany and France. Also the spatial correlation coefficients are very similar for all models. The CMAQ correlation is slightly lower than the other models (0.89). On average for the considered period, the bias is negative for all models in the range [-0.84 K, -0.66 K] for CAMX, CHIM, EMEP and LOTO. RCGC displays a very low absolute bias close to zero, and CMAQ displays the lowest negative bias (-1.57 K).

Wind speed

All the models show comparable correlation over the whole domain (R > 0.68) with better performances in Central Europe. Also the spatial geographical distribution of the correlation coefficients is very similar for all models. The RCGC model shows higher correlation coefficients over northern Europe (Finland and Sweden). On average the bias is positive and close to +0.5 m s^{-1}. The wind speeds in RCGC and CMAQ are almost unbiased. This specific behaviour for RCGC and CMAQ is illustrated in Figure 6.1 with usually lower wind speed for these models. Significant differences are found in Belarus and west of Russia, with a quite different wind speeds in CMAQ and RCGC compared to the other models. In Belarus the bias is closed to 1.5 m s^{-1} for CAMX, CHIM, EMEP and LOTO, 1 m s^{-1} for CMAQ and 0.1 m s^{-1} for RCGC. This clearly displays a problem in some regions for IFS U10 fields that are directly ingested by the CTM pre-processor for emission calculations. According to Ingleby *et al*. (2013) ECMWF 10 m wind speeds are slightly overestimated especially at night. In the IFS only

10m winds are used from ships over the oceans for data assimilation (problem of station representativeness for inland stations). Moreover, errors on wind speed measurements are stronger for low winds.

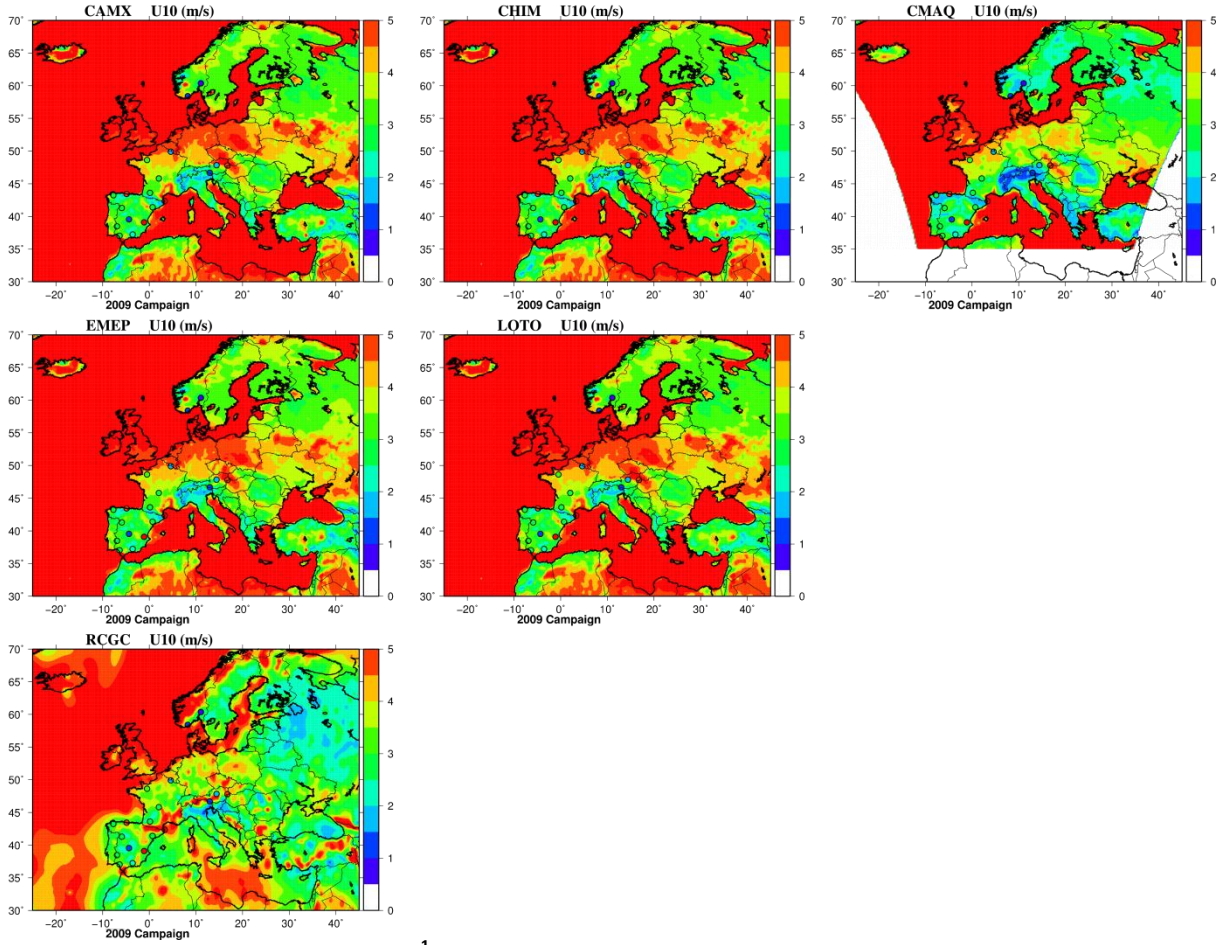

Figure 6.1: Average wind speed (m s^{-1}) for the whole 2009 campaign for all the models. The circles are the observed values at EMEP sites only

The diurnal cycles in Figure 6.2 display an overestimation of the modelled U10 at night except for RCGC and CMAQ in France and Great Britain. During the afternoon the models are closer to the observations except CMAQ and RCGC which underestimate the wind speed. Regarding the temperature, the models underestimate the measured T2M as previously described, with the exception of RCGC which overestimate the temperature from 01:00 to 8:00 UT in the morning.

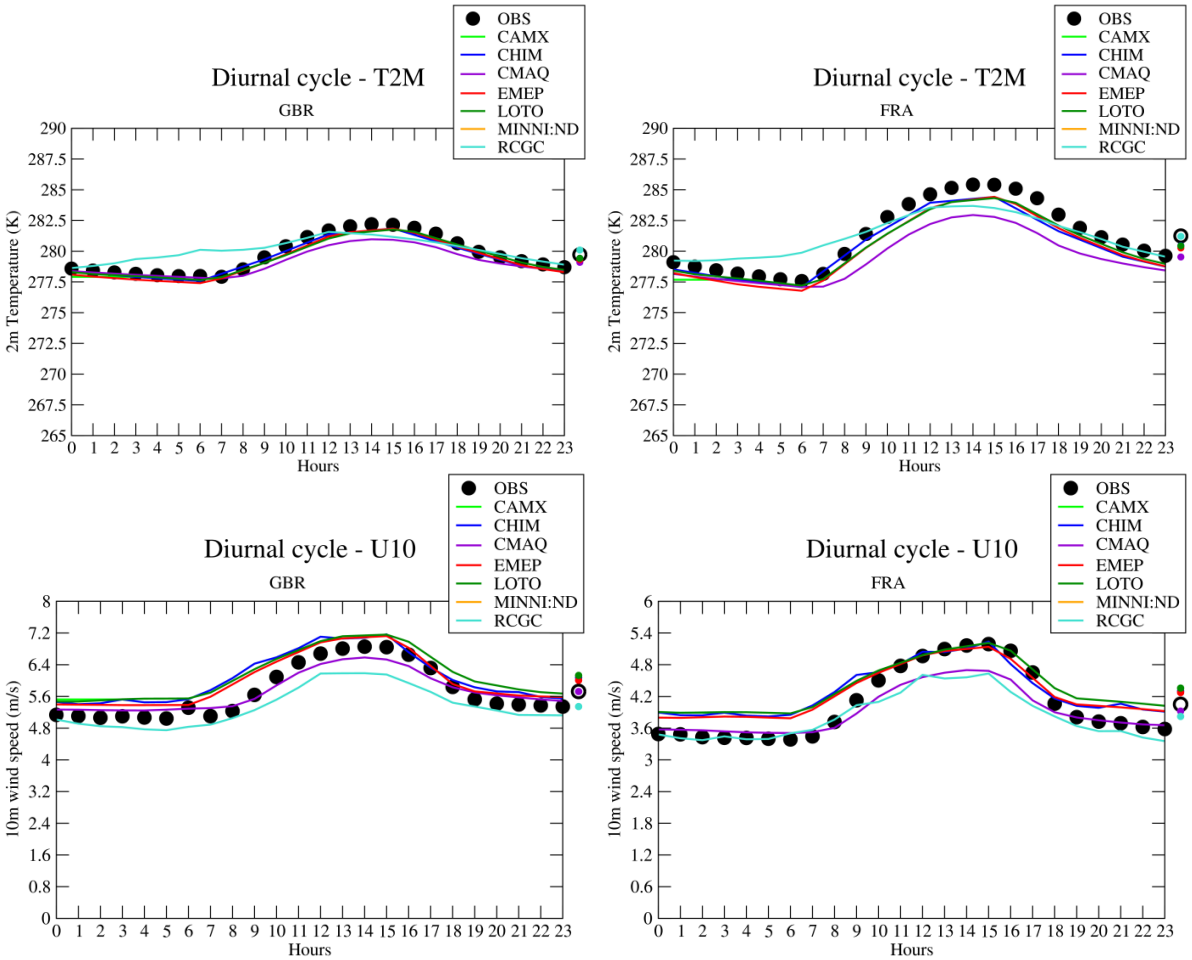

Figure 6.2: Average U10 and T2M diurnal cycle for the whole 2009 campaign for all the models in France (FRA) and Great Britain (GBR)

6.2 Precipitation

Table 6.2: Model evaluation for RAIN (in mm/day). Correlations in time and space (*Cor.*), Biases (in mm/day) and Root Mean Square Errors in (*RMSE* in mm/day) are computed for the period of intensive measurements of 2009 based on daily values. Observation data are from EMEP sites and are based on daily samples. *Nb* is the number of available observations for a given variable. The best model performance in terms of RMSE is displayed in bold characters.

Pollutant	Obs.	Model name	Model val.	Bias	Cor.	RMSE	Nb.
RAIN	1.95	CAMX	2.30	0.34	0.58	4.78	1920
		CHIM	2.12	0.17	0.58	4.68	
		CMAQ	1.18	-0.80	0.41	5.29	
		EMEP	2.19	0.23	0.58	4.72	
		LOTO	2.08	0.13	0.60	**4.65**	
		MINNI	2.32	0.37	0.59	4.73	
		RCGC	1.64	-0.32	0.18	6.89	

In Table 6.2, a slight positive bias is shown for CAMX, CHIM, EMEP, MINNI and LOTO with a correlation near 0.6 with a RMSE of about 4.7 mm/day. These error statistics are rather good for such a variable that has a strong spatial variability. RCGC and CMAQ display negative biases and lower correlation coefficients (in time and space) compared to the other models. In RCGC, lower

precipitation values in Scandinavia and also from Germany to Ukraine are in a better agreement with observations compared to the other models (Figure 6.3).

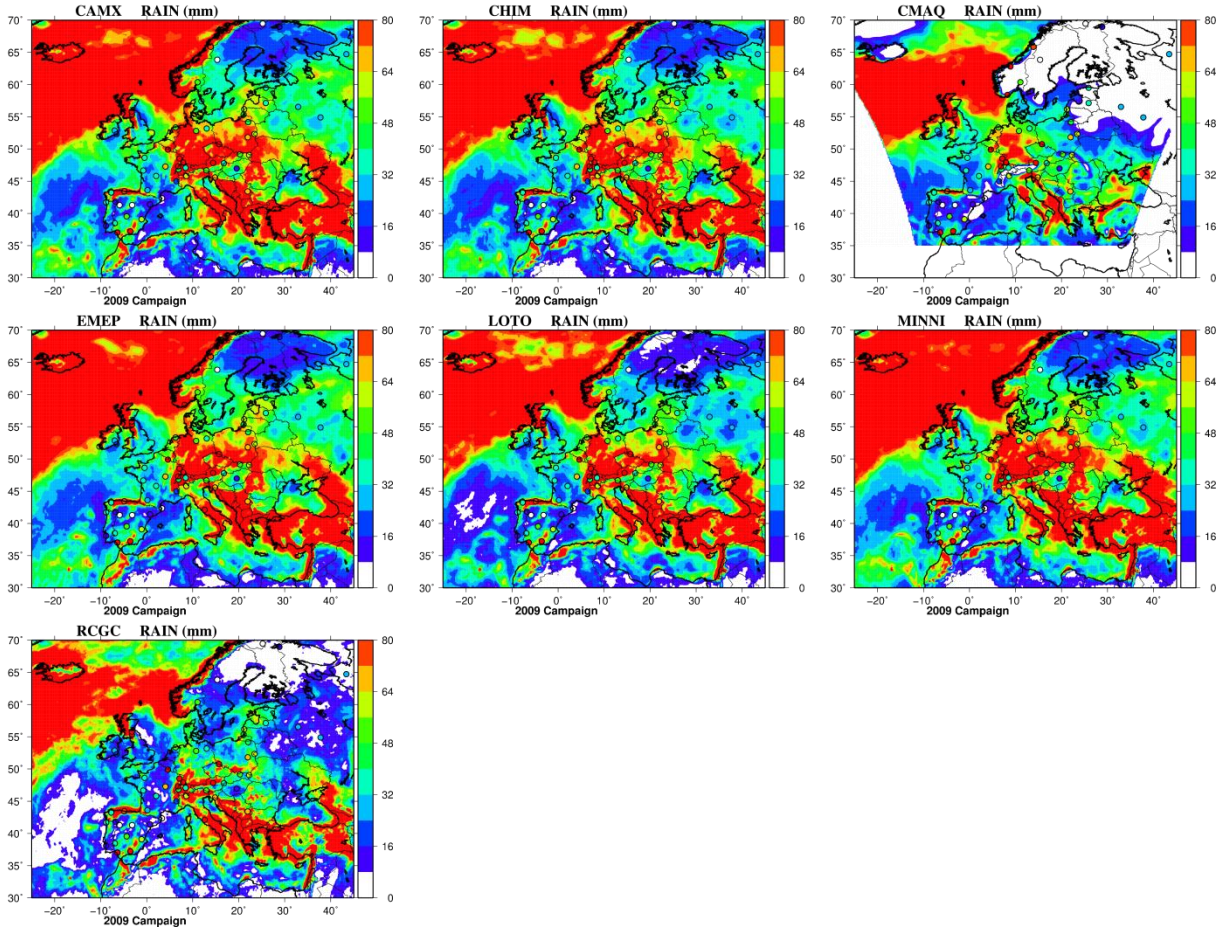

Figure 6.3: Total precipitation (in mm) for the whole 2009 campaign for all the models. The circles are the observed values at EMEP sites only

6.3 Planetary Boundary Layer

Table 6.3: Model evaluation for PBL (in m) at 12:00 UTC. Correlations in time and space (*Cor.*), Biases (in m) and Root Mean Square Errors in (*RMSE* in m) are computed for the whole 2009 campaign based on values at 12:00 UTC. *Nb* is the number of available observations for a given variable. The best model performance in terms of RMSE is displayed in bold characters.

Pollutant	Obs.	Model name	Model val.	Bias	Cor.	RMSE	Nb.
PBL	1269.27	CAMX	1115.04	-154.23	0.73	**478.26**	1497
		CHIM	1115.04	-154.23	0.73	478.26	
		CMAQ	1097.84	-171.43	0.58	582.06	
		EMEP	1005.06	-264.21	0.58	597.66	
		LOTO	1055.82	-213.45	0.73	497.76	
		MINNI	754.47	-514.80	0.56	753.99	
		RCGC	1064.79	-204.49	0.62	558.45	

As explained in section 4.1, the observed PBL is calculated at 12:00 because of methodology hypotheses. In terms of bias, correlation and RMSE, the best model performances are observed for PBL heights in CAMX and CHIM which are taken from IFS, they are biased by -154 m compared to PBL heights observed at noon (Table 6.3). The largest underestimation of PBL height is found for MINNI (-

515 m) and EMEP (-264 m); and the correlation coefficients for these models are lower compared to the others.

Figure 6.4 shows the diurnal profile of the PBL height in Romania, Sweden, Great Britain and France. Note that in the EMEP model PBL heights are calculated on a 3-hour basis. The shape of the PBL diurnal cycle is very similar in CAMX, CHIM, RCGC and LOTO, with the latter being shifted by one hour in advance. CMAQ, EMEP and MINNI, to a lesser extent, have quite different shapes of PBL diurnal cycle, with night time PBL being higher compared to the other models.

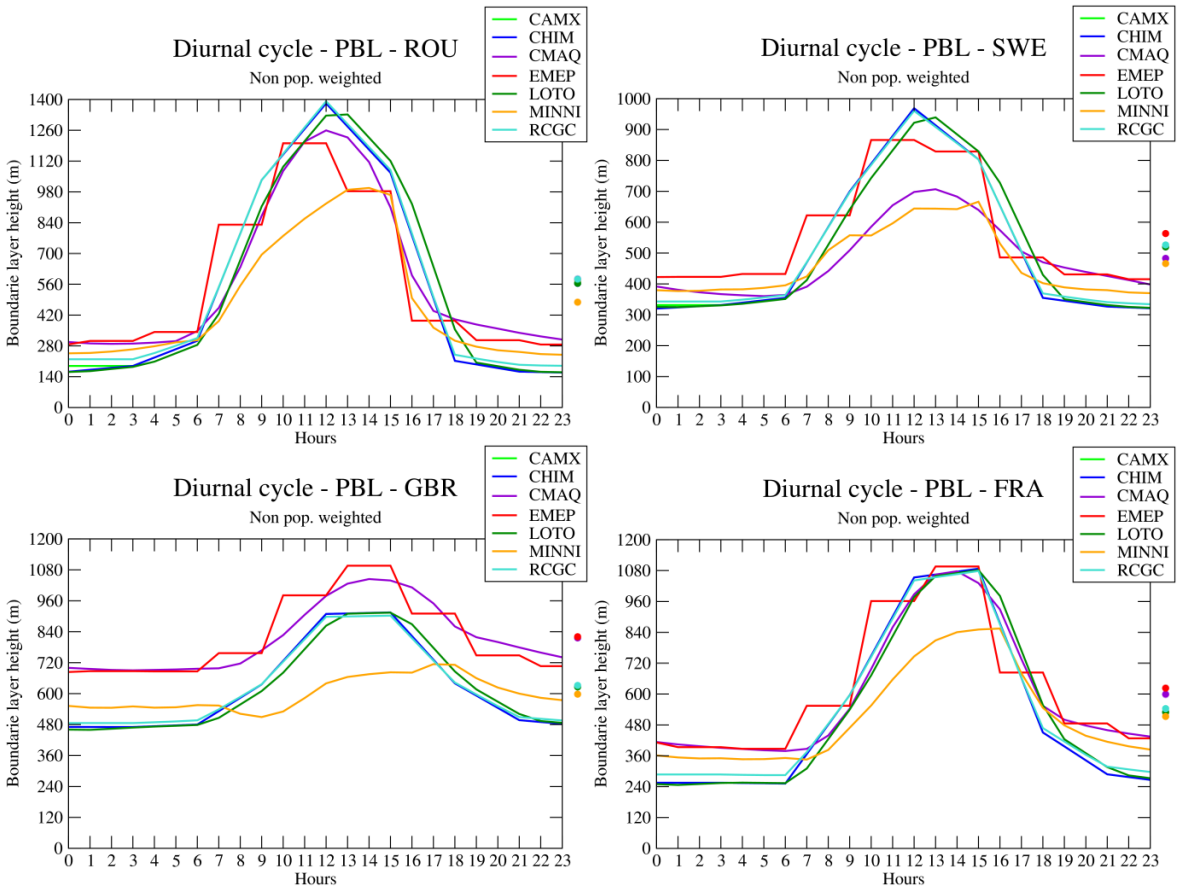

Figure 6.4: Average modelled diurnal cycles of the PBL height in Romania (top left), Sweden (top right), Great Britain (bottom left) and France (bottom right). For a given country the grid cell are averaged.

In order to investigate the hourly variation of the PBL height, we make use of observations at the SIRTA station close to Paris (see section 4). In Figure 6.5, the bias is positive for CMAQ and EMEP and negative for all other models, these two models exhibit the lowest correlation coefficients. However, if we consider nocturnal PBL (between 00:00 and 06:00 UT) CMAQ and EMEP exhibit the lowest absolute bias (about -50 m) whereas the other models display large negative biases up to -200 m for CAMX, CHIM and LOTO. Regarding the diurnal PBL (between 10:00 and 16:00) all models overestimate the PBL height. LOTO and MINNI show the lowest overestimation and also the best correlation coefficients (0.58).

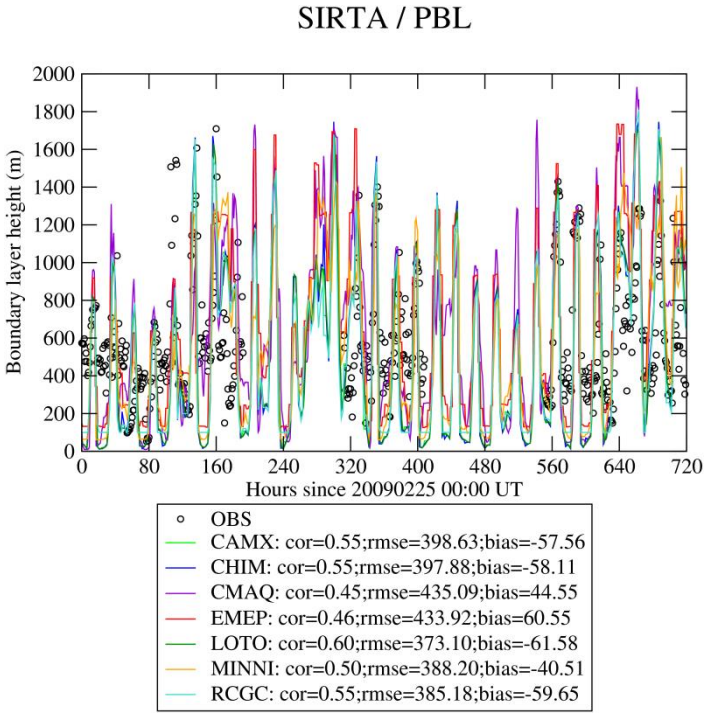

Figure 6.5: Time series of the PBL height in SIRTA (with error statistics) for the 2009 campaign for all models compare to observations retrieved with LIDAR data post-treatments

6.4 Influence of meteorology on NO_2 concentrations (with CAMX)

Pollutant concentrations are strongly influenced by the reconstruction of meteorological fields. In this section a comparison of modelling performances in reproducing wind speed and NO_2 concentrations is presented and discussed. Furthermore, Planetary Boundary Layer (PBL) height data, collected at SIRTA site (Paris) have been used too. Being mainly related to emission processes, NO_2 has been selected as a good tracer of the influence of dispersion on pollutant concentrations.
The analysis has been performed over the whole domain as well as over three smaller areas, namely: a) the whole Germany (DE), The Po Valley (POV) and the Paris area (PAR). The first two areas have been selected because are characterized by opposite level of performance, while the Paris area has been selected in order to focus the analysis on both wind and PBL height.
NO_2 observed data set has been set up from Airbase database, selecting just background stations, having more than 75% valid data over the whole 2009. Finally, as already mentioned, PBL heights derived at SIRTA site has been included too. Modelled concentrations have been derived from the CAMX simulation results, while modelled meteorological fields have been derived from IFS.

Figure 6.6 shows the spatial distribution of the NO_2 concentrations, averaged over the whole 2009 campaign, observed at both rural (RB, left top panel) and suburban/urban (SBUB, right top panel) sites. Bottom panels show the corresponding Mean Normalized Bias (NMB) of the computed hourly mean concentrations. At rural sites the observed concentration ranges between 4 and 14 ppb, while at SBUB sites it ranges between 8 and 24. Bottom panels clearly show that the model is rather skilful in reproducing the mean concentration at RB sites, while it underestimates at most of SBUB sites. This comparison suggests that at SBUB sites the model performance are influenced not only by meteorology but also by other systematic effects, such as emissions and station representativeness, that enhances the model low bias. For this reason the analysis of the influence of meteorological fields has been focused just on RB sites.
Figure 6.7 shows the time series of the hourly box plots comparing the distribution of the observed and computed NO_2 concentration at Airbase RB sites, over the whole domain. A similar comparison, concerning wind speed, is shown in Figure 6.8. The temporal evolution of the observed concentrations is clearly influenced by the corresponding variability in the observed wind speed. It is

worth noting, as an example, that the lowest NO_2 concentrations take place during 8-10 and 23-25 of March, that are characterized by the highest values of observed wind speed.

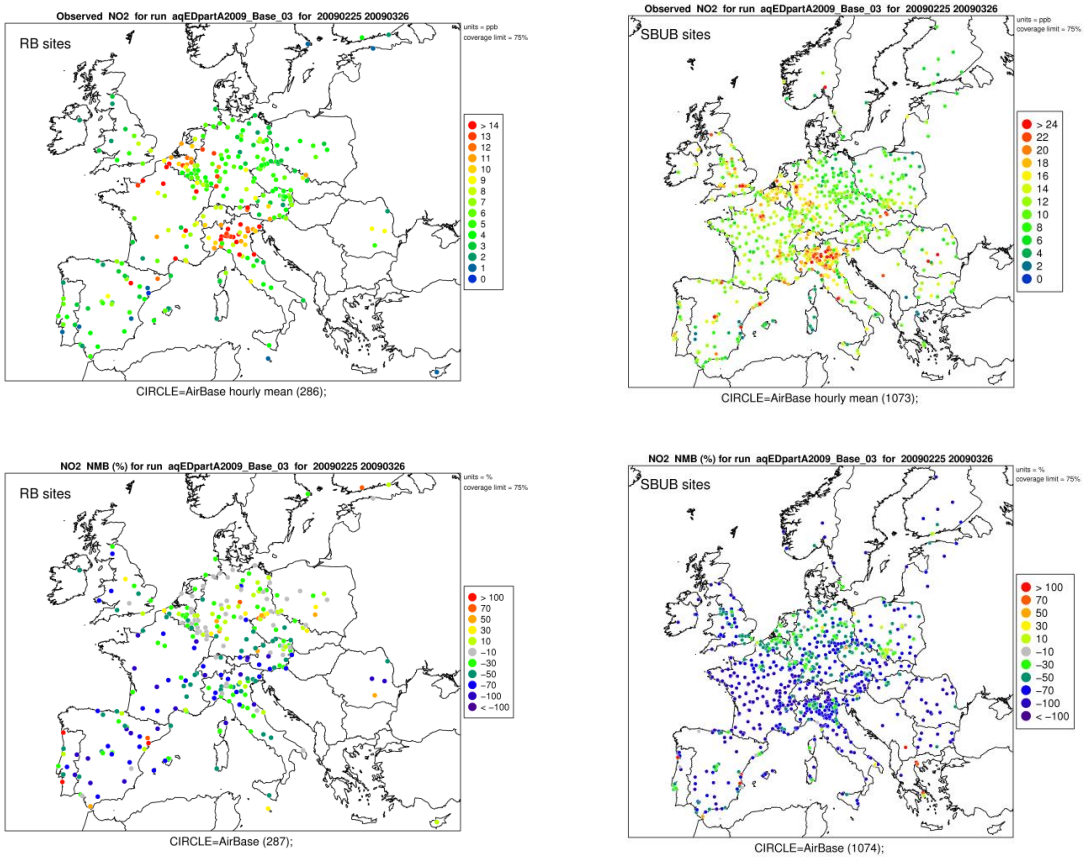

Figure 6.6: Top panels show the NO_2 mean concentration observed at rural (left, RB) and suburban/urban (right, SBUB) background Airbase sites. Bottom panels show the corresponding distribution of the Normalized Mean Bias, computed for NO_2 hourly concentrations over the whole 2009 campaign.

The CAMX model is able to reproduce the temporal variability of the observed NO_2 concentrations both in term of median values as well as range of variability among the set of stations (displayed by the hourly boxes). On average CAMx tends to slightly underestimate the observed concentration, as shown by the comparison of the modelled (3.7 ppb) and observed (4.9 ppb) median concentrations. Conversely, highest percentiles show a stronger discrepancy, suggesting that the model underestimation is not homogenously distributed but is more enhanced during peak episodes.
The differences between modelled and observed concentrations present two main features probably related to different causes. Firstly, CAMX shows a prolonged underestimation during 25-27 of February and 22-26 of March, characterized by a corresponding and rather constant overestimation of wind speed. Furthermore, CAMX shows also a systematic bias during daytime hours, when modelled concentrations are often underestimated. The latter seems not related to a corresponding discrepancy in modelled wind speed, thus being probably due to an imprecise reconstruction of the daily cycle of the PBL height.

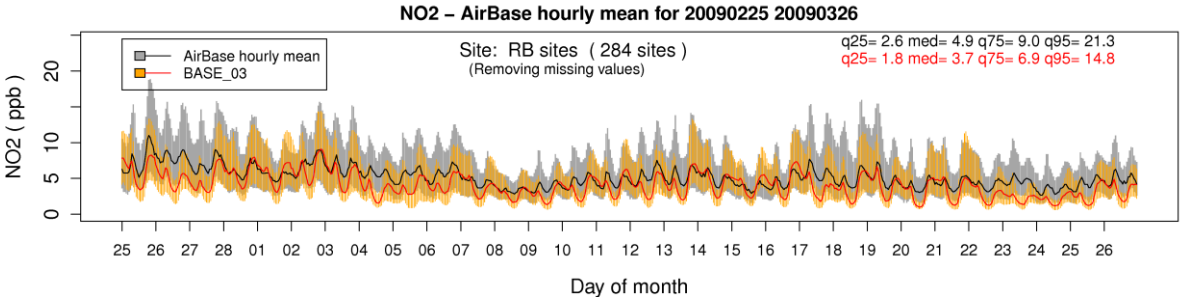

Figure 6.7: Time series of hourly Box plots showing the distribution of the observed and computed NO_2 concentration. Observations are in black/grey; CAMX in red/orange. Bars show the 25th -75th quantile interval, while the median is displayed by the continuous line. The 25th, 50th, 75th, and 95th quantile of the whole campaign are reported too. Comparison of computed and observed boxplot time series evaluated at Airbase RB sites over the whole domain.

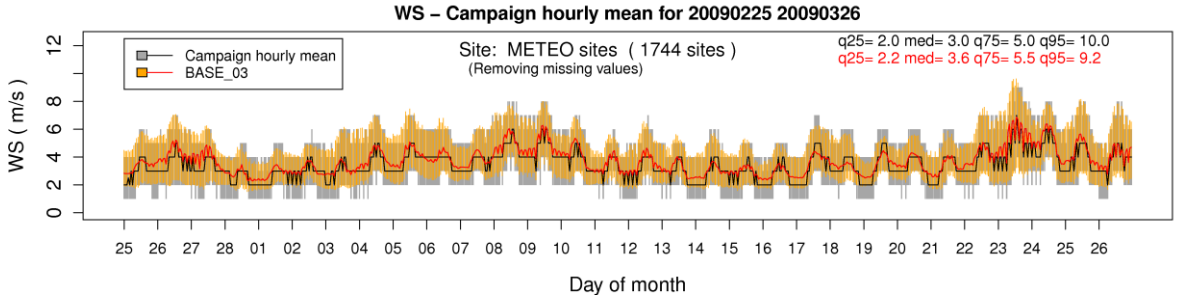

Figure 6.8: Time series of hourly Box plots showing the distribution of the observed and computed wind speed. Observations are in black/grey; modelled values in red/orange. Bars show the 25th -75th quantile interval, while the median is displayed by the continuous line. The 25th, 50th, 75th, and 95th quantile of the whole campaign are reported too. Comparison of computed and observed boxplot time series evaluated at meteorological sites over the whole domain.

In order to better investigate the influence of meteorological fields, the same analysis has been performed over the three subregions previously defined. At DE sites (Figure 6.9) the observed wind speed, ranging between 2 and 8 m s^{-1} is very well reproduced by the IFS model, both in term of statistical distribution as well as temporal variability. The NO_2 concentrations exhibit a corresponding behaviour in terms of high a low concentrations. On average, observed concentrations are very well reproduced by CAMX, as proved by the comparison of the main quantiles, but the model seems to introduce a stronger daily variability, with a positive bias during night-time and low bias during daytime. Once again, this systematic effect can be probably related more to the PBL evolution than the wind speed.

In the Po valley, as expected, the wind speed is generally lower than Germany, showing a median value of 2.0 m s^{-1}, corresponding to an half of the same metric for Germany. Also in this case the temporal evolution and the distribution of the wind speed is very well reproduced by IFS model, particularly during low wind speed conditions. But in this case, we do not observe a corresponding performance for the CAMX model that tends to strongly underestimate the observed NO_2 concentrations. Considering that the model proved to be very skilful in reproducing the wind speed, we can assume that in the Po valley the meteorological model tends to systematically overestimate the intensity of the vertical turbulent forcing during the whole day. It is worth noting that CAMx fails in reproducing the observed concentrations over the whole period, but the discrepancies are more relevant during weak circulation conditions, probably characterized by stronger stability conditions, not captured by the models.

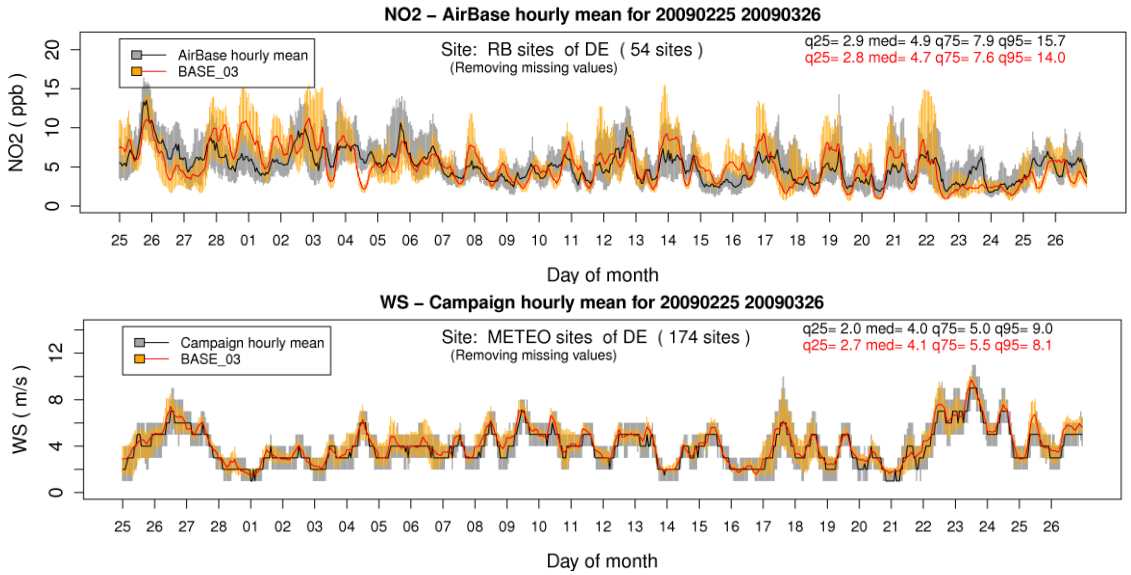

Figure 6.9: Time series of hourly Box plots showing the distribution of the observed and computed NO_2 concentration (top) and wind speed (bottom). Observations are in black/grey; modelled values in red/orange. Bars show the 25th -75th quantile interval, while the median is displayed by the continuous line. The 25th, 50th, 75th, and 95th quantile of the whole campaign are reported too. Comparison of computed and observed boxplot time series evaluated at Airbase and meteorological sites, available over Germany.

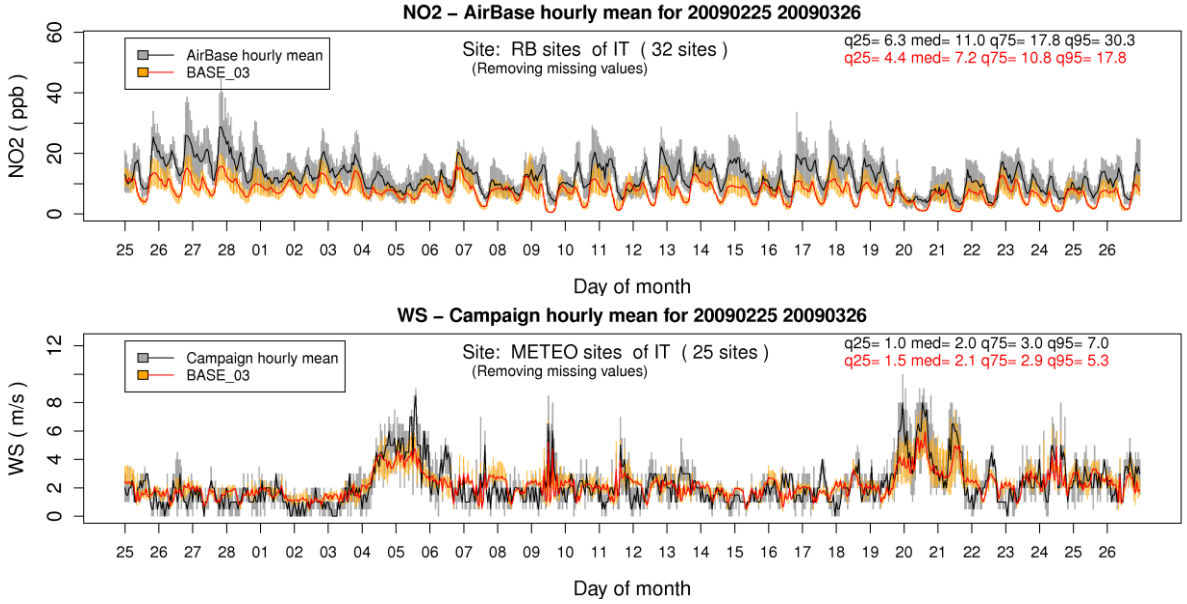

Figure 6.10: Time series of hourly Box plots showing the distribution of the observed and computed NO_2 concentration (top) and wind speed (bottom). Observations are in black/grey; modelled values in red/orange. Bars show the 25th -75th quantile interval, while the median is displayed by the continuous line. The 25th, 50th, 75th, and 95th quantile of the whole campaign are reported too. Comparison of computed and observed boxplot time series evaluated at Airbase and meteorological sites, available over the Po valley (Italy).

Finally, the same analysis has been carried out for the Paris area, where PBL height observations were available too. Also in this case, the meteorological model showed a very good performance in reproducing the observed wind speed, whose temporal evolution clearly influences the corresponding temporal variability of NO_2 concentrations. Also the PBL height is quite well reproduced by the model, though the model tends to underestimate the night-time minima and, conversely, to overestimate some diurnal peaks.

Within the Paris area NO_2 observations are quite well reproduced by CAMX, showing a low bias of the median value lower than 2 ppb, corresponding to less than 20% of the observed median concentration. The availability of both wind speed and PBL height observations, allow the influence of both processed to be clearly detected. For example 3-4, 10 and 25 of March, the underestimation showed by CAMX seems well related to a corresponding overestimation of the PBL rather than the wind speed. Conversely during night hours of March 5, CAMX results are more influenced by the wind speed.

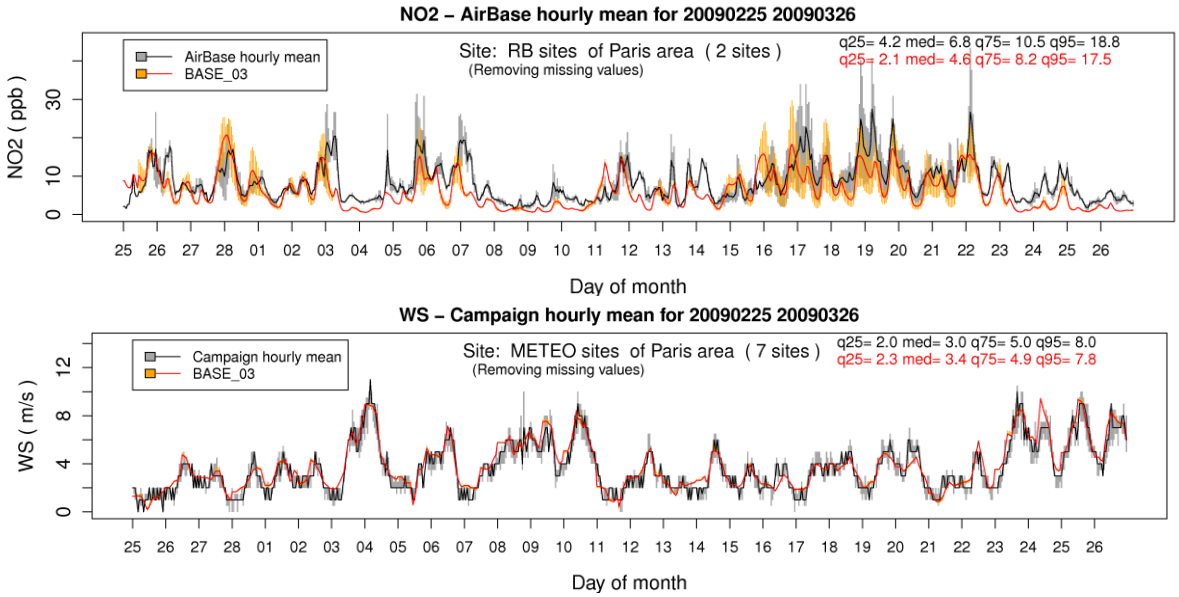

Figure 6.11: Time series of hourly Box plots showing the distribution of the observed and computed NO_2 concentration (top) and wind speed (bottom). Observations are in black/grey; modelled values in red/orange. Bars show the 25th -75th quantile interval, while the median is displayed by the continuous line. The 25th, 50th, 75th, and 95th quantile of the whole campaign are reported too. Comparison of computed and observed boxplot time series evaluated at Airbase and meteorological sites, available over the Paris area.

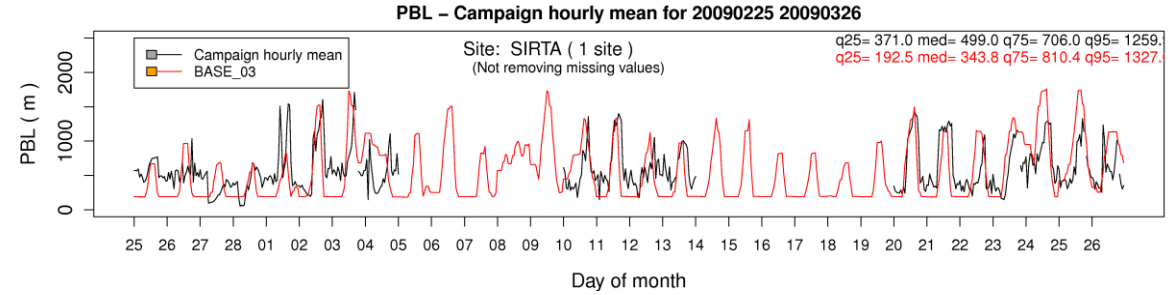

Figure 6.12: Time series of hourly Box plots showing the distribution of the observed and computed PBL height. Observations are in black/grey; modelled values in red/orange. Bars show the 25th -75th quantile interval, while the median is displayed by the continuous line. The 25th, 50th, 75th, and 95th quantile of the whole campaign are reported too. Comparison of computed and observed boxplot time series evaluated at SIRTA site.

The analysis has been completed comparing the diurnal cycle of both NO_2 and meteorological variables, reported from Figure 6.13 to Figure 6.15. At German sites NO_2 concentrations are slightly overestimated during night-time and underestimated during daytime. This behaviour does not seem strictly related to wind speed, particularly during night-time, thus being probably more related to vertical turbulence. At Po valley sites, NO_2 values are systematically underestimated, while wind speed is correctly reproduced, even partially underestimated during daytime hours. NO_2 modelled concentrations show a clear low bias during night-time, probably related to an imprecise

reconstruction of the strong stable conditions that characterize this area during the cold season. The difficulty of model is enhanced during the morning hours, when the model is not able to capture the strength of the observed peak. The discrepancy is probably caused by a too rapid growth of the PBL during the first daytime hours. Late in the afternoon the NO_2 bias tends to decrease, probably thanks to a very quick collapse of PBL height after sunset.

At Paris sites, NO_2 modelled concentrations show a behaviour similar to the Po valley area. The availability of both wind speed and PBL height observations, allows most of the previous comments to be confirmed. Particularly it is worth noting that at SIRTA site, PBL height shows a too rapid increase during morning hours followed by a too strong decrease just after sunset.

In conclusion the comparison of modelled concentrations against wind speed and PBL heights confirmed that meteorology strongly influences CTMs performance. Particularly the temporal evolution of wind speed is most responsible of model skilfulness in reproducing the daily variability of pollutant concentrations (*e.g.* the development of peak episodes), while the reconstruction of the PBL diurnal cycle seems more influencing in driving the corresponding pollutant diurnal and hence the presence of systematic positive and negative bias detectable on daily basis.

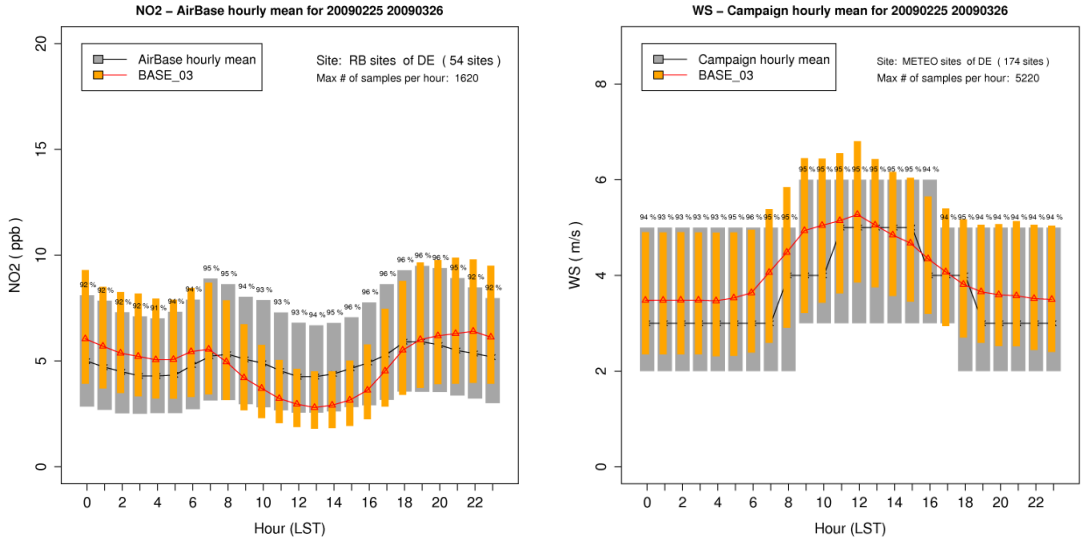

Figure 6.13: Time series of hourly Box plots showing the distribution of the diurnal cycle observed and computed NO_2 concentration (left) and wind speed (right). Observations are in black/grey; modelled values in red/orange. Bars show the 25th -75th quantile interval, while the median is displayed by the continuous line. The 25th, 50th, 75th, and 95th quantile of the whole campaign are reported too. Comparison of computed and observed boxplot time series evaluated at Airbase and meteorological sites, available over Germany. Wind speed is in UTC time.

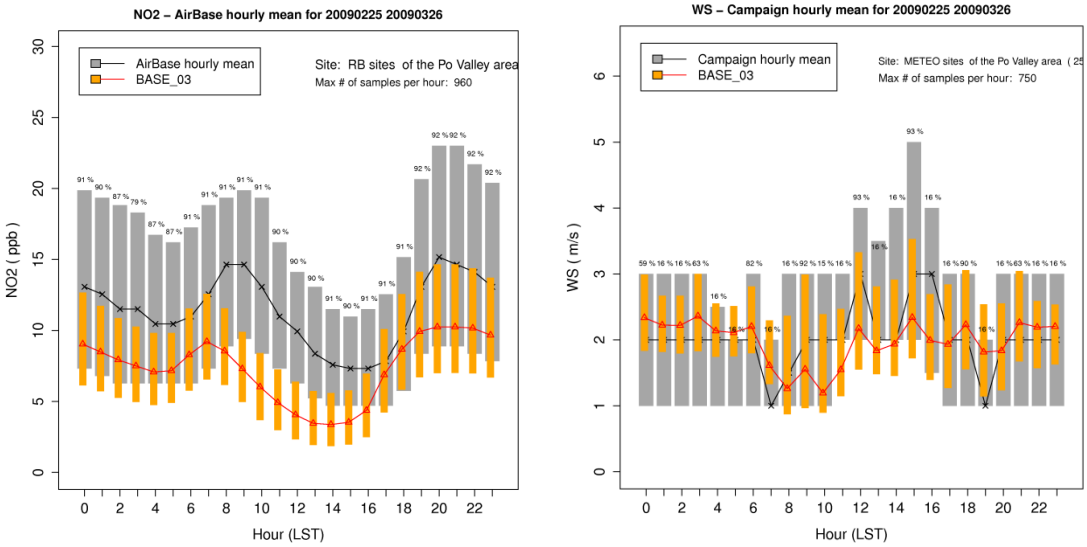

Figure 6.14: Time series of hourly Box plots showing the distribution of the diurnal cycle observed and computed NO_2 concentration (left) and wind speed (right). Observations are in black/grey; modelled values in red/orange. Bars show the 25th -75th quantile interval, while the median is displayed by the continuous line. The 25th, 50th, 75th, and 95th quantile of the whole campaign are reported too. Comparison of computed and observed boxplot time series evaluated at Airbase and meteorological sites, available over the Po valley. Wind speed is in UTC time.

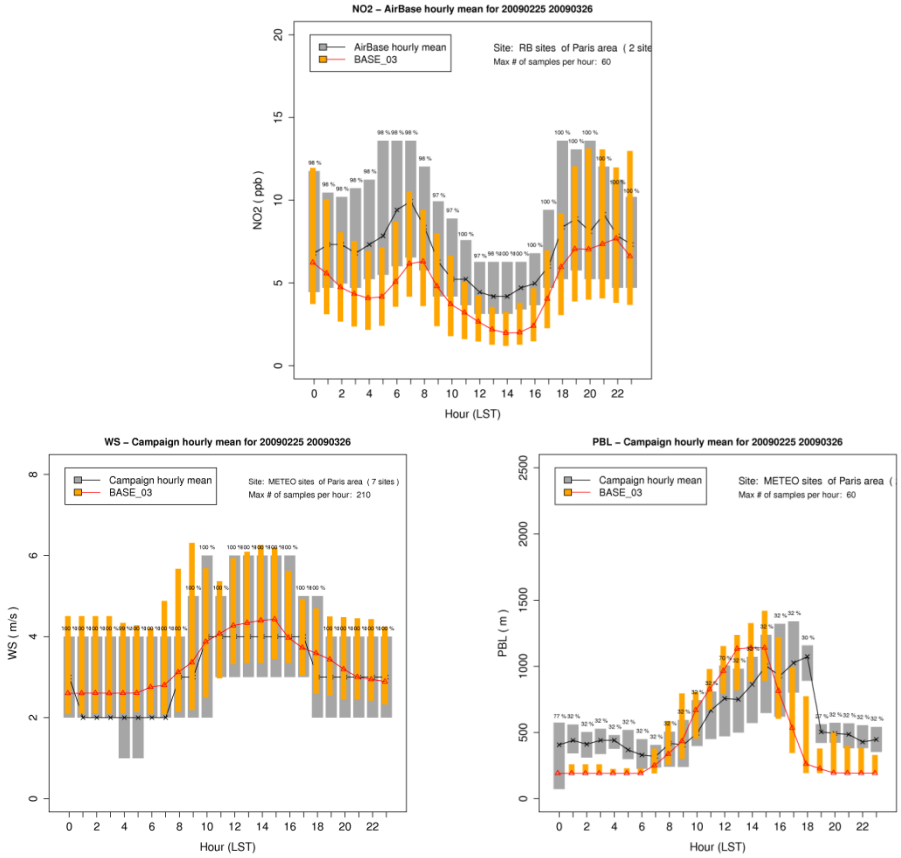

Figure 6.15: Time series of hourly Box plots showing the distribution of the diurnal cycle observed and computed NO_2 concentration (top), wind speed (bottom left) and PBL height (bottom right). Observations are in black/grey; modelled values in red/orange. Bars show the 25th -75th quantile interval, while the median is displayed by the continuous line. The 25th, 50th, 75th, and 95th quantile of the whole campaign are reported too. Comparison of computed and observed boxplot time series evaluated at Airbase and meteorological sites, available over the Paris area. Wind speed and PBL height are in UTC time.

6.5 Impact of the PBL parameterization (with MINNI results)

As shown in section 6.3, MINNI underestimates the PBL heights calculated at 12:00 from measurements (Table 6.3) but it is in a good agreement with hourly data available at SIRTA (Figure 6.5). In order to test the effect of PBL heights on air quality predictions, the MINNI model has been run using the PBL_{IFS} instead of its own parameterization for PBL heights. Figure 6.16 shows the average PBL heights and the average concentrations of O_3, NO_2 and PM_{10} using MINNI's parameterizations (left graphs) and the percentage difference between the average concentrations calculated with PBL heights given by IFS (PBL_{IFS}) and by MINNI's parameterizations (PBL_{MINNI}) (right graphs) using the following formula: $(PBL_{IFS}-PBL_{MINNI})/PBL_{MINNI}$.

It can be seen that over the sea, on average, PBL heights calculated with MINNI's parameterizations (PBL_{MINNI}) are lower than PBL heights given by IFS (PBL_{IFS}) but over the land PBL_{MINNI} is higher than PBL_{IFS} in coastal areas, North Africa, Scandinavian mountains and middle of Russian plains, and lower over the rest. Over the sea, PBL_{IFS} are higher than PBL_{MINNI} more than 50% while over the land the differences are between -30 and +30%.

Figure 6.16 also shows that the O_3 concentrations increase in correspondence of the increase of PBL heights up to 10% and more, and decrease where the PBL heights decrease. This behaviour is explained by the fact that with a higher PBL more O_3 is entrained from high altitudes where O_3 concentrations are higher than at surface (see Section 0). Since the NO_2 sources are mainly at surface, the NO_2 concentrations generally decrease with the increase of PBL heights and increase with the decrease of PBL heights as a consequence of more or, respectively, less effective dilution. Over most of Europe, the NO_2 concentrations decrease up to 8% when PBL_{IFS} heights are used. The PM_{10} concentrations respond to PBL heights variation in the same way as NO_2. The use of PBL_{IFS} heights produces ca. 4 % decrease of PM_{10} concentrations in most parts of Europe but also increases of 6-8% in coastal areas and Russian plains.

In terms of statistics, the use of the IFS PBL in MINNI slightly improves the correlations mainly driven by an improvement of time correlations. PM_{10}, PM_{25} and NO_2 concentrations are decreased by less than 0.5 μg m^{-3}, improving all error statistics reported in Table 5.1 for MINNI. An increase of 2.75 μg m^{-3} is observed for O_3 concentrations. It is also worth to mention that the variations in pollutant concentrations are small (over the land below 10% generally) in comparison to the variations of PBL height, therefore other factors such as emissions spatial distribution, meteorology (*e.g.* advection and vertical dispersion, especially in low-wind areas), gas phase chemistry, aerosol physics and chemistry have to be investigated for improving model performances.

These results clearly show the importance of having good estimates of PBL heights but they also demonstrates that more investigations are necessary in order to identify the best parameterization of PBL heights which improves the simulated concentrations over the whole Europe.

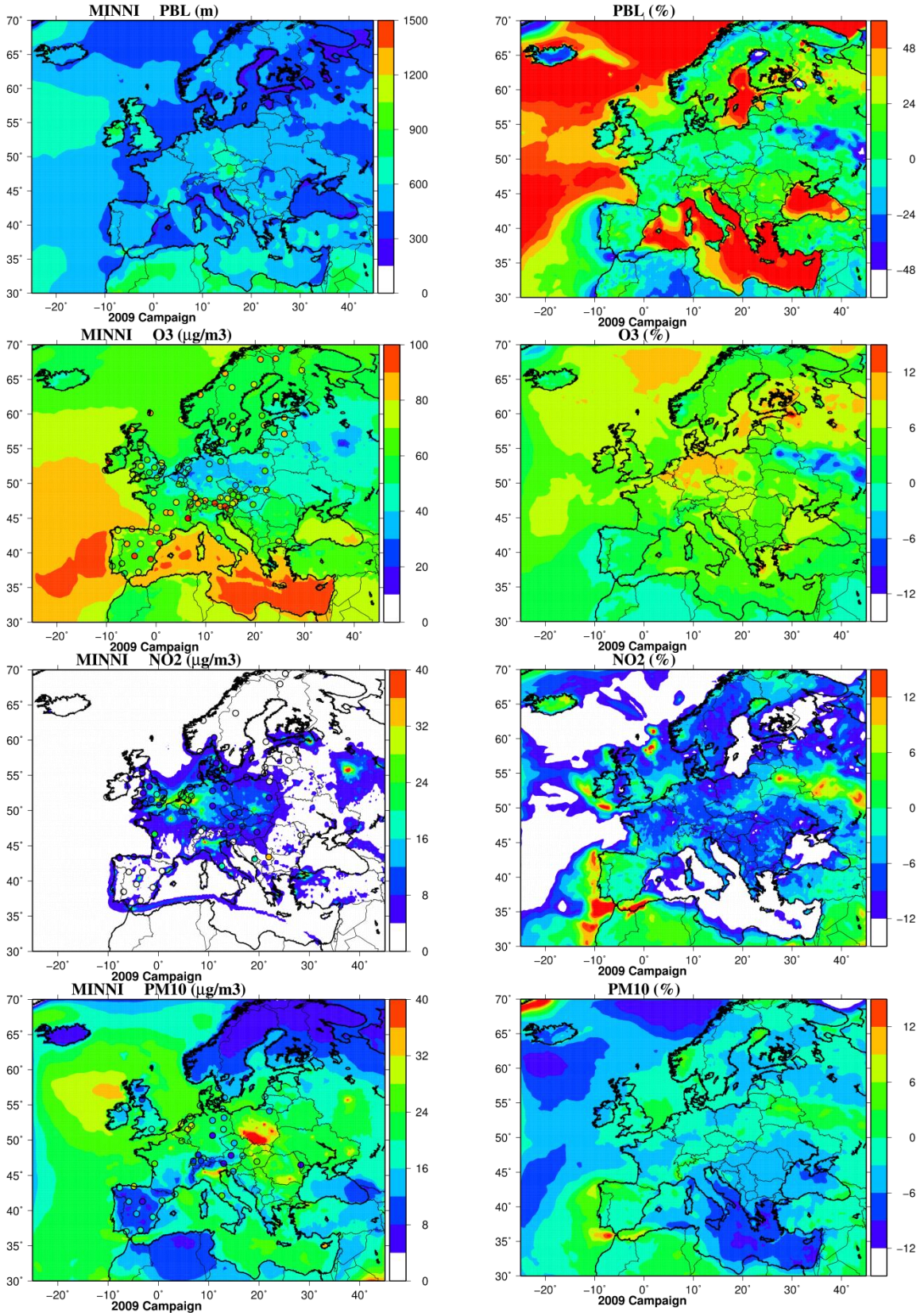

Figure 6.16: Left graphs show the average PBL heights and the average concentrations for O_3, NO_2 and PM_{10} using MINNI's parameterizations. Right graphs show the percentage difference between the average concentrations calculated with PBL heights given by IFS (PBL_{IFS}) and by MINNI's parameterizations (PBL_{MINNI}).

7 Evaluation of deposition

Reduced and oxidised N wet deposition (WNHx and WNOx respectively), as well as S wet deposition (WSOx) estimated by all the models have been compared and evaluated against observations. For dry deposition (DNHx, DNOx and DSOx), only an intercomparison between models has been possible due to the lack of an experimental database.

In order to facilitate the analysis, in the following sections the *Deposition/Concentration* ratio for dry deposition and *Deposition/Concentration/Rain* for wet deposition (from now on, "deposition capability") have been calculated. These variables can give some insight into how effective models are for deposition processes. Figure 7.2, Figure 7.9 and Figure 7.14 , that will be later discussed, show model deposition capability for some countries, estimated as the average of the model capability found at all grid-cells in a given country. Bars and crosses in these figures represent dry and wet deposition model capability, respectively. Note that the efficiencies of wet and dry deposition for any single model are not directly comparable in the figures presented in the next sections.

It is important also to remark that model daily outputs correspond to the 0:00-23:00 period (06:00-06:00 for the EMEP model), whereas daily sampling periods do usually start later in the morning (with the exception of CH02, CH05, GB48, IT01, IE05 and IE09, starting at 0:00h). Therefore temporal behaviour cannot be fairly evaluated, and just an overall and qualitative idea can be taken from time series included in next sections. Some statistics considering the accumulated wet deposition values were computed at each site.

7.1 NHx deposition

7.1.1 Wet Deposition

Maps showing WNHx accumulated during the 2009 intensive measurements period are presented in Figure 7.1. In an overall perspective, EMEP is clearly providing the highest deposition values. A quite good correlation is found between these maps and the wet deposition capability exposed in Figure 7.2 (crosses in the figure), with EMEP presenting the highest deposition capability (e.g. double as high as that from the rest of the models in Germany). The low capability observed in Figure 7.2 for MINNI could be related to the high TNH4 air concentration estimated by this model, with the largest positive bias (discussed in section 10).

Maps in Figure 7.1 also include accumulated WNHx observations in coloured circles. Just sites with less than 5 invalid measured values were included in the map, as well as in the bar plots presented in Figure 7.3 and Figure 7.4. As gaps of measurements were not filled, considering sites with more invalid measurements could have led to a false model overestimating map. The highest observed wet depositions were found at DE03, FR08 and FR14 (Figure 7.3 and Figure 7.4). At these sites all the models underestimate observations, with EMEP presenting the best performance. The highest efficiency of this model also leads to better results in terms of accumulated deposition in PL02, PL05, LT15 (in spite of a peak not captured by any model), RU18, RU20, SE14, FR09 and PT03. All the models strongly underestimate observations at some specific sites, namely BY04 (high values over this period not captured by any model; EMEP gives the best results, but still far from observations), RU13 or ES07. At this latter underestimation seems to be due to problems with modelled precipitation, highly underpredicted, as illustrated in Figure 7.6. In the Northern part of the domain, just CAMX and EMEP try to capture the peak around 22 mgN m^{-2} observed at NO01, as it can be inferred from Figure 7.5. Note that the time delay between observed and modelled values can drive to false results in terms of statistics, and thus these figures should be considered just in a qualitative way.

On the contrary, both maps in Figure 7.1 and bar diagrams in Figure 7.3 and Figure 7.4, suggest an overestimation of accumulated deposition by EMEP at AT48 (see also time series in the right side of Figure 7.5), AT02 (CHIM presents the best agreement), FR10, FR13, FR15 (CHIM overestimates even more), FR17 (CHIM overestimates even more), FR18 (CHIM overestimates even more), HU02, SI08, DEO2 (in spite of a punctual underestimation) and CH02 (also CHIM). All the models, with the exception of CMAQ, overestimate observed deposition at CH05, although this seems to be due to some periods with overestimated precipitation (rain is not overestimated in CMAQ). In Ireland, IE05 and IE09 sites are also overestimated by EMEP, as well as by CHIM. At these sites MINNI and LOTO provide the best results. The highest values of EMEP model, above 160 mgN m^{-2} over Northern Germany, Northern Italy and Austria (orange-red colour in the map of Figure 7.1) cannot be fairly evaluated, as there is no site over some of these areas to decide on EMEP behaviour, except AT48 site in Austria. At this site, as said before, the model seems to overestimate measured values.

Table 7.1 includes some statistics for WNHx, computed as the average of statistics at all sites. At each site the accumulated deposition value was considered. According to this table EMEP presents the lowest mean bias and LOTO the lowest RMSE values and better spatial correlation.

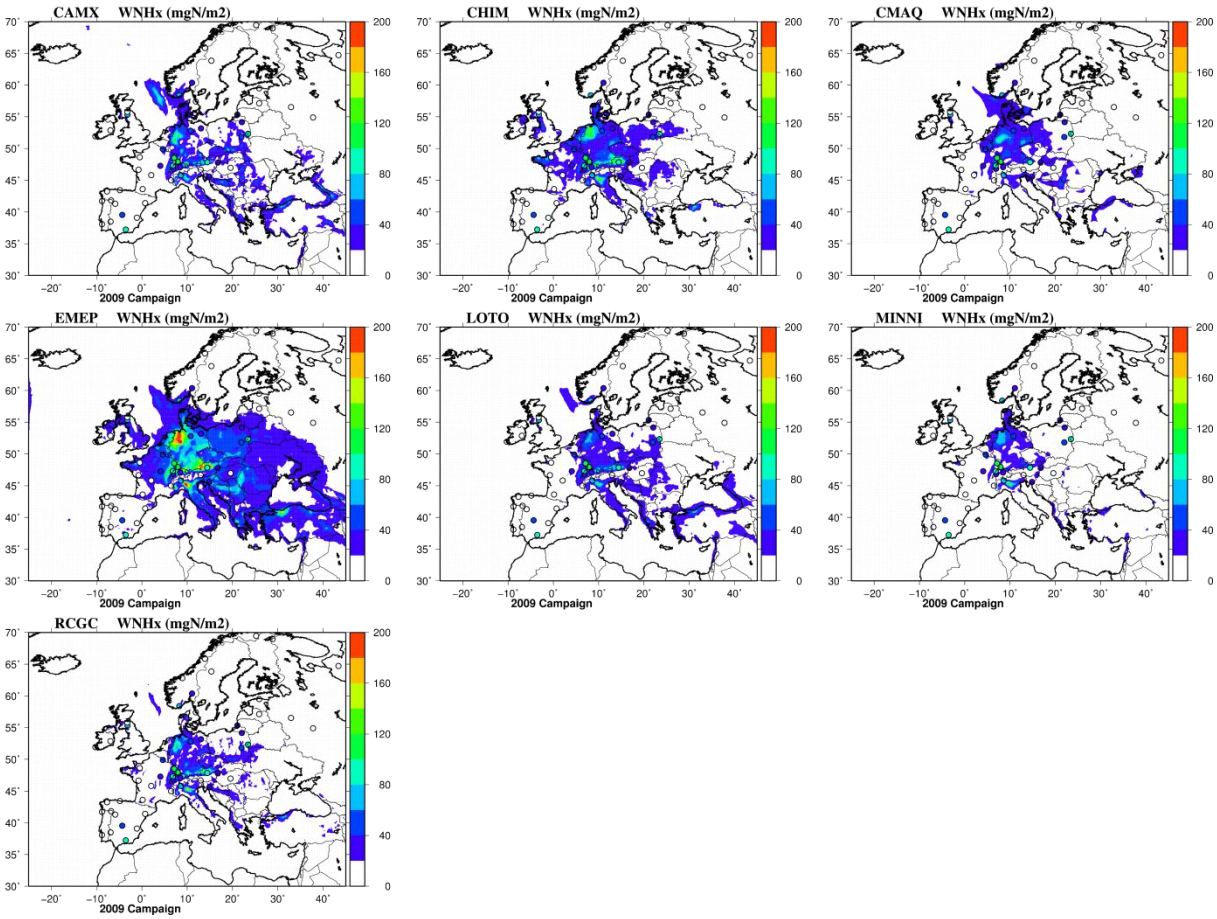

Figure 7.1: Accumulated NHx wet deposition over the 2009 intensive measurement period for all the models

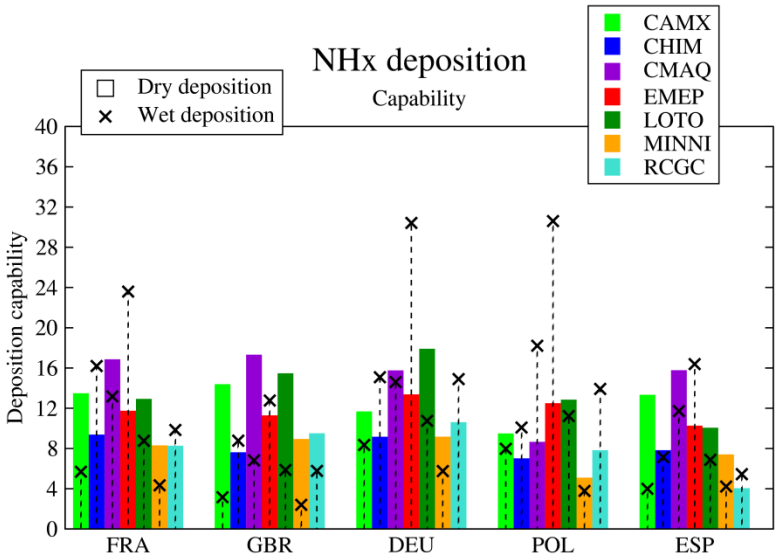

Figure 7.2: Model NHx deposition capability, estimated as Deposition/Concentration for dry deposition and Deposition/Concentration/Rain for wet deposition based on average variables over the 2009 campaign for five countries (France, Great Britain, Germany, Poland and Spain).

Table 7.1: Model evaluation for wet deposition. Correlations in space (Spat.*Cor.*), Biases (in mgN/m^2 or mgS/m^2) and Root Mean Square Errors in (*RMSE* in mgN/m^2 or mgS/m^2) are the average of statistics at all sites, considering for every site the accumulated deposition values. *Nsites* is the number of sites for a given variable. The best model performance in terms of RMSE is displayed in bold characters.

Pollutant	Obs	Model name	Model val.	Bias	Spat. Cor.	RMSE	Nsites
WNHx	31.3	CAMX	14.55	-16.76	0.71	28.9	37
		CHIM	22.68	-8.62	0.51	30.21	37
		CMAQ	11.94	-19.37	0.66	32.55	37
		EMEP	36.08	4.78	0.62	29.65	37
		LOTO	16.4	-14.9	0.72	**28.01**	37
		MINNI	9.27	-22.03	0.59	35.66	37
		RCGC	15.08	-16.22	0.62	30.52	37
WNOx	23.16	CAMX	8.32	-14.83	0.8	23.72	37
		CHIM	19.76	-3.39	0.78	**17.14**	37
		CMAQ	10.42	-12.74	0.81	21.93	37
		EMEP	18.16	-4.99	0.78	17.61	37
		LOTO	13.84	-9.32	0.84	18.83	37
		MINNI	3.73	-19.42	0.61	30.47	37
		RCGC	6.17	-16.99	0.8	27.31	37
WSOx	24.32	CAMX	12.2	-12.12	0.58	19.7	38
		CHIM	9.19	-15.13	0.37	23.38	38
		CMAQ	23.94	-0.38	0.69	**15.6**	38
		EMEP	22.62	-1.7	0.47	18.34	38
		LOTO	10.91	-13.41	0.54	21	38
		MINNI	6.05	-18.27	0.46	25.2	38
		RCGC	5.08	-19.24	0.47	26	38

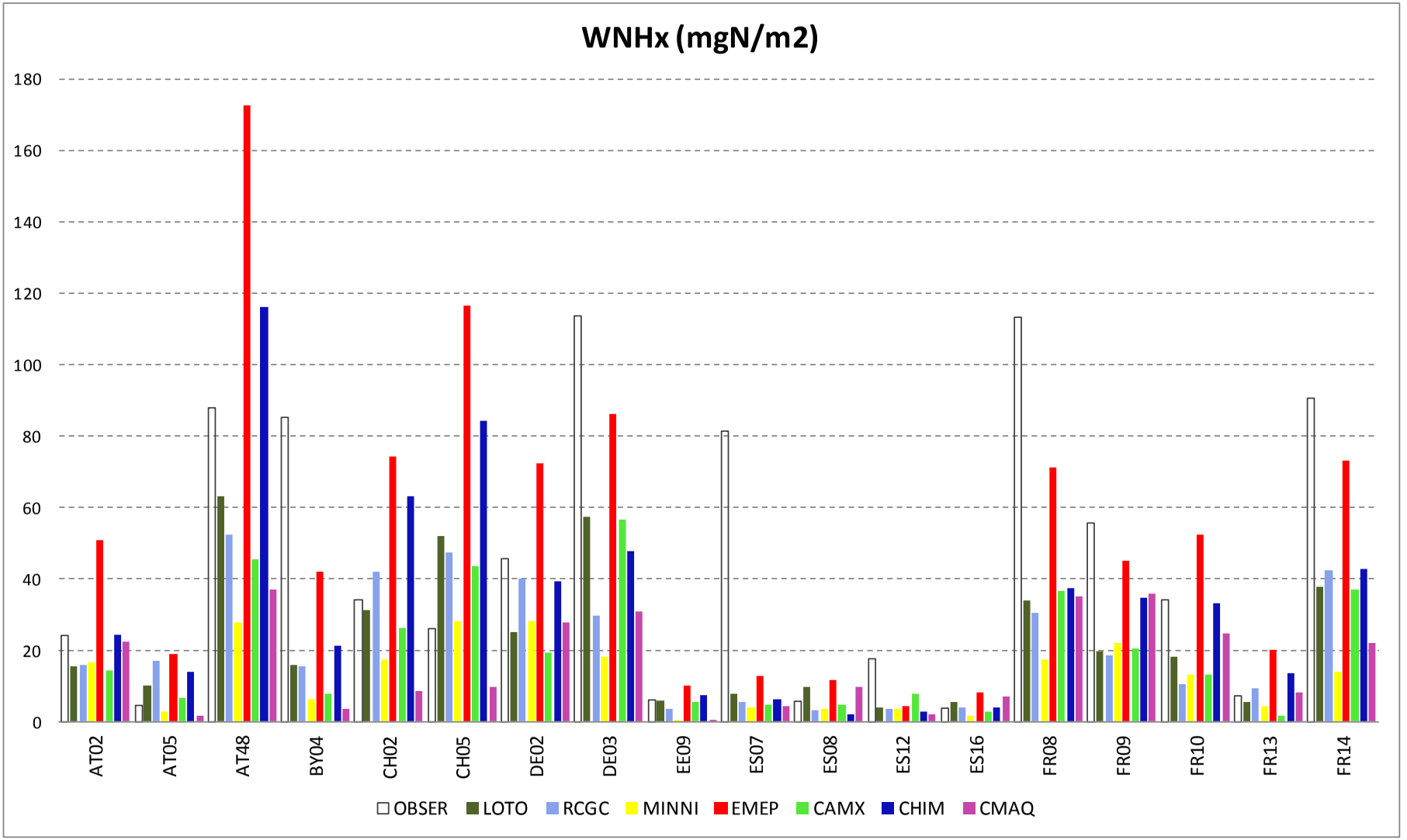

Figure 7.3: Observed and Modelled WNHx accumulated over the 2009 campaign for all the models (AT02-FR14)

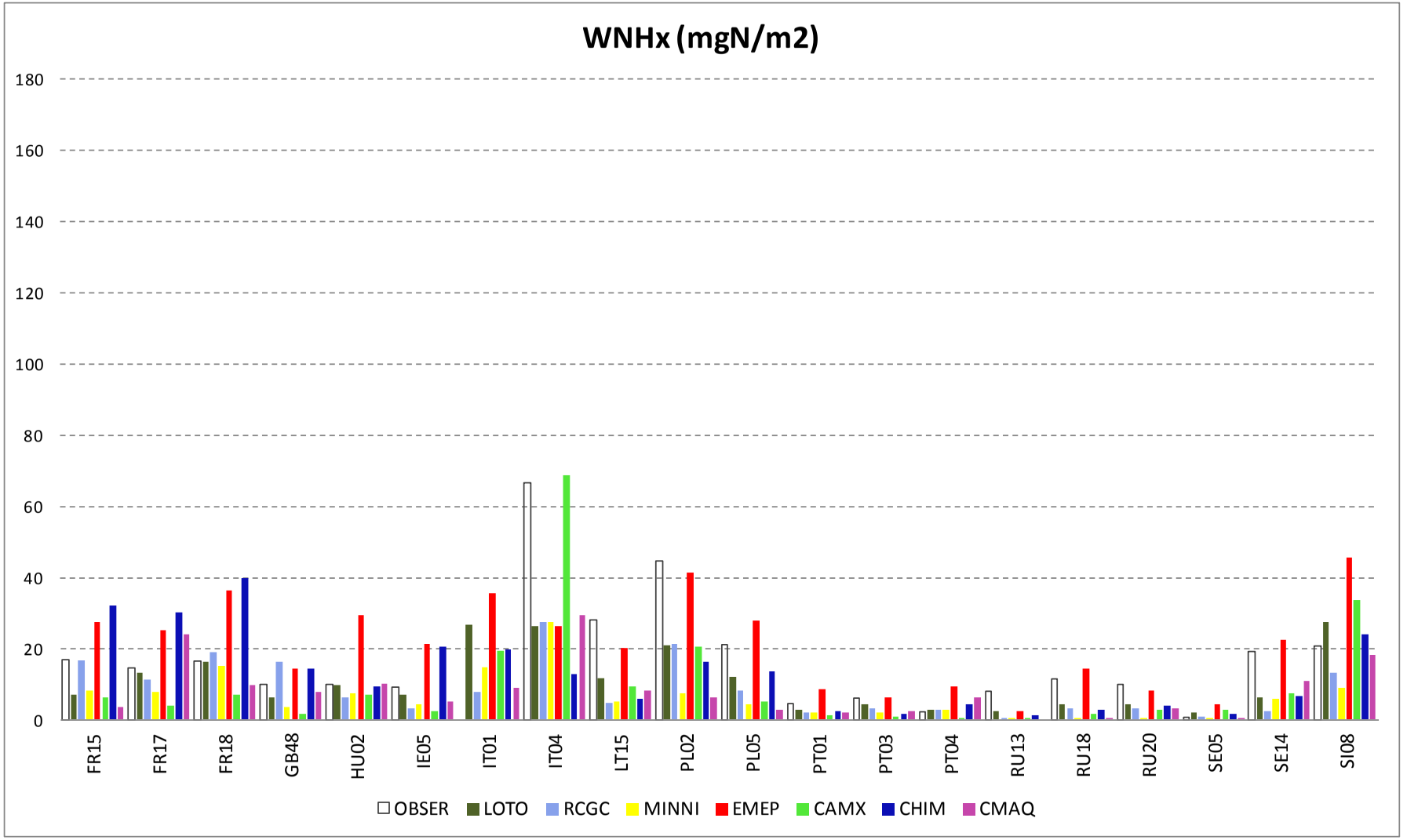

Figure 7.4: Observed and Modelled WNHx accumulated over the 2009 campaign for all the models (FR15- SI08)

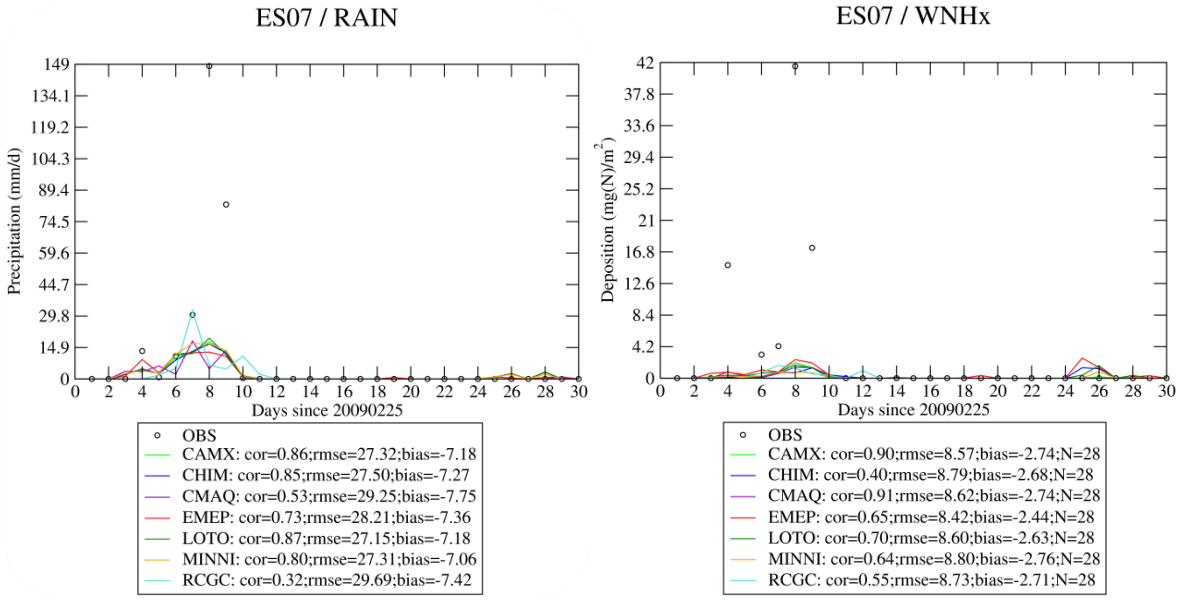

Figure 7.5: Time series showing precipitation and WNHx at ES07. Underestimation of WNHx correlates to the underestimation of rain.

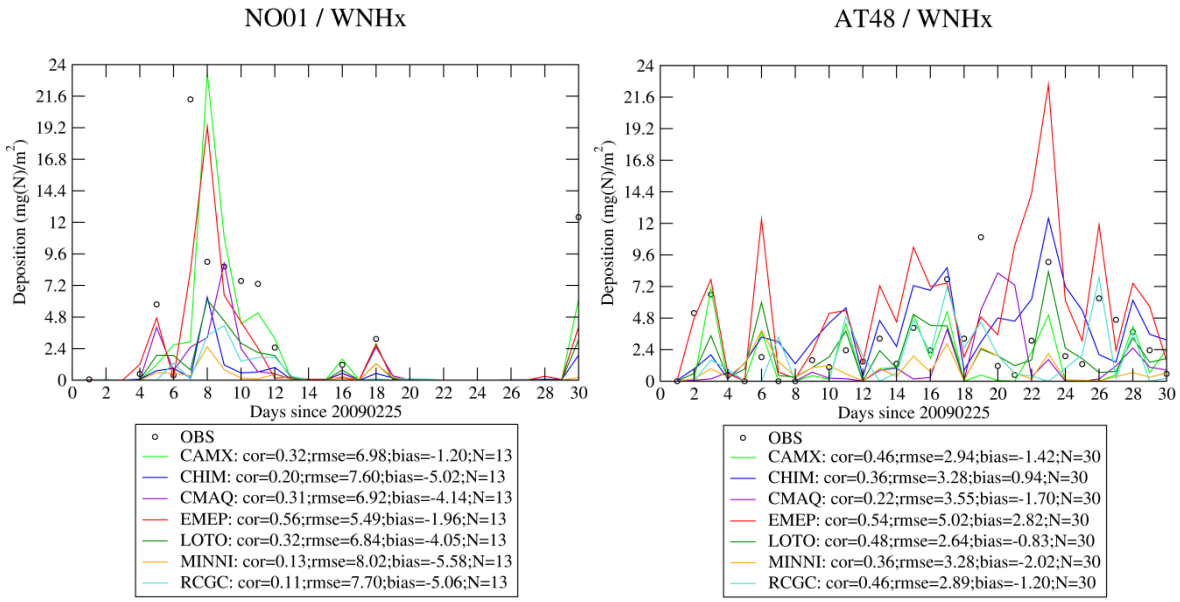

Figure 7.6: Time series of WNHx at a Norwegian (NO01) and Austrian (AT48) sites. Note that observed and modelled values present a time delay, and thus these graphics can also be used in a qualitative way.

7.1.2 Dry deposition

Model efficiency and deposition maps of DNHx deposition are presented in Figure 7.2 and Figure 7.7 respectively. CMAQ presents the highest model capability over some areas (France, Great Britain and Spain) and LOTO over Germany and Poland. Also CAMX and EMEP capability for DNHx is in the high range. No evaluation on model performance for this variable can be done due to the lack of measurements. All the models show the highest dry deposition on the North-western France area, North-western Germany and Northern Italy.

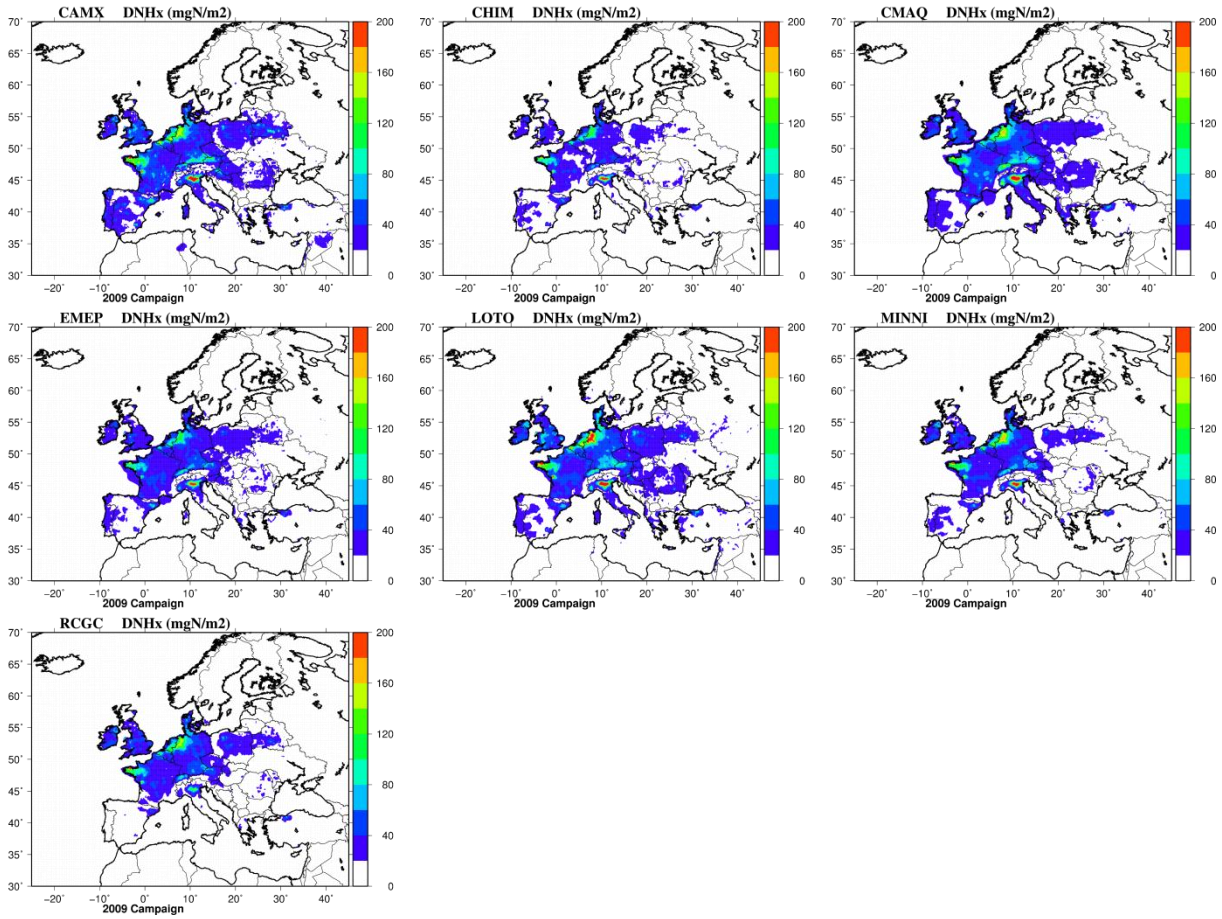

Figure 7.7: Accumulated DNHx over the 2009 campaign for all the models

7.2 NOx deposition

7.2.1 Wet Deposition

The WNOx maps (Figure 7.8) show that CHIM, EMEP and LOTO calculate higher deposition than the rest of models. This appears to correspond with the results for TNO3 air concentrations (see section 10), showing that MINNI, RCGC, CAMX and CMAQ strongly overestimate TNO3, whereas CHIM, EMEP and LOTO slightly underestimate it. In this case CHIM is the model with the highest deposition capability (Figure 7.9), although not over all the countries. For example, in Spain EMEP presents the highest deposition capability for this period. Differences between models in terms of this ratio are very significant; in Poland, differences between EMEP and MINNI achieve a factor of 6.

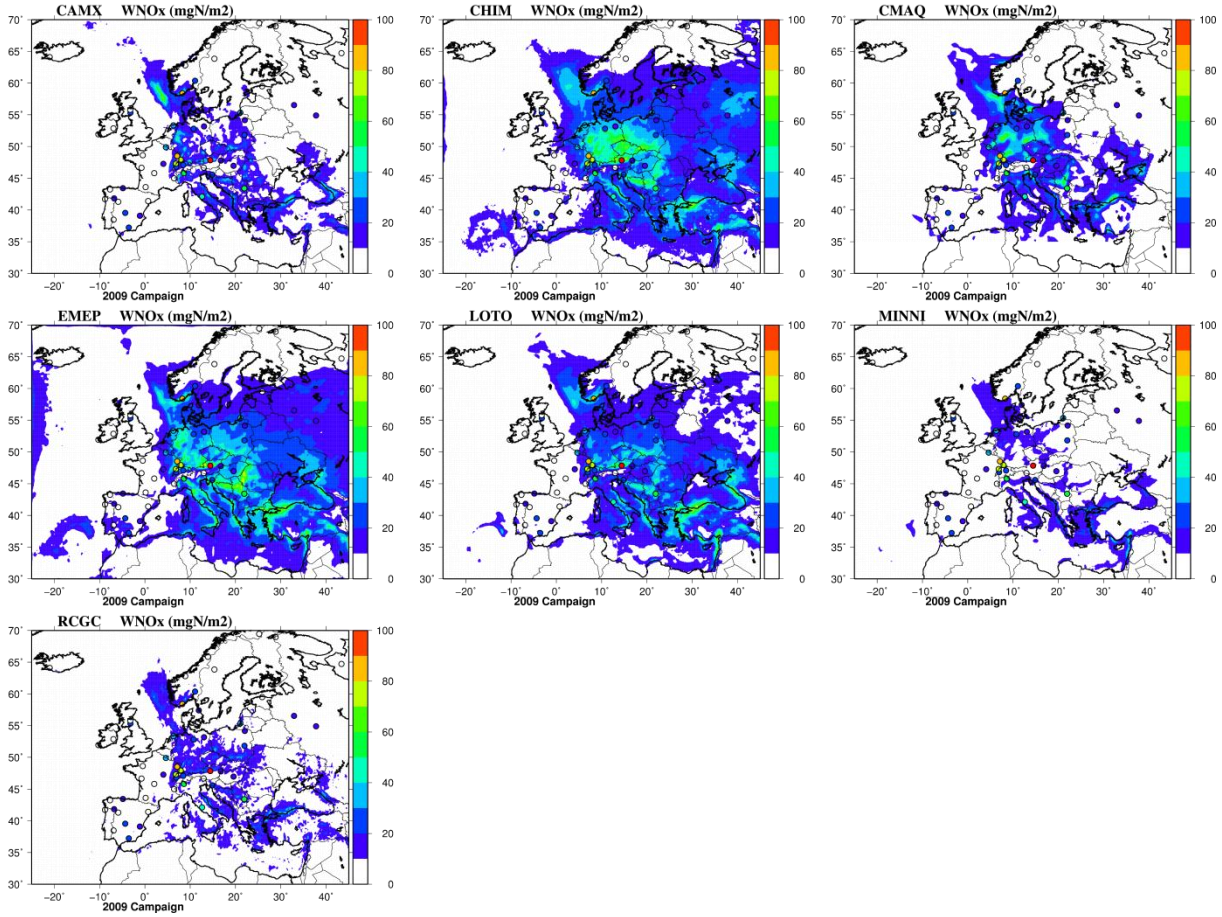

Figure 7.8: Accumulated NOx wet deposition over the 2009 campaign for all the models

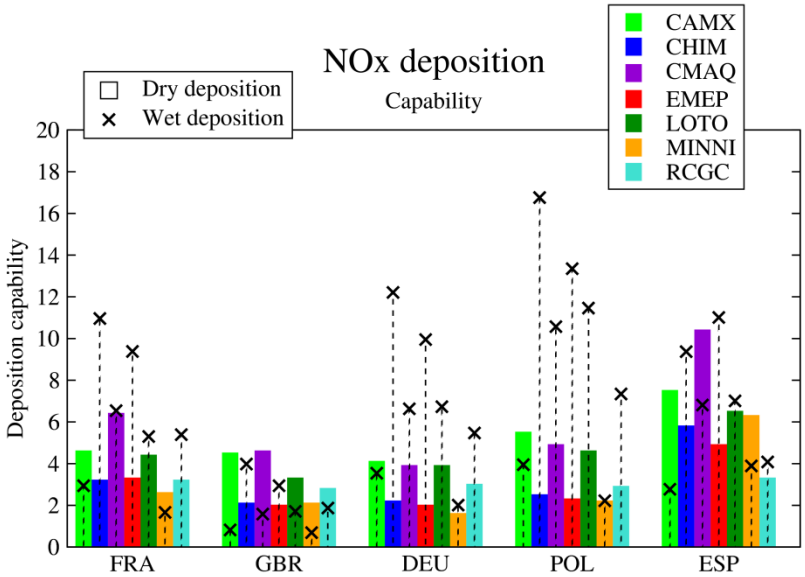

Figure 7.9: Model NOx deposition capability, estimated as Deposition/Concentration for dry deposition and Deposition/Concentration/Rain for wet deposition based on average variables over the 2009 campaign for five countries (France, Great Britain, Germany, Poland and Spain).

According to the maps in Figure 7.8 and to the bar diagram (Figure 7.11 and **Figure 7.12**) the higher values calculated by CHIM, EMEP and LOTO are in a better agreement with observations, although there is a general tendency to underpredict the highest accumulated wet depositions. In the central area, high values registered at FR08, FR14, DE03 and AT48 (see also time series in the right of Figure 7.10 for AT48) are not captured by any model, although spatial patterns of CHIM, EMEP and LOTO try

to represent a high-valued area encompassing these sites. Other sites in France (FR15), Spain (ES07, ES12), Italy (IT04), LT15 and RS05 are underestimated by all the models, although with important differences between them. Some of these underestimates (ES07, as discussed for WNHx) can be attributed to a strong rain underestimation. In Norway, just EMEP captures (a bit overestimates) the high daily values registered at NO01 (left graphic of Figure 7.10).

On the contrary, some sites are overestimated by CHIM and EMEP. CHIM overestimates AT02 (also EMEP), CH02, CH05 (also EMEP and LOTO), DE02, EE09 (also EMEP), RU18 or SI08 (EMEP even more). For the models in the low range, there is a considerable general underestimation. CAMX and CMAQ, although with also low deposition estimates, present higher variability than MINNI and RCGC, with values in the low range for some sites but others in the upper range.

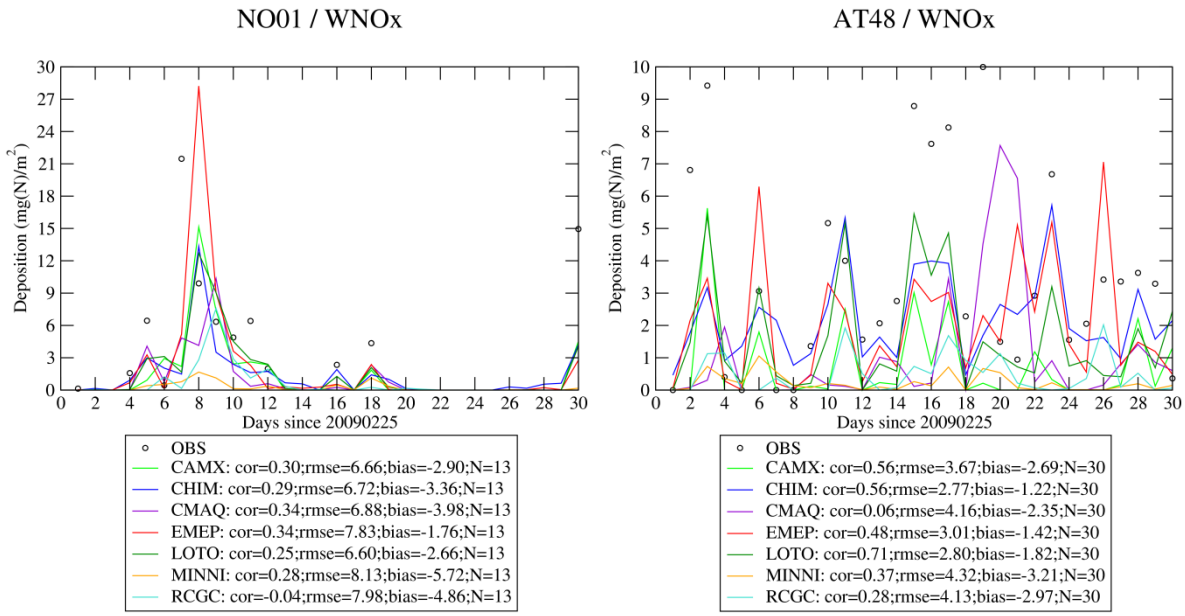

Figure 7.10: Time series showing WNOx at NO01 (left) and AT48 (right)

Results in Table 7.1 confirm the lowest bias and RMSE for CHIM, followed by EMEP and LOTO.

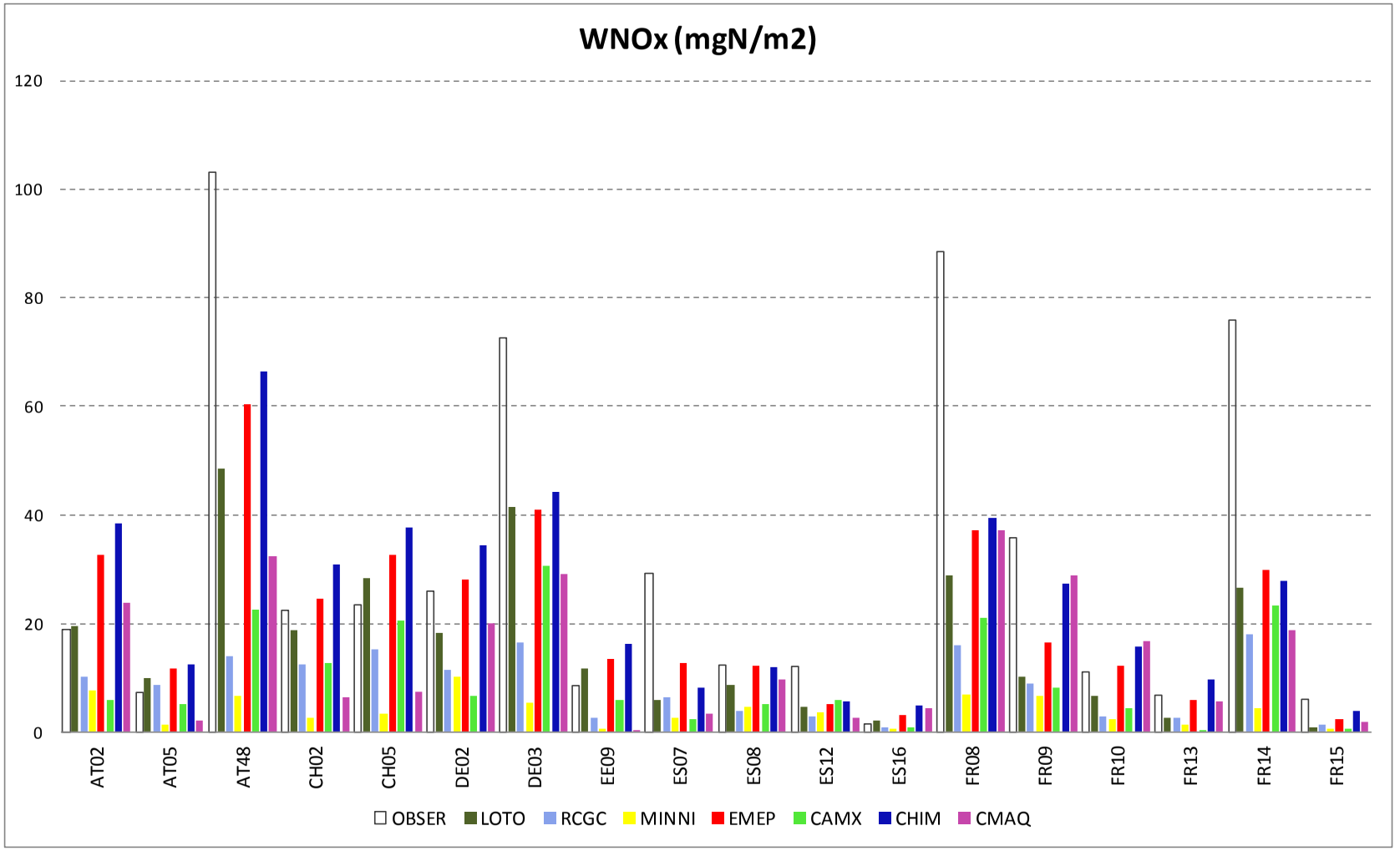

Figure 7.11: Observed and Modelled WNOx accumulated over the 2009 campaign for all the models (AT02-FR15)

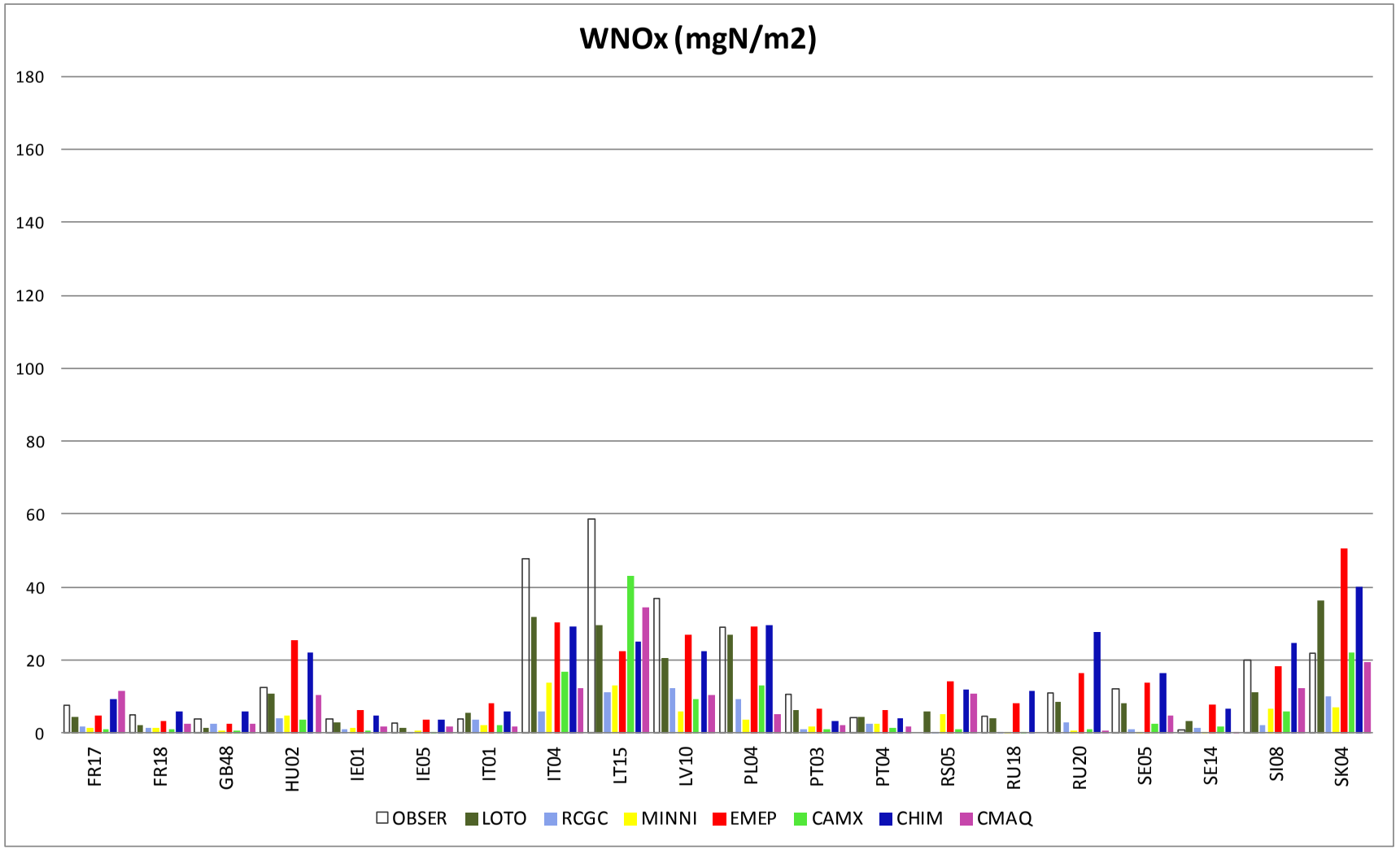

Figure 7.12: Observed and Modelled WNOx accumulated over the 2009 campaign for all the models (FR17-SK04)

7.2.2 Dry deposition

There are strong differences between models regarding dry deposition (Figure 7.13). For this pollutant CMAQ provides the highest deposition over the Mediterranean area and the eastern part of the domain. For the rest of models, CAMX, LOTO and MINNI present higher DNOx than CHIM, EMEP and RCGC. In terms of deposition capability CMAQ, CAMX and LOTO are the most efficient models. The strong differences in DNOx between CMAQ, CAMX/LOTO/MINNI group and CHIM/RCGC/EMEP group, make it necessary to obtain any kind of measurement to evaluate model behaviour for dry deposition processes.

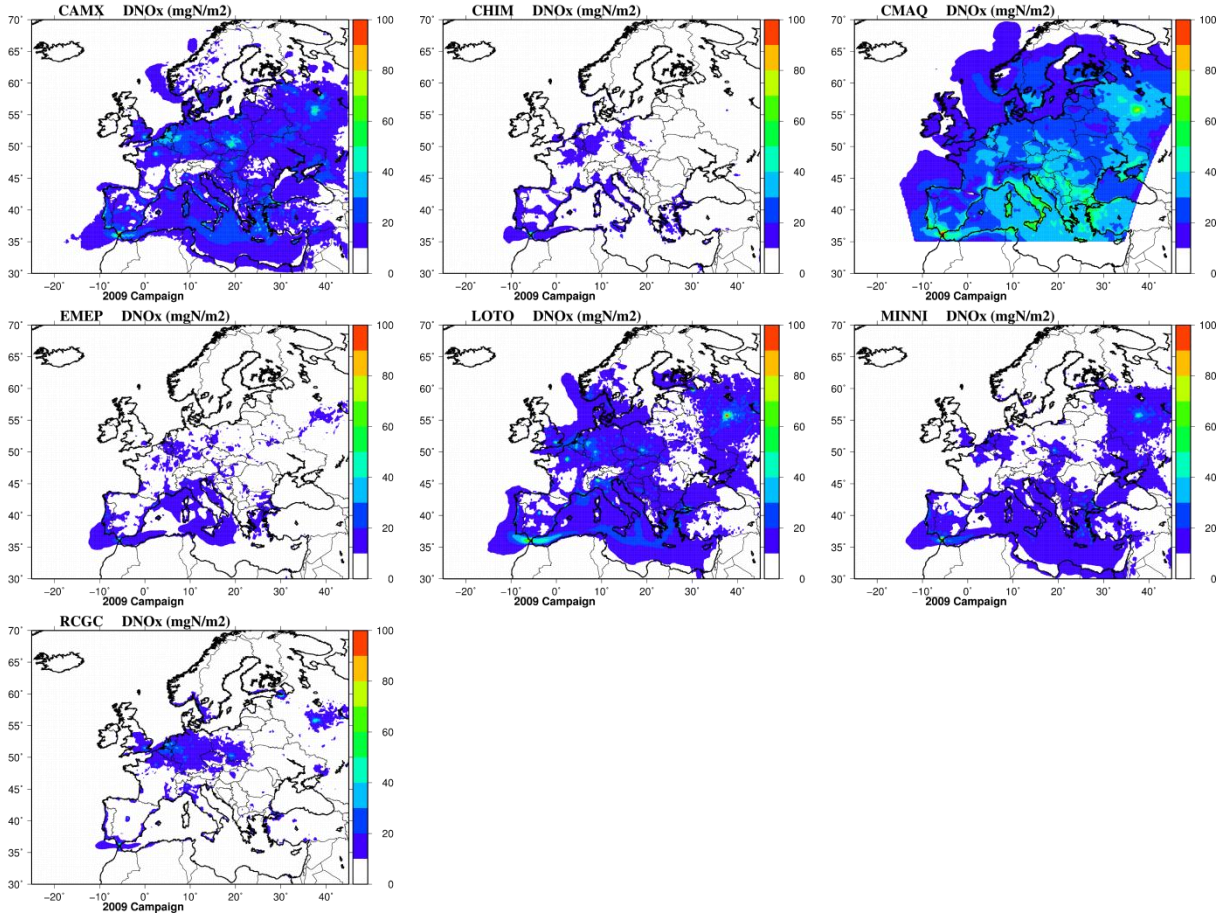

Figure 7.13: Accumulated DNOx deposition over the 2009 campaign for all the models

7.3 SOx deposition

7.3.1 Wet Deposition

For the evaluation of model performance regarding WSOx it is important to remark that the measurements of sulphur concentrations in precipitation used in this work were those not corrected for sea salt sulphate. Among the models, only CMAQ considers sulphate contribution from sea salt.
In this case, CMAQ present the highest “wet deposition capability” at Atlantic countries (Spain, Great Britain and France), followed by EMEP, whose capability for WSOx is the highest in Germany or Poland. RCGC presents the lowest WSOx capabilty, as it can be seen in Figure 7.14. As for WNHx, differences between models are also high for this parameter, especially over some countries.

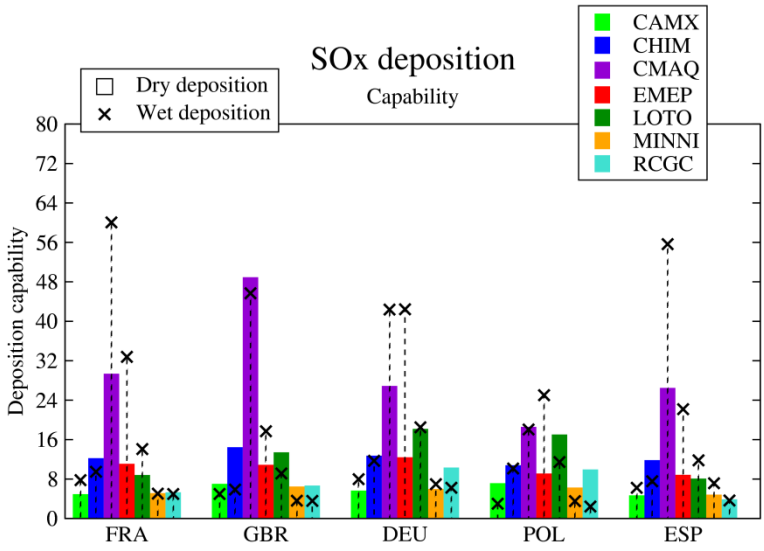

Figure 7.14: Model SOx deposition capability, estimated as Deposition/Concentration for dry deposition and Deposition/Concentration/Rain for wet deposition, based on average variables over the 2009 campaign for five countries (France, Great Britain, Germany, Poland and Spain).

Important differences in the spatial WSOx pattern are observed between the two models with the higher deposition capability, that is, CMAQ and EMEP. Also, there are strong differences with the rest of models. Unfortunately, there is an insufficient number and uneven distribution of monitoring sites, which makes it difficult to decide on model performance in some areas of Europe. For example, in the eastern part of the domain there is no observation, and maps for EMEP display much more deposition than the rest of the models.

Where observations available, CMAQ is providing the best performance for the highest observed values (bar diagram in Figure 7.17 and Figure 7.18) most of them registered at the Atlantic area (ES08, Figure 7.17). This fact seems to be related to the natural SO_4^{2-} emissions associated to sea salt processes that this model considers. On the contrary, this model presents some overestimation at certain sites over this area (FR17, FR10, ES16 or GB48), as well as at DE02 (Figure 7.17) where also EMEP is overestimating observations. This latter also shows some overestimation at HU02. In general, as illustrated in Table 7.1, CMAQ present the best performance, with the lowest bias and RMSE, followed by EMEP, and the highest spatial correlation. The rest of models present a general and significant underestimation at most of the sites.

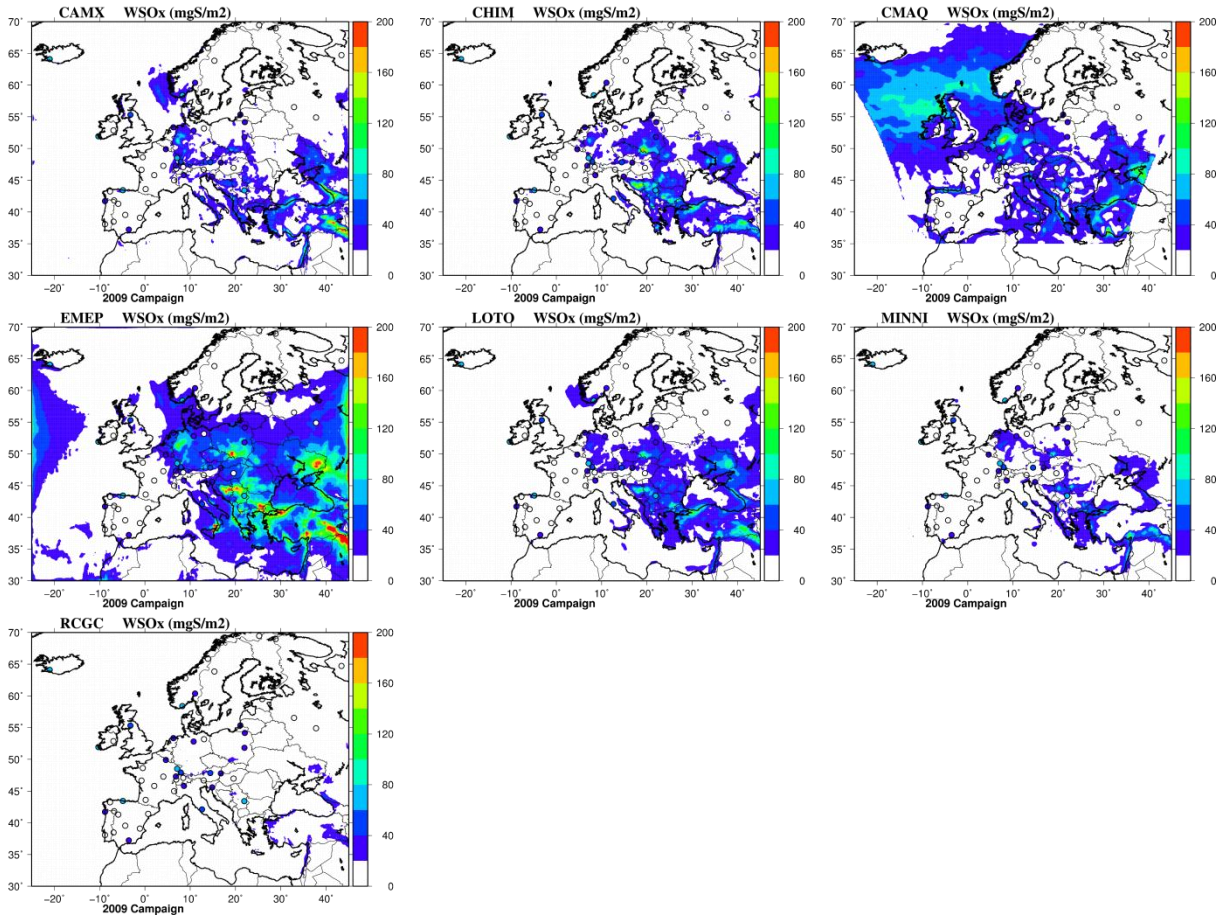

Figure 7.15: Accumulated SOx wet deposition over the 2009 campaign for all the models

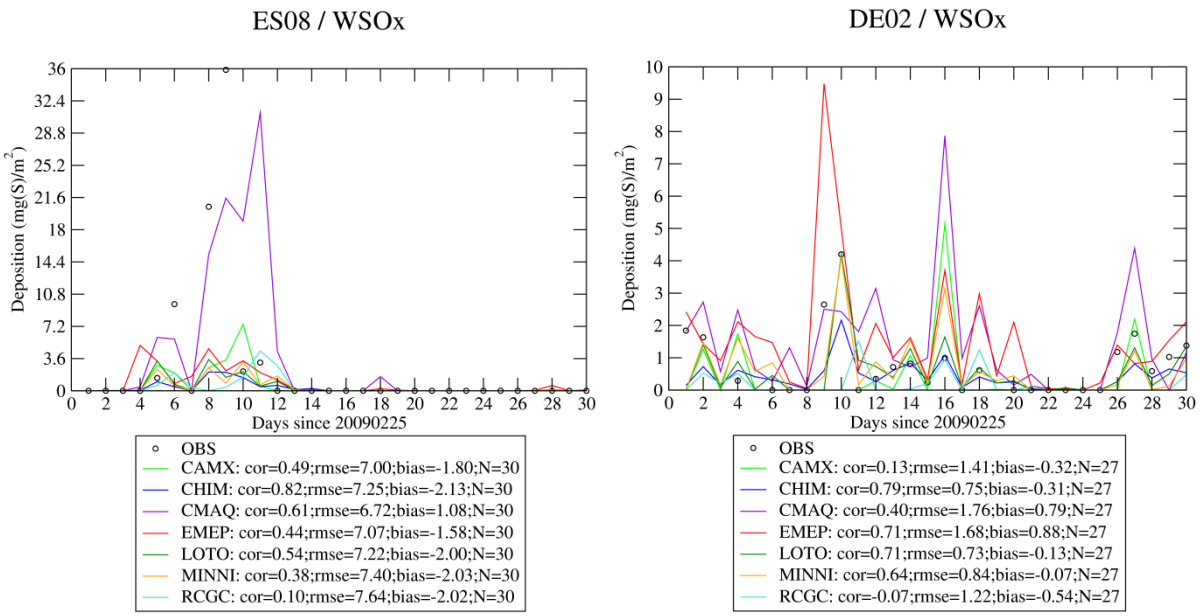

Figure 7.16: Time series showing modelled and observed WSOx over the 2009 campaign at AT48 (left) and DE02 (right)

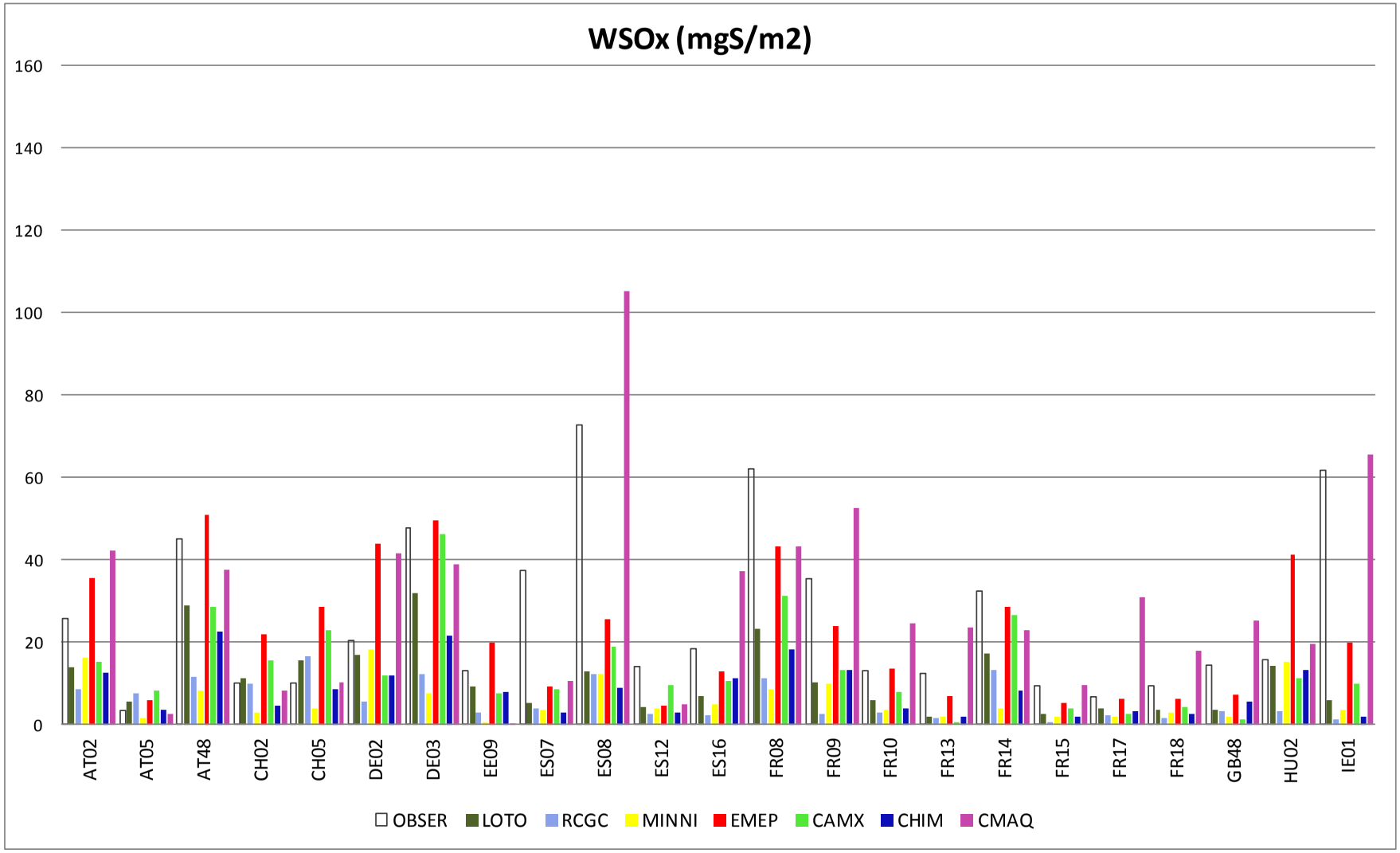

Figure 7.17: Observed and Modelled WSOx accumulated over the 2009 campaign for all the models (AT02-IE01)

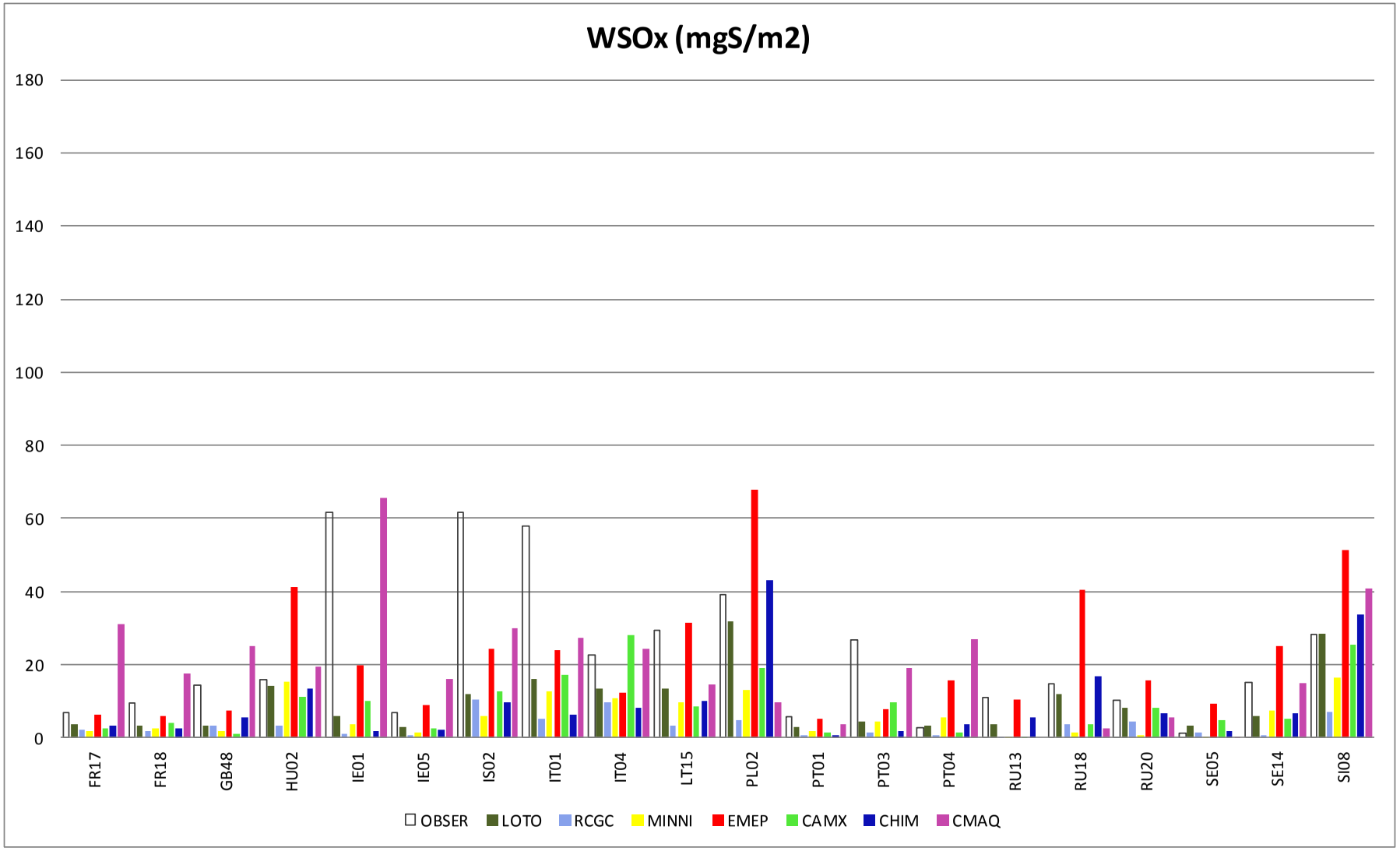

Figure 7.18: Observed and Modelled WSOx accumulated over the 2009 campaign for all the models (FR17-SI08)

7.3.2 Dry deposition

For DSOx, CMAQ is estimating the highest values (Figure 7.19). Strong differences can be observed between models, with EMEP and MINNI with the lowest values. The importance of having any kind of methodology to evaluate dry deposition is clear, in the light of the results shown in these figures.

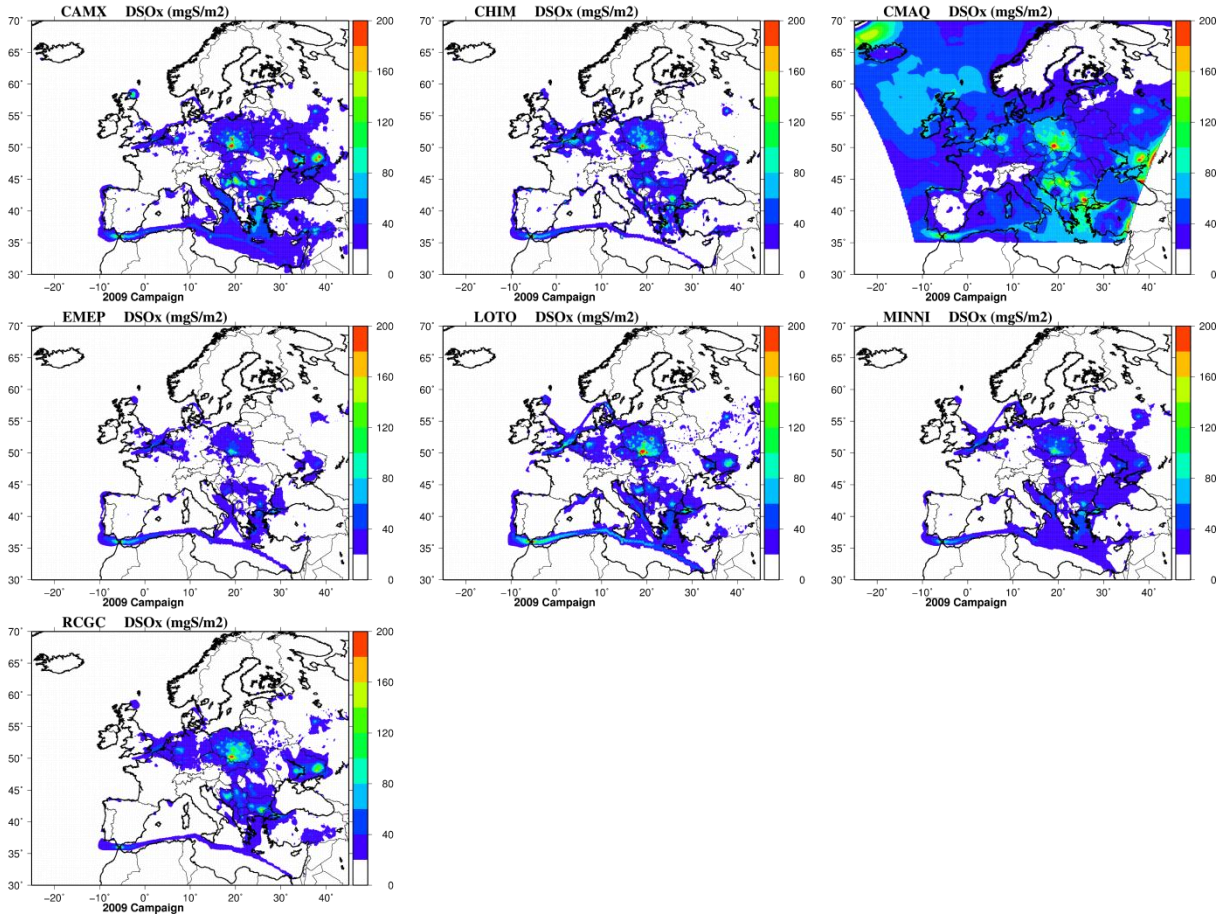

Figure 7.19: Accumulated SOx dry deposition over the 2009 campaign for all the models

8 Evaluation of Carbonaceous compounds

8.1 Elemental carbon

Elemental carbon in the $PM_{2.5}$ fraction (particle diameter <2.5 µm as EC-25) is underestimated by most models, particularly EMEP and CMAQ. EC-10 concentrations are globally overestimated by the models by up to 50-60% for CHIM, RCGC and MINNI, only EMEP has a null bias. Elemental carbon is a non-reactive species we can track in the models, the discrepancies can be due to problems with deposition, transport /mixing or emissions. The negative bias of EMEP for EC-25 is also coherent with overestimates of the PBL.

The statistic evaluation between EC-25 and EC-10 is performed on different groups of stations. In Figure 8.1, a coherent behaviour of models can be observed in the Melpitz station (DE44) with a quite well reproduction of the time variability. In Melpitz, 14% of the EC is in the coarse fraction (between 2.5 and 10 µm) according to the observations; the coarse EC fractions is 0%, 0%, 13%, 16%, 17%, 22% and 23% for MINNI, CMAQ, CHIM, RCGC, LOTO, CAMX and EMEP respectively. The exaggerated coarse EC fraction by EMEP and CAMX might be due to too efficient removal of fine EC, whilst too slow removal of the coarse EC.

At ES09 station (Campisabalos) the EC ratio in the coarse fraction is 12% while the models predict a value in the range 0 – 4.6 %. At this station EMEP predicts rather well the average concentrations either for the fine and coarse fractions while the other models slightly overestimate the EC concentrations.

Table 8.1: Model evaluation for EC-25, EC-10 concentrations (µg m^{-3}). Correlations in time and space (*Cor.*), Biases (in µg m^{-3}) and Root Mean Square Errors in (*RMSE in* µg m^{-3}) are computed for the whole 2009 campaign based on daily values. Observation values (*Obs.* in µg m^{-3}) and model values (in µg m^{-3}) are the average concentrations for the 2009 campaign. *Nb* is the number of available observations for a given pollutant. The best model performance for the RMSE is displayed in bold characters.

Pollutant	Obs.	Model name	Model val.	Bias	Cor.	RMSE	Nb.
EC-10	0.40	CAMX	0.57	0.17	0.84	0.32	123
		CHIM	0.63	0.23	0.84	0.38	
		CMAQ	0.49	0.09	0.80	0.32	
		EMEP	0.40	0.00	0.84	**0.22**	
		LOTO	0.56	0.16	0.82	0.31	
		MINNI	0.59	0.20	0.84	0.30	
		RCGC	0.68	0.28	0.74	0.50	
EC-25	0.95	CAMX	0.74	-0.21	0.42	1.19	91
		CHIM	0.94	-0.01	0.51	**1.11**	
		CMAQ	0.87	-0.08	0.34	1.35	
		EMEP	0.50	-0.45	0.46	1.25	
		LOTO	0.84	-0.10	0.49	1.13	
		MINNI	0.86	-0.09	0.35	1.22	
		RCGC	0.77	-0.18	0.22	1.30	

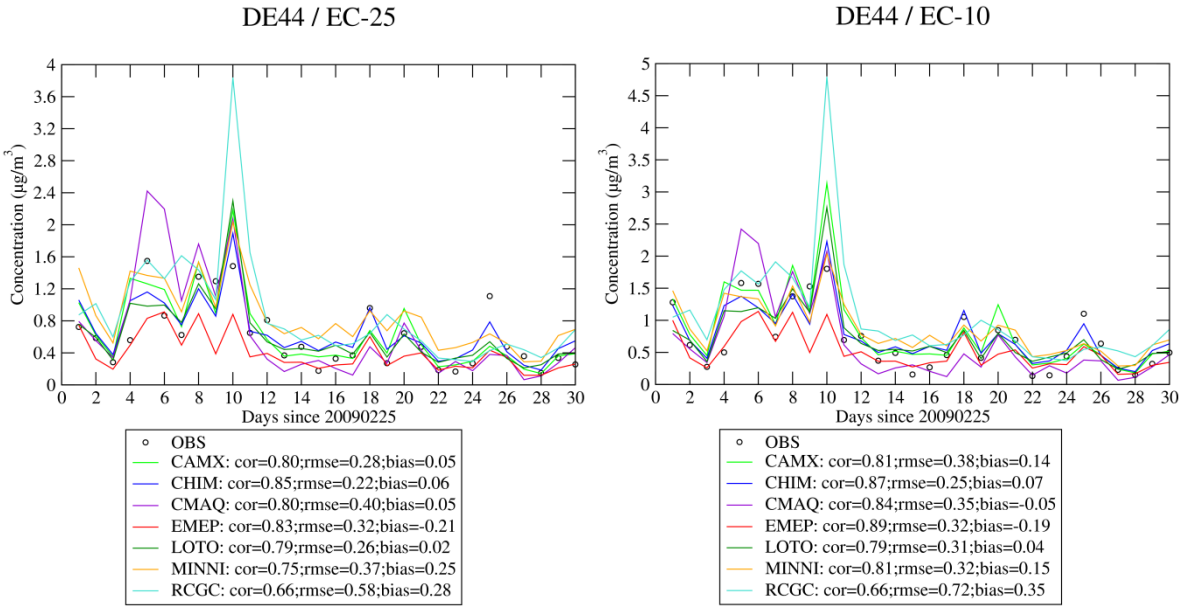

Figure 8.1: Daily time series of Elemental Carbon concentrations in the $PM_{2.5}$ and PM_{10} fractions in Melpitz (DE44, Germany)

EC-25 is considered as an inert chemical component originating from anthropogenic primary PM emissions notably from combustion sources. This species makes possible to evaluate the ability of models to simulate an urban signal over populated areas. Figure 8.2 is an average diurnal cycle for Germany and Poland of the ratio defined as $\frac{C_{pop}-C_{non\,pop}}{C_{non\,pop}}$ (a proxy for gradients between populated and background areas), $\frac{C_{pop}-C_{non\,pop}}{C_{non\,pop}}$ where for a given country C_{pop} is the population weighted concentrations and C_{nonpop} is the non weighted concentrations. We notice that all models are able to reproduce a positive signal from densely populated regions to remote places. This signal is more pronounced during the morning and afternoon emission peaks. The EC gradient values are very different from country to country. CHIM, EMEP and LOTO have the highest gradients; CMAQ exhibits the lowest gradients meaning that concentrations are not so different between rural and urban areas. MINNI, RCGC and CAMX are in between.

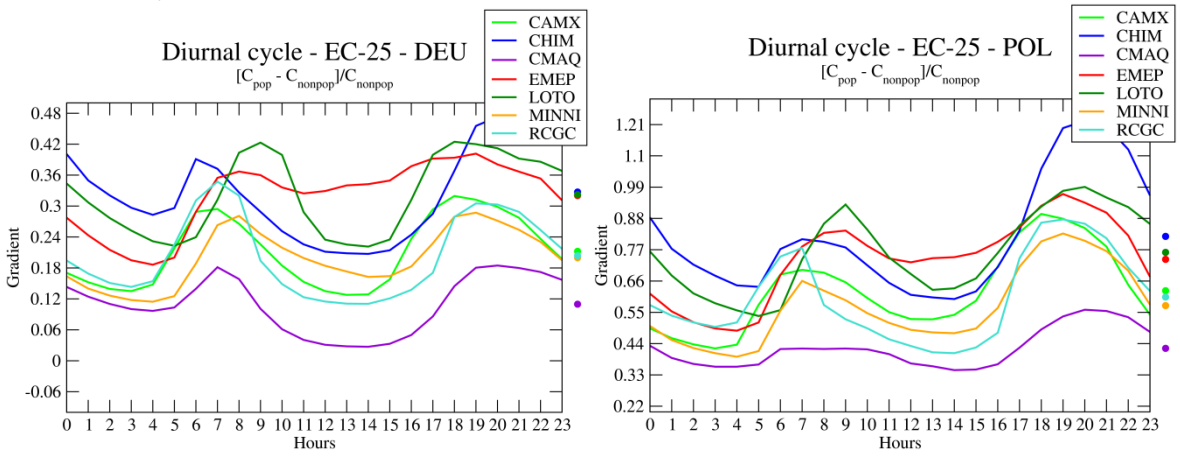

Figure 8.2: Gradient of EC-25 concentrations between populated and background area for Germany (left) and Poland (right)

8.2 Organic matter

8.2.1 Secondary and primary organic aerosols

The total organic matter concentrations are dominated by the primary emitted organics over large emitting areas (central Europe, Balkan countries, and major urbanized / industrialized areas) as shown in Figure 8.3. As the SOA schemes are very different in the models, the secondary fractions are quite different, however all the models show that this fraction is higher in remote areas. EMEP and CHIM gives higher SOA fraction near the borders of the domain mainly because a large fraction of OM issued from the boundary conditions is allocated to SOA species in the regional models. In the EMEP model, OC boundary conditions from the MACCA dataset has been calculated as a separate component and added in a proportion 50%/50% to TPOM and SOA concentrations in the post-processing. This was done in order to avoid too complicated model modifications. CMAQ displays low levels of SOA fractions in the rang 10-20% on the north of the domain. Relatively higher levels of SOA in the EMEP results can partly be explained by a constant background value of 0.5 µgC m^{-3} applied in the model.

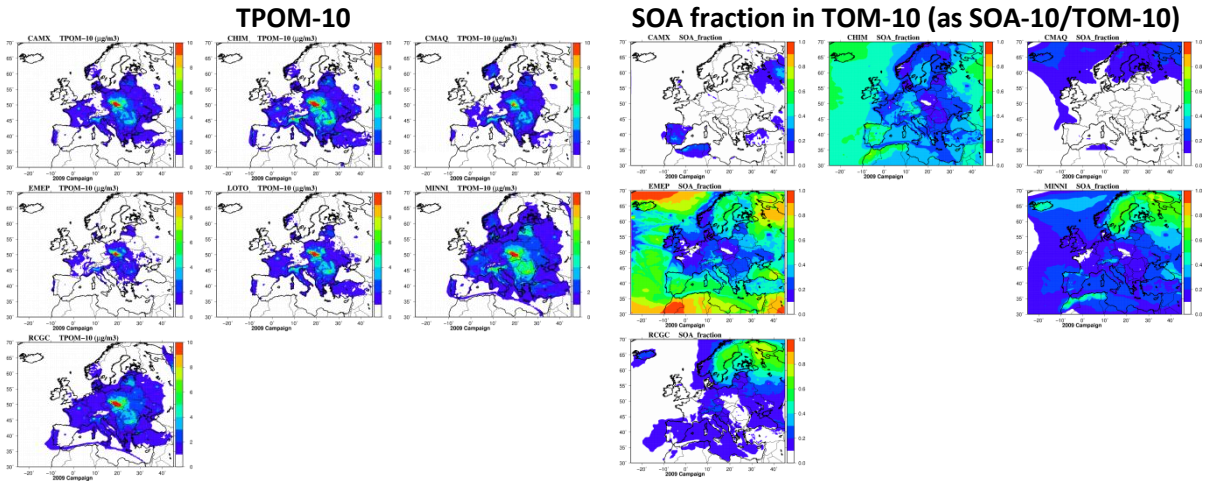

Figure 8.3: Average Total primary organic matter concentrations (left panel) and secondary fraction of organic aerosols (right panel) in the PM_{10} fraction over the 2009 campaign period for all models.

The anthropogenic modelled SOA is generally low; models simulate concentrations less than 1 µg m^{-3}, with CAMX and CMAQ calculating specially low anthropogenic SOA concentrations. MINNI simulates high concentrations in the Eastern countries, whilst EMEP gives higher concentrations over the Mediterranean Sea (probably from shipping and southern boundary conditions). CHIM, MINNI and EMEP have a specific hot spot pattern over the north of Italy (Figure 8.4).

The contribution of Biogenic SOA is high in Scandinavia and Finland for MINNI and RCGC causing high SOA concentrations in those regions. CHIM and EMEP calculate quite similar spatial patterns of both anthropogenic and biogenic SOA. CHIM, EMEP and MINNI give higher biogenic SOA concentrations, whereas CAMX and CMAQ simulate rather low BSOA concentrations everywhere.

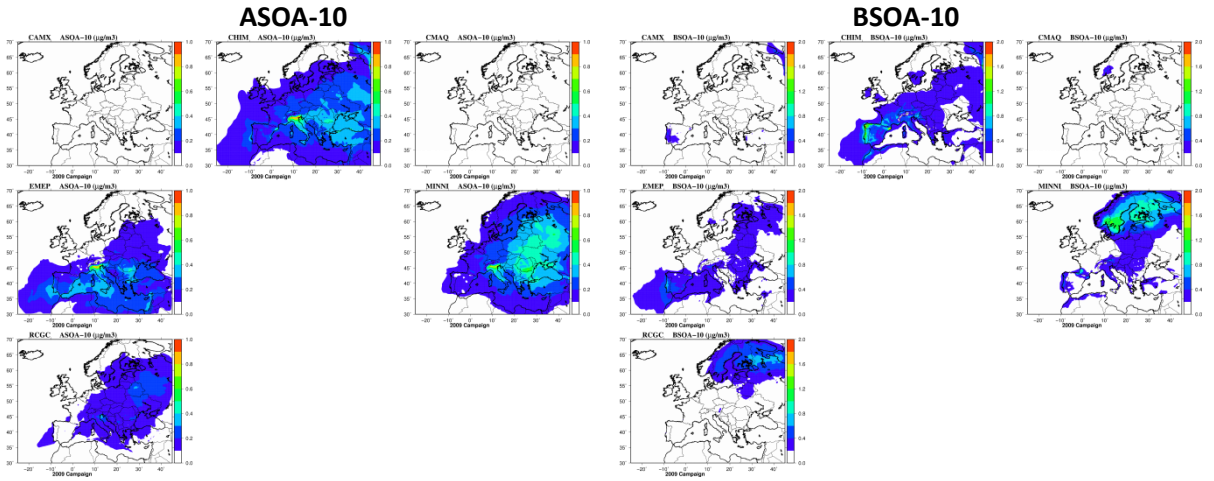

Figure 8.4: Average anthropogenic (left panel) and biogenic (right panel) secondary organic aerosol concentrations (in µg m^{-3}) over the 2009 campaign period for all models.

8.2.2 Total organic matter

Very few measurements were available during the 2009 campaign, but different types of measurement provide coherent results reported in Table 8.2. Models provide Organic matter (OM) whilst observational can be either organic matter or organic carbon (OC), in the latter case OC is multiplied by 1.6 to be converted in OM.

On average, all models underestimate the measured total organic matter concentrations in both fine and coarse fractions. MINNI and CHIM seem to have the lowest negative bias. For daily TOM-25 concentrations, correlations are close to 0.4 for daily values (and better for hourly values) for most of models except RCGC that displays a correlation of 0.27.

Table 8.2: Model evaluation for TOM-25 and TOM-10 concentrations (µg m^{-3}). Correlations in time and space (*Cor.*), Biases (in µg m^{-3}) and Root Mean Square Errors in (*RMSE in* µg m^{-3}) are computed for the whole 2009 campaign based on daily values (left table) and hourly values (right table). Observation values (*Obs.* in µg m^{-3}) and model values (in µg m^{-3}) are the average concentrations for the 2009 campaign. *Nb* is the number of available observations for a given pollutant. The best model performance for the RMSE is displayed in bold character.

Daily basis

Pollutant	Obs.	Model name	Model val.	Bias	Cor.	RMSE	Nb.
TOM-25	5.53	CAMX	1.22	-4.31	0.40	13.60	183
		CHIM	2.11	-3.43	0.40	**13.10**	
		CMAQ	1.42	-4.12	0.36	13.34	
		EMEP	1.09	-4.44	0.39	13.67	
		LOTO	1.25	-4.29	0.39	13.55	
		MINNI	2.70	-2.84	0.33	13.10	
		RCGC	1.53	-4.01	0.27	13.66	
TOM-10	2.91	CAMX	0.80	-2.11	0.65	2.57	123
		CHIM	1.26	-1.66	0.71	**2.12**	
		CMAQ	0.67	-2.24	0.57	2.71	
		EMEP	0.66	-2.26	0.72	2.70	
		LOTO	0.65	-2.26	0.63	2.73	
		MINNI	1.64	-1.27	0.39	2.12	
		RCGC	1.13	-1.78	0.50	2.38	

Hourly basis

Pollutant	Obs.	Model name	Model val.	Bias	Cor.	RMSE	Nb.
TOM-25	2.61	CAMX	0.93	-1.68	0.62	2.71	3065
		CHIM	1.42	-1.19	0.65	2.31	
		CMAQ	0.98	-1.63	0.59	2.62	
		EMEP	0.82	-1.79	0.55	2.83	
		LOTO	0.79	-1.82	0.47	2.90	
		MINNI	2.30	-0.31	0.50	**2.20**	
		RCGC	1.41	-1.20	0.47	2.52	
TOM-10	ND	CAMX	ND	ND	ND	ND	ND
		CHIM	ND	ND	ND	ND	
		CMAQ	ND	ND	ND	ND	
		EMEP	ND	ND	ND	ND	
		LOTO	ND	ND	ND	ND	
		MINNI	ND	ND	ND	ND	
		RCGC	ND	ND	ND	ND	

The models display similar geographical patterns with higher concentrations in Poland, Central Europe up to the Balkans countries and Romania (Figure 8.5). The north of Italy and large cities exhibit high concentrations, the high values in Ispra station (IT04, Italy) are not reproduced by the models; this could be related to a combination of emissions patterns and circulation features in the pre-Alpine area and the nearby Po Valley that are difficult to capture at the modelled resolution. In Germany, Spain and Sweden concentrations are very low that is coherent with low PM emissions compared to the other countries (particularly for SNAP2 emissions). As previously mentioned MINNI

and CHIM provide the highest concentrations values. The high values displayed for MINNI can partly be due to the low PBL used by the model as shown in section 6.5. CHIM provides higher values because of higher SOA concentrations both anthropogenic and biogenic fractions.

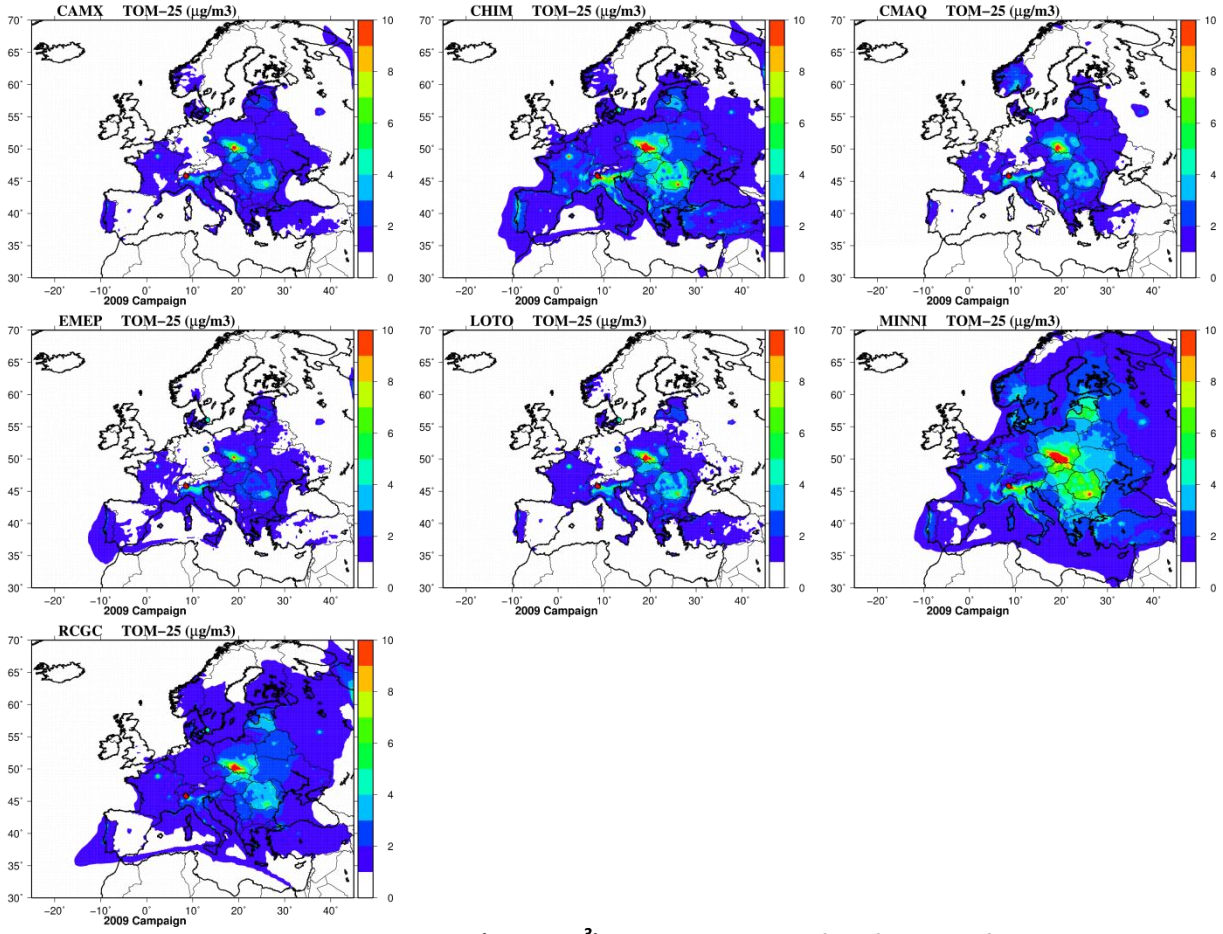

Figure 8.5: Average Total organic matter (in µg m^{-3}) concentrations in fine fraction of PM over the 2009 campaign period for all the models. The colour circles are the observed values at EMEP sites.

The diurnal cycles of the Total organic matter is displayed in Figure 8.6. For stations SE11 and DE44 high concentrations are usually found at night with a significant decrease in the afternoon. This behaviour is well reproduced by all models but with a negative bias for models except MINNI as previously explained and confirmed by the statistics. The cycle is rather flat in station GR02 in the observations, a slight increase is observed at night; the models capture this observed flat profile but a small peak is simulated in the morning by CHIM, LOTO, RCGC and MINNI. For the Payerne station (CH02) two peaks are observed in the measurements, a first one at 09:00 and a second around midnight. Whereas the midnight peak is captured by the models, the first peak is not very well simulated, a slight increase is observed but earlier in the morning at 06:00 – 07:00. Only LOTO seems to have a small signal at 09:00.

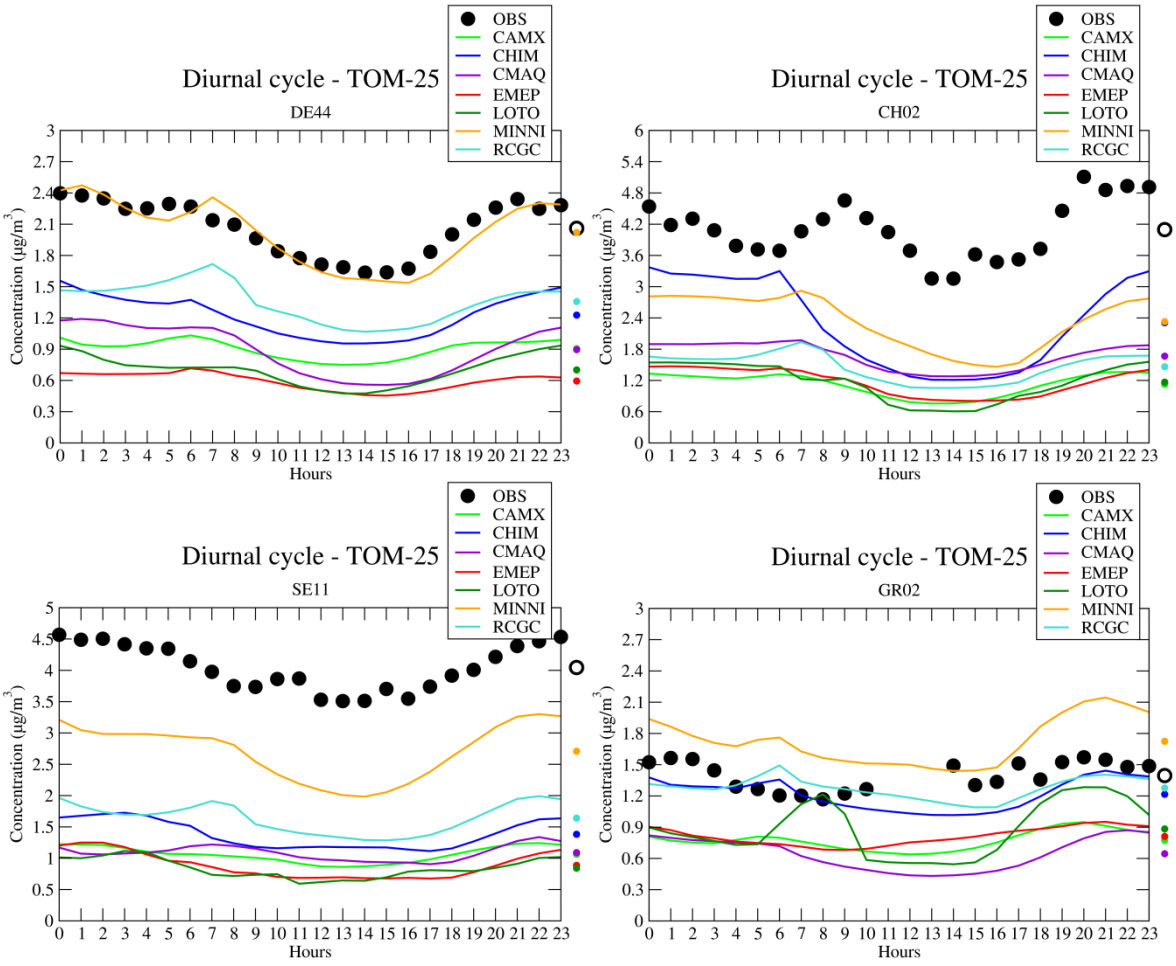

Figure 8.6: Average diurnal cycle of the total organic matter for the whole 2009 campaign for all the models compared to the observations at four stations

8.3 Tracking SNAP2 emissions and secondary organic contributions in PM concentrations

RCGC and CHIM were the only models to run the models separating the primary emissions issued from SNAP2 emissions in the fine fraction of PM (called POMS2-25 in models) in order to track the wood burning combustion. We assume that PM emissions in SNAP2 is mainly due to wood combustion (around 90% in France for instance according to French data). At station Montseny (ES78) located in Spain close to Barcelona, we found a considerable overestimation of observed POMS2-25 concentrations by RCGC and CHIM (Figure 8.7). Error statistics are similar for both models. This overestimation could come from the altitude of the site that makes irrelevant the comparison with the models because the coarse resolution to resolve topography. Moreover as shown in Figure 2.1, Barcelona exhibit too high PM emissions that could affect the modelled concentrations in Montseny. It could be related to a too high transport of pollutant from Barcelona, we can also observe this behaviour with a primary species like EC-25 displaying a very high overestimation too (not shown here). In Melpitz (DE44), the timing of BBOA peaks are quite well reproduced with CHIM unfortunately the first part of the campaign is not covered by measurements. In Vavihill (SE11) the timing of the main peaks are well reproduced by both models with sometime a slight time lag for RCGC.

Regarding SOA-25 concentrations, on average modelled SOA-25 is much lower than OOA observed concentrations (Figure 8.8). CHIM exhibits the lowest underestimations particularly in ES78 but with a low correlation. In Melpitz and Vavihill the amplitude of OOA peaks are not reproduced by the

models with SOA-25. At this stage, it is difficult to say more on this comparison because a part of OOA can have a primary origin. Indeed, the observed OOA (Oxidized Organic Aerosols) and BBOA (Biomass Burning Organic Aerosols) concentrations peaks seem correlated particularly in Vavihill (SE11).

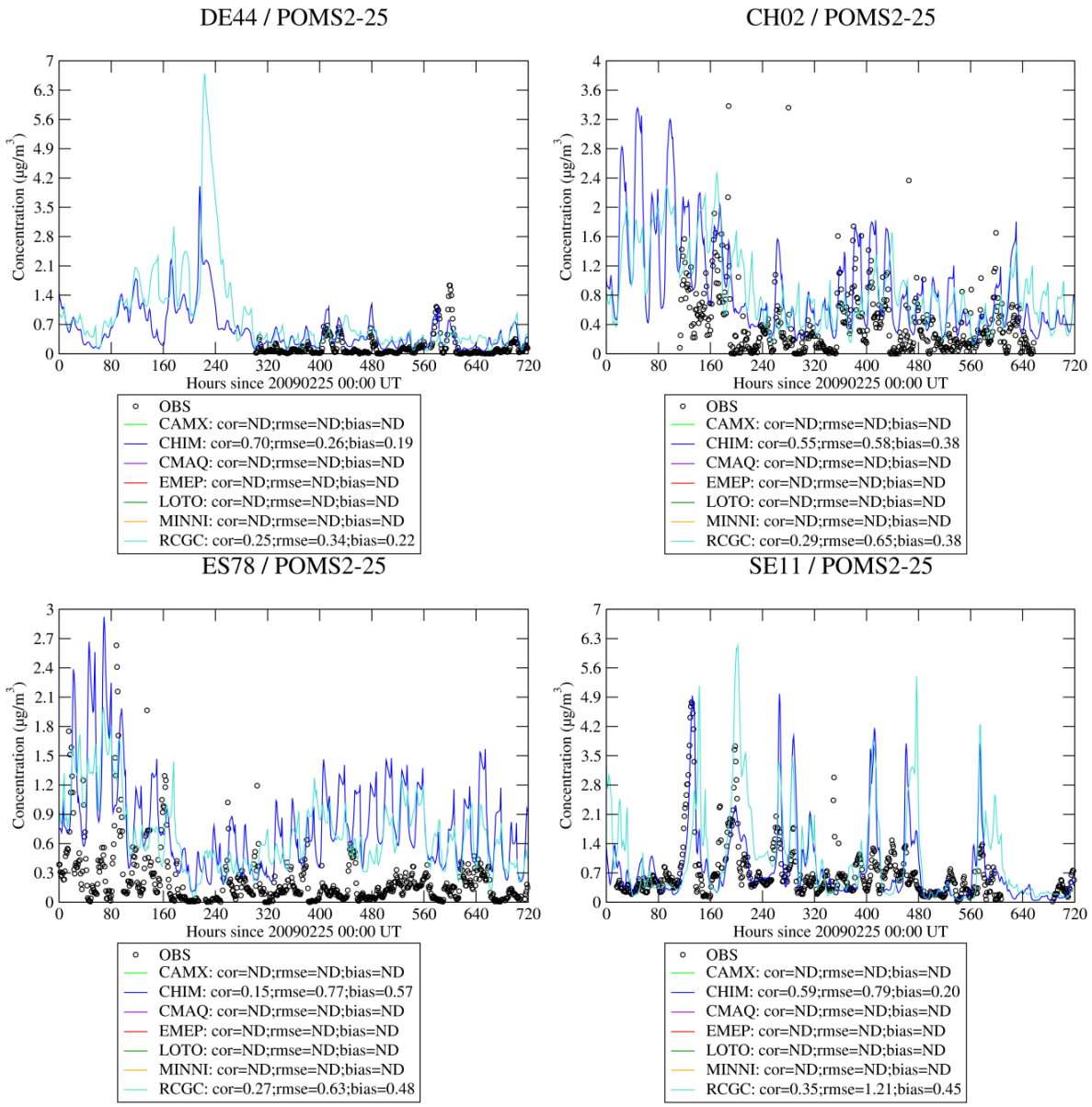

Figure 8.7: Time series of Biomass Burning Organic Aerosol (BBOA in measurements compared to POMS2-25 in models) in the fine fraction of PM.

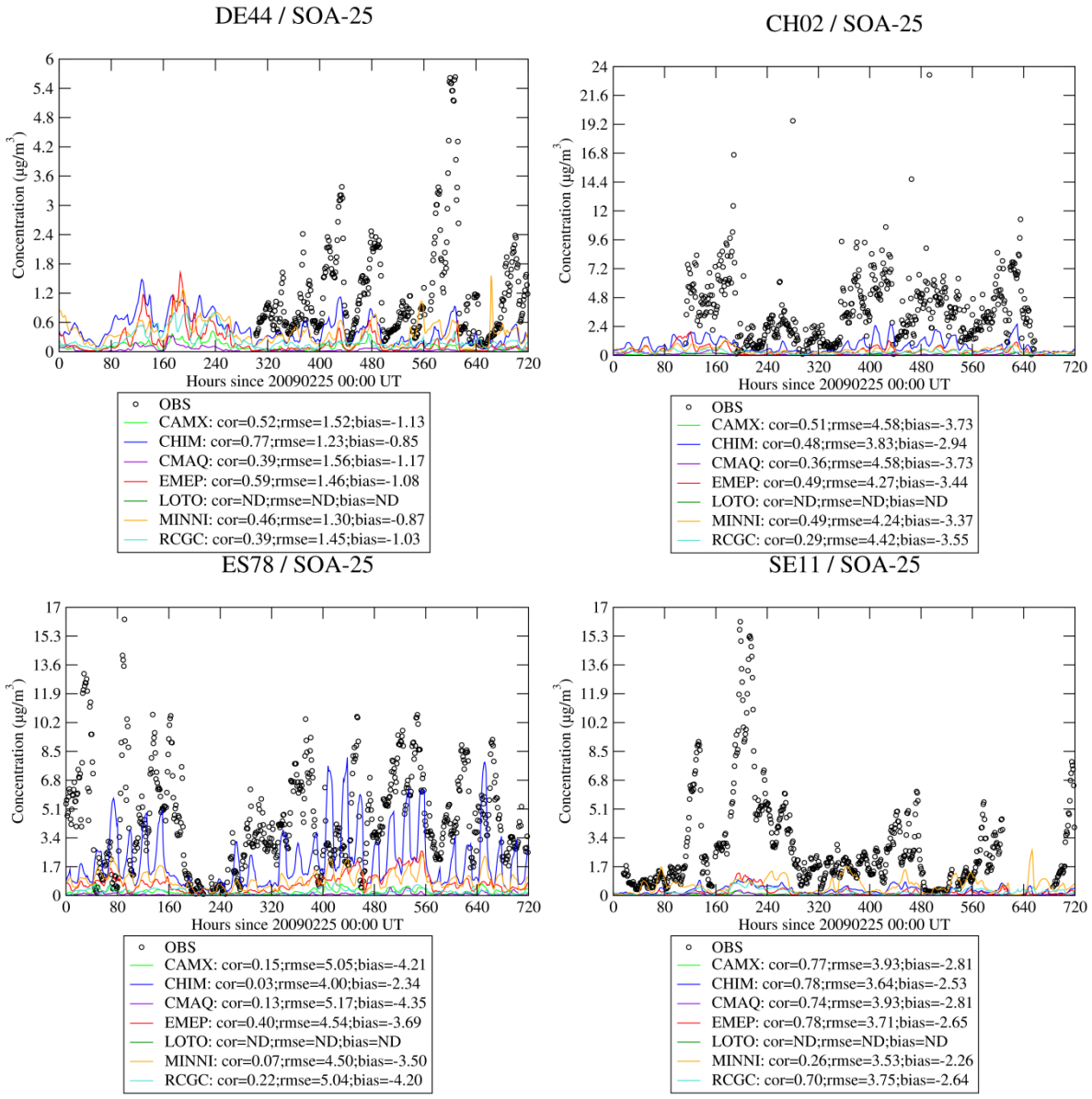

Figure 8.8: Time series of Secondary Organic Aerosols (OOA in measurements compared to SOA-25 in models) in the fine fraction of PM.

9 Sulphur dioxide and sulphate

9.1 Overall error statistics

For SO_2 concentrations, CHIM, EMEP, CMAQ and LOTO show the lowest RMSE compared with both daily and hourly measurements (Table 9.1). For all models the correlation coefficient declines from 0.5 to 0.3 from daily to hourly measurements, suggesting difficulties for the models to capture the diurnal cycle. The largest biases are found for CAMX, MINNI and RCGC. The observed diurnal cycle is rather flat with a slight increase at noon (Figure 9.1), whereas all models display a peak in the morning in the period 06:00 to 09:00, with a decrease in the afternoon. The relatively poor statistics for SO_2 is due to the "punctual" characteristic of industrial sources that makes difficult for chemistry transport models to describe the dilution of industrial plumes at coarse model resolutions. In addition, CAMX injects all sources at the ground level for the simulation of the 2009 campaign**.**

For SO4-10 concentrations, the correlations are slightly higher, ranging between 0.46-0.55 for daily measurements (though not for CAMX, CMAQ and RCGC). CMAQ, EMEP and LOTO have the highest RMSE mainly driven by a low bias compared to the other models. CHIM exhibits the highest overestimation with (+33%). EMEP and LOTO display the best correlation coefficients, while underestimating measured concentrations.
Regarding diurnal cycles, at CH02 for example, we observe a rather slight variability for sulphate concentrations with two small peaks at 11:00 and 23:00. While most of the models can reproduce the evening peak, CHIM, CAMX, MINNI and EMEP calculate the first peak at 06:00. The time of occurrence of the morning peak is calculated more accurately by RCGC and CMAQ, whereas the LOTO's diurnal cycle anti-correlates with observations.

Table 9.1: Model evaluation for SO_2 and SO4-10 (µg m^{-3}). Correlations in time and space (*Cor.*), Biases (in µg m^{-3}) and Root Mean Square Errors in (*RMSE in* µg m^{-3}) are computed for the whole 2009 campaign based on daily values (left table) and hourly values (right table). *Nb* is the number of available observations for a given pollutant. The best model performance with respect to RMSE is displayed in bold character.

Daily basis

Pollutant	Obs.	Model name	Model val.	Bias	Cor.	RMSE	Nb.
SO2	1.10	CAMX	2.73	1.63	0.49	2.85	1618
		CHIM	0.89	-0.21	0.48	**1.33**	
		CMAQ	1.47	0.36	0.49	1.60	
		EMEP	1.09	-0.01	0.50	1.37	
		LOTO	1.19	0.08	0.48	1.33	
		MINNI	2.35	1.25	0.49	2.23	
		RCGC	2.49	1.39	0.49	2.50	
		MACCA	ND	ND	ND	ND	
SO4-10	2.03	CAMX	2.10	0.07	0.46	1.82	1829
		CHIM	2.81	0.78	0.51	2.31	
		CMAQ	1.84	-0.19	0.47	1.64	
		EMEP	1.58	-0.46	0.55	**1.61**	
		LOTO	1.20	-0.83	0.55	1.69	
		MINNI	2.31	0.28	0.52	1.76	
		RCGC	1.87	-0.17	0.40	1.87	
		MACCA	2.16	0.12	0.43	1.94	

Hourly basis

Pollutant	Obs.	Model name	Model val.	Bias	Cor.	RMSE	Nb.
SO2	1.24	CAMX	3.26	2.01	0.27	3.98	20403
		CHIM	1.00	-0.24	0.37	**1.73**	
		CMAQ	1.58	0.34	0.31	2.19	
		EMEP	1.24	0.00	0.39	1.89	
		LOTO	1.33	0.08	0.31	1.83	
		MINNI	2.54	1.30	0.36	2.68	
		RCGC	2.93	1.69	0.28	3.30	
SO4-10	2.20	CAMX	1.76	-0.45	0.46	1.80	1650
		CHIM	2.48	0.28	0.62	1.68	
		CMAQ	1.62	-0.58	0.35	1.88	
		EMEP	2.19	-0.01	0.52	2.12	
		LOTO	1.22	-0.99	0.57	1.84	
		MINNI	2.45	0.25	0.59	**1.62**	
		RCGC	1.64	-0.56	0.42	1.83	

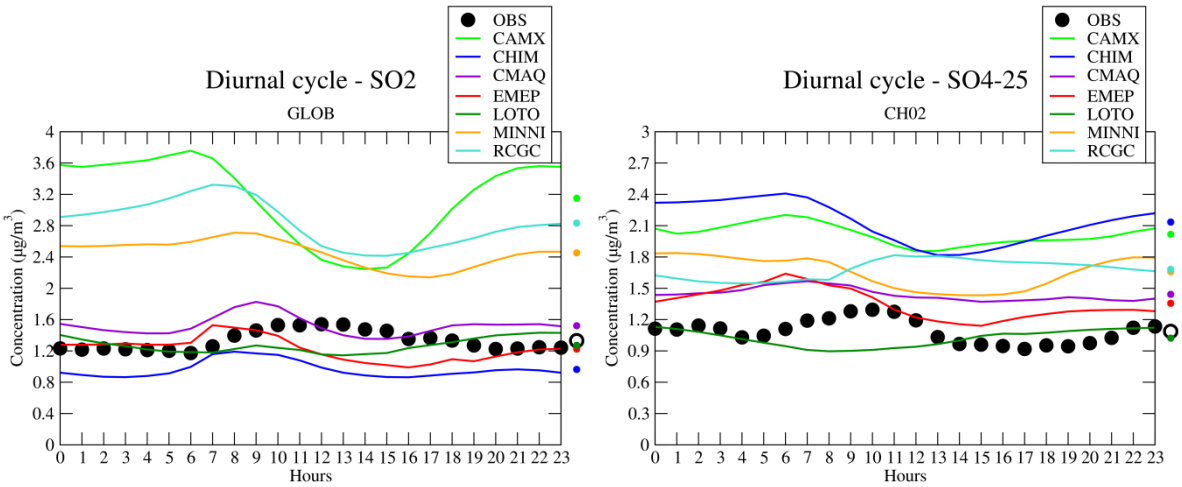

Figure 9.1: Average diurnal cycles of SO_2 concentrations for all EMEP stations (GLOB) in Europe (left panel) and fine sulphate concentrations in station CH02 (right panel)

We look closer at the results of CHIM, LOTO and EMEP. These three models have a low bias for SO2 concentrations. As previously described, EMEP is the best to reproduce SOx deposition and exhibits the highest wet deposition capability for SOx. However, EMEP underestimates observed sulphate concentrations and this negative bias might be higher because the sulphate boundary conditions are overestimated. Certainly the chemical formation of sulphate is too weak in EMEP counterbalanced by high deposition efficiency. For CHIM, it is the opposite, the chemical production of sulphate is too high and certainly the removal efficiency of SOx is too low. For LOTO, the wet deposition is underestimated but the sulphate concentrations are rather low, probably the chemical production of sulphate is too low associated with a higher dry deposition.

9.2 Regional patterns

CAMX, MINNI and RCGC overestimate mean SO_2 concentrations in all regions, giving better results for UK and Ireland. CHIM, EMEP and LOTO calculate SO_2 levels quite close to the measured concentrations in France, Benelux, Denmark, Germany, Austria and the Mediterranean basin whilst underestimating in UK (Figure 9.2). According to the spatial correlation coefficients all models capture the spatial variability with correlation in the range 0.52 (CAMX) – 0.63 (RCGC), this range is rather low because the footprint of SO_2 concentrations is driven by emissions however RCGC and CMAQ better capture the spatial variability. The highest values of SO_2 concentrations are generally modelled in Central and Eastern Europe. The shipping lines are clearly identified in all model outputs.

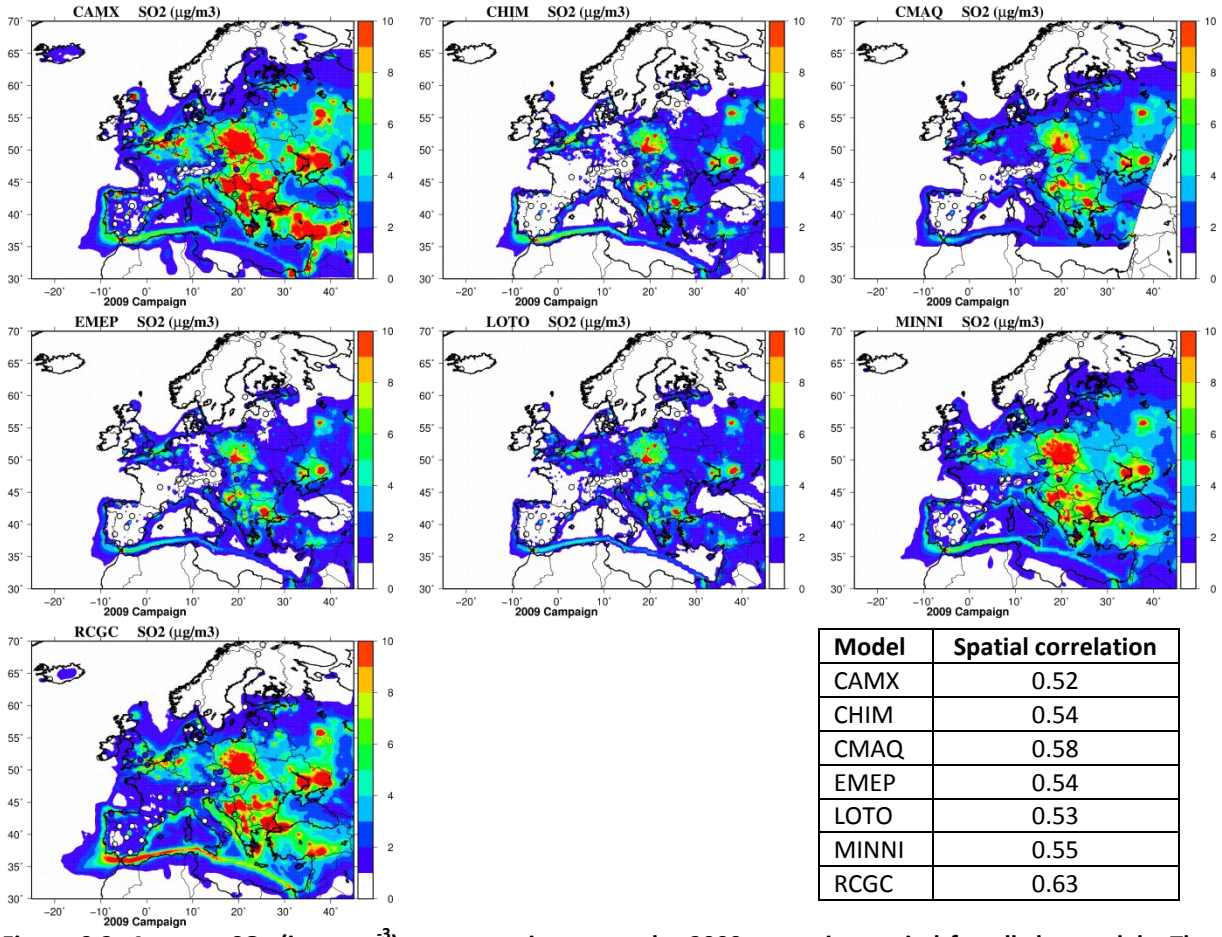

Model	Spatial correlation
CAMX	0.52
CHIM	0.54
CMAQ	0.58
EMEP	0.54
LOTO	0.53
MINNI	0.55
RCGC	0.63

Figure 9.2: Average SO_2 (in µg m^{-3}) concentrations over the 2009 campaign period for all the models. The colour circles are the observed values at EMEP sites. Spatial correlation coefficients are reported in the table for the daily mean measurements.

Figure 9.3 displays the average sulphate concentrations for the whole considered period. Compared to the SO_2 concentrations, spatial patterns of sulphate calculated by all models are smoother, displaying a west-east gradient with enhanced concentrations in the east of the domain. This pattern is due to the boundary conditions which come from the global MACC analysis (MACCA in Figure 9.3). Calculated sulphate fields are visibly influenced by the boundary conditions. The MACC analysis (MACCA) has the lowest spatial correlation among the models for sulphate. The MACCA boundary conditions negatively influences sulphate concentrations from the ED III models at eastern parts of the domain. However, it is difficult to say how far west this effect propagates and to what degree it worsens the evaluation results. Still, the spatial correlations of sulphate concentrations are lower than those for SO_2.EMEP has the highest spatial correlations reaching 0.5 for the latter.
Among possible reasons for models discrepancies are the differences in:

- Treatment of emission plume rise
- PBL heights calculations
- Aqueous oxidation of SO_2 to sulphate (pH dependence). Some tests performed by INERIS do not produced important changes assuming different constant pH instead of varying pH as it is the case in CHIM.
- Dry deposition parameterisations (*e.g.* accounting for co-deposition of SO_2 and NH_3 in the EMEP model)
- Wet scavenging
- Sulphate boundary conditions, the MACC analysis has a small bias of +0.12 µg m^{-3} that can partly explain a part of the positive bias of models, and a rather low spatial correlation.

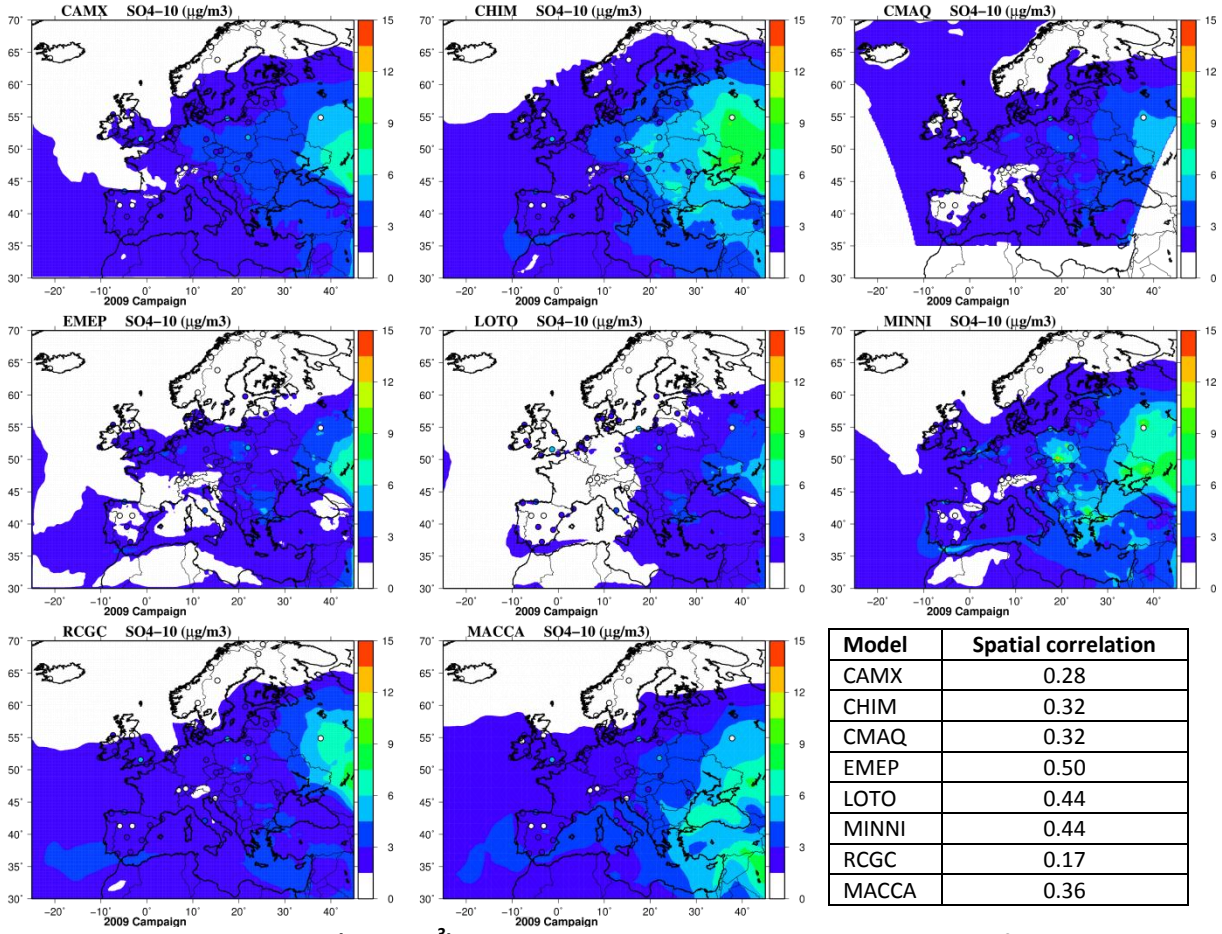

Model	Spatial correlation
CAMX	0.28
CHIM	0.32
CMAQ	0.32
EMEP	0.50
LOTO	0.44
MINNI	0.44
RCGC	0.17
MACCA	0.36

Figure 9.3: Average Sulphate (in µg m^{-3}) concentrations over the 2009 campaign period for all the models. The colour circles are the observed values at EMEP sites. Spatial correlation coefficients are reported in the table for the daily mean measurements.

10 Nitrate and Ammonium

10.1 Overall error statistics

Table 10.1 presents all statistics for the secondary inorganic aerosols in PM_{10} and $PM_{2.5}$ fractions on daily and hourly bases. The models differ in the implementation of nitrate and ammonium (Table 3.2). EMEP is the only one using MARS equilibrium model, whereas the other models use ISORROPIA. In addition, EMEP, LOTO, CMAQ and RCGC account for coarse nitrate formation. For nitrate in the PM_{10} fraction, the correlation coefficients are rather high compared to other compounds particularly on an hourly basis. On a daily basis, CHIM, EMEP and LOTO underestimate nitrate concentrations both in PM_{10} and $PM_{2.5}$ fractions. Conversely, MINNI, RCGC, CMAQ and CAMX overestimate NO_3 in both PM_{10} and $PM_{2.5}$. For CAMX one has to consider that the mechanism considers the SIA just in the fine fraction, actually SIA is rather a bulk concentration coming from ISORROPIA and all placed in the $PM_{2.5}$ fraction. This is why, generally, CAMX has a positive bias for SIA species in the fine mode and a negative bias for SIA species in the coarse mode. EMEP also puts all SIA in the fine fraction of PM. For ammonium, all models except EMEP and LOTO overestimate the concentrations when looking at daily measurements. The average values of hourly measurements are the double of daily ones.

Table 10.1: Model evaluation for NO3-10, NO3-25, NH4-10, NH4-25, SO4-10, SO4-25 concentrations (µg m^{-3}). Correlations in time and space (*Cor.*), Biases (in µg m^{-3}) and Root Mean Square Errors in (*RMSE in* µg m^{-3}) are computed for the whole 2009 campaign based on daily values (left table) and hourly values (right table). *Nb* is the number of available observations for a given pollutant. The best model performance for the RMSE is displayed in bold character.

Daily basis

Pollutant	Obs.	Model name	Model val.	Bias	Cor.	RMSE	Nb.
NO3-10	2.58	CAMX	3.22	0.64	0.65	2.98	1026
		CHIM	2.19	-0.38	0.76	**2.26**	
		CMAQ	3.01	0.44	0.52	3.28	
		EMEP	2.31	-0.27	0.68	2.46	
		LOTO	2.14	-0.44	0.64	2.56	
		MINNI	3.51	0.93	0.64	3.07	
		RCGC	3.65	1.08	0.58	3.20	
NO3-25	3.00	CAMX	4.44	1.43	0.76	3.68	225
		CHIM	2.75	-0.26	0.75	**3.11**	
		CMAQ	3.65	0.64	0.66	3.69	
		EMEP	2.21	-0.79	0.61	3.85	
		LOTO	2.55	-0.46	0.60	3.79	
		MINNI	4.43	1.42	0.70	3.67	
		RCGC	2.93	-0.07	0.50	4.09	
NH4-10	1.12	CAMX	1.79	0.66	0.71	1.36	919
		CHIM	1.73	0.61	0.75	1.18	
		CMAQ	1.67	0.55	0.63	1.37	
		EMEP	0.99	-0.13	0.76	**0.92**	
		LOTO	1.02	-0.10	0.66	1.04	
		MINNI	2.05	0.93	0.70	1.52	
		RCGC	1.43	0.31	0.61	1.26	
NH4-25	1.30	CAMX	2.19	0.89	0.71	1.77	192
		CHIM	1.77	0.47	0.66	1.52	
		CMAQ	1.75	0.45	0.60	1.64	
		EMEP	1.10	-0.20	0.63	**1.51**	
		LOTO	1.20	-0.10	0.60	1.58	
		MINNI	2.18	0.88	0.63	1.74	
		RCGC	1.51	0.21	0.43	1.77	
SO4-10	2.03	CAMX	2.10	0.07	0.46	1.82	1829
		CHIM	2.81	0.78	0.51	2.31	
		CMAQ	1.84	-0.19	0.47	1.64	
		EMEP	1.58	-0.46	0.55	**1.61**	
		LOTO	1.20	-0.83	0.55	1.69	
		MINNI	2.31	0.28	0.52	1.76	
		RCGC	1.87	-0.17	0.40	1.87	
SO4-25	2.06	CAMX	2.46	0.40	0.38	2.16	226
		CHIM	3.00	0.94	0.41	2.43	
		CMAQ	1.81	-0.24	0.49	**1.76**	
		EMEP	1.50	-0.55	0.28	2.06	
		LOTO	1.32	-0.73	0.33	2.05	
		MINNI	2.47	0.41	0.41	1.98	
		RCGC	2.12	0.06	0.38	2.04	

Hourly basis

Pollutant	Obs.	Model name	Model val.	Bias	Cor.	RMSE	Nb.
NO3-10	4.95	CAMX	4.58	-0.38	0.85	**2.98**	1409
		CHIM	5.47	0.52	0.78	4.07	
		CMAQ	3.92	-1.03	0.78	3.58	
		EMEP	3.10	-1.85	0.77	3.87	
		LOTO	2.74	-2.21	0.84	3.94	
		MINNI	5.03	0.08	0.83	3.18	
		RCGC	4.52	-0.43	0.67	4.16	
NO3-25	2.41	CAMX	4.09	1.67	0.67	4.08	3290
		CHIM	2.69	0.28	0.72	2.59	
		CMAQ	3.91	1.49	0.59	4.14	
		EMEP	1.84	-0.57	0.65	2.54	
		LOTO	2.40	-0.02	0.66	**2.43**	
		MINNI	4.27	1.85	0.69	3.64	
		RCGC	3.18	0.76	0.52	3.30	
NH4-10	2.43	CAMX	2.12	-0.31	0.80	1.50	1265
		CHIM	2.59	0.15	0.77	1.59	
		CMAQ	1.85	-0.58	0.71	1.82	
		EMEP	1.71	-0.72	0.73	1.83	
		LOTO	1.24	-1.20	0.79	2.14	
		MINNI	2.61	0.18	0.81	**1.48**	
		RCGC	1.77	-0.66	0.61	2.06	
NH4-25	0.95	CAMX	2.08	1.14	0.61	2.00	3290
		CHIM	1.75	0.81	0.62	1.41	
		CMAQ	1.86	0.91	0.59	1.68	
		EMEP	1.02	0.08	0.63	**0.89**	
		LOTO	1.19	0.24	0.63	0.89	
		MINNI	2.13	1.18	0.63	1.68	
		RCGC	1.61	0.66	0.45	1.44	
SO4-10	2.20	CAMX	1.76	-0.45	0.46	1.80	1650
		CHIM	2.48	0.28	0.62	1.68	
		CMAQ	1.62	-0.58	0.35	1.88	
		EMEP	2.19	-0.01	0.52	2.12	
		LOTO	1.22	-0.99	0.57	1.84	
		MINNI	2.45	0.25	0.59	**1.62**	
		RCGC	1.64	-0.56	0.42	1.83	
SO4-25	1.54	CAMX	2.56	1.01	0.31	2.64	3312
		CHIM	3.20	1.65	0.42	3.05	
		CMAQ	1.94	0.40	0.41	**1.92**	
		EMEP	1.61	0.07	0.13	2.25	
		LOTO	1.37	-0.18	0.27	1.99	
		MINNI	2.52	0.98	0.44	2.20	
		RCGC	2.23	0.68	0.34	2.37	

The error statistics for the nitric acid are very poor for all models (Table 10.2), the correlation is slightly negative for the daily datasets, while positive, but rather low, for the hourly dataset. The best

improvement of the correlation from daily to hourly data is for CHIM. The biases are negative and considerably large for all models for hourly results compared with the daily dataset (with the exception of CMAQ and CAMX).

For NH_3, the average hourly value is strongly affected by measurements at one particular station that gives very high values (NL11) and is certainly not representative of NH_3 background values (crop fields in the vicinity). Considering the daily dataset, an underestimation is found for all models, with RCGC, MINNI and LOTO having lowest biases. Also absolute values are quite comparable between the models. NH_3 from LOTO, which accounts for re-emission of deposited ammonia, tends to be higher than other models. As a crude approximation of the compensation point, EMEP does not allow deposition of NH_3 over growing crops. Correlations of daily values are on average around 0.6 for most models. The daily profile of NH_3 concentrations differs however between models and regions, with strong diurnal cycles for RCGC, LOTO and CAMX, and nearly constant concentrations for EMEP. There are several issues that make it difficult to represent ammonia correctly in regional models. Ammonia emissions are dominated by agriculture. Emissions are rather local, so that for example rural stations in the Netherlands that are in agricultural areas have far higher observed concentrations than modelled ones due to the mixing over relatively large model grid cells. This idea is supported by the notion that stations outside the agricultural areas the modelled values are in quite good agreement with observations. The other issue is that ammonia emissions strongly depend on meteorological conditions, whereas in the model these emissions are determined by a calendar. This may lead to poor correlations during some periods of the year, in particular in periods and areas where manure spreading takes place.

Table 10.2: Model evaluation for TNO3, HNO3, TNH4 and NH3 concentrations (µg m^{-3}). Correlations in time and space (*Cor.*), Biases (in µg m^{-3}) and Root Mean Square Errors in (*RMSE in* µg m^{-3}) are computed for the whole 2009 campaign based on daily values (left table) and hourly values (right table). *Nb* is the number of available observations for a given pollutant. The best model performance for the RMSE is displayed in bold character.

Daily basis

Pollutant	Obs.	Model name	Model val.	Bias	Cor.	RMSE	Nb.
HNO3	0.90	CAMX	0.95	0.05	-0.15	1.83	347
		CHIM	0.31	-0.60	0.00	**1.57**	
		CMAQ	0.73	-0.17	0.07	1.57	
		EMEP	0.22	-0.68	0.07	1.58	
		LOTO	0.23	-0.67	-0.05	1.61	
		MINNI	0.43	-0.47	-0.10	1.63	
		RCGC	0.26	-0.64	-0.14	1.64	
NH3	2.97	CAMX	1.60	-1.38	0.60	5.30	359
		CHIM	1.48	-1.49	0.61	5.49	
		CMAQ	1.09	-1.88	0.51	5.84	
		EMEP	1.69	-1.28	0.68	5.25	
		LOTO	2.17	-0.80	0.64	4.94	
		MINNI	2.35	-0.62	0.61	5.01	
		RCGC	2.50	-0.47	0.64	**4.91**	
TNO3	2.73	CAMX	4.17	1.44	0.66	3.12	1269
		CHIM	2.24	-0.49	0.72	2.00	
		CMAQ	3.91	1.18	0.57	3.23	
		EMEP	2.55	-0.18	0.68	2.11	
		LOTO	2.44	-0.29	0.69	**1.96**	
		MINNI	4.08	1.35	0.67	2.90	
		RCGC	3.87	1.14	0.60	2.99	
TNH4	2.14	CAMX	3.01	0.87	0.58	2.47	1132
		CHIM	2.76	0.62	0.64	1.91	
		CMAQ	2.49	0.35	0.52	2.22	
		EMEP	2.29	0.16	0.66	**1.79**	
		LOTO	2.53	0.39	0.63	1.81	
		MINNI	3.47	1.34	0.62	2.55	
		RCGC	3.17	1.04	0.65	2.14	

Hourly basis

Pollutant	Obs.	Model name	Model val.	Bias	Cor.	RMSE	Nb.
HNO3	0.27	CAMX	0.44	0.17	0.08	0.75	687
		CHIM	0.33	0.06	0.30	0.28	
		CMAQ	0.36	0.09	0.19	0.69	
		EMEP	0.09	-0.18	0.16	0.24	
		LOTO	0.05	-0.22	0.14	0.25	
		MINNI	0.13	-0.14	0.09	**0.22**	
		RCGC	0.26	-0.01	0.26	0.58	
NH3	9.50	CAMX	3.46	-6.04	0.41	12.18	2067
		CHIM	2.77	-6.74	0.43	12.51	
		CMAQ	2.20	-7.30	0.30	13.24	
		EMEP	3.32	-6.19	0.50	12.03	
		LOTO	4.63	-4.88	0.40	11.74	
		MINNI	4.84	-4.67	0.45	**11.34**	
		RCGC	5.03	-4.48	0.43	11.37	
TNO3	ND	CAMX	ND	ND	ND	ND	0
		CHIM	ND	ND	ND	ND	
		CMAQ	ND	ND	ND	ND	
		EMEP	ND	ND	ND	ND	
		LOTO	ND	ND	ND	ND	
		MINNI	ND	ND	ND	ND	
		RCGC	ND	ND	ND	ND	
TNH4	ND	CAMX	ND	ND	ND	ND	0
		CHIM	ND	ND	ND	ND	
		CMAQ	ND	ND	ND	ND	
		EMEP	ND	ND	ND	ND	
		LOTO	ND	ND	ND	ND	
		MINNI	ND	ND	ND	ND	
		RCGC	ND	ND	ND	ND	

For nitric acid (HNO_3), the models show in general the same patterns, with highest concentrations in the Mediterranean, and with relatively high values for CAMX, MINNI and RCGC. The correspondence with measurements is very poor, with either serious over- or underestimations for most locations. Models have a very strong daily cycle which is not found in the few available observations, and the daily cycle differs between the models. Averaged over France for example, all models exhibit an

early-afternoon maximum. Averaged over the Netherlands however, some models (RCGC and EMEP), also have a similar maximum, whereas other models have very flat distribution (LOTO, CHIM) or even a night-time maximum (CAMX).

For the total nitrate (TNO3), there is a clear difference between one group of models (MINNI, RCGC, CMAQ and CAMX) which strongly overestimate the concentrations and the other one (CHIM, EMEP and LOTO) which slightly underestimate the total nitrate concentrations. It is coherent with the results found for particulate nitrate. Two possible reasons explain these results, (i) too large production of nitric acid in the chemical mechanism and (ii) a inefficient deposition for the first model group (as shown in section 7.2).

For total ammonium (TNH4), EMEP, LOTO and CMAQ have the lowest biases, MINNI and RCGC the highest positive biases. The high positive bias for MINNI can be partly explained by its tendency to underestimate the PBL, for RCGC the bias is mainly driven by high NH_3 concentrations. EMEP has the smallest bias.

10.2 Regional patterns

All models have highest nitrate concentration in the Po valley, with a slight shift towards the East for RCGC (Figure 10.1). However, overall absolute values and gradients differ considerably between the models. MINNI has the highest concentrations; whereas EMEP calculates the lowest NO_3 levels. CHIM has relatively high concentrations in Benelux but the lowest concentration in the Mediterranean area mainly due to the missing formation of coarse nitrate. LOTO has overall the lowest concentrations. The observed gradients, with high concentrations in the Benelux and low concentrations in Scandinavia and Poland are poorly represented by all models: models either have good levels in hot spot locations and too high values elsewhere, or concentrations are too low at hot spot locations and have the right magnitude in locations with low observed values. As seen in the table embedded in Figure 10.1, CHIM has the best spatial correlations with 0.81 (west-east gradient better reproduced and higher values in Benelux) the other models are in the range 0.44 – 0.72. The specific patterns for RCGC off the coast of south Portugal is mainly due to a high formation of coarse nitrate over the ocean.

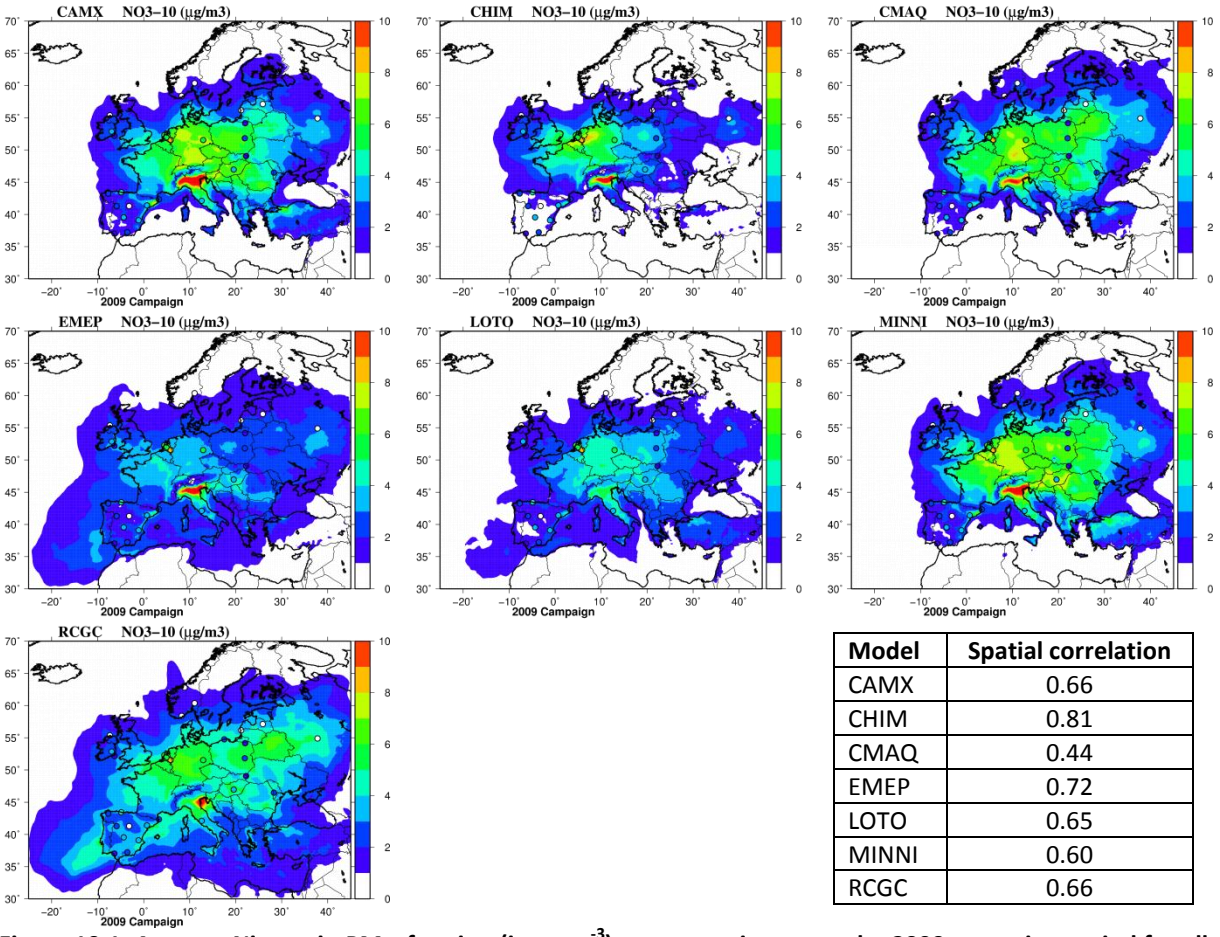

Model	Spatial correlation
CAMX	0.66
CHIM	0.81
CMAQ	0.44
EMEP	0.72
LOTO	0.65
MINNI	0.60
RCGC	0.66

Figure 10.1: Average Nitrate in PM_{10} fraction (in µg m^{-3}) concentrations over the 2009 campaign period for all the models. The colour circles are the observed values at EMEP sites. Spatial correlation coefficients are reported in the table for the daily mean measurements.

For ammonium, the spatial patterns show large differences in absolute values between the models (Figure 10.2). LOTO and EMEP have the lowest concentrations, CAMX and MINNI the highest. Most models show the high concentrations in the Po Valley, but for other parts of Europe the location of the maximum concentrations differ (Poland versus Western Germany/Netherlands) between the models. RCGC has a specific hot spot pattern close to Venice. The observed spatial variability is captured by the models with different accuracy, with spatial correlation coefficient ranging from 0.59 for CMAQ to 0.81 for CHIM and EMEP.

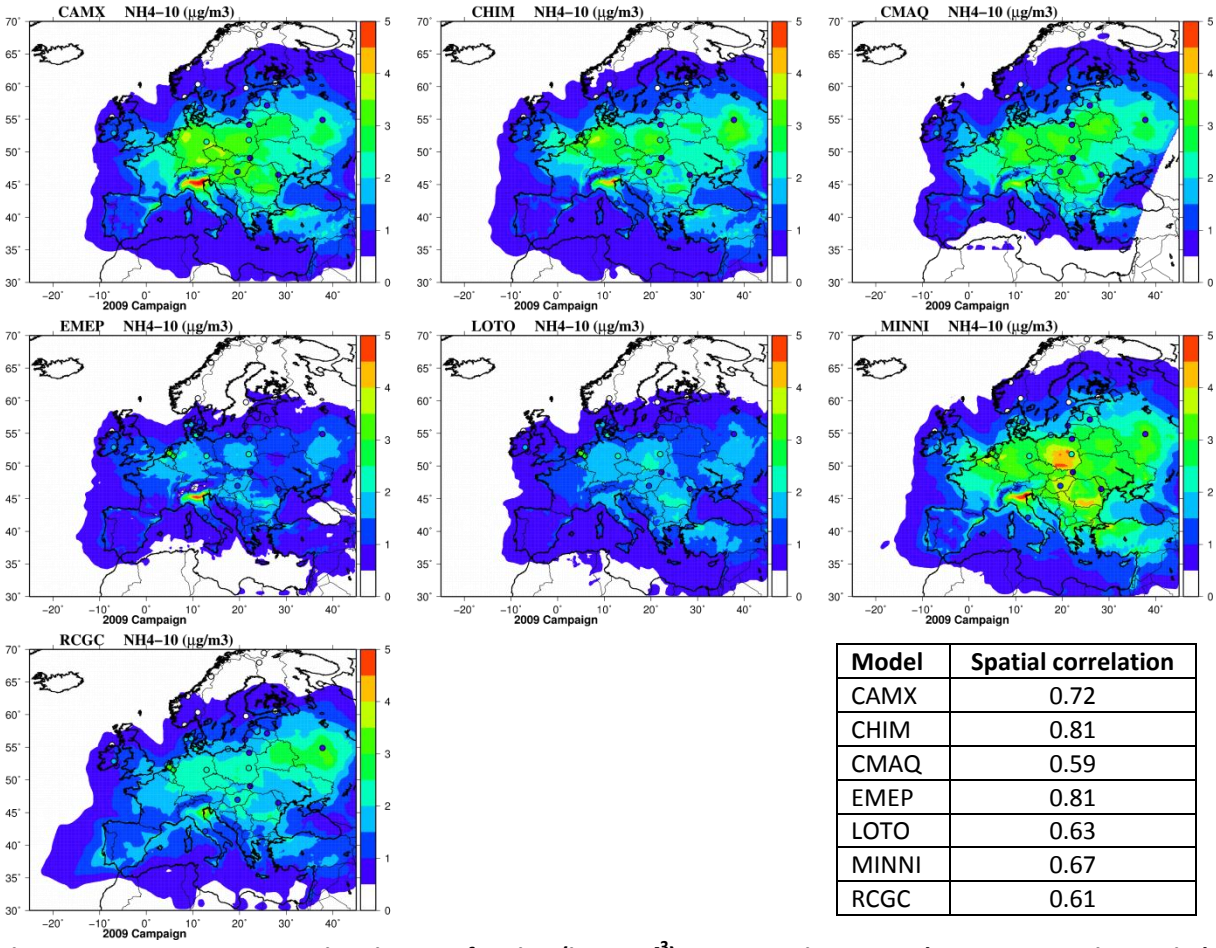

Model	Spatial correlation
CAMX	0.72
CHIM	0.81
CMAQ	0.59
EMEP	0.81
LOTO	0.63
MINNI	0.67
RCGC	0.61

Figure 10.2: Average Ammonium in PM_{10} fraction (in µg m^{-3}) concentrations over the 2009 campaign period for all the models. The colour circles are the observed values at EMEP sites. Spatial correlation coefficients are reported in the table for the daily mean measurements.

10.3 Discussion and implications on SIA chemistry

Nitrate, ammonium and sulphate are secondary inorganic aerosols (SIA) and are formed from gaseous emissions of SO_2, NO_x and NH_3. Typically, the models calculate aerosol/gas partitioning assuming SIA being in a temperature and relative humidity dependent equilibrium with nitric acid, sulphuric acid, ammonia, chloride acid and some base cations (Na, Ca, K, Mg). The latter are not always taken into account. Models use different gas phase chemistry schemes. Most models except EMEP use a version of ISORROPIA to simulate the multiphase partitioning of inorganic aerosol and their precursors. The poor representation of HNO_3 in the models is one of the reasons for inaccurate modelling of nitrate and ammonium partitioning. This is consistent with findings reported in Aas et al. (2012). The role of NH_3 in SIA formation is also central and will be considered below. An analysis of one or the rare available complete hourly time series of HNO_3, NO_3^-, NH_3, NH_4^+ and SO_4^{2-} of good quality (with 2006 and 2007 EMEP intensive campaigns in Aas et al., 2012) showed that there are significant partitioning errors between gas- and particle phase (Schaap *et al.*, 2011) when using ISORROPIA, with a too strong daily cycle for HNO_3. A lack of good HNO_3 observations at other locations hampers further conclusions, but results indicate that all models should be improved with respect to HNO_3 formation.

The diurnal cycles in Melpitz reported in Figure 10.3 show that all models reproduce the morning peak at 06:00 and the lower afternoon concentrations for the nitrate and ammonium species. The diurnal cycle of nitrate and ammonium are very well simulated by EMEP and LOTO. All other models overestimate ammonium in relation with their overestimation of sulphate and nitrate

concentrations. In Payerne, the diurnal cycle for all SIA species displays two peaks at 10:00 – 12:00 and at nighttime. The timing of the daytime peak is not captured by any of the models which modelled a peak at 06:00. Except EMEP and LOTO, all models tends to overestimate the measured concentrations of SIA in $PM_{2.5}$, however since the measurements are performed over a fine fraction of PM with the AMS instrument (particle diameter < 1µm), this overestimation can be partly explained.

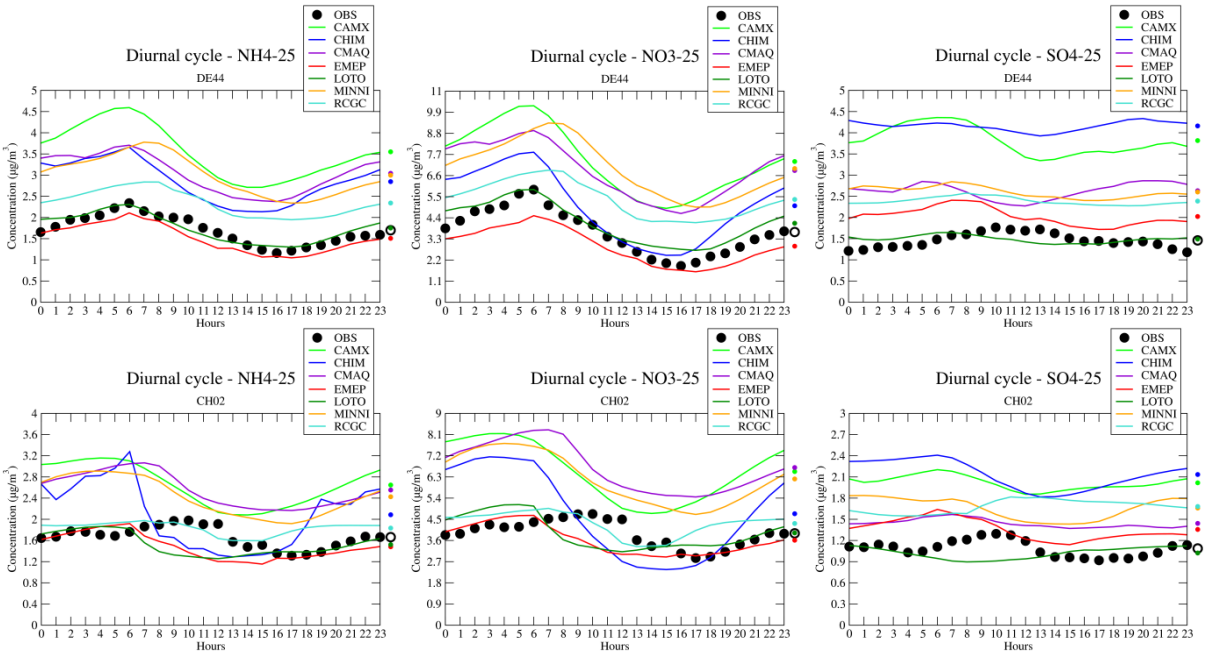

Figure 10.3: Diurnal cycles of Ammonium, Nitrate and Sulphate concentrations in the fine fraction of PM at Payerne (CH02, Switzerland) and Melpitz (DE44, Germany) stations.

Figure 10.4 represents the average concentrations of free ammonia (*F-NH$_X$*). The free ammonia is defined as the difference in molar concentrations of the total ammonium and of sulphate concentrations as follows: $F\text{-}NH_x = TNH4 - 2 \times SO_4^{2-}$. The free ammonia is the amount of ammonia available for ammonium nitrate formation, after all sulphate is neutralized. To complete the SIA analysis the G_{ratio} is used (Ansari and Pandis, 1998 in Pay *et al.*, 2012). This ratio indicates whether fine-particle nitrate formation is limited by the availability of HNO_3 or NH_3. All the terms in the following equation are expressed on a molar basis: $G_{ratio} = \frac{F\text{-}NH_x}{TNO3}$:

- G_{ratio} > 1 indicates that nitric acid is limiting,
- G_{ratio} < 0 indicates the absence of free ammonia,
- G_{ratio} between 0 and 1 indicates that ammonia is available for reaction with nitric acid, but ammonia is the limiting species.

The charts of G_{ratio} in Figure 10.4 show that the models simulate an overall limitation of ammonium nitrate formation by the nitric acid, with severe limitations occurring in ammonia hot spot emission areas, like the Netherlands. The G_{ratio} is very different from country to country for a given model. In general, LOTO, EMEP and CHIM give the the highest G_{ratio} while CMAQ gives systematically the lowest G_{ratio}. This will have a direct implication on ammonia reduction scenarios analysis with different responses expected from model to model, CMAQ being probably the most sensitive to ammonia emission reductions.

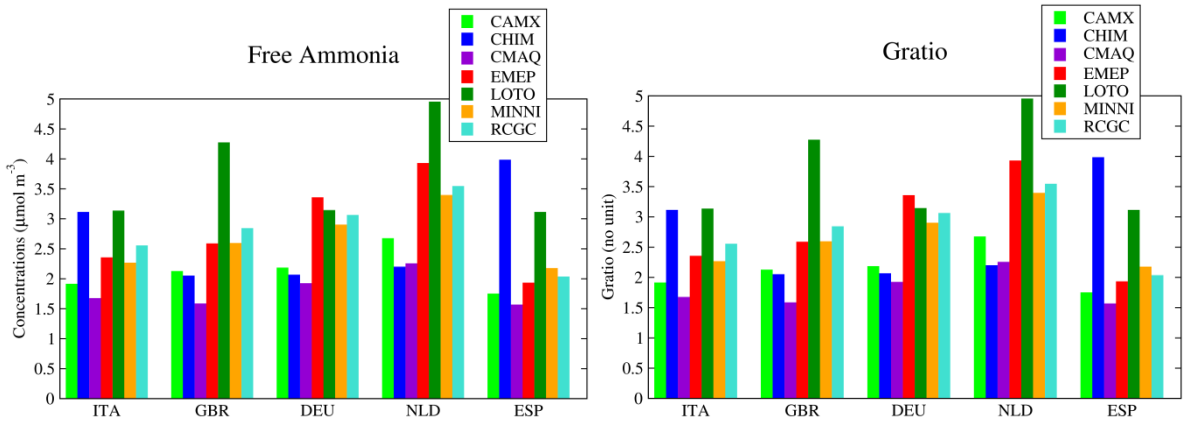

Figure 10.4: Mean free ammonia concentrations (left panel) and G_{ratio} (right panel) for the 2009 campaign for five countries (Italy, Great Britain, Germany, the Netherlands, Spain) for the models.

11 Natural aerosols

11.1 Sodium (from Sodium Chloride)

As expected, all the models simulate high concentrations of sea salt sodium over the oceans and seas with some differences because of the parameterisation used (**Error! Reference source not found.**). n average the spatial correlation is very good in the range 0.90 – 0.95 for all models. CHIM and MINNI give the highest values over lands and clearly show an overestimate as reported in Table 11.1. This overestimate can be explained by lower PBL for MINNI, for CHIM this is more a problem related to the tuning of the emission parameterisation. EMEP, LOTO and RCGC are in better agreement with the observations.

Table 11.1: Model evaluation for Sodium concentrations (µg m^{-3}) in the PM_{10} and $PM_{2.5}$ fractions. Correlations in time and space (*Cor.*), Biases (in µg m^{-3}) and Root Mean Square Errors in (*RMSE in* µg m^{-3}) are computed for the whole 2009 campaign based on daily values (left table) and hourly values (right table). *Nb* is the number of available observations for a given pollutant. The best model performance for the RMSE is displayed in bold character.

Daily basis

Pollutant	Obs.	Model name	Model val.	Bias	Cor.	RMSE	Nb.
NA-10	0.95	CAMX	ND	ND	ND	ND	779
		CHIM	1.66	0.71	0.75	1.31	
		CMAQ	1.22	0.26	0.76	1.17	
		EMEP	1.09	0.13	0.87	**0.86**	
		LOTO	0.86	-0.10	0.79	0.92	
		MINNI	1.95	0.99	0.81	1.66	
		RCGC	0.80	-0.16	0.81	0.87	
NA-25	0.24	CAMX	ND	ND	ND	ND	65
		CHIM	0.53	0.29	0.18	0.58	
		CMAQ	0.06	-0.18	0.06	0.35	
		EMEP	0.07	-0.17	0.61	0.31	
		LOTO	0.16	-0.09	0.29	**0.30**	
		MINNI	0.12	-0.12	0.16	0.33	
		RCGC	0.10	-0.14	-0.09	0.36	

Hourly basis

Pollutant	Obs.	Model name	Model val.	Bias	Cor.	RMSE	Nb.
NA-10	0.76	CAMX	ND	ND	ND	ND	1692
		CHIM	2.00	1.24	0.38	1.77	
		CMAQ	1.27	0.51	0.47	1.44	
		EMEP	1.67	0.92	0.69	1.56	
		LOTO	1.33	0.58	0.48	0.97	
		MINNI	2.28	1.52	0.60	2.12	
		RCGC	0.79	0.03	0.35	**0.84**	
NA-25	ND	CAMX	ND	ND	ND	ND	0
		CHIM	ND	ND	ND	ND	
		CMAQ	ND	ND	ND	ND	
		EMEP	ND	ND	ND	ND	
		LOTO	ND	ND	ND	ND	
		MINNI	ND	ND	ND	ND	
		RCGC	ND	ND	ND	ND	

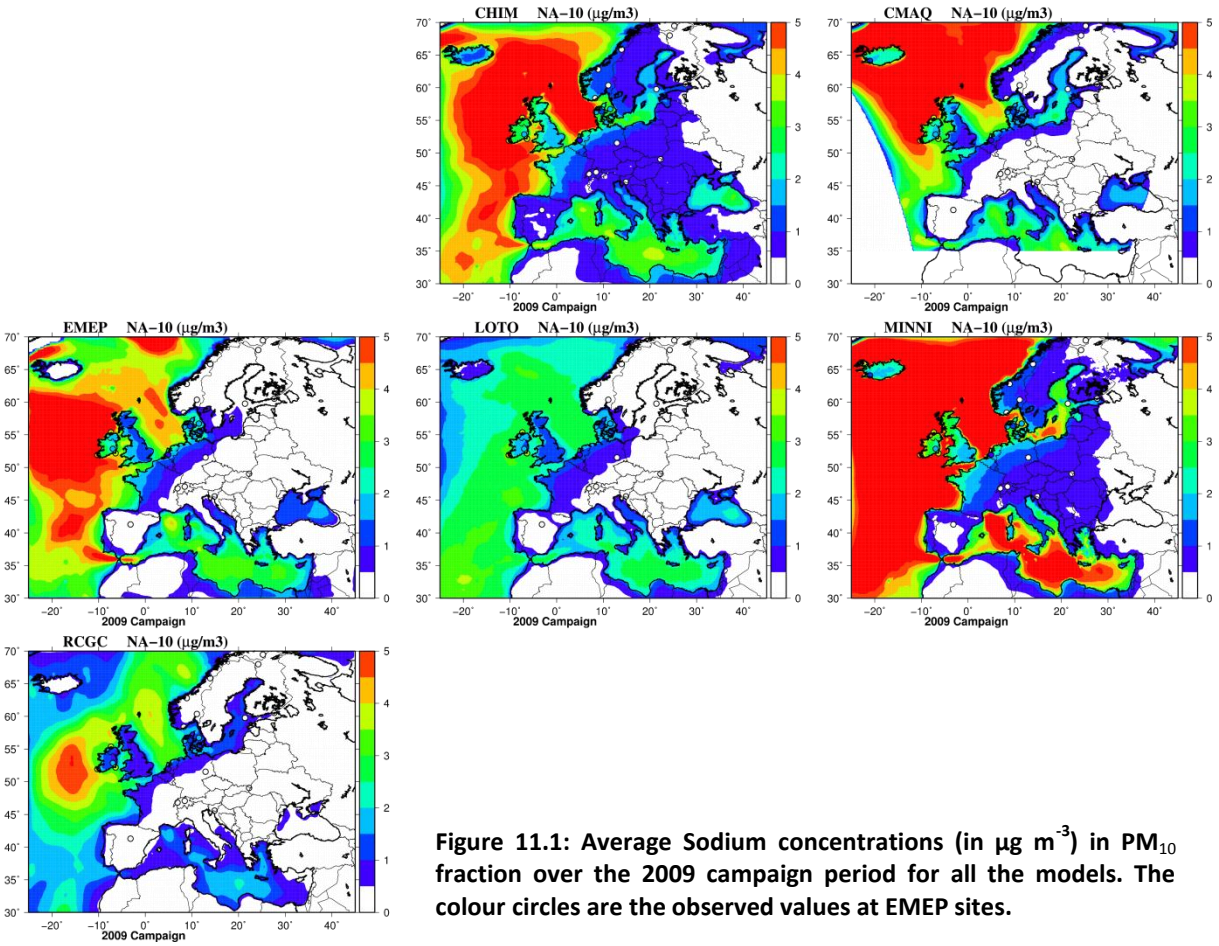

Figure 11.1: Average Sodium concentrations (in µg m^{-3}) in PM_{10} fraction over the 2009 campaign period for all the models. The colour circles are the observed values at EMEP sites.

11.2 Dust

As discussed in section 4.1, dust concentrations from models are compared against measurements of Calcium multiplied by a factor of 8. CAMX and CHIM only transport dust from the boundary conditions, with CHIM giving higher concentrations in the centre of the domain. The MACC analysis provides a pattern similar to those from CHIM and CAMX. The EMEP model accounts also for windblown dust, besides on the concentrations map, large cities can be identified as contributors to the dust load due to the road traffic resuspension schemes. In RCGC outputs, the resuspension schemes create a uniform value over the continent with a dust contribution in the range 1 – 3 µg m^{-3}. In the southern border of the domain, the dust contribution is larger due to the wind blown dust parametrisation in this area. In LOTO, the activated parametrisation does not produce any significant dust concentrations on average in Europe.

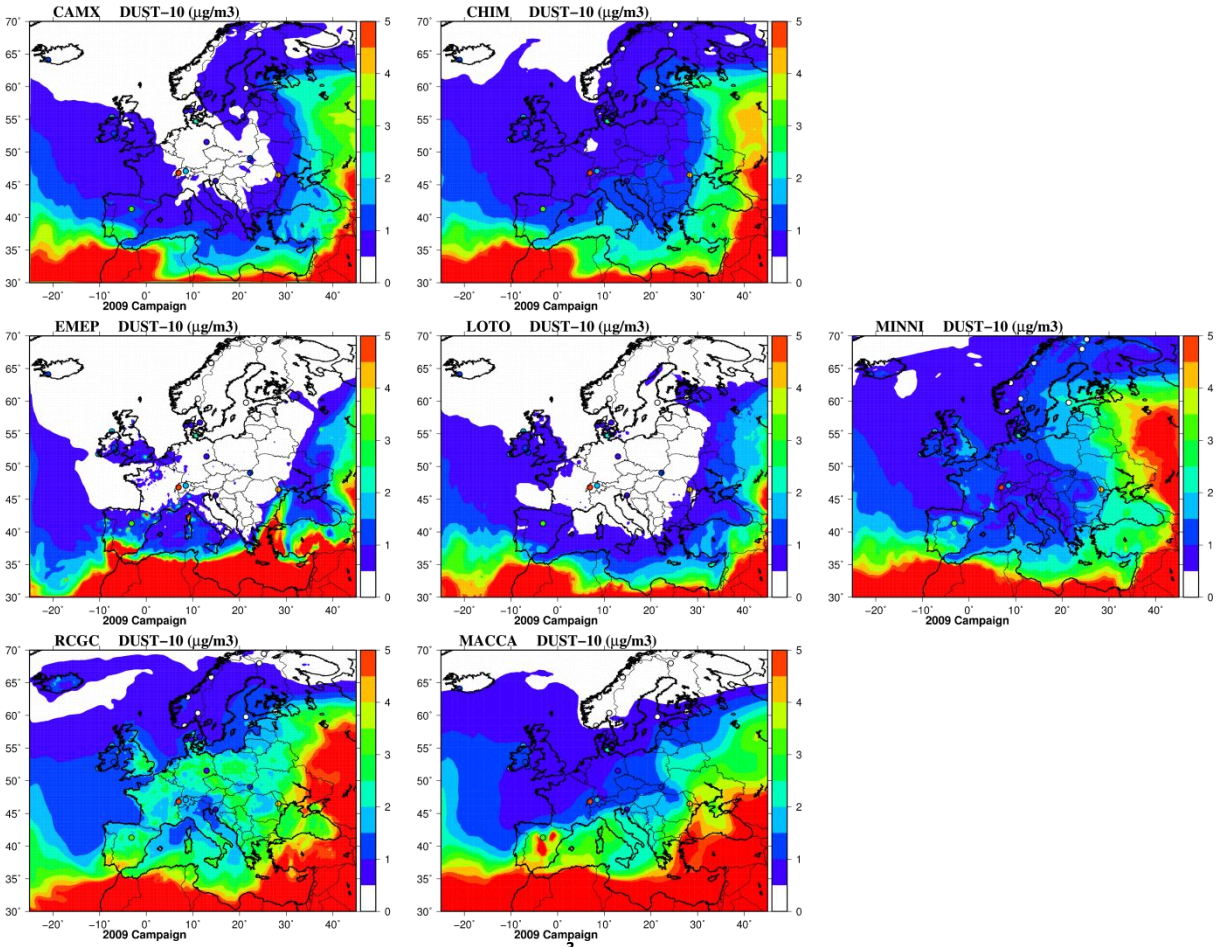

Figure 11.2: Average Dust concentrations (in µg m^{-3}) in the PM_{10} fraction over the 2009 campaign period for all the models. The colour circles are the observed values at EMEP sites.

Due to the differences in dust calculations setup in the models, the biases reported in Table 11.2 should be considered carefully. EMEP and LOTO simulate the lowest values, whereas RCGC and MINNI the highest ones. The correlations in time and space for dust concentrations in the PM_{10} fraction are close to zero for all models, the spatial correlations are better for LOTO and RCGC (0.50) and EMEP (0.62) and near zero for all other models. This large difference on correlations between EMEP, LOTO and RCGC with the other models shows that the dust parameterisations used in these models were more successful in reproducing dust events during the considered period. However, the

temporal correlations impair the statistics for all models suggesting discrepancies of models to get right concentration peaks at the right time.

Table 11.2: Model evaluation for Dust concentrations (µg m^{-3}) in the PM_{10} and $PM_{2.5}$ fraction. Correlations in time and space (*Cor.*), Biases (in µg m^{-3}) and Root Mean Square Errors in (*RMSE in* µg m^{-3}) are computed for the whole 2009 campaign based on daily values. *Nb* is the number of available observations for a given pollutant. The best model performance for the RMSE is displayed in bold character.

Pollutant	Obs.	Model name	Model val.	Bias	Cor.	RMSE	Nb.
DUST-25	1.10	CAMX	1.13	0.03	0.76	2.30	64
		CHIM	1.68	0.59	0.81	2.22	
		CMAQ	ND	ND	ND	ND	
		EMEP	1.66	0.56	0.89	2.80	
		LOTO	1.24	0.14	0.75	2.39	
		MINNI	1.77	0.67	0.86	**1.91**	
		RCGC	3.11	2.02	0.53	5.40	
DUST-10	1.31	CAMX	0.55	-0.77	0.04	3.69	802
		CHIM	0.78	-0.53	0.05	3.73	
		CMAQ	ND	ND	ND	ND	
		EMEP	0.31	-1.01	0.09	3.70	
		LOTO	0.38	-0.93	0.15	**3.64**	
		MINNI	1.13	-0.18	0.04	3.82	
		RCGC	1.53	0.21	0.05	3.82	

A dust event was captured in the PM measurements in Cyprus and confirmed with the calcium measurements in the fine fraction of PM. As displayed in Figure 11.3, on March 7th and 8th, a large increase of dust concentrations is observed. Both models equipped with dust parameterisation and models only using boundary conditions (as CAMX and CHIM) are able to capture this event, only RCGC seems to get this event one day later. In Melpitz, the correlation coefficients are generally poor in the range 0.37 – 0.60. All models capture a peak on March 6th, whereas observations remain below 2 µg m^{-3}. As CHIM and CAMX transport only dust boundary conditions, these modelled dust mainly come from the domain borders. The long distance transport can be evaluated at IE01, CHIM, RCGC and LOTO seems to get a better time correlation at this station, however a systematic bias is observed for all models. This bias is also observed in several stations in this area up to Iceland.

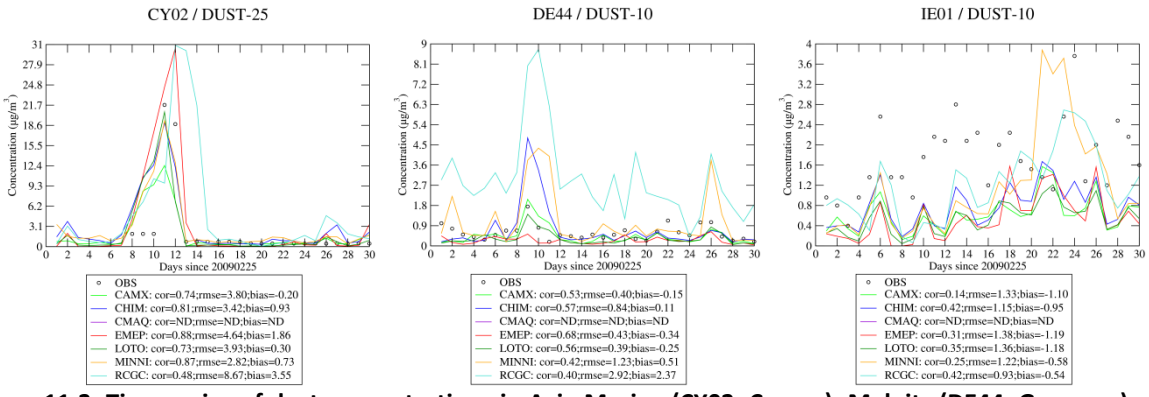

Figure 11.3: Time series of dust concentrations in Ayia Marina (CY02, Cyprus), Melpitz (DE44, Germany) and Valentia Observatory (IE01, Ireland) for the 2009 campaign

12 Model behaviour during episodes

12.1 Statistics for high concentrations

In order to study the behaviour of models during episodes, Table 12.1 and Table 12.2 summarize the error statistics for the 10% highest observed values respectively for regulatory pollutants and PM components. High O_3 concentrations are underestimated of more than 10 µg m^{-3}, however this species is not concerned by episodes during this season. All models underestimate NO_2 concentrations except CMAQ that have a slight positive bias.
For SO_2, models have different behaviour from a large underestimation for CHIM and LOTO to a large overestimation for CAMX, MINNI and RCGC. For the PM_{10} and $PM_{2.5}$, all models underestimate the PM concentrations during episodes, with LOTO, CMAQ and EMEP showing the largest negative biases.

To understand which component is responsible for this PM underestimation during episodes, a close look at Table 12.2 brings clear explanations. If models are in good agreement with elemental carbon concentrations suggesting also a good estimation of the meteorology (EC being a primary species and is mainly affected by the meteorology), the models show a clear tendency to underestimate the total organic matter in the PM_{10} and $PM_{2.5}$ fractions. During episodes, models underestimate the organic matter by a factor of 2 to 6.
The models behaviour for nitrates shows a clear difference between the group LOTO/EMEP/CHIM which underestimate the nitrate concentrations (-30 to -40%) with the other models which have a slight overestimate. For CHIM this behaviour is consistent with an overestimate of sulphate concentrations in this simulation. For the sulphate, all the model except CHIM exhibit a significant underestimate of concentrations.

Table 12.1: Model evaluation for regulatory pollutants concentrations (µg m^{-3}) for the 10% highest values. Correlations in time and space (*Cor.*), Biases (in µg m^{-3}) and Root Mean Square Errors in (*RMSE in* µg m^{-3}) are computed for the whole 2009 campaign based on daily values. *Nb* is the number of available observations for a given pollutant. The best model performance for the RMSE is displayed in bold character.

Pollutant	Obs.	Model name	Model val.	Bias	Cor.	RMSE	Nb.
O3	86.68	CAMX	72.51	-14.17	0.55	**19.06**	436
		CHIM	75.64	-11.03	0.12	19.14	
		CMAQ	72.27	-14.40	0.06	25.15	
		EMEP	72.42	-14.25	0.41	19.63	
		LOTO	71.47	-15.21	0.22	21.54	
		MINNI	64.10	-22.58	0.48	25.97	
		RCGC	67.29	-19.39	0.47	23.19	
NO2	14.65	CAMX	9.10	-5.55	0.59	10.68	321
		CHIM	10.23	-4.42	0.60	10.55	
		CMAQ	17.04	2.39	0.54	12.98	
		EMEP	10.43	-4.22	0.58	10.39	
		LOTO	10.04	-4.61	0.59	10.42	
		MINNI	10.82	-3.84	0.58	**10.32**	
		RCGC	8.69	-5.96	0.54	11.27	
SO2	2.32	CAMX	4.05	1.73	0.53	3.58	221
		CHIM	1.35	-0.97	0.48	2.43	
		CMAQ	2.25	-0.07	0.53	2.42	
		EMEP	1.86	-0.46	0.54	**2.25**	
		LOTO	1.65	-0.67	0.51	2.26	
		MINNI	3.32	1.00	0.52	2.81	
		RCGC	3.36	1.04	0.53	3.00	
PM10	36.28	CAMX	22.62	-13.66	0.07	34.90	184
		CHIM	23.26	-13.02	0.24	32.78	
		CMAQ	20.11	-16.17	0.03	36.13	
		EMEP	20.94	-15.33	0.61	**30.17**	
		LOTO	15.69	-20.59	0.37	35.84	
		MINNI	25.86	-10.42	0.19	32.27	
		RCGC	22.99	-13.29	0.18	33.42	
PM25	27.85	CAMX	21.14	-6.71	0.38	16.60	122
		CHIM	20.48	-7.38	0.50	**15.21**	
		CMAQ	17.62	-10.23	0.33	18.61	
		EMEP	17.01	-10.84	0.48	17.29	
		LOTO	12.53	-15.32	0.46	20.63	
		MINNI	22.53	-5.32	0.40	15.26	
		RCGC	18.95	-8.91	0.30	17.39	

Table 12.2: Model evaluation for PM components concentrations (µg m^{-3}) for the 10% highest values. Correlations in time and space (*Cor.*), Biases (in µg m^{-3}) and Root Mean Square Errors in (*RMSE in* µg m^{-3}) are computed for the whole 2009 campaign based on daily values. *Nb* is the number of available observations for a given pollutant. The best model performance for the RMSE is displayed in bold character.

Carbonaceous species

Pollutant	Obs.	Model name	Model val.	Bias	Cor.	RMSE	Nb.
TOM-25	17.79	CAMX	2.23	-15.56	0.10	36.06	23
		CHIM	3.47	-14.32	0.13	35.45	
		CMAQ	3.09	-14.70	0.10	35.66	
		EMEP	1.96	-15.83	0.07	36.23	
		LOTO	1.86	-15.93	0.19	36.08	
		MINNI	4.26	-13.53	0.01	**35.42**	
		RCGC	2.48	-15.30	-0.03	36.11	
TOM-10	6.32	CAMX	1.92	-4.39	-0.01	4.64	15
		CHIM	2.75	-3.57	-0.08	3.87	
		CMAQ	1.72	-4.60	-0.05	4.81	
		EMEP	1.49	-4.82	0.08	4.97	
		LOTO	1.42	-4.90	0.06	5.06	
		MINNI	2.92	-3.40	0.00	**3.75**	
		RCGC	2.51	-3.81	0.06	4.30	
EC-25	2.51	CAMX	1.17	-1.34	-0.46	3.08	12
		CHIM	1.35	-1.16	-0.14	**2.94**	
		CMAQ	1.28	-1.23	-0.43	3.26	
		EMEP	0.74	-1.77	-0.28	3.17	
		LOTO	1.24	-1.27	-0.20	2.97	
		MINNI	1.16	-1.35	-0.48	3.09	
		RCGC	1.24	-1.27	-0.31	3.17	
EC-10	1.09	CAMX	1.24	0.16	0.73	0.53	15
		CHIM	1.35	0.26	0.82	0.56	
		CMAQ	1.22	0.14	0.82	0.49	
		EMEP	0.80	-0.29	0.85	0.42	
		LOTO	1.13	0.05	0.85	0.39	
		MINNI	1.09	0.00	0.82	**0.34**	
		RCGC	1.44	0.35	0.59	1.00	

Secondary Inorganic Aerosols

Pollutant	Obs.	Model name	Model val.	Bias	Cor.	RMSE	Nb.
NO3-10	6.27	CAMX	6.88	0.61	0.61	5.07	131
		CHIM	4.75	-1.53	0.76	**4.10**	
		CMAQ	6.21	-0.07	0.51	5.31	
		EMEP	5.10	-1.18	0.68	4.40	
		LOTO	4.04	-2.23	0.66	4.89	
		MINNI	6.58	0.31	0.67	4.46	
		RCGC	6.45	0.18	0.60	4.72	
NO3-25	7.35	CAMX	8.00	0.65	0.83	**4.95**	32
		CHIM	4.85	-2.50	0.82	5.73	
		CMAQ	5.94	-1.42	0.73	6.09	
		EMEP	4.24	-3.11	0.57	7.78	
		LOTO	3.65	-3.70	0.71	7.74	
		MINNI	6.98	-0.38	0.74	5.83	
		RCGC	4.70	-2.66	0.41	8.33	
NH4-10	2.91	CAMX	3.58	0.67	0.68	1.93	119
		CHIM	3.25	0.34	0.73	**1.60**	
		CMAQ	3.17	0.27	0.57	1.93	
		EMEP	2.10	-0.80	0.75	1.71	
		LOTO	1.95	-0.96	0.60	2.07	
		MINNI	3.72	0.81	0.69	1.86	
		RCGC	3.01	0.10	0.45	2.14	
NH4-25	3.16	CAMX	4.07	0.91	0.73	2.60	27
		CHIM	2.90	-0.26	0.72	**2.53**	
		CMAQ	3.04	-0.12	0.58	2.81	
		EMEP	2.04	-1.11	0.45	3.32	
		LOTO	1.90	-1.25	0.56	3.29	
		MINNI	3.59	0.43	0.54	2.96	
		RCGC	2.48	-0.67	0.25	3.49	
SO4-10	4.68	CAMX	3.88	-0.80	0.21	2.86	232
		CHIM	5.40	0.72	0.38	2.99	
		CMAQ	3.08	-1.59	0.21	3.01	
		EMEP	3.12	-1.56	0.32	2.92	
		LOTO	2.32	-2.36	0.41	3.19	
		MINNI	3.95	-0.73	0.38	**2.51**	
		RCGC	3.38	-1.30	0.24	2.89	
SO4-25	4.72	CAMX	4.32	-0.40	0.02	4.03	29
		CHIM	5.17	0.44	0.05	4.31	
		CMAQ	3.06	-1.66	0.34	**3.48**	
		EMEP	2.54	-2.18	0.01	4.08	
		LOTO	2.22	-2.51	-0.05	4.30	
		MINNI	3.72	-1.01	0.13	3.57	
		RCGC	3.29	-1.44	0.23	3.73	

12.2 The 2009 campaign splitted in three periods

The performance of air quality models is highly dependent on input data such us emissions and meteorological conditions. Temporal distributions of anthropogenic emissions take into account monthly, daily and hourly variations and thus, for a given month, they do not vary from one week to another. Since this EMEP campaign practically covers only March, an inter-comparison of models results was performed in relation to the meteorological parameters, looking in particular at the temperature variations. According to the temperature analysis, the campaign was divided in three periods (see maps in Annexe 5):

- **T01** : 25 February to 2 March,
- **T02** : 3 March to 21 March,
- **T03** : 22 March to 26 March.

The three periods T01, T02 and T03 are characterised by cold, warm and cold weather, respectively. Similar description is given in Knote *et al*. (2011) that identified this month as a period of typical European spring with cold weather on 1-2 March and after 20 March. The analysis was carried out for species whose formation/destruction or emission depend on temperature such as ozone, nitrogen dioxide and, to some extent, PM_{10} and $PM_{2.5}$ since both biogenic secondary organic aerosol

(BSOA) and anthropogenic secondary organic aerosol (ASOA) may be affected by variations in temperature, in particular when isoprene and monoterpenes are produced with BVOC emissions model.

As expected, the decrease of the simulated NO_2 concentrations from period T01 to T03 is coupled with the increase of the simulated O_3 concentrations. For a given period, all the models exhibit the same pattern for the NO_2 concentrations, with the highest concentrations in the Po Valley, Belgium, South Poland and around Moscow.

All models show an increase of ozone concentrations from T01 to T03, over the whole Europe, particularly higher over the Mediterranean area. Since the temperature does not increase substantially from period T01 to period T03, this behaviour is probably caused by the increase of incoming solar radiation. During period T03, characterised by higher ozone concentrations, all models reproduce better the observations in the North of Europe. In addition to that, as for NO_2, the patterns of ozone concentrations simulated by models are similar for a given period.

The modelled concentrations of PM_{10} and $PM_{2.5}$ are also lower during T03 with respect to T01 for all the models reflecting a lower contribution of inorganic and organic secondary aerosol and/or more dispersive meteorological conditions. For a given model and period, the spatial distributions of PM_{10} and $PM_{2.5}$ over the land are similar reflecting that $PM_{2.5}$ account for most of the aerosol mass in the absence of dust and sea-salt transport. On the contrary, for a given period, the maps of PM concentrations show different patterns between the CTMs due to the fact that they include different models/parameterizations for aerosol microphysics and chemistry.

The patterns of ISOP, BSOA and ASOA average simulated concentrations (not shown here) exhibit important differences between the models and between periods. While ozone concentrations show a net increase from period 1 to period 3, the concentrations of ISOP, BSOA and ASOA have no such a definite behaviour suggesting a weaker dependency on radiation and temperature. Other simulations and comparison with observations (not available for this campaign) are needed in order to understand and explain the differences in model results.

13 Evaluation of O_3 vertical profiles

The common way to evaluate simulated O_3 is against surface observations because of the model's primary goal is to simulate pollutants to which human are exposed. Although models performance to simulate free tropospheric O_3 has been less evaluated, a precise simulation of O_3 total column is crucial from the point of view of air quality. In that sense, it is important to evaluate O_3 long-range transport from source regions and the downward exchange between free troposphere and the boundary layer (Zyryanov *et al*., 2012). This section evaluates the models abilities to reproduce O_3 free tropospheric concentrations.

13.1 Model vertical resolution and set-up for boundary condition

Table 13.1 indicates the vertical model structure for each Chemical Transport Model (CTM) participating in the present study. CTMs differ in the number of vertical layers, model top and depth of the lowest level.

Table 13.1. Vertical model structure of the CTMs used in the present study

MODEL	Vertical layers / top	Depth first layer (m)	Lateral BC from MACC: interpolation type/proxy	Top BC from MACC: yes/no
EMEP	20 sigma / 100 hPa (~16.400 m)	90	linear wrt StandAtm pressure (v)/distance-weighted(h)	yes
CHIM	9 sigma / 500 hPa	20	Linear / pressure	yes
LOTO	4 (3 dynamic layers and a surface layer) / 3500 m	25	Linear /pressure	yes
RCGC	5 fixed terrain following layers / 3000 m	25	Linear/pressure	yes
CMAQ	30 sigma/ 100 hPa	36	Linear/pressure	no
MINNI	16 fixed terrain-following layers / 10000 m	40	Linear (v) / distance-weighted (h)	yes
CAMX	33 sigma / 8000 m	20	Linear/pressure	no

MACC reanalysis global fields provide hourly varying boundary conditions for O_3 to the CTMs used in the present study. MACC analysis is available every 3 hours with a horizontal resolution of 1.125° x 1.125° and with 60 vertical levels up to 0.1hPa. As MACC data has not the same vertical resolution as CTMs, each modelling group interpolates by pressure O_3 from MACC to their own vertical levels. Since the top of the models is not bigger than 10 hPa, only the first 54 levels of MACC fields are used.

The MACC data assimilation system for chemically reactive gases was constructed by extending ECMWF's IFS to include fields for O_3, CO, NOx and HCHO. Source and sink terms for these gases are supplied by the MOZART-3 CTM which is coupled to the IFS. MACC O_3 reanalysis assimilates **GOME**, **MIPAS** or **MLS** retrievals with their vertically resolved information in the stratosphere together with total column O_3 data of **OMI**[18] and **SCIAMACHY**[19]. MIPAS and MLS measure in the mid-infrared and microwave part of the spectrum, respectively, and are the only ozone data used in the MACC

[18] The Ozone Monitoring Instrument (OMI) is on board the NASA Aura. OMI can distinguish between aerosol types, such as smoke, dust, and sulfates, and can measure cloud pressure and coverage, which provide data to derive tropospheric ozone.

[19] SCIAMACHY is an imaging spectrometer whose primary mission objective is to perform global measurements of trace gases in the troposphere and in the stratosphere.

reanalysis that are available independent of illumination condition, including during the polar night. Together with the GOME O_3 profile retrievals, they are also the only assimilated O_3 profile data with higher vertical resolution, which had been shown in the past to be crucial for obtaining a realistic vertical O_3 distribution in MACC and ECMWF analyses (Inness *et al*., 2013).

13.2 Model evaluation

For evaluating O_3 profiles, modelled and observed O_3 values are directly compared. Horizontally, models and observations are compared selecting the grid point where the station is located. Vertically, we interpolate modelled and measured O_3 concentration to a common vertical profile using a linear interpolation. The selected altitudes above ground levels are (in meters) 50, 100, 200, 400, 600, 800, 1000, 500, 2000, 3000, 4000, 5000, and 6000 covering the lower and middle troposphere. The upper troposphere is not evaluated in the present study because most of the models do not simulate this region (Table 4.1). Concerning time, we use the closest hourly model time step respect to the mean observation time.

Model comparison to measurements is evaluated using classical statistics such as mean bias (MB), root mean squared error (RMSE), mean gross error (MGE) and correlation coefficient (r) integrated for the whole period and as a function of the altitude.

In the present study, MACC data is evaluated against measurements together with the vertical profiles for models. For this purpose, MACC data in 1.125º x 1.125º horizontal resolution are remap to the EURODELTA grid (0.25º x 0.25º). Note that only data for pressure (not temperature) is provided with MACC dataset in this study, so the calculation of O_3 profiles as a function of altitude is estimated using the hydrostatic assumption as follows:

where *h* is the height for corresponding to each pressure, *R* is equal to 287.05 J/kgK, *g* is 9.81 m/m^2, T is fixed at 297.65 K and P_{surf} is the pressure at surface and equal to 101325 Pa. This approach introduces some errors that should be taken into account during the evaluation of the results.

13.3 Model evaluation at boundaries

The nearest stations to the boundaries are STN043 (Great Britain), STN318 (Ireland), STN308 (Spain) and STN348 (Turkey). Figure 13.1 shows the direct comparison of O_3 profiles simulated with CTMs against in-situ observations available from sondes at the nearest stations to the boundaries for the day 11/03/2009. Measurements and models are plotted by their own altitude.

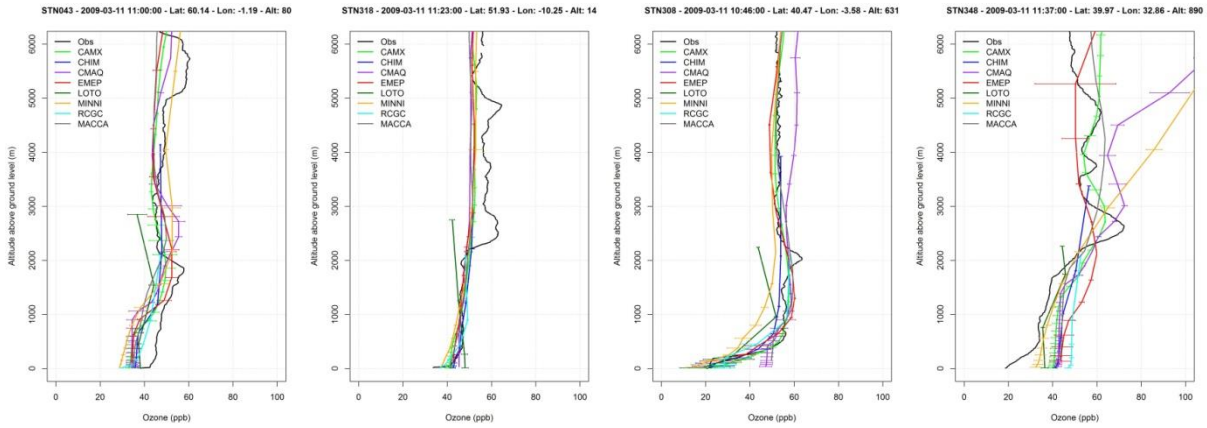

Figure 13.1: O_3 vertical profiles at the nearest stations to the boundaries the 11/03/2009. The horizontal lines by the model profiles are the standard deviation of the mean over the closest day of the measurement day.

At these stations all models show a similar behaviour. Overall the models follow the tendency of measured vertical profiles. However, they depict deficiencies to reproduce inversions ~2-3 km between low and middle troposphere. The behaviour of the models (O_3 mixing ration value and tendency) shows the biggest differences at STN348 in the southern boundary and located at high altitude (890 m a.s.l.). These differences increase with height. Overall, models show a tendency to overestimate O_3 mixing ratio under 2 km. High differences between models are also found at STN043 (O_3 mixing ratio value and tendency) in the northern domain. In contrast to southern boundary, models tend to underestimate O_3 mixing ratio under 2 km.
Overall MACC profiles are in accordance with the general behaviour of all the models.

13.4 Evaluation of the mean vertical profiles

With the objective of evaluating the performance of the models over the study period, Figure 13.2 shows the O_3 mean profiles at WOUDC station, including global statistics such as r, RMSE and MB for each model. Overall, models and measurements depict a good agreement with correlation coefficients bigger than 0.57. Only LOTO show anti-correlations at the STN318 stations in Ireland (r=--0.36). Most models (CAMx, CHIM, CMAQ, EMEP, MINNI and RCGC) show the lowest performance at STN348 station (Turkey, 890 m) with large positive bias between 7 and 14 ppb and RMSE between 9 and 18 ppb.
In order to analyse the overall model behaviour, Figure 13.3 depicts the mean profiles for all models against measurements at each station. Overall, models tend to underestimate the O_3 profiles. MACCA profiles are illustrative, hydrostatic assumption includes inconsistencies at surface for high altitude stations (> 450 m, STN631, STN348 and STN156)

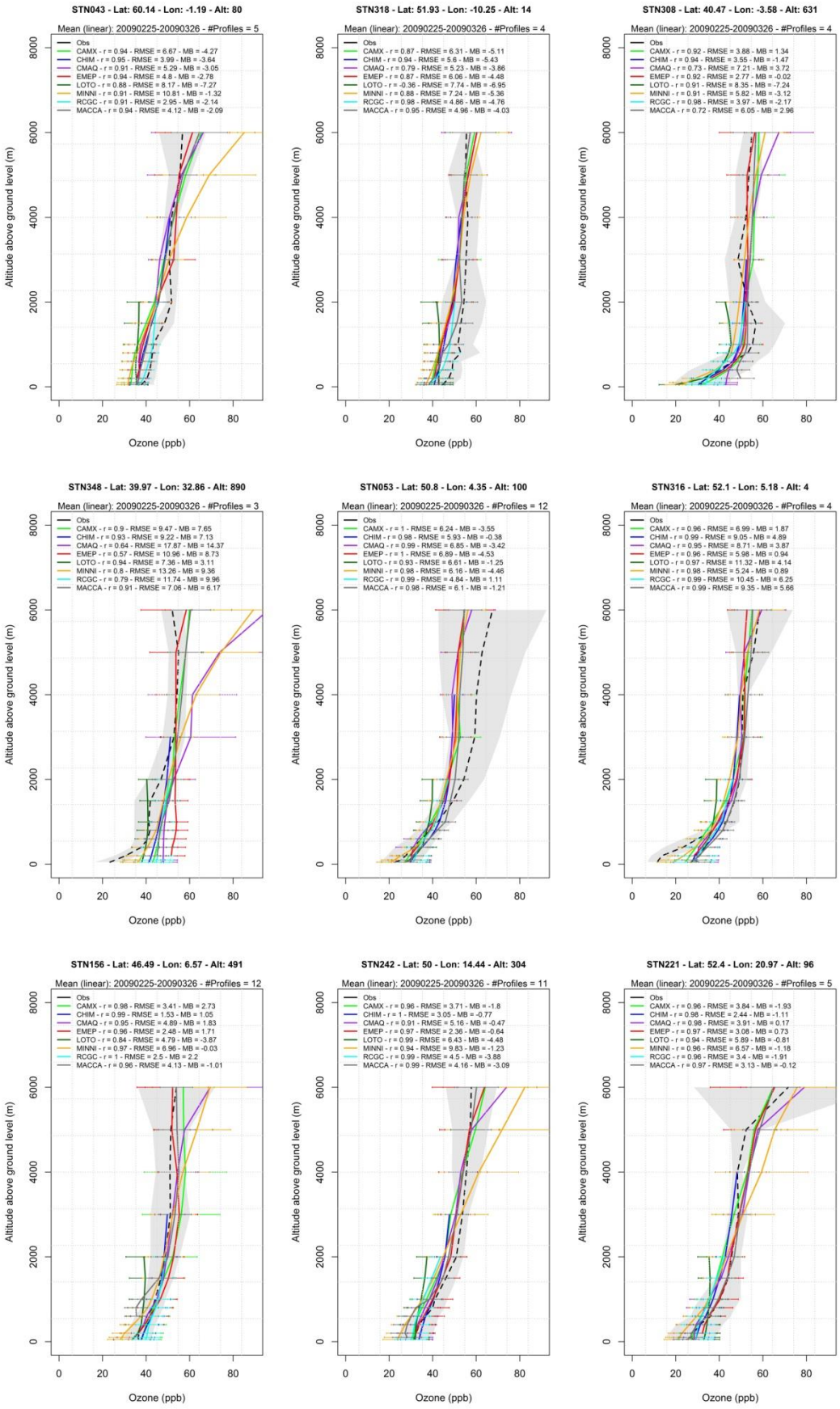

Figure 13.2. O_3 vertical profiles for WOUDC stations during the study period for each model, MACC data and measurements. The horizontal lines by the models profiles are the standard deviation of the mean. Grey shaded area shows the standard deviation of the mean measurements.

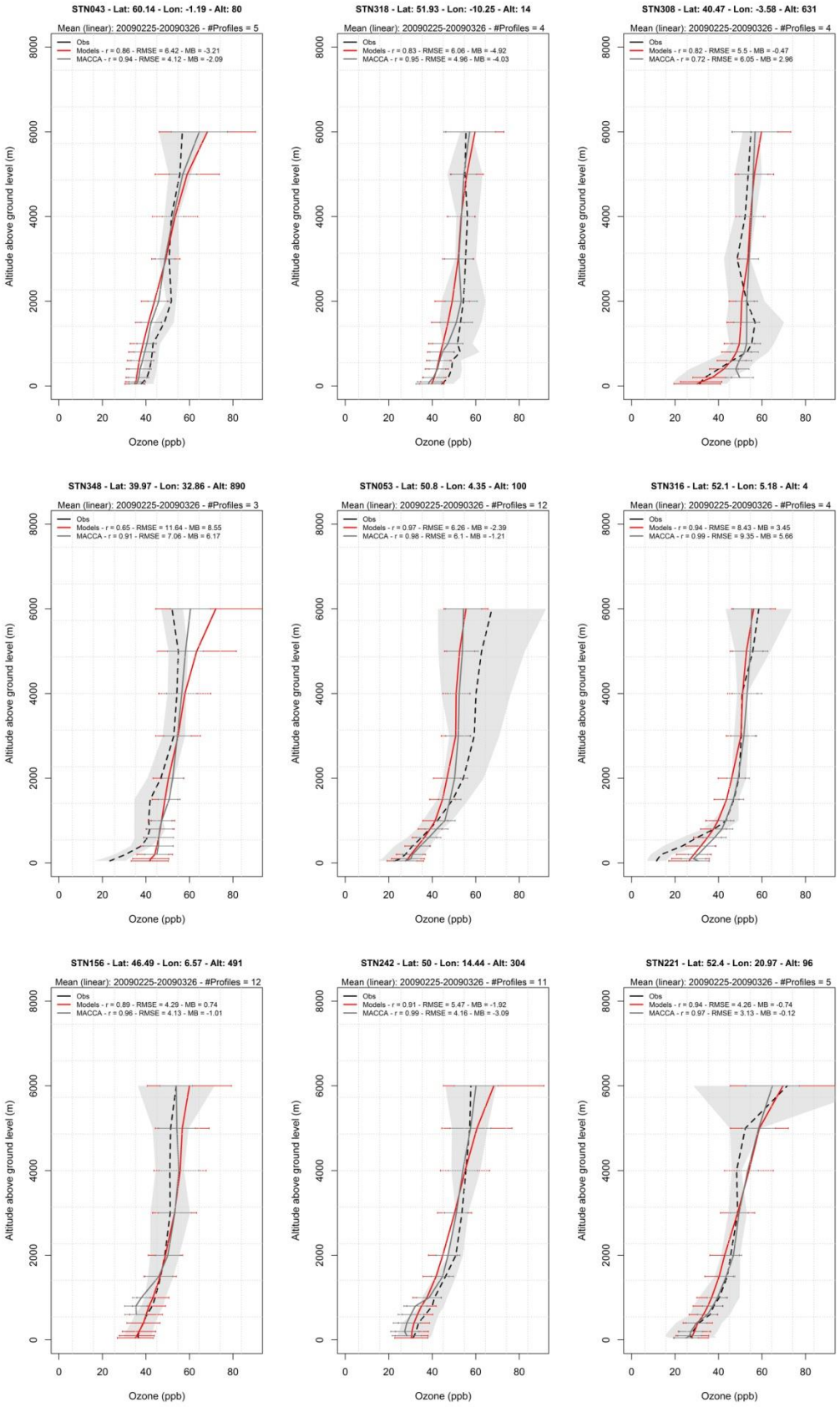

Figure 13.3. O_3 vertical profiles for WOUDC stations during the study period for the mean of the models (red), MACC data (grey) and measurements (black). The horizontal lines by the mean profiles are the standard deviation of the mean. Grey shaded area shows the standard deviation of the mean measurements.

Figure 13.4 shows the mean O_3 vertical profiles over all study period and WOUDC stations for O_3 soundings, MACCA and the mean of all models. The mean O_3 vertical profile for MACC shows a higher agreement with measurements than model's mean behaviour presenting lower RMSE (6 vs 7 ppb) and higher r (0.85 vs 0.79). Below 1 km, MB and RMSE for MACC are higher than the mean model's behaviour and no tendency is found for the correlation. Above 1 km, statistics significantly improve for MACC showing MB ~±1 ppb and RMSE ~ 4 ppb which are almost constant.

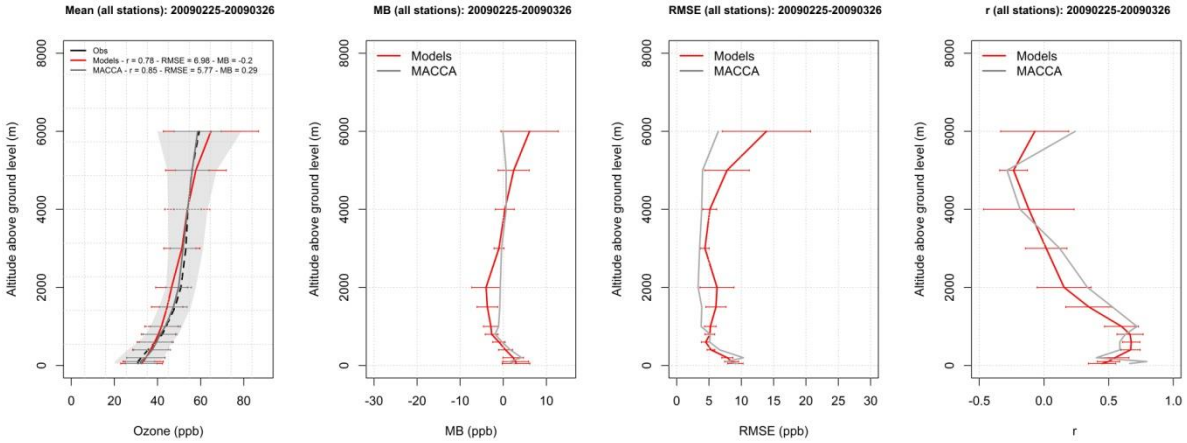

Figure 13.4. Mean O_3 vertical profiles for all models (red), MACC data (grey), and measurements (black) (a) and associated MB (b), RMSE (c) and r (d) in each level over all WOUDC stations during the study period. The horizontal lines by the mean profiles are the standard deviation of the mean. Grey shaded area shows the standard deviation of the mean measurements.

Table 13.2. Mean O_3 mixing ratio and standard deviation (SD) both in ppb for observation (obs), all models and MACC data for 2 altitude range (1) 0-2 km and (2) >2-8 km over the study period. Statistics are: mean bias (MB), mean gross error (MGE), root mean squared error (RMSE) and correlation coefficient (r).

Altitude range	Models		MACCA	
	0-2km	>2-8km	0-2km	>2-8km
Mean (obs/mod*, ppb)	41.98 / 39.91	57.53 / 61.44	33.6 / 40.69	56.81 / 59.79
SD (obs/mod*, ppb)	10.70 / 8.24	5.44 / 8.99	16.09 / 8.90	0.94 / 3.43
MB (ppb)	-1.4 (-3%)	-6.8 (7%)	7.1 (21%)	3.0 (5%)
MGE (ppb)	5.5 (-13%)	8.1 (14%)	7.2 (21%)	3.0 (5%)
RMSE(ppb)	7.2 (17%)	10.6 (18%)	10.11 (30%)	4.1 (7%)
r	0.75	0.06	0.98	0.25

**mod is equal to the mean of all the models in the case of "Models" column and mod is equal to MACC data in the case of "MACCA" column.*

Table 13.2 shows statistical evaluation as a function of two ranges of altitude: the Planetary Boundary Layer (0-2 km height) and the middle troposphere (2-8 km height). Models show better performances in the low than in the middle troposphere (the opposite happens to MACC). Models show better performance than MACC in the lower atmosphere. The models skills to represent low troposphere region (0-2km) O_3 mixing ratio are in the range of values obtained in Zyryano *et al*. (2012). We have calculated relative MB of 3%, RMSE of 17% and correlation of 0.75. This is not valid for MACC data skills, which exhibits poorer statistics: MB of 21%, RMSE of 30%, maybe due to hydrostatic assumption to estimate height. In the middle troposphere height region (2-8km) models data skills show similar values for bias and RMSE, but not for correlation. In this region MACC display better statistics than Zyryano *et al*. (2012), except for the correlation.

13.5 Discussion

In this exercise, the run setup for all models has been harmonized with respect to anthropogenic emissions, meteorology, chemical boundary condition and horizontal resolution, whereas the models are characterized with different vertical structure and employ different physical and chemical schemes. O_3 chemical boundary condition come from MACC reanalysis which is available every 3 hours with a horizontal resolution of 1.125º x 1.125º and with 60 vertical levels up to 0.1hPa. As MACC data has not the same vertical resolution as CTMs, each modelling group interpolates by pressure O_3 from MACC to their own vertical levels.

The evaluation at the nearest stations to the boundaries (STN043 in Great Britain, STN318 in Ireland, STN308 in Spain and STN348 in Turkey) shows that overall the models follow the tendency of measured vertical profiles. However, they depict deficiencies to reproduce inversions ~2-3 km between low and middle troposphere.

Although all the models show similar trends reproducing vertical profiles, some differences appear with the altitude. Between 1-2 km (low troposphere), the LOTO model systematically underestimates showing slightly deviations of O_3 mixing ratio (~5-10 ppb) respect to the models' mean behaviour, meanwhile between 2-8 km (middle troposphere) the MINNI models display the highest overestimations of O_3 mixing ratio (~5-10 ppb).

The evaluation at the WOUDC stations allows sorting the models by their performance in two groups, a first group which includes LOTO, MINNI, and RCGC with RMSE ~3-11 ppb and MB between -7 to 6 ppb. The second group comprises EMEP, CAMx, CHIM and CMAQ with RMSE ~1-9 ppb and MB ±5 ppb. This classification excludes the STN318 station in Turkey, where the models depicts the lowest performance ($7 < MB < 14$ ppb and $9 < RMSE < 18$ ppb).

The models skills to represent PBL O_3 mixing ratio are in the range of values obtained in Zyryano *et al*. (2012). We have calculated relative bias of 3%, RMSE of 17% and correlation of 0.75. This is not valid for MACC data skills: 21%, RMSE of 30% and 0.98, maybe due to hydrostatic assumption to estimate height. The evaluation of MACC data shows a better agreement with measurement in the middle than in the lower troposphere, with MB ~ 5-21%. These results are in accordance with Inness *et al*. (2013) which indicate that evaluation of MACC O_3 reanalysis agrees with O_3 sondes data to within ±10% in most situations. In the troposphere the reanalysis shows bias of -5% to 10% with respect to O_3 sondes.

14 Conclusions

This report summarises the main outcomes of a model inter-comparison over the **25/02 – 26/ 03 2009 period** which coincides with EMEP intensive measurement period so that an extended set of observational data were available. Thus, in addition to EMEP operational monitoring data, also size disaggregated (in $PM_{2.5}$ and PM_{10}) aerosols and hourly measurements for studying diurnal cycles have been employed. The exercise was performed under strict requirements: same domain, horizontal resolution, emission dataset, meteorology and boundary conditions.
We can clearly observe a rather large variability of model outputs and related performances statistics for all modelled species. Processes implemented in the model and pre-processing of input data can explain this variability in model performance. For instance, the comparison of meteorological data as used in the models displays differences on diagnosed variable like the PBL and even on directly used data like wind speed or temperature because of some differences on interpolation processes. For the wind speed some discrepancies can be observed on native IFS data. The comparison of modelled concentrations against wind speed and PBL heights confirmed that meteorology strongly influences CTMs performance. Particularly the temporal evolution of wind speed is most responsible of model skilfulness in reproducing the daily variability of pollutant concentrations (e.g. the development of peak episodes), while the reconstruction of the PBL diurnal cycle seems more influencing in driving the corresponding pollutant diurnal and hence the presence of systematic positive and negative bias detectable on daily basis.

For each species groups, we draw some general conclusions for the studied period that cannot be extrapolated to a full year.

Ozone and nitrogen dioxide
The models (with some exceptions) are found to underestimate observed ozone concentrations. EMEP, CHIM and CMAQ display the highest ozone concentrations with particularly over water surfaces but still below the observations. This negative bias is partly explained by a systematic bias produced by the boundary conditions. MINNI and RCGC show the highest negative biases but totally explained at Mace Head by the bias on boundary conditions. The spatial correlations are rather different among the models: 0.35 for CMAQ; 0.59 for CHIM, EMEP and LOTO; 0.64 for CAMX and 0.66 for MINNI and up to 0.67 for RCGC.
The performances for NO_2 are similar between all models (with five of the models underestimating and two overestimating the observations); the highest positive bias is given for CMAQ. For all models the correlations in time and space are close to 0.6.
Regarding the ozone profiles, the models skills to represent PBL O3 mixing ratio are in the range of values obtained in other studies. We have calculated relative bias of 3%, RMSE of 17% and correlation of 0.75. This is not valid for MACC data skills: 21%, RMSE of 30% and 0.98, maybe due to hydrostatic assumption to estimate height. The evaluation of MACC data shows a better agreement with measurement in the middle than in the lower troposphere, with MB ~ 5-21%. In the troposphere the reanalysis shows bias of -5% to 10% with respect to O_3 sondes.

PM_{10} and $PM_{2.5}$
For PM_{10} concentrations the variability of model results is significant and is mostly associated with model treatments of natural PM (dust and sea salts). The main hotspot in Poland and Po valley are simulated by all models. MINNI and CHIM results are found to be closer to the PM_{10} and $PM_{2.5}$ observations in term of bias; EMEP has the best correlation coefficient. Usually, all models underestimate the highest values, MINNI and CHIM can overestimate some low values. For most of

stations the error on PM_{10} is dominated by a problem of a time correlation, for LOTO it is more mixed with a problem of correlation and standard deviation.
The spatial variability is poorly represented by the models, the gradient from low to high values is too low compared to observations.

Deposition
Regarding wet deposition most of the models show a better agreement with observations at sites with relatively low and medium measured accumulated wet deposition values. For WNHx most of the models underestimate the highest observed values, with EMEP presenting the lowest mean bias. The lowest mean RMSE is obtained by LOTOS, with also the better spatial correlation. In the case of WNOx there is a general tendency to underpredict the highest accumulated wet depositions, with some differences between the models: CHIM, EMEP and LOTO calculate higher values than the other models for this period, being closer to observations. In the case of WSOx, CMAQ is providing the best performance for the highest observed values, most of them registered in the Atlantic area. This fact seems to be related to the natural sulphate emissions associated to sea salt processes that this model considers (note that SO4 observed in precipitations were not corrected for sea salt sulphate). Unfortunately, the uneven distribution of monitoring sites makes it difficult to decide on model performance in some areas of Europe with strong differences between models.
Regarding dry deposition and in the case of DNOx, CMAQ estimates the highest deposition over the Mediterranean area and the eastern part of the domain. Strong differences are found between this model and the rest, with CHIM/RCGC/EMEP group presenting the lowest values. For DSOx, CMAQ is also estimating the highest values, and EMEP and MINNI the lowest ones. For DNHx differences between models are not as strong as those found for DSOx and DNOx, with all the models presenting a quite similar spatial pattern. The importance of having any kind of methodology to evaluate dry deposition is clear, in the light of the results, especially for SOx and NOx.

Sulphur compounds
On average EMEP, CHIM and LOTO have the lowest bias for SO_2 concentrations. In this exercise CAMX has too high concentrations because all SO_2 was injected at the ground level, high concentrations are also displayed for RCGC. The correlation coefficients between calculated and measured SO_2 are quite similar for the models. EMEP, CMAQ and MINNI behave the best for sulphate concentrations when looking at the RMSE. CHIM has the highest overestimation of sulphate concentrations. The results from all models have to some extend been affected by overestimated MACCA boundary conditions at the eastern boarders. Even if the sulphur chemistry is well known, the co-analysis of sulphur depositions and concentrations suggest that some improvements can be done yet on this topic, which has a direct influence on SIA chemistry.

Nitrate and ammonium
Nitrate and ammonium are the species simulated by the models the best in this exercise; the main regional footprint is coherent between models with some local differences over the Benelux and the Po valley. However differences appear between models. For nitrates, LOTO and EMEP simulate the lowest concentration values, CHIM simulates low values in the south of Europe. For the total nitrate (TNO3), there is clearly a difference between one group of models MINNI, RCGC, CMAQ and CAMX which strongly overestimate the concentrations with the other group CHIM, EMEP and LOTO which slightly underestimate the total nitrate concentrations.

CHIM, EMEP and LOTO underestimate the highest values of nitrate concentrations. The models behaviour for nitrates shows a clear difference between the group LOTO/EMEP/CHIM which underestimate the high nitrate concentrations (-30 to -40%) with the other models which have a slight overestimate.

Carbonaceous species

EC-10 concentrations are on average overestimated by the models, with biases up to 50-60% for CHIM, RCGC and MINNI, only EMEP has a null bias.

Regarding SOA concentrations in models, a first comparison with OOA measurements tends to support the assumption that models underestimate concentrations. CHIM exhibits the lowest underestimations particularly in ES78 but with a low correlation. In Melpitz and Vavihill the amplitude of OOA peaks are not reproduced by the models with SOA. At this stage, it is difficult to say more on this comparison because a part of OOA can have a primary origin. Indeed, the observed OOA and BBOA concentrations peaks seem correlated particularly in Vavihill (SE11). The implementation of more sophisticated module and a work on the harmonization of POA emissions is a pressing issue. For the highest values, all models underestimate the organic matter by a factor of 2 to 6.

Natural aerosols

All the models simulate high concentrations of sea salt sodium over the oceans and seas with some differences because of the parameterisation. On average the spatial correlation is very good in the range 0.90 – 0.95 for all models. CHIM and MINNI give the highest values over lands and clearly display an overestimation.

EMEP and LOTO simulate the lowest dust concentrations values, whereas RCGC and MINNI the highest ones. The correlations in time and space for dust concentrations in the PM_{10} fraction are close to zero for all models, the spatial correlations are better for LOTO and RCGC (0.50) and EMEP (0.62) and near zero for all other models. This large difference on correlations between EMEP, LOTO and RCGC with the other models shows that the dust parameterisations used in these models were more successful in reproducing dust events during the considered period.

Acknowledgements

The EBAS database has largely been funded by the CLRTAP-EMEP programme, AMAP and by NILU internal resources. Specific developments have been possible due to projects like EUSAAR (EBAS web interphase), EBAS-Online (upgrading of database platform) and HTAP (import and export routines to build a secondary repository for in support of www.htap.org. A large number of specific projects have supported development of data and metadata reporting schemes in dialog with data providers (CREATE, ACTRIS and others). For a complete list of programmes and projects for which EBAS serves as a database, please consult the information box in the Framework filter of the web interface. These are all highly acknowledged for their support.

INERIS was financed by the French Ministry in charge of Ecology. **RSE** contribution to this work has been financed by the Research Fund for the Italian Electrical System under the Contract Agreement between RSE S.p.A. and the Ministry of Economic Development - General Directorate for Nuclear Energy, Renewable Energy and Energy Efficiency in compliance with the Decree of March 8, 2006.

15 References

Aas, W., Tsyro, S., Bieber, E., Bergström, R., Ceburnis, D., Ellermann, T., Fagerli, H., Frölich, M., Gehrig, R., Makkonen, U., Nemitz, E., Otjes, R., Perez, N., Perrino, C., Prévôt, A. S. H., Putaud, J.-P., Simpson, D., Spindler, G., Vana, M., and Yttri, K. E. (2012) Lessons learnt from the first EMEP intensive measurement periods, Atmos. Chem. Phys., 12, 8073-8094.

Aksoyoglu, S., Keller, J., Barmpadimos, I., Oderbolz, D., Lanz, V. A., Prévôt, A. S. H., and Baltensperger, U. (2011) Aerosol modelling in Europe with a focus on Switzerland during summer and winter episodes, *Atmos. Chem. Phys.,* 11, 7355-7373, doi:10.5194/acp-11-7355-2011.

Ansari, A.S., Pandis, S. (1998) Response of inorganic PM to precursor concentrations. *Environ. Sci. Technol*, 32, 2706-2714.

Banzhaf, S., M. Schaap, A. Kerschbaumer, E. Reimer,R. Stern, E. van der Swaluw, P. Builtjes (2012) Implementation and evaluation of pH-dependent cloud chemistry and wet deposition in the chemical transport model REM-Calgrid, *Atmos. Environ*., Volume 49, Pages 378–390.

Beltman, J.B., Hendriks, C., Tum, M., Schaap, M. (2013) The impact of large scale biomass production on ozone air pollution in Europe, *Atmos. Environ*, Volume 71, Pages 352-363.

Benedetti, A., Morcrette, J.-J., Boucher, O., Dethof, A., Engelen, R. J., Fisher, M., Flentje, H., Huneeus, N., Jones, L., Kaiser, J. W., Kinne, S., Mangold, A., Razinger, M., Simmons, A. J., Suttie, M., and the GEMS-AER team (2009) Aerosol analysis and forecast in the European Centre for Medium-Range Weather Forecasts Integrated Forecast System: 2. Data assimilation, *J. Geophys. Res*., 114.

Bessagnet, B. *et al*. (2012) The CHIMERE atmospheric model, *EC4MACS publications*, http://www.ec4macs.eu/content/report/EC4MACS_Publications/MR_Final%20in%20pdf/Chimere_Methodologies_Final.pdf

Bessagnet B., L. Menut, G. Curci, A. Hodzic, B. Guillaμme, C. Liousse, S. Moukhtar, B. Pun, C. Seigneur, M. Schulz (2009) Regional modelling of carbonaceous aerosols over Europe - Focus on Secondary Organic Aerosols, *Journal of Atmospheric Chemistry*, 61, 175-202.

Binkowski, F. and Shankar, U. (1995) The Regional Particulate Matter Model .1. Model description and preliminary results, *J. Geophys. Res*., 100, 26191–26209.

Binkowski F. S. (1999): The aerosol portion of Models-3 CMAQ. In Science Algorithms of the EPA Models-3 Community Multiscale Air Quality (CMAQ) Modeling System. Part II: Chapters 9-18. D.W. Byun, and J.K.S. Ching (Eds.). EPA-600/R-99/030, National Exposure Research Laboratory, U.S. *Environmental Protection Agency*, Research Triangle Park, NC, 10-1-10-16.

Binkowski, F S., Roselle, S. J. (2003) Models-3 Community Multiscale Air Quality (CMAQ) model aerosol component 1: Model Description. *J. Geophys. Res*., Vol 108, No D6, 4183 doi:10.1029/2001JD001409.

Bott, A. (1989) A Positive Definite Advection Scheme Obtained by Nonlinear Renormalization of the Advective Fluxes. *Mon. Wea. Rev*., 117, 1006-1015.

Businger, J.A. (1971) Comments on free convection in the turbulent Ekman layer of the atmosphere, J. Atmos. Sci. 28, 298-299.

Byun, D., Schere, K.L. (2006) Review of the governing equations, computational algorithms, and other components of the models-3 Community Multiscale Air Quality (CMAQ) modeling system. *Applied Mechanics Reviews,* 59, 51-77.

Carson, D.J. (1973) The development of a dry inversion-capped convectively unstable boundary layer. *Q. J. R. Met. Soc.*, 99, 450-467.

Carlton, A. G., Bhave, P. V., Napelenok, S. L., Edney, E. O., Sarwar, G., Pinder, R. W., Pouliot, G. A., and Houyoux, M. (2010) Model representation of secondary organic aerosol in CMAQv4.7, *Environ. Sci. Technol.*, 44, 8553-8560.

Carter W.P.L. (2000a) Documentation of the SAPRC-99 Chemical Mechanism for VOC Reactivity Assessment," Draft report to the California Air Resources Board, Contracts 92-329 and 95-308, May 8, available at http://www.cert.ucr.edu/~carter/absts.htm#saprc99).

Carter W.P.L. (2000b) Implementation of the SAPRC-99 Chemical Mechanism into the Models-3 Framework," Report to the United States Environmental Protection Agency, January 29. Available at http://www.cert.ucr.edu/~carter/absts.htm#s99mod3).

Chang, J.S., R.A. Brost, I.S.A. Isaksen, S. Madronich, P. Middleton, W.R. Stockwell, and C.J, Walcek (1987) A Three-dimensional Eulerian Acid Deposition Model: Physical Concepts and Formulation. *J. Geophys. Res*., 92, 14,681-14,700.

Cheinet, S. (2002) The parameterization of clear and cloudy convective boundary layers. Ph.D. Thesis, Ecole Polytechnique, Paris, France.

Claiborn, C., Lamb, B., Miller, A., Beseda, J., Clode, B., Vaughan, J., Kang, L., and Nevine, C. (1998) Regional measurements and modelling of windblown agricultural dust: The Columbia Plateau PM_{10} Program, *J. Geophys. Res*., 103(D16), 19 753-19 767.

Clarke, A. D., Owens, S. R., and Zhou, J. C. (2006) An ultrafine sea-salt flux from breaking waves Implications for cloud condensation nuclei in the remote marine atmosphere, *J. Geophys. Res*., 111, D06202, doi:10.1029/2005JD006565.

Colella, P., Woodward (1984) The piecewise parabolic method (PPM) for gas dynamical simulation. *J. Comput. Phys*., 54, 174-201.

Crippa, M., Canonaco, F., Lanz, V. A., Äijälä, M., Allan, J. D., Carbone, S., Capes, G., Dall'Osto, M., Day, D. A., DeCarlo, P. F., Di Marco, C. F., Ehn, M., Eriksson, A., Freney, E., Hildebrandt Ruiz, L., Hillamo, R., Jimenez, J.-L., Junninen, H., Kiendler-Scharr, A., Kortelainen, A.-M., Kulmala, M., Mensah, A. A., Mohr, C., Nemitz, E., O'Dowd, C., Ovadnevaite, J., Pandis, S. N., Petäjä, T., Poulain, L., Saarikoski, S., Sellegri, K., Swietlicki, E., Tiitta, P., Worsnop, D. R., Baltensperger, U., and Prévôt, A. S. H. (2013) Organic aerosol components derived from 25 AMS datasets across Europe using a newly developed ME-2 based source apportionment strategy, *Atmos. Chem. Phys. Discuss*., 13, 23325-23371, doi:10.5194/acpd-13-23325-2013.

Denier van der Gon, H., Jozwicka, M., Hendriks, E., Gondwe, M., and Schaap, M. (2010) Mineral dust as a component of particulate matter, Tno, bop - wp2 - report, report 500099003, TNO Delft, The Netherlands, www.pbl.nl, iSSN:1875–2322 (print) ISSN: 1875- 2314 (on line).

Doms, G., J., F., Heise, E., Herzog, H.-J., Mrionow, D., Raschendorfer, M., Reinhart, T., Ritter, B., Schrodin, R., Schulz, J.-P. and Vogel, G. (2011) A Description of the Nonhydrostatic Regional COSMO Model. Part II: Physical Parameterization, *Tech. Rep., Deutscher Wetterdienst*, http://www.cosmo-model.org/content/ model/documentation/core/cosmoPhysParamtr.pdf.

Emberson, L.D., Ashmore, M.R., Simpson, D., Tuovinen, J.-P., Cambridge, H.M. (2000a) Towards a model of ozone deposition and stomatal uptake over Europe. *EMEP/MSC-W 6/2000, Norwegian Meteorological Institute*, Oslo, Norway, 57 pp.

Emberson, L.D., Ashmore, M.R., Simpson, D., Tuovinen, J.-P., Cambridge, H.M. (2000b) Modelling stomatal ozone flux across Europe. *Water, Air and Soil Pollution 109*, 403-413.

EMEP (2003) Transboundary acidification, eutrophication and ground level ozone in Europe. Part I: Unified EMEP model description. *EMEP status Report 1/2003.*

Gong, S.L. (2003) A parameterization for sea-salt aerosol source function for sub- and super-micron particle sizes. *Biogeochemical Cycles*, 17, 1097-1104.

Guenther, A., Karl, T., Harley, P., Wiedinmyer, C., Palmer, P. I., and Geron, C. (2006) Estimates of global terrestrial isoprene emissions using MEGAN (Model of Emissions of Gases and Aerosols from Nature), *Atmos. Chem. Phys*., 6, 3181-3210, doi:10.5194/acp-6-3181-2006.

Guenther, A. B., Jiang, X., Heald, C. L., Sakulyanontvittaya, T., Duhl, T., Emmons, L. K., and Wang, X. (2012) The Model of Emissions of Gases and Aerosols from Nature version 2.1 (MEGAN2.1): an extended and updated framework for modellingbiogenic emissions, *Geosci. Model Dev*., 5, 1471-1492, doi:10.5194/gmd-5-1471-2012.

Guinot, B., Cachier, H., and Oikonomou, K. (2007) Geochemical perspectives from a new aerosol chemical mass closure, *Atmos. Chem. Phys.,* 7, 1657-1670, doi:10.5194/acp-7-1657-2007.

Gong, S., Barrie, L., and Blanchet, J. (1997) Modelling sea-salt aerosols in the atmosphere .1. Model development, *J. Geophys. Res*., 102, 3805–3818, doi:10.1029/96JD02953.

Gong, S. (2003) A parameterization of sea-salt aerosol source function for sub- and super-micron particles, *Global Biogeochemical Cycles*, Volume 17, Issue 4, DOI: 10.1029/2003GB002079.

Hanna, S. R., Schulman, L. L., Paine, R. J., Pleim, J. E., and Baer, M. (1985) Development and evaluation of the offshore and coastal dispersion model, *J. Air Pollut. Control Assoc*., 35, 1039–1047.

Hayami, H., Sakurai, T., Han, Z., Ueda, H., Carmichael, G.R., Streets, D., Holloway, T., Wang, Z., Thongboonchoo, N., Engardt, M., Bennet, C., Fung, C., Chang, A., Park, S.U., Kajino, M., Sartelet, K., Matsuda, K., Amann, M. (2008) MICS-Asia II: model intercomparison and evaluation of particulate sulfate, nitrate and ammonium. *Atmos. Environ*., 42, 3510e3527

Holtslag, A.A.M. and van Ulden, A.P. (1983) A simple scheme for daytime estimates of the surface fluxes from routine weather data. *J. Clim. and Appl. Meteor*., 22, 517-529.

Hosker, R. P. (1974) A comparison of estimation procedures for over-water plume dispersion. ATDL contribution file ; no.99. Oak Ridge, Tenn.: Air Resources Atmospheric Turbulence and Diffusion Laboratory.

Ingleby, B., Isaksen, L. And Dahoui, M. (2013) Comparison of Met Office and ECMWF Background Fields with Conventional Observations, Sixth WMO Symposium on Data Assimilation, 7-11 October 2013.

Inness, A., Baier, F., Benedetti, A., Bouarar, I., Chabrillat, S., Clark, H., Clerbaux, C., Coheur, P., Engelen, R. J., Errera, Q., Flemming, J., George, M., Granier, C., Hadji-Lazaro, J., Huijnen, V., Hurtmans, D., Jones, L., Kaiser, J. W., Kapsomenakis, J., Lefever, K., Leitão, J., Razinger, M., Richter, A., Schultz, M. G., Simmons, A. J., Suttie, M., Stein, O., Thépaut, J.-N., Thouret, V., Vrekoussis, M., Zerefos, C., and the MACC team (2013) The MACC reanalysis: an 8 yr data set of atmospheric composition, *Atmos. Chem. Phys*., 13, 4073-4109, doi:10.5194/acp-13-4073-2013.

Jeričevič, A., Kraljevič, L., Grisogono, B., Fagerli, H., and Večenaj, Ž. (2010) Parameterisation of vertical diffusion and the atmospheric boundary layer height determination in the EMEP model, *Atmos. Chem. Phys.,* 10, 341-364; doi:10.5194/acp-10-341-2010.

Knote C., Brunner D., Vogel H., Allan, Asmi J.A., Aijala M., Carbone S., van der Gon H. D., Kiendler-Scharr A., Mohr C., Poulain L., Prevot A. S. H., Swietlicki E., and Vogel B. (2011) Towards an online-coupled chemistry-climate model: evaluation of trace gases and aerosols in COSMO-ART, *Geosci. Model Dev.,* 4, 1077–1102.

Koeble, R. and Seufert, G. (2001) Novel Maps for Forest Tree Species in Europe, in: A Changing Atmosphere, 8th European Symposium on the Physico-Chemical Behaviour of Atmospheric Pollutants, Torino, Italy, 17–20 September, 2001, http://ies.jrc.ec.europa.eu/Units/cc/events/torino2001/torinocd/ Documents/Terrestrial/TP35.htm.

Köhler, I., Sausen, R., and Klenner, G. (1995) NOx production from lightning, The impact of NOx emissions from aircraft upon the atmosphere at flight altitudes 8–15 km (AERONOX), edited by: Schumann, U., final report to the Commission of the European Communities, Deutch Luft und Raumfart, Oberpfaffenhofen, Germany.

Kuenen, J., H. Denier van der Gon, A. Visschedijk, H. van der Burgh, R. van Gijlswijk (2011) MACC European emission inventory 2003-2007, *TNO report*, TNO-060-UT-2011-00588.

Loosemore, G. A. and Hunt, J. R. (2000) Dust resuspension without saltation, *J. Geophys. Res*., 105(D16), 20663-20671.

Lindfors V. and Laurila T. (2000) Biogenic volatile organic compound (VOC) emissions from forests in Finland, *Bor. Env. Res*., 5: 95–113.

McKeen, S., Chung, S.H., Wilczak, J., Grell, G., Djalalova, I., Peckham, S., Gong, W., Bouchet, V., Moffet, R., Tang, Y., Carmichael, G.R., Mathur, R., Yu, S. (2007) Evaluation of several real-time $PM_{2.5}$ forecast models using data collected during the ICARTT/NEAQS 2004 field study. *J. of Geo. Res*., 112 (D10S20), 20, doi:10.1029/2006JD007608.

Martensson, E., Nilsson, E., de Leeuw, G., Cohen, L., and Hansson, H.-C. (2003) Laboratory simulations and parameterisation of the primary marine aerosol production, *J. Geophys. Res*., 108, 4297, doi:10.1029/2002JD002263.

Matthias V., Aulinger A., Quante M. (2008) Adapting CMAQ to investigate air pollution in North Sea coastal regions . *Environmental Modelling & Software*, 23, 356-368.

Maul, P.R. (1980) Atmospheric transport of sulfur compound pollutants. Central Electricity Generating Bureau MID, SSD/80/0026/R, Nottingham. England.

Minguillón, M. C., Perron, N., Querol, X., Szidat, S., Fahrni, S. M., Alastuey, A., Jimenez, J. L., Mohr, C., Ortega, A. M., Day, D. A., Lanz, V. A., Wacker, L., Reche, C., Cusack, M., Amato, F., Kiss, G., Hoffer, A., Decesari, S., Moretti, F., Hillamo, R., Teinilä, K., Seco, R., Peñuelas, J., Metzger, A., Schallhart, S., Müller, M., Hansel, A., Burkhart, J. F., Baltensperger, U., and Prévôt, A. S. H. (2011) Fossil versus contemporary sources of fine elemental and organic carbonaceous particulate matter during the DAURE campaign in Northeast Spain, *Atmos. Chem. Phys*., 11, 12067-12084, doi:10.5194/acp-11-12067-2011.

Mol, W.J.A., Leeuw F.A.A.M. de (2005) AirBase: A Valuable Tool in Air Quality Assessments in: The Proceedings of the 5th International Conference on Urban Air Quality, Valencia Spain 29-31 March 2005, Editors R.S. Sokhi, M.M. Millán and N. Moussiopoulos.

Monahan, E. C. (1986). In The Role of Air-Sea Exchange in Geochemical Cycling, chapter The ocean as a source of atmospheric particles, pages 129–163. Kluwer Academic Publishers, Dordrecht, Holland.

Nenes, A, C. Pilinis, and S.N. Pandis (1998) ISORROPIA: A New Thermodynamic Model for Multiphase Multicomponent Inorganic Aerosols. Aquatic Geochemistry, 4, 123-152.

Nenes, A., Pilinis, C., and Pandis, S. N. (1999) Continued development and testing of a new thermodynamic aerosol module for urban and regional air quality models, *Atmos. Environ*., 33, 1553–1560.

Oderbolz, D. C., Aksoyoglu, S., Keller, J., Barmpadimos, I., Steinbrecher, R., Skjøth, C. A., Plaß-Dülmer, C., and Prévôt, A. S. H. (2013) A comprehensive emission inventory of biogenic volatile organic compounds in Europe: improved seasonality and land-cover, *Atmos. Chem. Phys*., 13, 1689-1712, doi:10.5194/acp-13-1689-2013.

O'Brien J.J. (1970) A note on the vertical structure of the eddy exchange coefficient in the planetary boundary layer. *J Atmos Sci*, 27:1213–1215

Pal, S., Haeffelin, M., Batchvarova E. (2013) Exploring a geophysical process-based attribution technique for the determination of the atmospheric boundary layer depth using aerosol lidar and near-surface meteorological measurements, *in press*, *Journal of Geophysical Research (Atmospheres)*, 118, 1–19, doi:10.1002/jgrd.50710.

Pay, M.T., Jiménez-Guerrero. P., Baldasano, J.M. (2012) Assessing sensitivity regimes of secondary inorganic aerosol formation in Europe with the CALIOPE-EU modellingsystem. *Atmos. Environ.*, 51, 146-164.

Perniogotti *et al*. (2013) POMI: a model inter-comparison exercise over the Po Valley, *Air Qual Atmos Health*, DOI 10.1007/s11869-013-0211-1.

Pleim, J. (2007) A combined local and nonlocal closure model for the atmospheric boundary layer. Part I: model description and testing. *J. Appl. Met. Climatology*, 46, 1383---1395.

Putaud, J.-P., Van Dingenen, R., Dell'Acqua, A., Raes, F., Matta, E., Decesari, S., Facchini, M. C., and Fuzzi, S. (2004) Size-segregated aerosol mass closure and chemical composition in Monte Cimone (I) during MINATROC, *Atmos. Chem. Phys*., 4, 889-902, doi:10.5194/acp-4-889-2004.

Reimer, E. and Scherer, B. (1992) An operational meteorological diagnostic system for regional air pollution analysis and long term modelling, In: Air Pollution Modelling and its Application IX, edited by: H. v. Dop, and G. Kallos (Eds.), *NATO Challenges of Modern Society, Kluwer Academic/Plenum Publisher*, New York.

Schaap, M., Manders, A.M.M., Hendriks, E.C.J., Cnosse, J.M, Segers, A.J.S., Denier van der Gon, H.A.C., Jozwicka, M., Sauter, F., Velders, G., Matthijsen, J., Builtjes, P.J. H. (2009) Regional modelling of particulate matter for the Netherlands, *BOP report 500099008, PBL, the Netherlands*.

Schell, B., Ackermann, I.J., Hass, H., Binkowski, F.S., Ebel, A. (2001) Modelling the formation of secondary organic within a comprehensive air quality model system. *J. Geophys. Res*., 106, 28275-28293.

Seinfeld, J.H. and S.N. Pandis (1998) Atmospheric Chemistry and Physics, From Air Pollution to Climate Change. *John Wiley and Sons, Inc., NY*.

Simpson, D., Winiwarter, W., Börjesson, G., Cinderby, S., Ferreiro, A., Guenther, A., Hewitt, C. N., Janson, R., Khalil, M. A. K., Owen, S., Pierce, T. E., Puxbaum, H., Shearer, M., Skiba, U., Steinbrecher, R., Tarrason, L., and Öquist, M. G. (1999) Inventorying emissions from Nature in Europe, *J. Geophys. Res.*, 104, 8113– 8152.

Simpson, D., Benedictow, A., Berge, H., Bergström, R., Emberson, L. D., Fagerli, H., Flechard, C. R., Hayman, G. D., Gauss, M., Jonson, J. E., Jenkin, M. E., Nyíri, A., Richter, C., Semeena, V. S., Tsyro, S., Tuovinen, J.-P., Valdebenito, Á., and Wind, P. (2012) The EMEP MSC-W chemical transport model – technical description. *Atmos. Chem. Phys*., 12, 7825–7865.

Smyth, S.C., Jiang, W., Roth, H., Moran, M.D., Makar, P.A., Yang, F., Bouchet, V.S., Landry, H. (2009) A comparative performance evaluation of the AURAMS and CMAQ air quality modelling systems. *Atmos. Environ*., 43, 1059e1070.

Solazzo, E., Roberto Bianconi, Guido Pirovano, Volker Matthias, Robert Vautard, Michael D. Moran, K. Wyat Appel, Bertrand Bessagnet, Jørgen Brandt, Jesper H. Christensen, Charles Chemel, Isabelle Coll, Joana Ferreira, Renate Forkel, Xavier V. Francis, Georg Grell, Paola Grossi, Ayoe B. Hansen, Ana Isabel Miranda, Uarporn Nopmongcol, Marje Prank, Karine N. Sartelet, Martijn Schaap, Jeremy D. Silver, Ranjeet S. Sokhi, Julius Vira, Johannes Werhahn, Ralf Wolke, Greg Yarwood, Junhua Zhang, S. Trivikrama Rao, Stefano Galmarini, (2012) Operational model evaluation for particulate matter in Europe and North America in the context of AQMEII, *Atmos. Environ*., Volume 53, Pages 75-92, ISSN 1352-2310, http://dx.doi.org/10.1016/j.atmosenv.2012.02.045.

Sorensen, J.H. (1998) Sensitivity of the DERMA long-range gaussian dispersion model to meteorological input and diffusion parameters. *Atmos. Environ.*, 32 (24), 4195-4206.

Stern, R., Builtjes, P., Schaap, M., Timmermans, R., Vautard, R., Hodzic, A., Memmesheimer, M., Feldmann, H., Renner, E., Wolke, R., Kerschbaumer, A. (2008) A model inter-comparison study focussing on episodes with elevated PM_{10} concentrations. *Atmos. Environ,* 42, 4567e4588.

Strader, R., F. Lurmann, and S.N. Pandis (1999) Evaluation of secondary organic aerosol formation in winter. *Atmos. Environ*., 33, 4849-4863.

Terrenoire, E., Bessagnet, B., Rouïl, L., Tognet, F., Pirovano, G., Létinois, L., Colette, A., Thunis, P., Amann, M., and Menut, L. (2013) High resolution air quality simulation over Europe with the chemistry transport model CHIMERE, *Geosci. Model Dev. Discuss*., 6, 4137-4187, doi:10.5194/gmdd-6-4137-2013.

Thunis P., C. Cuvelier, P. Roberts, L. White, L. Post, L. Tarrason, S. Tsyro, R. Stern, A. Keschbaμmer, L.Rouil, B. Bessagnet, R. Bergstrom, M. Schaap, G. Boersen, P. Builtjes (2008) EuroDelta-II, Evaluation of a Sectorial Approach to Integrated Assessment Modelling including the Mediterranean Sea. *JRC Scientific and Technical Reports* – EUR 23444 EN 2008.

Thunis, P., A. Pederzoli, D. Pernigotti, (2012) Performance criteria to evaluate air quality modelling applications., *Atmos. Environ*., 59, 476-482.

Troen, I. and L. Mahrt (1986) A simple model of the atmospheric boundary layer: Sensitivity to surface evaporation. *Bound.-Layer Meteorol.*, 37, 129-148.

Tsyro, S., Aas, W., Soares, J., Sofiev, M., Berge, H., and Spindler, G. (2011) Modelling of sea salt concentrations over Europe: key uncertainties and comparison with observations, *Atmos. Chem. Phys.*, 11, 10367–10388, doi:10.5194/acp-11-10367-2011.

Tuovinen, J.-P., Ashmore, M., Emberson, L., and Simpson, D. (2004) Testing and improving the EMEP ozone deposition module, *Atmos. Environ*., 38, 2373–2385.

Van Loon, M., R. Vautard, M. Schaap, R. Bergström, B. Bessagnet, J. Brandt, P.J.H. Builtjes, J. H. Christensen, C. Cuvelier, A. Graf, J.E. Jonson, M. Krol, J. Langner, P. Roberts, L. Rouil, R. Stern, L. Tarrasón, P. Thunis, E. Vignati, L. White, P. Wind (2007) Evaluation of long-term ozone simulations from seven regional air quality models and their ensemble average. *Atmos. Environ*., 41, 2083-2097.

Vautard, R., B. Bessagnet, M. Chin, and L. Menut (2005) On the contribution of natural Aeolian sources to particulate matter concentrations in Europe: testing hypotheses with a modelling approach, *Atmos. Environ.*, 39, 3291–3303.

Vautard, R., M. Van Loon, M. Schaap, R. Bergström, B. Bessagnet, J. Brandt, P.J.H. Builtjes, J. H. Christensen, C. Cuvelier, A. Graf, J.E. Jonson, M. Krol, J. Langner, P. Roberts, L. Rouil, R. Stern, L. Tarrasón, P. Thunis, E. Vignati, L. White, P. Wind (2006) Is regional air quality model diversity representative of uncertainty for ozone simulation? *Geophys. Res. Lett.*, 33, L24818, doi:10.1029/2006GL027610.

Vautard, R., P.H.J. Builtjes, P. Thunis, C. Cuvelier, M. Bedogni, B. Bessagnet, C. Honoré, N. Moussiopoulos, G. Pirovano, M. Schaap, R. Stern, L. Tarrason, P. Wind (2007) Evaluation and intercomparison of Ozone and PM_{10} simulations by several chemistry transport models over four European cities within the CityDelta project, *Atmos. Environ*., Volume 41, Issue 1, Pages 173-188, ISSN 1352-2310, http://dx.doi.org/10.1016/j.atmosenv.2006.07.039.

Vautard R., M. Schaap, R. Bergström, B. Bessagnet, J. Brandt, P.J.H. Builtjes, J.H. Christensen, C. Cuvelier, V. Foltescu, A. Graff, A. Kerschbaumer, M. Krol, P. Roberts, L. Rouïl, R. Stern, L. Tarrason, P. Thunis, E. Vignati, P. Wind (2009) Skill and uncertainty of a regional air quality model ensemble, *Atmos. Environ.*, Volume 43, Issue 31, Pages 4822-4832, ISSN 1352-2310, 10.1016/j.atmosenv.2008.09.083.

van Leer B. (1984) Multidimensional explicit difference schemes for hyperbolic conservation laws, in Computing Methods in Applied Sciences and Engineering VI, *edited by R. Growinski and J. L. Lions Elsevier, Amsterdam*.

van Loon M., R. Vautard, M. Schaap, R. Bergström, B. Bessagnet, J. Brandt, P.J.H. Builtjes, J.H. Christensen, C. Cuvelier, A. Graff, J.E. Jonson, M. Krol, J. Langner, P. Roberts, L. Rouil, R. Stern, L. Tarrasón, P. Thunis, E. Vignati, L. White, P. Wind (2007) Evaluation of long-term ozone simulations from seven regional air quality models and their ensemble, *Atmos. Environ.*, Volume 41, Issue 10, Pages 2083-2097.

Van Zanten, M.C., Sauter, F.J., Wichink Kruit, R.J., Van Jaarsveld, J.A., Van Pul, W.A.J. (2010) Description of the DEPAC module: Dry deposition modelling with DEPAC_GCN2010. *RIVM report* 680180001/2010, Bilthoven, the Netherlands.

Venkatram, A. and Pleim, J. (1999) The electrical analogy does not apply to modelling dry deposition of particles, *Atmos. Environ*., 33, 3075-3076.

Venkatram, A. (1980) Estimation of Turbulence Velocity Scales in Stable and Unstable Boundary Layer for Dispersion Applications. Eleventh NATO-CCMS International Technical Meeting on Air Pollution Modellingand its Application.

Vestreng, V. , G. Myhre, H. Fagerli, S. Reis, and L. Tarrason (2007) Twenty-five years of continuous sulphur dioxide emission reduction in Europe, *Atmos. Chem. Phys*., 7, 3663–3681.

Walcek, C. J. (2000) Minor flux adjustment near mixing ratio extremes for simplified yet highly accurate monotonic calculation of tracer advection. *Journal of Geophysical Research* D: Atmosphere 105 (D7), 9335-9348.

Walcek, C.J. and Taylor, G.R. (1986) A theoretical method for computing vertical distribution of acidity and sulphate production within cumulus clouds. *J. Atmos. Sci*., 43, 339-355.

Wesely, M.L. (1989) Parameterization of Surface Resistances to Gaseous Dry Deposition in Regional-Scale Numerical Models. *Atmos. Environ*., 23, 1293-1304.

Wyngaard, J.C. (1992) Atmospheric Turbulence. *Ann. Rev. Fluid Mech*., 24, 205-33.

Yamartino, R.J., J. Scire, G.R. Carmichael, and Y.S. Chang (1992) The CALGRID mesoscale photochemical grid model---I. Model formulation, *Atmos. Environ*., 26A (1992), 1493---1512.

Yamartino, R.J. (1993) Nonnegative, conserved scalar transport using grid-cell-centered, spectrally constrained Blackman cubics for applications on a variable-thickness mesh. *Mon. Wea. Rev*., 121, 753-763.

Yamartino, R.J. (2003) Refined 3d Transport and Horizontal Diffusion for the REM/CALGRID Air Quality Model. Freie Universiträt Berlin, Institut für Meteorologie.

Yarwood. G., S. Rao, M. Yocke, and G.Z. Whitten (2005b) Updates to the Carbon Bond chemical mechanism: CB05. Final Report prepared for US EPA. Available at http://www.camx.com/publ/pdfs/CB05_Final_Report_120805.pdf.

Zilitinkevich, S., Baklanov, A. (2002) Calculation of the height of the stable boundary layer in practical applications. *Boundary Layer Meteorology*, 105(3), 389-409.

Zender, C. S., H. Bian, and D. Newman (2003) Mineral Dust Entrainment And Deposition (DEAD) model: Description and 1990s dust climatology*, J. Geophys. Res*., 108(D14), 4416.

Zhang, L., S. Gong, J. Padro, L. Barrie (2001) A size-segregated particle dry deposition scheme for an atmospheric aerosol module. *Atmos. Environ*., 35, 549-560.

Zhang, L., J. R. Brook, and R. Vet (2003) A revised parameterization for gaseous dry deposition in air-quality models. *Atmos. Chem. Phys*., 3, 2067–2082.

Zhang, K. M., Knipping, E. M., Wexler, A. S., Bhave, P. V., and Tonnesen, G. S. (2005) Size distribution of sea-salt emissions as a function of relative humidity, *Atmos. Environ*., 39(18), 3373-3379.

Zyryanov, D., Foret, G., Eremenko, M., Beekmann, M., Cammas, J.-P., *et al*. (2012) 3-D evaluation of tropospheric ozone simulations by an ensemble of regional Chemistry Transport Model. *Atmos. Chem. Phys*., 12, 3219-3240.

16 ANNEX 1: Available stations for daily basis comparisons

Available stations for daily basis comparisons

Pollutant	Number	Sites
O3	134	AM01 AT02 AT05 AT30 AT32 AT34 AT37 AT38 AT40 AT41 AT42 AT43 AT44 AT45 AT46 AT47 AT48 AT49 BE01 BE32 BE35 BG53 CH01 CH02 CH03 CH04 CH05 CY02 CZ01 DE01 DE02 DE03 DE07 DE08 DE09 DK05 DK31 DK41 EE09 EE11 ES01 ES07 ES08 ES09 ES10 ES11 ES12 ES13 ES14 ES16 ES17 FI09 FI17 FI22 FI37 FI96 FR08 FR09 FR10 FR12 FR13 FR14 FR15 FR16 FR17 FR18 FR19 FR30 GB02 GB06 GB13 GB14 GB15 GB31 GB33 GB35 GB36 GB37 GB38 GB39 GB43 GB45 GB48 GB49 GB50 GB51 GB52 GB53 GR01 GR02 HU02 IE01 IE31 IT01 LT15 LV10 LV16 MK07 NL07 NL09 NL10 NL11 NL91 NO01 NO15 NO39 NO42 NO43 NO52 NO55 NO56 NO58 NO89 PL02 PL03 PL04 PL05 PT04 SE05 SE11 SE12 SE13 SE14 SE32 SE35 SE39 SI08 SI31 SI32 SI33 SK02 SK04 SK06 SK07
NO2	89	AM01 AT02 AT05 AT48 BE01 BE32 BE35 CH01 CH02 CH03 CH04 CH05 CZ01 CZ03 DE01 DE02 DE03 DE07 DE08 DE09 DK05 DK08 EE09 EE11 ES01 ES07 ES08 ES09 ES10 ES11 ES12 ES13 ES14 ES16 ES17 FI09 FI17 FI22 FI37 FI96 FR08 FR09 FR13 FR15 GB02 GB13 GB14 GB31 GB33 GB36 GB37 GB38 GB43 GB45 GB48 GB50 GB51 GB53 GR01 HU02 IE01 IT01 LT15 LV10 LV16 MD13 ME08 MK07 NL07 NL09 NL10 NL11 NL91 NO01 NO15 NO39 NO55 NO56 PL02 PL03 PL04 PL05 RS05 SE05 SE11 SE12 SE14 SI08 SK02
SO2	63	AM01 AT02 AT05 AT48 CH01 CH02 CH04 CH05 CY02 CZ01 CZ03 DK03 DK05 DK08 DK31 EE09 EE11 ES01 ES07 ES08 ES09 ES10 ES11 ES12 ES13 ES14 ES16 ES17 FI09 FI17 FI36 FR09 FR13 FR15 FR30 GB36 GB37 GB38 GB43 GB45 GB48 GR01 HU02 IE01 IS02 IT01 LT15 LV10 LV16 MD13 ME08 NL07 NL08 NL09 NL10 NL11 NL91 NO01 NO15 NO39 NO42 NO55 NO56
PM10	58	AT02 AT05 AT48 CH01 CH02 CH03 CH04 CH05 CY02 CZ01 CZ03 DE01 DE02 DE03 DE07 DE08 DE09 DE44 DK05 DK41 ES01 ES06 ES07 ES08 ES09 ES10 ES11 ES12 ES13 ES14 ES16 ES17 ES78 FR09 FR13 FR15 FR18 GB06 GB36 GB43 GB48 GR02 HU02 IT01 LV10 LV16 MD13 MK07 MY29 NL07 NL09 NL10 NL91 PL05 SE11 SE12 SE14 SI08
PM25	38	AT02 CH02 CH05 CY02 CZ03 DE02 DE03 DE44 ES01 ES07 ES08 ES09 ES10 ES11 ES12 ES13 ES14 ES16 ES78 FR09 FR13 FR15 FR18 GB36 GB48 IE31 IT04 LV10 LV16 NL09 NL10 NL11 NL91 PL05 SE11 SE12 SE14 SI08
SO4-10	73	AM01 AT02 CH01 CH02 CH05 CZ01 CZ03 DE44 DK03 DK05 DK08 DK31 ES01 ES07 ES08 ES09 ES10 ES11 ES12 ES13 ES14 ES16 ES17 ES78 FI09 FI17 FI36 FR09 FR13 FR15 GB02 GB06 GB07 GB13 GB14 GB36 GB48 HU02 IE01 IE05 IE06 IE08 IS02 IT01 KZ01 LT15 LV10 LV16 MD13 NL08 NL09 NL10 NL11 NL91 NO01 NO15 NO39 NO42 NO55 NO56 NO77 PL02 PL03 PL04 PL05 RU18 SE05 SE11 SE12 SE14 SI08 SK02 SK06
NO3-10	44	AM01 AT02 DE44 ES01 ES07 ES08 ES09 ES10 ES11 ES12 ES13 ES14 ES16 ES17 ES78 GB36 GB48 HU02 IE05 IE06 IE08 IT01 KZ01 LV10 LV16 MD13 NL08 NL10 NL11 NL91 NO01 NO15 NO39 NO42 NO55 NO56 NO77 PL02 PL03 PL04 PL05 RU18 SK02 SK06
NH4-10	39	AM01 AT02 DE44 DK03 DK05 DK08 DK31 ES09 ES78 FI09 FI17 FI36 GB36 GB48 HU02 IE05 IE06 IE08 IT01 LV10 LV16 MD13 NL08 NL10 NL11 NL91 NO01 NO15 NO39 NO42 NO55 NO56 NO77 PL02 PL03 PL04 PL05 RU18 SK06

Pollutant	Number	Sites
WNHx	62	AT02 AT05 AT48 BY04 CH02 CH05 CZ03 DE02 DE03 DE07 EE09 ES01 ES07 ES08 ES09 ES11 ES12 ES13 ES14 ES16 ES17 FR08 FR09 FR10 FR13 FR14 FR15 FR17 FR18 GB02 GB48 HU02 IE01 IE05 IE09 IT01 IT04 LT15 LV10 LV16 NL09 NO01 NO15 NO39 NO55 NO56 PL02 PL04 PL05 PT01 PT03 PT04 RS05 RU01 RU13 RU18 RU20 SE05 SE14 SI08 SK04 SK06
WNOx	63	AT02 AT05 AT48 BY04 CH02 CH05 CZ03 DE02 DE03 DE07 EE09 ES01 ES07 ES08 ES09 ES11 ES12 ES13 ES14 ES16 ES17 FR08 FR09 FR10 FR13 FR14 FR15 FR17 FR18 GB02 GB48 HU02 IE01 IE05 IE09 IS02 IT01 IT04 LT15 LV10 LV16 NL09 NO01 NO15 NO39 NO55 NO56 PL02 PL04 PL05 PT01 PT03 PT04 RS05 RU01 RU13 RU18 RU20 SE05 SE14 SI08 SK04 SK06
WSOx	63	AT02 AT05 AT48 BY04 CH02 CH05 CZ03 DE02 DE03 DE07 EE09 ES01 ES07 ES08 ES09 ES11 ES12 ES13 ES14 ES16 ES17 FR08 FR09 FR10 FR13 FR14 FR15 FR17 FR18 GB02 GB48 HU02 IE01 IE05 IE09 IS02 IT01 IT04 LT15 LV10 LV16 NL09 NO01 NO15 NO39 NO55 NO56 PL02 PL04 PL05 PT01 PT03 PT04 RS05 RU01 RU13 RU18 RU20 SE05 SE14 SI08 SK04 SK06

Pollutant	Number	Sites
CA-1	1	ES78
CA-10	34	AM01 AT02 CH02 CH05 DE44 DK03 DK05 DK08 DK31 ES09 ES78 FI09 FI17 FI36 GB36 GB48 IE01 IE05 IE06 IE08 IS02 MD13 NL08 NL09 NL10 NO01 NO15 NO39 NO42 NO55 NO56 NO77 SI08 SK06
CA-25	4	CY02 DE44 ES09 ES78
EC-10	5	DE44 ES09 ES78 GB36 SE12
EC-25	5	CZ03 DE44 ES09 ES78 IT04
HNO3	17	AM01 AT02 GB48 HU02 IT01 MD13 NL11 NO01 NO15 NO39 NO42 NO55 NO56 NO77 PL05 SK02 SK06
NA-1	1	ES78
NA-10	32	AM01 AT02 CH02 CH05 DE44 DK03 DK05 DK08 DK31 ES09 ES78 FI09 FI17 FI36 GB36 GB48 IE01 IE05 IE06 IE08 IS02 MD13 NL11 NO01 NO15 NO39 NO42 NO55 NO56 NO77 SI08 SK06
NA-25	4	CY02 DE44 ES09 ES78
NH3	15	AM01 AT02 DK03 DK05 DK08 DK31 GB48 HU02 IT01 MD13 NL07 NL11 NL91 PL05 SK06
NH4-1	1	ES78
NH4-25	10	CH02 CY02 DE44 ES09 ES78 FI50 FR30 GR02 IT04 SE11
NO3-1	1	ES78
NO3-25	11	CH02 CY02 DE44 ES09 ES78 FI50 FR30 GR02 IT01 IT04 SE11
POMS2-25	6	CH02 DE44 ES78 FI50 NL11 SE11
RAIN	68	AT02 AT05 AT48 BY04 CH02 CH05 CZ03 DE02 DE03 DE07 EE09 ES01 ES07 ES08 ES09 ES10 ES11 ES12 ES13 ES14 ES16 ES17 FR08 FR09 FR10 FR13 FR14 FR15 FR16 FR17 FR18 GB02 GB48 HU02 IE01 IE05 IE09 IS02 IT01 IT04 LT15 LV10 LV16 NL09 NO01 NO15 NO18 NO39 NO55 NO56 PL02 PL03 PL04 PL05 PT01 PT03 PT04 RS05 RU01 RU13 RU18 RU20 SE05 SE14 SI08 SK02 SK04 SK06
SO4-1	2	CH01 ES78
SO4-25	11	CH02 CY02 DE44 ES09 ES78 FI50 FR30 GR02 IT01 IT04 SE11
SOA-25	6	CH02 DE44 ES78 FI50 NL11 SE11
T2M	32	AT02 AT05 AT48 BG01 ES01 ES07 ES08 ES09 ES10 ES11 ES12 ES13 ES14 ES16 ES17 FI50 FR08 FR09 FR10 FR12 FR13 FR14 FR15 FR16 FR17 FR18 IT04 NO01 NO02 NO42 NO56 NO58
TNH4	43	AM01 AT02 CH02 CH05 CZ01 CZ03 DK03 DK05 DK08 DK31 ES01 ES07 ES08 ES09 ES10 ES11 ES12 ES13 ES14 ES16 ES17 FI09 FI17 FI36 FR09 FR13 FR15 HU02 IE01 IT01 LT15 LV10 LV16 MD13 PL02 PL03 PL04 PL05 SE05 SE11 SE12 SE14 SI08
TNO3	50	AM01 AT02 CH02 CH05 CZ01 CZ03 DK03 DK05 DK08 DK31 ES01 ES07 ES08 ES09 ES10 ES11 ES12 ES13 ES14 ES16 ES17 FI09 FI17 FI36 FR09 FR13 FR15 HU02 IE01 IT01 LT15 LV10 LV16 MD13 NO01 NO15 NO39 NO42 NO55 NO56 NO77 PL02 PL03 PL04 PL05 SE05 SE11 SE12 SE14 SI08
TOM-10	5	DE44 ES09 ES78 GB36 SE12
TOM-25	9	CH02 CZ03 DE44 ES09 ES78 FI50 GR02 IT04 SE11
U10	31	AT02 AT05 AT48 BG01 ES01 ES07 ES08 ES09 ES10 ES11 ES12 ES13 ES14 ES16 ES17 FI50 FR08 FR09 FR10 FR12 FR13 FR14 FR15 FR16 FR17 FR18 NO01 NO02 NO42 NO56 NO58

POMS2-25 is compared to observed BBOA, SOA-25 is compared OOA. CA is Calcium measurement.

Available stations for hourly basis comparisons

Pollutant	Number	Sites
O3	134	AM01 AT02 AT05 AT30 AT32 AT34 AT37 AT38 AT40 AT41 AT42 AT43 AT44 AT45 AT46 AT47 AT48 AT49 BE01 BE32 BE35 BG53 CH01 CH02 CH03 CH04 CH05 CY02 CZ01 DE01 DE02 DE03 DE07 DE08 DE09 DK05 DK31 DK41 EE09 EE11 ES01 ES07 ES08 ES09 ES10 ES11 ES12 ES13 ES14 ES16 ES17 FI09 FI17 FI22 FI37 FI96 FR08 FR09 FR10 FR12 FR13 FR14 FR15 FR16 FR17 FR18 FR19 FR30 GB02 GB06 GB13 GB14 GB15 GB31 GB33 GB35 GB36 GB37 GB38 GB39 GB43 GB45 GB48 GB49 GB50 GB51 GB52 GB53 GR01 GR02 HU02 IE01 IE31 IT01 LT15 LV10 LV16 MK07 NL07 NL09 NL10 NL11 NL91 NO01 NO15 NO39 NO42 NO43 NO52 NO55 NO56 NO58 NO89 PL02 PL03 PL04 PL05 PT04 SE05 SE11 SE12 SE13 SE14 SE32 SE35 SE39 SI08 SI31 SI32 SI33 SK02 SK04 SK06 SK07
NO2	48	BE01 BE32 BE35 CH01 CZ03 DK05 DK08 ES01 ES07 ES08 ES09 ES10 ES11 ES12 ES13 ES14 ES16 ES17 FI09 FI17 FI22 FI37 FI96 FR08 FR09 FR13 FR15 GB02 GB13 GB14 GB31 GB33 GB36 GB37 GB38 GB43 GB45 GB48 GB50 GB51 GB53 GR01 MK07 NL07 NL09 NL10 NL11 NL91
SO2	30	AT02 AT05 AT48 CY02 CZ03 ES01 ES07 ES08 ES09 ES10 ES11 ES12 ES13 ES14 ES16 ES17 FR30 GB36 GB37 GB38 GB43 GB45 GB48 GR01 NL07 NL08 NL09 NL10 NL11 NL91
PM10	17	FR09 FR13 FR15 FR18 GB06 GB36 GB43 GB48 GR02 HU02 MK07 NL07 NL09 NL10 NL91 SE11 SE12
PM25	9	FR09 FR13 FR15 FR18 GB36 GB48 IE31 SE11 SE12
SO4-10	3	GB36 GB48 NL11
NO3-10	3	GB36 GB48 NL11
NH4-10	3	GB36 GB48 NL11

Pollutant	Number	Sites
HNO3	2	GB48 NL11
NA-10	3	GB36 GB48 NL11
NH3	4	GB48 NL07 NL11 NL91
NH4-25	6	CH02 DE44 FI50 FR30 GR02 SE11
NO3-25	6	CH02 DE44 FI50 FR30 GR02 SE11
POMS2-25	6	CH02 DE44 ES78 FI50 NL11 SE11
RAIN	11	ES01 ES07 ES08 ES09 ES10 ES11 ES12 ES13 ES14 ES16 ES17
SO4-25	5	CH02 DE44 FI50 FR30 GR02
SOA-25	6	CH02 DE44 ES78 FI50 NL11 SE11
T2M	28	AT02 AT05 AT48 ES01 ES07 ES08 ES09 ES10 ES11 ES12 ES13 ES14 ES16 ES17 FI50 FR08 FR09 FR10 FR12 FR13 FR14 FR15 FR17 FR18 IT04 NO01 NO02 NO56
TOM-25	5	CH02 DE44 FI50 GR02 SE11
U10	27	AT02 AT05 AT48 ES01 ES07 ES08 ES09 ES10 ES11 ES12 ES13 ES14 ES16 ES17 FI50 FR08 FR09 FR10 FR12 FR13 FR14 FR15 FR17 FR18 NO01 NO02 NO56

POMS2-25 is compared to observed BBOA, SOA-25 is compared OOA.

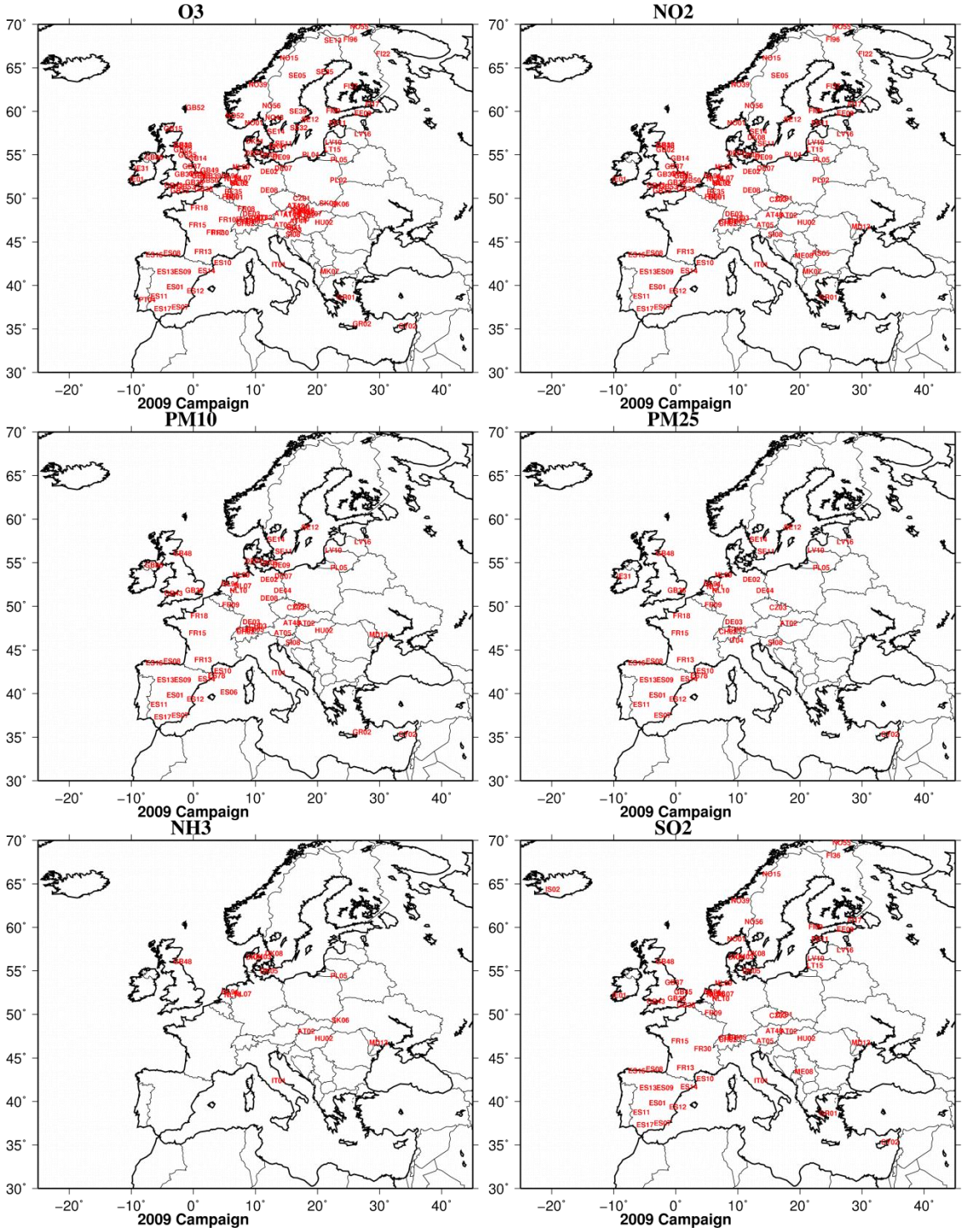
O3
NO2
PM10
PM25
NH3
SO2
2009 Campaign

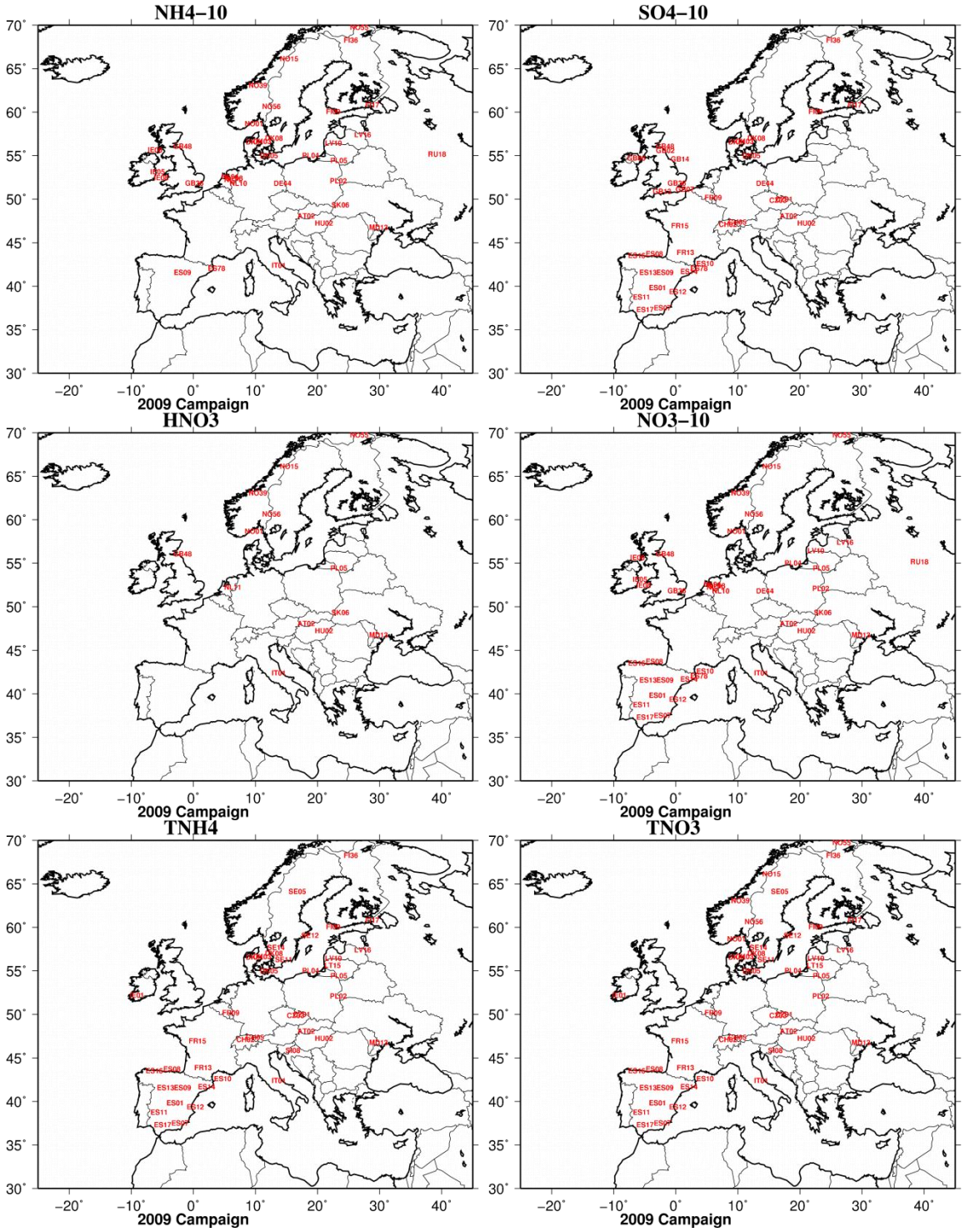
NH4–10
SO4–10
HNO3
NO3–10
TNH4
TNO3
2009 Campaign

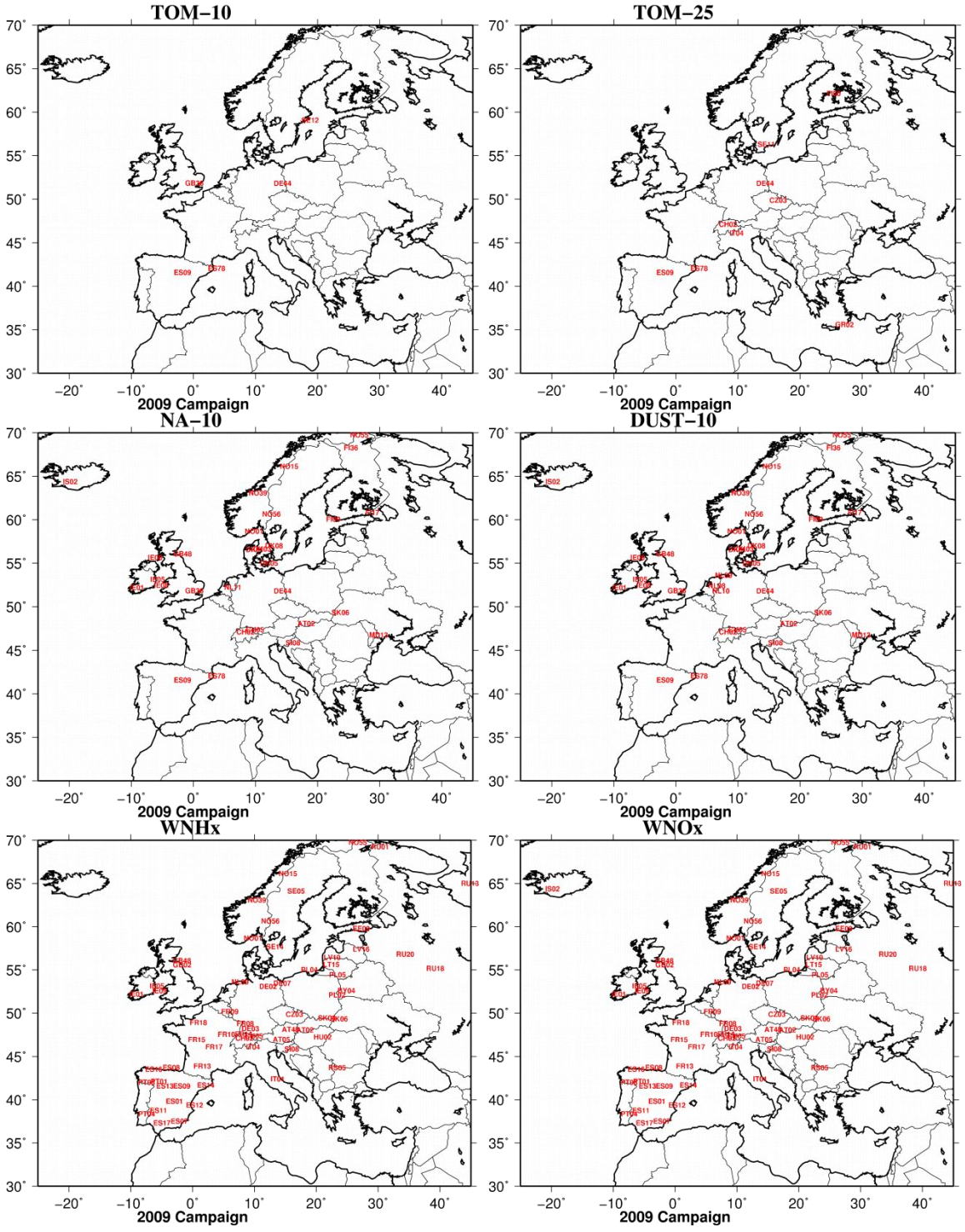
TOM−10
TOM−25
NA−10
DUST−10
WNHx
WNOx
2009 Campaign

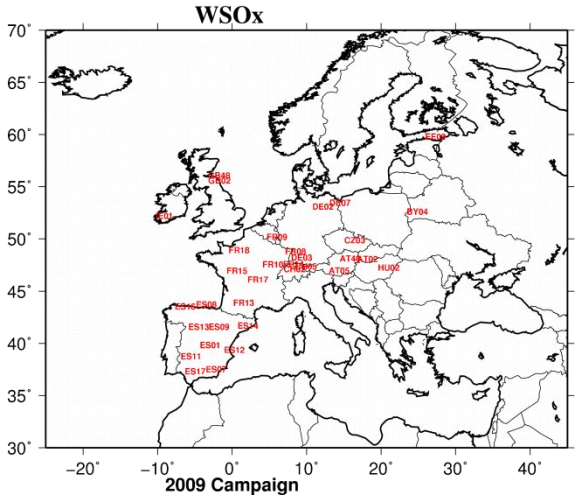
WSOx
70°
65°
60°
55°
50°
45°
40°
35°
30°
−20°
−10°
0°
10°
20°
30°
40°
2009 Campaign

17 ANNEX 2: Coordinates of EMEP stations

Site code	EMEP code	Site name	Latitude (°N)	Longitude (°E)	Altitude (m)
AT02	AT0002R	Illmitz	47.7667	16.7667	117
AT05	AT0005R	Vorhegg	46.6778	12.9722	1020
AT30	AT0030R	Pillersdorf bei Retz	48.7211	15.9422	315
AT32	AT0032R	Sulzberg	47.5292	9.9267	1020
AT40	AT0040R	Masenberg	47.3481	15.8822	1170
AT41	AT0041R	Haunsberg	47.9731	13.0161	730
AT42	AT0042R	Heidenreichstein	48.8786	15.0467	570
AT43	AT0043R	Forsthof	48.1061	15.9194	581
AT44	AT0044R	Graz Platte	47.1131	15.4706	651
AT45	AT0045R	Dunkelsteinerwald	48.3711	15.5467	320
AT46	AT0046R	Gnserndorf	48.3347	16.7306	161
AT47	AT0047R	Stixneusiedl	48.0508	16.6767	240
AT48	AT0048R	Zoebelboden	47.8386	14.4414	899
BE01	BE0001R	Offagne	49.8778	5.2036	430
BE32	BE0032R	Eupen	51.4575	6.0028	295
BE35	BE0035R	Vezin	50.5033	4.9894	160
BY04	BY0004R	Vysokoe	52.3333	23.4333	163
CH02	CH0002R	Payerne	46.8131	6.9447	489
CH03	CH0003R	Tnikon	47.4797	8.9047	539
CH04	CH0004R	Chaumont	47.0497	6.9794	1137
CH05	CH0005R	Rigi	47.0675	8.4639	1031
CY02	CY0002R	Ayia Marina	35.0389	33.0581	532
CZ01	CZ0001R	Svratouch	49.7333	16.0500	737
CZ03	CZ0003R	Kosetice	49.5833	15.0833	534
DE01	DE0001R	Westerland	54.9256	8.3097	12
DE02	DE0002R	Waldhof	52.8022	10.7594	74
DE03	DE0003R	Schauinsland	47.9147	7.9086	1205
DE07	DE0007R	Neuglobsow	53.1667	13.0333	62
DE08	DE0008R	Schmcke	50.6500	10.7667	937
DE09	DE0009R	Zingst	54.4333	12.7333	1
DE44	DE0044R	Melpitz	51.5300	12.9300	86
DK03	DK0003R	Tange	56.3500	9.6000	13
DK05	DK0005R	Keldsnor	54.7333	10.7333	10
DK08	DK0008R	Anholt	56.7167	11.5167	40
DK31	DK0031R	Ulborg	56.2833	8.4333	10
DK41	DK0041R	Lille Valby	55.6869	12.1261	10
EE09	EE0009R	Lahemaa	59.5000	25.9000	32
EE11	EE0011R	Vilsandi	58.3833	21.8167	6
ES01	ES0001R	San Pablo de los Montes	39.5478	-4.3486	917
ES06	ES0006R	Mahn	39.8667	4.3167	78
ES07	ES0007R	Vznar	37.2333	-3.5333	1265
ES08	ES0008R	Niembro	43.4422	-4.8503	134
ES09	ES0009R	Campisabalos	41.2811	-3.1428	1360
ES10	ES0010R	Cabo de Creus	42.3194	3.3169	23
ES11	ES0011R	Barcarrola	38.4758	-6.9228	393
ES12	ES0012R	Zarra	39.0861	-1.1019	885
ES13	ES0013R	Penausende	41.2833	-5.8667	985
ES14	ES0014R	Els Torms	41.4000	0.7167	470
ES16	ES0016R	O Saviao	43.2311	-7.6997	506
ES17	ES0017R	Doana	37.0303	-6.3317	5

Site code	EMEP code	Site name	Latitude (°N)	Longitude (°E)	Altitude (m)
ES78	ES1778R	Montseny	41.7667	2.3500	700
FI09	FI0009R	Ut	59.7792	21.3772	7
FI17	FI0017R	Virolahti II	60.5267	27.6861	4
FI22	FI0022R	Oulanka	66.3203	29.4017	310
FI36	FI0036R	Pallas (Matorova)	68.0000	24.2397	340
FI37	FI0037R	htri II	62.5833	24.1833	180
FI50	FI0050R	Hyytil	61.8500	24.2833	181
FI96	FI0096G	Pallas (Sammaltunturi)	68.0000	24.1500	340
FR08	FR0008R	Donon	48.5000	7.1333	775
FR09	FR0009R	Revin	49.9000	4.6333	390
FR10	FR0010R	Morvan	47.2667	4.0833	620
FR13	FR0013R	Peyrusse Vieille	43.6167	0.1833	200
FR14	FR0014R	Montandon	47.3000	6.8333	836
FR15	FR0015R	La Tardire	46.6500	-0.7500	133
FR17	FR0017R	Montfranc	45.8000	2.0667	810
FR18	FR0018R	La Coulonche	48.6333	-0.4500	309
FR30	FR0030R	Puy de Dme	45.7667	2.9500	1465
GB02	GB0002R	Eskdalemuir	55.3131	-3.2042	243
GB06	GB0006R	Lough Navar	54.4431	-7.8700	126
GB07	GB0007R	Barcombe Mills	50.8667	-0.0331	8
GB13	GB0013R	Yarner Wood	50.5964	-3.7131	119
GB14	GB0014R	High Muffles	54.3344	-0.8075	267
GB15	GB0015R	Strath Vaich Dam	57.7344	-4.7744	270
GB31	GB0031R	Aston Hill	52.5039	-3.0331	370
GB33	GB0033R	Bush	55.8586	-3.2050	180
GB35	GB0035R	Great Dun Fell	54.6833	-2.4500	847
GB36	GB0036R	Harwell	51.5731	-1.3167	137
GB37	GB0037R	Ladybower Res.	53.3989	-1.7533	420
GB38	GB0038R	Lullington Heath	50.7928	0.1794	120
GB39	GB0039R	Sibton	52.2939	1.4631	46
GB43	GB0043R	Narberth	51.2333	-4.7000	160
GB45	GB0045R	Wicken Fen	52.2983	-0.2928	5
GB48	GB0048R	Auchencorth Moss	55.7933	-3.2447	260
GB49	GB0049R	Weybourne	52.9506	1.1219	16
GB50	GB0050R	St. Osyth	51.7781	1.0822	8
GB51	GB0051R	Market Harborough	52.5544	-0.7722	145
GB52	GB0052R	Lerwick	60.1392	-1.1853	85
GB53	GB0053R	Charlton Mackrell	51.0561	-2.6833	54
GR01	GR0001R	Aliartos	38.3667	23.0833	110
GR02	GR0002R	Finokalia	35.3167	25.6667	250
HU02	HU0002R	K-puszta	46.9667	19.5833	125
IE01	IE0001R	Valentia Observatory	51.9397	-10.2444	11
IE05	IE0005R	Oak Park	52.8686	-6.9247	59
IE06	IE0006R	Malin Head	55.3750	-7.3428	20
IE08	IE0008R	Carnsore Point	52.1850	-6.3683	9
IE09	IE0009R	Johnstown Castle	52.2989	-6.5108	62
IE31	IE0031R	Mace Head	53.1667	-9.5000	15
IS02	IS0002R	Irafoss	64.0833	-21.0167	66
IT01	IT0001R	Montelibretti	42.1000	12.6333	48
IT04	IT0004R	Ispra	45.8000	8.6333	209

Site code	EMEP code	Site name	Latitude (°N)	Longitude (°E)	Altitude (m)
LT15	LT0015R	Preila	55.3500	21.0667	5
LV10	LV0010R	Rucava	56.1619	21.1731	18
LV16	LV0016R	Zoseni	57.1353	25.9056	188
MD13	MD0013R	Leova II	46.4883	28.2833	166
ME08	ME0008R	Zabljak	43.1500	19.1333	1450
MK07	MK0007R	Lazaropole	41.3200	20.4200	1332
NL07	NL0007R	Eibergen	52.0833	6.5667	20
NL08	NL0008R	Bilthoven	52.1167	5.2000	5
NL09	NL0009R	Kollumerwaard	53.3339	6.2772	1
NL10	NL0010R	Vredepeel	51.5411	5.8536	28
NL11	NL0011R	Cabauw	51.9700	4.9300	60
NL91	NL0091R	De Zilk	52.3000	4.5000	4
NO01	NO0001R	Birkenes	58.3833	8.2500	190
NO02	NO0002R	Birkenes II	58.3883	8.2519	219
NO15	NO0015R	Tustervatn	65.8333	13.9167	439
NO39	NO0039R	Krvatn	62.7833	8.8833	210
NO43	NO0043R	Prestebakke	59.0000	11.5333	160
NO52	NO0052R	Sandve	59.2000	5.2000	15
NO55	NO0055R	Karasjok	69.4667	25.2167	333
NO56	NO0056R	Hurdal	60.3722	11.0781	300
PL02	PL0002R	Jarczew	51.8167	21.9833	180
PL04	PL0004R	Leba	54.7500	17.5333	2
PL05	PL0005R	Diabla Gora	54.1500	22.0667	157
PT01	PT0001R	Braganca	41.8167	-6.7667	690
PT03	PT0003R	Viana do Castelo	41.7000	-8.8000	16
PT04	PT0004R	Monte Velho	38.0833	-8.8000	43
RS05	RS0005R	Kamenicki vis	43.4000	21.9500	813
RU01	RU0001R	Janiskoski	68.9333	28.8500	118
RU13	RU0013R	Pinega	64.7000	43.4000	28
RU18	RU0018R	Danki	54.9000	37.8000	150
RU20	RU0020R	Lesnoy	56.5300	32.9400	340
SE05	SE0005R	Bredklen	63.8500	15.3333	404
SE11	SE0011R	Vavihill	56.0167	13.1500	175
SE12	SE0012R	Aspvreten	58.8000	17.3833	20
SE13	SE0013R	Esrange	67.8833	21.0667	475
SE14	SE0014R	R	57.3939	11.9139	5
SE32	SE0032R	Norra-Kvill	57.8167	15.5667	261
SE35	SE0035R	Vindeln	64.2500	19.7667	225
SE39	SE0039R	Grims	59.7278	15.4719	132
SI08	SI0008R	Iskrba	45.5667	14.8667	520
SI31	SI0031R	Zarodnje	46.4286	15.0033	770
SI33	SI0033R	Kovk	46.1286	15.1139	600
SK04	SK0004R	Star Lesn	49.1500	20.2833	808
SK06	SK0006R	Starina	49.0500	22.2667	345
SK07	SK0007R	Topolniky	47.9600	17.8606	113

18 ANNEX 3 List of station with full characteristics used for the analysis for PM with the delta tool

Station Name	Stat Code	Stat abbr	LON	LAT	Altitude	Region	Cntry	City	Type
Amberd	AM0001R	AM01	44.2606	40.3844	2080	Caviar	AM	remote	Mountain
Illmitz	AT0002R	AT02	16.7667	47.7667	117	Mozart	AT	Vienna	Plain
Achenkirch	AT0003R	AT03	11.7167	47.55	960	Mozart	AT	remote	Valley
St_Koloman	AT0004R	AT04	13.2	47.65	851	Mozart	AT	remote	Valley
Vorhegg	AT0005R	AT05	12.9722	46.6778	1020	Mozart	AT	remote	Valley
Pillersdorf_bei_Retz	AT0030R	AT30	15.9422	48.7211	315	Mozart	AT	Vienna	Plain
Sulzberg	AT0032R	AT32	9.9267	47.5292	1020	Mozart	AT	remote	Valley
Stolzalpe_bei_Murau	AT0033R	AT33	14.2039	47.1292	1302	Mozart	AT	remote	Valley
Sonnblick	AT0034G	AT34	12.9583	47.0544	3106	Mozart	AT	remote	Mountain
Zillertaler_Alpen	AT0037R	AT37	11.87	47.1369	1970	Mozart	AT	remote	Mountain
Gerlitzen	AT0038R	AT38	13.915	46.6936	1895	Mozart	AT	remote	Mountain
Masenberg	AT0040R	AT40	15.8822	47.3481	1170	Mozart	AT	Vienna	Valley
Haunsberg	AT0041R	AT41	13.0161	47.9731	730	Mozart	AT	remote	Valley
Heidenreichstein	AT0042R	AT42	15.0467	48.8786	570	Mozart	AT	Vienna	Valley
Forsthof	AT0043R	AT43	15.9194	48.1061	581	Mozart	AT	Vienna	Valley
Graz_Platte	AT0044R	AT44	15.4706	47.1131	651	Mozart	AT	Vienna	Valley
Dunkelsteinerwald	AT0045R	AT45	15.5467	48.3711	320	Mozart	AT	Vienna	Plain
Ganserndorf	AT0046R	AT46	16.7306	48.3347	161	Mozart	AT	Vienna	Plain
Stixneusiedl	AT0047R	AT47	16.6767	48.0508	240	Mozart	AT	Vienna	Plain
Zoebelboden	AT0048R	AT48	14.4414	47.8386	899	Mozart	AT	remote	Valley
Grebenzen_bei_St_Lamprecht	AT0049R	AT49	14.33	47.0403	1648	Mozart	AT	remote	Mountain
Ivan_Sedlo	BA0006R	BA06	18.0333	43.7667	970	Olive	BA	remote	Valley
Offagne	BE0001R	BE01	5.2036	49.8778	430	Lowland	BE	Bruxelles	Plain
University_of_Gent	BE0005R	BE05	3.7167	51.05	0	Lowland	BE	Bruxelles	Plain
Koksijde	BE0014R	BE14	3.3	51.4664	4	Lowland	BE	Bruxelles	Plain
Eupen	BE0032R	BE32	6.0028	51.4575	295	Lowland	BE	Bruxelles	Plain
Vezin	BE0035R	BE35	4.9894	50.5033	160	Lowland	BE	Bruxelles	Plain
BEO_Moussala	BG0001R	BG01	23.5833	42.1667	2971	Goulash	BG	Sofia	Mountain
Rojen_peak	BG0053R	BG53	24.7386	41.6958	1750	Goulash	BG	Sofia	Mountain
Vysokoe	BY0004R	BY04	23.4333	52.3333	163	Caviar	BY	remote	Plain
Jungfraujoch	CH0001G	CH01	7.985	46.5475	3578	Cheese	CH	remote	Mountain
Payerne	CH0002R	CH02	6.9447	46.8131	489	Cheese	CH	remote	Plain
Tanikon	CH0003R	CH03	8.9047	47.4797	539	Cheese	CH	remote	Valley
Chaumont	CH0004R	CH04	6.9794	47.0497	1137	Cheese	CH	remote	Valley
Rigi	CH0005R	CH05	8.4639	47.0675	1031	Cheese	CH	remote	Valley
Sion	CH0031R	CH31	7.3419	46.2203	483	Cheese	CH	remote	Plain
Ayia_Marina	CY0002R	CY02	33.0581	35.0389	532	Olive	CY	remote	Valley
Svratouch	CZ0001R	CZ01	16.05	49.7333	737	Goulash	CZ	remote	Valley
Kosetice	CZ0003R	CZ03	15.0833	49.5833	534	Goulash	CZ	Prague	Valley
Libus	CZ0099R	CZ99	15.0667	50.15	0	Goulash	CZ	Prague	Plain
Westerland	DE0001R	DE01	8.3097	54.9256	12	Goethe	DE	remote	Plain

Waldhof	DE0002R	DE02	10.7594	52.8022	74	Goethe	DE	Hambourg	Plain
Schauinsland	DE0003R	DE03	7.9086	47.9147	1205	Goethe	DE	remote	Mountain
Deuselbach	DE0004R	DE04	7.0519	49.7647	480	Goethe	DE	Cologne	Plain
Brotjacklriegel	DE0005R	DE05	13.2192	48.8194	1016	Goethe	DE	Munich	Mountain
Arkona	DE0006R	DE06	13.4333	54.6833	42	Goethe	DE	remote	Plain
Neuglobsow	DE0007R	DE07	13.0333	53.1667	62	Goethe	DE	Berlin	Plain
Schmucke	DE0008R	DE08	10.7667	50.65	937	Goethe	DE	remote	Mountain
Zingst	DE0009R	DE09	12.7333	54.4333	1	Goethe	DE	remote	Plain
Hohenwestedt	DE0011R	DE11	9.6667	54.1	75	Goethe	DE	Hambourg	Plain
Bassum	DE0012R	DE12	8.7	52.85	52	Goethe	DE	Hambourg	Plain
Rodenberg	DE0013R	DE13	9.3667	52.3167	148	Goethe	DE	Hambourg	Plain
Meinerzhagen	DE0014R	DE14	7.6333	51.1167	510	Goethe	DE	Cologne	Valley
Usingen	DE0015R	DE15	8.5333	50.3333	485	Goethe	DE	Cologne	Plain
Bad_Kreuznach	DE0016R	DE16	7.8667	49.8333	230	Goethe	DE	Cologne	Plain
Ansbach	DE0017R	DE17	10.5833	49.25	481	Goethe	DE	Munich	Plain
Rottenburg	DE0018R	DE18	8.9333	48.4833	427	Goethe	DE	remote	Plain
Starnberg	DE0019R	DE19	11.35	48.0167	729	Goethe	DE	Munich	Valley
Hof	DE0020R	DE20	11.8833	50.3167	568	Goethe	DE	remote	Valley
Ueckermunde	DE0026R	DE26	14.0667	53.75	1	Goethe	DE	Berlin	Plain
Wiesenburg	DE0031R	DE31	12.4667	52.1167	107	Goethe	DE	Berlin	Plain
Luckendorf	DE0035R	DE35	14.7667	50.8333	490	Goethe	DE	remote	Plain
Murnauer_Moos	DE0038R	DE38	11.2033	47.6514	622	Goethe	DE	Munich	Valley
Aukrug	DE0039R	DE39	9.7928	54.0747	15	Goethe	DE	Hambourg	Plain
Ohringen	DE0042R	DE42	9.4472	49.2433	283	Goethe	DE	remote	Plain
Hohenpeissenberg	DE0043G	DE43	11.0167	47.8	985	Goethe	DE	Munich	Mountain
Melpitz	DE0044R	DE44	12.93	51.53	86	Goethe	DE	Berlin	Plain
Schorfheide	DE0045R	DE45	13.65	52.9667	70	Goethe	DE	Berlin	Plain
Raisting	DE0046R	DE46	11.1	47.9	552	Goethe	DE	Munich	Valley
Falkenberg	DE0047R	DE47	14.1167	52.1667	73	Goethe	DE	Berlin	Plain
Schneefernerhaus	DE0054R	DE54	10.9817	47.4167	2650	Goethe	DE	Munich	Mountain
BOsel	DE0056R	DE56	7.9425	52.9981	40	Goethe	DE	remote	Plain
Faeroerne	DK0001R	DK01	-7.0667	62.03	210	Lowland	DK	remote	Plain
Tange	DK0003R	DK03	9.6	56.35	13	Lowland	DK	remote	Plain
Keldsnor	DK0005R	DK05	10.7333	54.7333	10	Lowland	DK	remote	Plain
Faeroerne-Akraberg	DK0007R	DK07	-6.6667	61.4	90	Lowland	DK	remote	Plain
Anholt	DK0008R	DK08	11.5167	56.7167	40	Lowland	DK	remote	Plain
Storebaelt	DK0009R	DK09	10.9167	58.3164	250	Lowland	DK	remote	Plain
Risoe	DK0012R	DK12	12.0856	55.6933	3	Lowland	DK	remote	Plain
Pedersker	DK0020R	DK20	14.9458	55.0169	5	Lowland	DK	remote	Plain
Sepstrup_Sande	DK0022R	DK22	9.6	55.0833	60	Lowland	DK	remote	Plain
Ulborg	DK0031R	DK31	8.4333	56.2833	10	Lowland	DK	remote	Plain
Frederiksborg	DK0032R	DK32	12.3333	55.9667	10	Lowland	DK	remote	Plain
Lille_Valby	DK0041R	DK41	12.1261	55.6869	10	Lowland	DK	remote	Plain
Syrve	EE0002R	EE02	22.1	57.95	2	Caviar	EE	remote	Plain
Lahemaa	EE0009R	EE09	25.9	59.5	32	Caviar	EE	remote	Plain
Vilsandi	EE0011R	EE11	21.8167	58.3833	6	Caviar	EE	remote	Plain

San_Pablo_de_los_Montes	ES0001R	ES01	-4.3486	39.5478	917	Olive	ES	Madrid	Valley
La_Cartuja	ES0002R	ES02	-3.6	37.2	720	Olive	ES	remote	Valley
Roquetas	ES0003R	ES03	0.4914	40.8206	44	Olive	ES	Valencia	Plain
Logrono	ES0004R	ES04	-2.5031	42.4578	445	Olive	ES	Bilbao	Plain
Noya	ES0005R	ES05	-8.9236	42.7281	683	Olive	ES	remote	Valley
Mahon	ES0006R	ES06	4.3167	39.8667	78	Olive	ES	remote	Plain
Viznar	ES0007R	ES07	-3.5333	37.2333	1265	Olive	ES	remote	Valley
Niembro	ES0008R	ES08	-4.8503	43.4422	134	Olive	ES	remote	Plain
Campisabalos	ES0009R	ES09	-3.1428	41.2811	1360	Olive	ES	Madrid	Valley
Cabo_de_Creus	ES0010R	ES10	3.3169	42.3194	23	Olive	ES	Barcelone	Plain
Barcarrola	ES0011R	ES11	-6.9228	38.4758	393	Olive	ES	Sevilla	Plain
Zarra	ES0012R	ES12	-1.1019	39.0861	885	Olive	ES	Valencia	Valley
Penausende	ES0013R	ES13	-5.8667	41.2833	985	Olive	ES	remote	Valley
Els_Torms	ES0014R	ES14	0.7167	41.4	470	Olive	ES	Barcelone	Plain
Risco_Llamo	ES0015R	ES15	-4.35	39.5167	1241	Olive	ES	Madrid	Valley
O_Savinao	ES0016R	ES16	-7.6997	43.2311	506	Olive	ES	remote	Valley
Donana	ES0017R	ES17	-6.3317	37.0303	5	Olive	ES	Sevilla	Plain
Montseny	ES1778R	ES78	2.35	41.7667	700	Olive	ES	Barcelone	Valley
ahtari	FI0004R	FI04	24.2217	62.5333	162	Caviar	FI	remote	Plain
Kokar	FI0006R	FI06	20.9167	59.9167	10	Caviar	FI	remote	Plain
Virolahti	FI0007R	FI07	27.6833	60.5167	8	Caviar	FI	remote	Plain
Kevo	FI0008R	FI08	27	69.75	80	Caviar	FI	remote	Plain
Uto	FI0009R	FI09	21.3772	59.7792	7	Caviar	FI	remote	Plain
Virolahti_II	FI0017R	FI17	27.6861	60.5267	4	Caviar	FI	remote	Plain
Oulanka	FI0022R	FI22	29.4017	66.3203	310	Caviar	FI	remote	Plain
Pallas_(Matorova)	FI0036R	FI36	24.2397	68	340	Caviar	FI	remote	Plain
ahtari_II	FI0037R	FI37	24.1833	62.5833	180	Caviar	FI	remote	Plain
Hyytiala	FI0050R	FI50	24.2833	61.85	181	Caviar	FI	remote	Plain
Hailuoto_II	FI0053R	FI53	24.6942	65	4	Caviar	FI	remote	Plain
Haapasaari	FI0090R	FI90	27.2	60.2833	15	Caviar	FI	remote	Plain
Hailuoto	FI0091R	FI91	24.6833	65	4	Caviar	FI	remote	Plain
Hietajarvi	FI0092R	FI92	30.7167	63.1667	173	Caviar	FI	remote	Plain
Kotinen	FI0093R	FI93	25.0667	61.2333	158	Caviar	FI	remote	Plain
Pesosjarvi	FI0094R	FI94	29.5	66.3	257	Caviar	FI	remote	Plain
Vuoskojarvi	FI0095R	FI95	26.95	69.7333	147	Caviar	FI	remote	Plain
Pallas_(Sammaltunturi)	FI0096G	FI96	24.15	68	340	Caviar	FI	remote	Plain
Vert-le-Petit	FR0001R	FR01	2.3667	48.5333	64	Cheese	FR	Paris	Plain
La_Crouzille	FR0003R	FR03	1.3833	46.1333	497	Cheese	FR	remote	Plain
La_Hague	FR0005R	FR05	-1.8333	49.6167	133	Cheese	FR	remote	Plain
Valduc	FR0006R	FR06	4.8667	47.5833	470	Cheese	FR	remote	Plain
Lodeve	FR0007R	FR07	3.3333	43.7	252	Cheese	FR	remote	Plain
Donon	FR0008R	FR08	7.1333	48.5	775	Cheese	FR	remote	Valley
Revin	FR0009R	FR09	4.6333	49.9	390	Cheese	FR	remote	Plain
Morvan	FR0010R	FR10	4.0833	47.2667	620	Cheese	FR	Lyon	Valley
Bonnevaux	FR0011R	FR11	6.1833	46.8167	836	Cheese	FR	Lyon	Valley
Iraty	FR0012R	FR12	-1.0833	43.0333	1300	Cheese	FR	remote	Valley

Peyrusse_Vieille	FR0013R	FR13	0.1833	43.6167	200	Cheese	FR	remote	Plain
Montandon	FR0014R	FR14	6.8333	47.3	836	Cheese	FR	remote	Valley
La_Tardiere	FR0015R	FR15	-0.75	46.65	133	Cheese	FR	remote	Plain
Le_Casset	FR0016R	FR16	6.4667	45	1750	Cheese	FR	remote	Mountain
Montfranc	FR0017R	FR17	2.0667	45.8	810	Cheese	FR	remote	Valley
La_Coulonche	FR0018R	FR18	-0.45	48.6333	309	Cheese	FR	remote	Plain
Pic_du_Midi	FR0019R	FR19	0.1419	42.9367	2877	Cheese	FR	remote	Mountain
Puy_de_Dome	FR0030R	FR30	2.95	45.7667	1465	Cheese	FR	remote	Valley
Aubur	FR0031R	FR31	7.1833	48.2167	1135	Cheese	FR	remote	Valley
Brennilis	FR0032R	FR32	-3.8667	48.35	220	Cheese	FR	remote	Plain
Porspoder	FR0090R	FR90	-4.75	48.5167	50	Cheese	FR	remote	Plain
Eskdalemuir	GB0002R	GB02	-3.2042	55.3131	243	Big Ben	GB	remote	Plain
Goonhilly	GB0003R	GB03	-5.1833	50.05	108	Big Ben	GB	remote	Plain
Stoke_Ferry	GB0004R	GB04	0.5	52.5667	15	Big Ben	GB	London	Plain
Ludlow	GB0005R	GB05	-2.6333	52.3667	190	Big Ben	GB	remote	Plain
Lough_Navar	GB0006R	GB06	-7.87	54.4431	126	Big Ben	GB	remote	Plain
Barcombe_Mills	GB0007R	GB07	-0.0331	50.8667	8	Big Ben	GB	London	Plain
Yarner_Wood	GB0013R	GB13	-3.7131	50.5964	119	Big Ben	GB	remote	Plain
High_Muffles	GB0014R	GB14	-0.8075	54.3344	267	Big Ben	GB	Leeds	Plain
Strath_Vaich_Dam	GB0015R	GB15	-4.7744	57.7344	270	Big Ben	GB	remote	Plain
Glen_Dye	GB0016R	GB16	-2.5889	56.9675	85	Big Ben	GB	remote	Plain
Heigham_Holmes	GB0017R	GB17	1.6167	52.7167	0	Big Ben	GB	remote	Plain
Aston_Hill	GB0031R	GB31	-3.0331	52.5039	370	Big Ben	GB	remote	Plain
Bush	GB0033R	GB33	-3.205	55.8586	180	Big Ben	GB	remote	Plain
Great_Dun_Fell	GB0035R	GB35	-2.45	54.6833	847	Big Ben	GB	Leeds	Valley
Harwell	GB0036R	GB36	-1.3167	51.5731	137	Big Ben	GB	London	Plain
Ladybower_Res.	GB0037R	GB37	-1.7533	53.3989	420	Big Ben	GB	Leeds	Plain
Lullington_Heath	GB0038R	GB38	0.1794	50.7928	120	Big Ben	GB	London	Plain
Sibton	GB0039R	GB39	1.4631	52.2939	46	Big Ben	GB	remote	Plain
Wharley_Croft	GB0041R	GB41	-2.4667	54.6167	26	Big Ben	GB	Leeds	Plain
Narberth	GB0043R	GB43	-4.7	51.2333	160	Big Ben	GB	remote	Plain
Somerton	GB0044R	GB44	-3.0481	51.2311	55	Big Ben	GB	remote	Plain
Wicken_Fen	GB0045R	GB45	-0.2928	52.2983	5	Big Ben	GB	London	Plain
CEH_Edingburgh	GB0046R	GB46	-3.2167	55.95	0	Big Ben	GB	remote	Plain
Auchencorth_Moss	GB0048R	GB48	-3.2447	55.7933	260	Big Ben	GB	remote	Plain
Weybourne	GB0049R	GB49	1.1219	52.9506	16	Big Ben	GB	remote	Plain
St_Osyth	GB0050R	GB50	1.0822	51.7781	8	Big Ben	GB	London	Plain
Market_Harborough	GB0051R	GB51	-0.7722	52.5544	145	Big Ben	GB	London	Plain
Lerwick	GB0052R	GB52	-1.1853	60.1392	85	Big Ben	GB	remote	Plain
Charlton_Mackrell	GB0053R	GB53	-2.6833	51.0561	54	Big Ben	GB	remote	Plain
Glen_Saugh	GB0054R	GB54	-2.5592	56.9072	85	Big Ben	GB	remote	Plain
East_Ruston	GB0090R	GB90	1.4667	52.8	5	Big Ben	GB	remote	Plain
Banchory	GB0091R	GB91	-2.5344	57.0767	120	Big Ben	GB	remote	Plain
Chillerton	GB0092R	GB92	-1.3	50.7	35	Big Ben	GB	London	Plain
Staxton_Wold	GB0093R	GB93	-0.4333	54.1833	35	Big Ben	GB	Leeds	Plain
Lough_Erne	GB0094R	GB94	-8.05	54.4	35	Big Ben	GB	remote	Plain

Driby	GB0095R	GB95	0.0667	53.2333	47	Big Ben	GB	Leeds	Plain
Chilton	GB0096R	GB96	-1.3167	51.5667	109	Big Ben	GB	London	Plain
Abastumani	GE0001R	GE01	42.8253	41.755	1650	Caviar	GE	remote	Mountain
Aliartos	GR0001R	GR01	23.0833	38.3667	110	Olive	GR	Athens	Plain
Finokalia	GR0002R	GR02	25.6667	35.3167	250	Olive	GR	remote	Plain
Livadi	GR0003R	GR03	23.25	40.5333	850	Olive	GR	remote	Valley
Zavizan	HR0004R	HR04	14.9833	44.8167	1594	Olive	HR	remote	Mountain
Kecskemet	HU0001R	HU01	19.5833	46.9667	125	Goulash	HU	Budapest	Plain
K-puszta	HU0002R	HU02	19.5833	46.9667	125	Goulash	HU	Budapest	Plain
Valentia_Observatory	IE0001R	IE01	-10.2444	51.9397	11	Big Ben	IE	remote	Plain
Turlough_Hill	IE0002R	IE02	-6.4	53.0367	420	Big Ben	IE	Dublin	Plain
The_Burren	IE0003R	IE03	-9.1	53	90	Big Ben	IE	remote	Plain
Ridge_of_Capard	IE0004R	IE04	-7.45	53.1167	340	Big Ben	IE	Dublin	Plain
Oak_Park	IE0005R	IE05	-6.9247	52.8686	59	Big Ben	IE	Dublin	Plain
Malin_Head	IE0006R	IE06	-7.3428	55.375	20	Big Ben	IE	remote	Plain
Glenveagh	IE0007R	IE07	-7.94	55.0519	44	Big Ben	IE	remote	Plain
Carnsore_Point	IE0008R	IE08	-6.3683	52.185	9	Big Ben	IE	Dublin	Plain
Johnstown_Castle	IE0009R	IE09	-6.5108	52.2989	62	Big Ben	IE	Dublin	Plain
Mace_Head	IE0031R	IE31	-9.5	53.1667	15	Big Ben	IE	remote	Plain
Rjupnahed	IS0001R	IS01	-21.85	64.0833	120	Salmon	IS	remote	Plain
Irafoss	IS0002R	IS02	-21.0167	64.0833	66	Salmon	IS	remote	Plain
Reykjavik	IS0090R	IS90	-21.9	64.1333	52	Salmon	IS	remote	Plain
Storhofdi	IS0091R	IS91	-20.2833	63.4	118	Salmon	IS	remote	Plain
Montelibretti	IT0001R	IT01	12.6333	42.1	48	Olive	IT	Rome	Plain
Stelvio	IT0002R	IT02	10.3833	46.35	1415	Olive	IT	remote	Valley
Vallombrosa	IT0003R	IT03	11.55	43.7333	1000	Olive	IT	remote	Valley
Ispra	IT0004R	IT04	8.6333	45.8	209	Olive	IT	Milan	Plain
Arabba	IT0005R	IT05	11.8833	46.5167	2030	Olive	IT	remote	Mountain
ISAC_Belogna	IT0008R	IT08	11.3333	44.4833	0	Olive	IT	remote	Plain
Mt_Cimone	IT0009R	IT09	10.7	44.1833	2165	Olive	IT	remote	Mountain
Nida	LT0003R	LT03	21.0667	55.35	17	Caviar	LT	remote	Plain
Preila	LT0015R	LT15	21.0667	55.35	5	Caviar	LT	remote	Plain
Rucava	LV0010R	LV10	21.1731	56.1619	18	Caviar	LV	remote	Plain
Zoseni	LV0016R	LV16	25.9056	57.1353	188	Caviar	LV	remote	Plain
Kemeri	LV0025R	LV25	23.4667	56.9167	0	Caviar	LV	remote	Plain
Leova	MD0012R	MD12	28.2667	46.5	156	Goulash	MD	remote	Plain
Leova_II	MD0013R	MD13	28.2833	46.4883	166	Goulash	MD	remote	Plain
Zabljak	ME0008R	ME08	19.1333	43.15	1450	Olive	ME	remote	Valley
Lazaropole	MK0007R	MK07	20.42	41.32	1332	Olive	MK	remote	Valley
Giordan_lighthouse	MT0001R	MT01	14.2	36.1	160	Olive	MT	remote	Plain
Witteveen	NL0002R	NL02	6.6667	52.8167	18	Lowland	NL	remote	Plain
Rekken	NL0005R	NL05	6.7167	52.1	25	Lowland	NL	remote	Plain
Appelscha	NL0006R	NL06	6.3	52.95	10	Lowland	NL	remote	Plain
Eibergen	NL0007R	NL07	6.5667	52.0833	20	Lowland	NL	remote	Plain
Bilthoven	NL0008R	NL08	5.2	52.1167	5	Lowland	NL	remote	Plain
Kollumerwaard	NL0009R	NL09	6.2772	53.3339	1	Lowland	NL	remote	Plain

Vredepeel	NL0010R	NL10	5.8536	51.5411	28	Lowland	NL	remote	Plain
Cabauw	NL0011R	NL11	4.93	51.97	60	Lowland	NL	remote	Plain
De_Zilk	NL0091R	NL91	4.5	52.3	4	Lowland	NL	remote	Plain
Birkenes	NO0001R	NO01	8.25	58.3833	190	Salmon	NO	remote	Plain
Birkenes_II	NO0002R	NO02	8.2519	58.3883	219	Salmon	NO	remote	Plain
Skreadalen	NO0008R	NO08	6.7167	58.8167	475	Salmon	NO	remote	Plain
Tustervatn	NO0015R	NO15	13.9167	65.8333	439	Salmon	NO	remote	Plain
Narbuvoll	NO0035R	NO35	11.6667	62.35	768	Salmon	NO	remote	Valley
Hummelfjell	NO0036R	NO36	11.2667	62.45	1539	Salmon	NO	remote	Mountain
Karvatn	NO0039R	NO39	8.8833	62.7833	210	Salmon	NO	remote	Plain
Osen	NO0041R	NO41	11.7833	61.25	440	Salmon	NO	remote	Plain
Prestebakke	NO0043R	NO43	11.5333	59	160	Salmon	NO	remote	Plain
Nordmoen	NO0044R	NO44	11.1	60.2667	200	Salmon	NO	remote	Plain
Jeloya	NO0045R	NO45	10.6	59.4333	5	Salmon	NO	remote	Plain
Svanvik	NO0047R	NO47	30.0333	69.45	30	Salmon	NO	remote	Plain
Voss	NO0048R	NO48	6.5333	60.6	500	Salmon	NO	remote	Plain
Sandve	NO0052R	NO52	5.2	59.2	15	Salmon	NO	remote	Plain
Karasjok	NO0055R	NO55	25.2167	69.4667	333	Salmon	NO	remote	Plain
Hurdal	NO0056R	NO56	11.0781	60.3722	300	Salmon	NO	remote	Plain
Andoya	NO0090R	NO90	16.0117	69.2783	380	Salmon	NO	remote	Plain
overbygd	NO0092R	NO92	19.3667	69.05	90	Salmon	NO	remote	Plain
Valdalen	NO0093R	NO93	12.1667	62.0833	800	Salmon	NO	remote	Valley
Mosvatn	NO0094R	NO94	8.3333	59.8333	940	Salmon	NO	remote	Valley
Ualand	NO0095R	NO95	6.3833	58.5167	220	Salmon	NO	remote	Plain
Solhomfjell	NO0097R	NO97	8.8	58.9333	260	Salmon	NO	remote	Plain
Karpdalen	NO0098R	NO98	30.4333	69.65	70	Salmon	NO	remote	Plain
Lista	NO0099R	NO99	6.5667	58.1	13	Salmon	NO	remote	Plain
Suwalki	PL0001R	PL01	22.95	54.1333	184	Caviar	PL	remote	Plain
Jarczew	PL0002R	PL02	21.9833	51.8167	180	Caviar	PL	Warsaw	Plain
Sniezka	PL0003R	PL03	15.7333	50.7333	1603	Caviar	PL	remote	Mountain
Leba	PL0004R	PL04	17.5333	54.75	2	Caviar	PL	remote	Plain
Diabla_Gora	PL0005R	PL05	22.0667	54.15	157	Caviar	PL	remote	Plain
Braganca	PT0001R	PT01	-6.7667	41.8167	690	Olive	PT	remote	Valley
Faro	PT0002R	PT02	-7.9667	37.0167	8	Olive	PT	remote	Plain
Viana_do_Castelo	PT0003R	PT03	-8.8	41.7	16	Olive	PT	remote	Plain
Monte_Velho	PT0004R	PT04	-8.8	38.0833	43	Olive	PT	Lisbon	Plain
Foia	PT0005R	PT05	-8.9	37.3167	902	Olive	PT	Lisbon	Valley
Rarau	RO0001R	RO01	25.45	47.45	1536	Goulash	RO	remote	Mountain
Stina_de_Vale	RO0002R	RO02	23.5333	46.6833	1111	Goulash	RO	remote	Valley
Semenic	RO0003R	RO03	25.9667	45.1167	1432	Goulash	RO	Bucarest	Valley
Paring	RO0004R	RO04	23.4667	45.3833	1585	Goulash	RO	remote	Mountain
Fundata	RO0005R	RO05	25.3	45.4667	1371	Goulash	RO	Bucarest	Valley
Turia	RO0006R	RO06	25.9833	46.1167	1008	Goulash	RO	Bucarest	Valley
Poiana_Stampei	RO0008R	RO08	25.1344	47.3247	908	Goulash	RO	remote	Valley
Kamenicki_vis	RS0005R	RS05	21.95	43.4	813	Goulash	RS	remote	Valley
Janiskoski	RU0001R	RU01	28.85	68.9333	118	Caviar	RU	remote	Plain

Lesogorsky	RU0008R	RU08	28.9667	61	39	Caviar	RU	remote	Plain
Pinega	RU0013R	RU13	43.4	64.7	28	Caviar	RU	remote	Plain
Pushkinskie_Gory	RU0014R	RU14	28.9	57	103	Caviar	RU	remote	Plain
Shepeljovo	RU0016R	RU16	29.1167	59.9667	4	Caviar	RU	remote	Plain
Danki	RU0018R	RU18	37.8	54.9	150	Caviar	RU	remote	Plain
Lesnoy	RU0020R	RU20	32.94	56.53	340	Caviar	RU	remote	Plain
Ekerod	SE0001R	SE01	13.7167	55.9	140	Salmon	SE	remote	Plain
Rorvik	SE0002R	SE02	11.9333	57.4167	10	Salmon	SE	remote	Plain
Velen	SE0003R	SE03	14.3	58.7833	127	Salmon	SE	remote	Plain
Bredkalen	SE0005R	SE05	15.3333	63.85	404	Salmon	SE	remote	Plain
Hoburgen	SE0008R	SE08	18.15	56.9167	58	Salmon	SE	remote	Plain
Vavihill	SE0011R	SE11	13.15	56.0167	175	Salmon	SE	remote	Plain
Aspvreten	SE0012R	SE12	17.3833	58.8	20	Salmon	SE	Stockholm	Plain
Esrange	SE0013R	SE13	21.0667	67.8833	475	Salmon	SE	remote	Plain
Rao	SE0014R	SE14	11.9139	57.3939	5	Salmon	SE	remote	Plain
AmmarnasH	SE0031R	SE31	16.2	65.9667	480	Salmon	SE	remote	Plain
Norra-Kvill	SE0032R	SE32	15.5667	57.8167	261	Salmon	SE	remote	Plain
Sannen	SE0033R	SE33	15.3333	56.3333	90	Salmon	SE	remote	Plain
Storulvsjoen	SE0034R	SE34	16.3	62.2667	420	Salmon	SE	remote	Plain
Vindeln	SE0035R	SE35	19.7667	64.25	225	Salmon	SE	remote	Plain
Grimso	SE0039R	SE39	15.4719	59.7278	132	Salmon	SE	remote	Plain
Arup	SE0051R	SE51	13.6667	55.75	157	Salmon	SE	remote	Plain
AmmarnasL	SE0094R	SE94	16.2	65.9667	140	Salmon	SE	remote	Plain
Gardsjon	SE0097R	SE97	12.0167	58.05	126	Salmon	SE	remote	Plain
Masun	SI0001R	SI01	14.3667	45.65	1026	Goulash	SI	remote	Valley
Iskrba	SI0008R	SI08	14.8667	45.5667	520	Goulash	SI	remote	Valley
Zarodnje	SI0031R	SI31	15.0033	46.4286	770	Goulash	SI	remote	Valley
Krvavec	SI0032R	SI32	14.5386	46.2994	1740	Goulash	SI	remote	Mountain
Kovk	SI0033R	SI33	15.1139	46.1286	600	Goulash	SI	remote	Valley
Chopok	SK0002R	SK02	19.5833	48.9333	2008	Goulash	SK	remote	Mountain
Stara_Lesna	SK0004R	SK04	20.2833	49.15	808	Goulash	SK	remote	Valley
Liesek	SK0005R	SK05	19.6833	49.3667	892	Goulash	SK	remote	Valley
Starina	SK0006R	SK06	22.2667	49.05	345	Goulash	SK	remote	Plain
Topolniky	SK0007R	SK07	17.8606	47.96	113	Goulash	SK	remote	Plain
Cubuk_II	TR0001R	TR01	33	40.5	1169	Olive	TR	remote	Valley
Svityaz	UA0005R	UA05	23.8833	51.5167	164	Caviar	UA	remote	Plain
Rava-Russkaya	UA0006R	UA06	23.6333	50.25	249	Caviar	UA	remote	Plain
Beregovo	UA0007R	UA07	22.6833	48.25	112	Caviar	UA	remote	Plain

19 ANNEX 4: Acronyms of EU countries and Cities

EU Countries

AT	Austria
BE	Belgium
BG	Bulgaria
CY	Cyprus
CZ	Czech Republic
DE	Germany
DK	Denmark
EE	Estonia
ES	Spain
FI	Finland
FR	France
GB	United Kingdom
GR	Greece
HU	Hungary
IE	Ireland
IT	Italy
LT	Lithuania
LU	Luxembourg
LV	Latvia
MT	Malta
NL	The Netherlands
PL	Poland
PT	Portugal
RO	Romania
SE	Sweden
SI	Slovenia
SK	Slovakia

EU cities

Bar	Barcelona
Ber	Berlin
Ham	Hamburg
Lon	London
Mad	Madrid
Pra	Pragues
Rom	Rome
Sev	Sevilla
Sto	Stockolm
Val	Valencia
Vie	Vienna

20 ANNEX 5: Average observed and modelled concentrations

Average observed (bullets) and modelled (map) concentrations of NO_2, O_3, PM_{10}, $PM_{2.5}$ over three periods: T01 (left column), T02 (middle column) and T03 (right column) for all models.

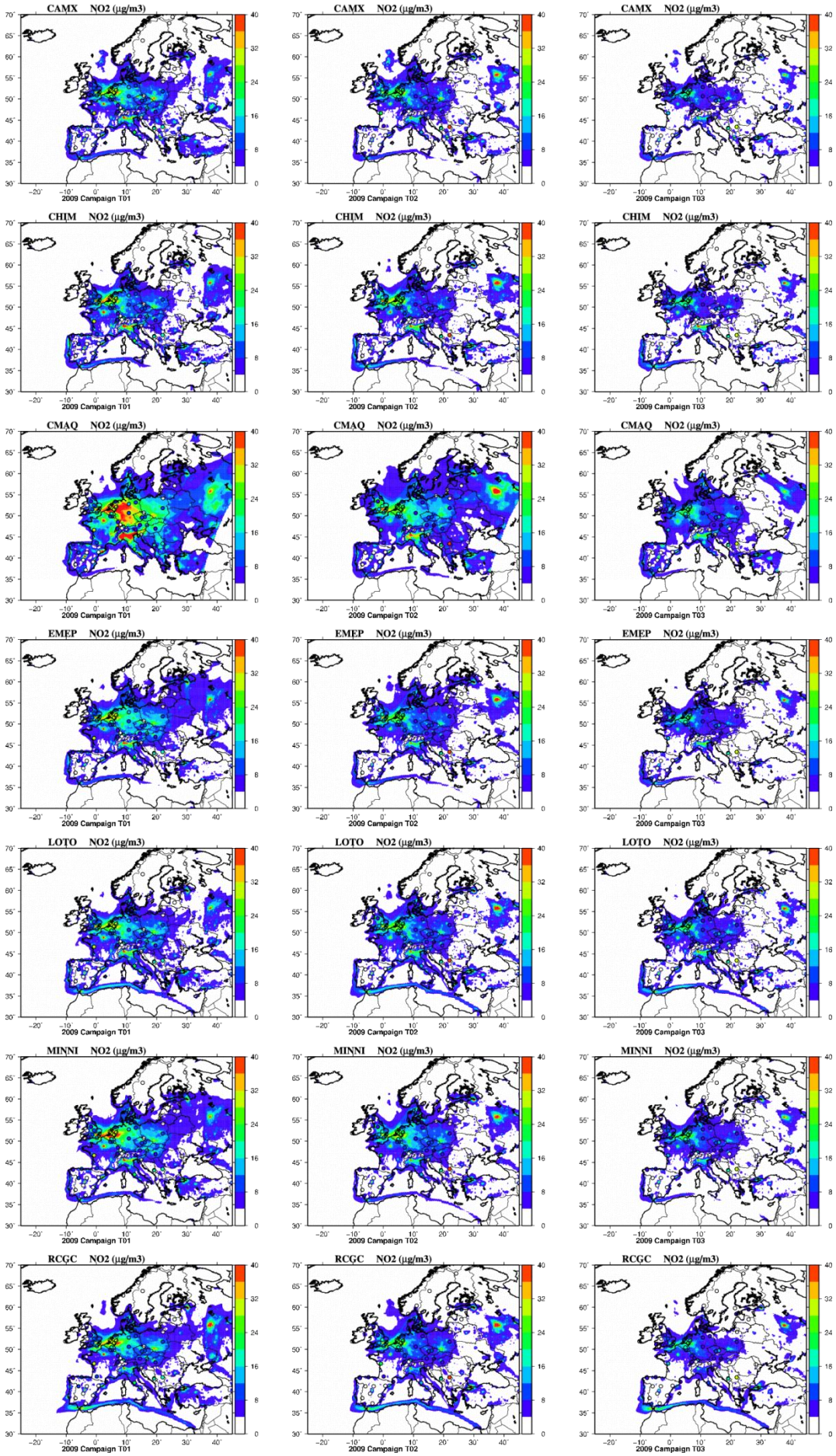
CAMX NO2 (µg/m3)
CAMX NO2 (µg/m3)
CAMX NO2 (µg/m3)
CHIM NO2 (µg/m3)
CHIM NO2 (µg/m3)
CHIM NO2 (µg/m3)
CMAQ NO2 (µg/m3)
CMAQ NO2 (µg/m3)
CMAQ NO2 (µg/m3)
EMEP NO2 (µg/m3)
EMEP NO2 (µg/m3)
EMEP NO2 (µg/m3)
LOTO NO2 (µg/m3)
LOTO NO2 (µg/m3)
LOTO NO2 (µg/m3)
MINNI NO2 (µg/m3)
MINNI NO2 (µg/m3)
MINNI NO2 (µg/m3)
RCGC NO2 (µg/m3)
RCGC NO2 (µg/m3)
RCGC NO2 (µg/m3)
2009 Campaign T01
2009 Campaign T02
2009 Campaign T03

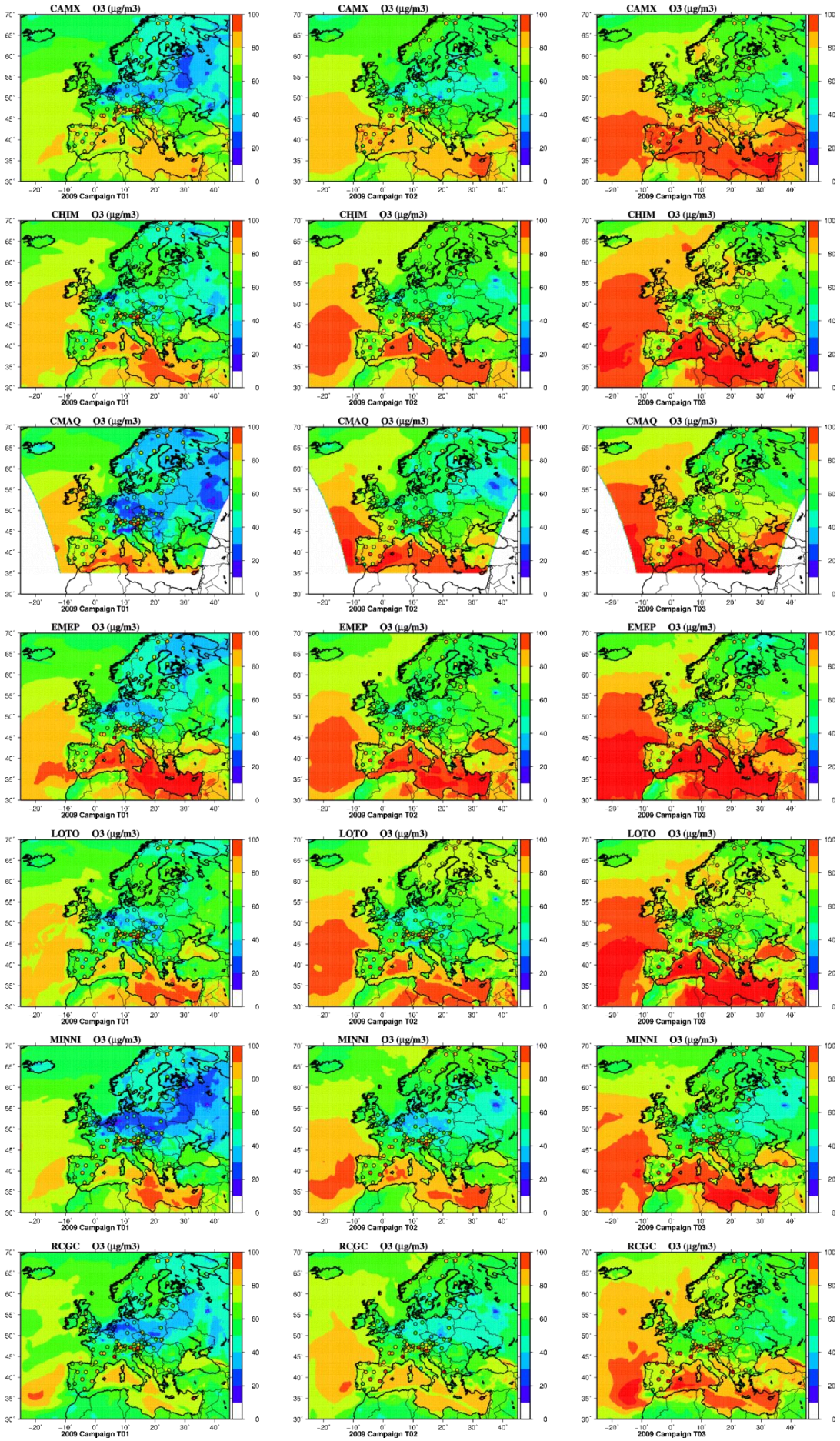
CAMX O3 (µg/m3)
CHIM O3 (µg/m3)
CMAQ O3 (µg/m3)
EMEP O3 (µg/m3)
LOTO O3 (µg/m3)
MINNI O3 (µg/m3)
RCGC O3 (µg/m3)
2009 Campaign T01
2009 Campaign T02
2009 Campaign T03

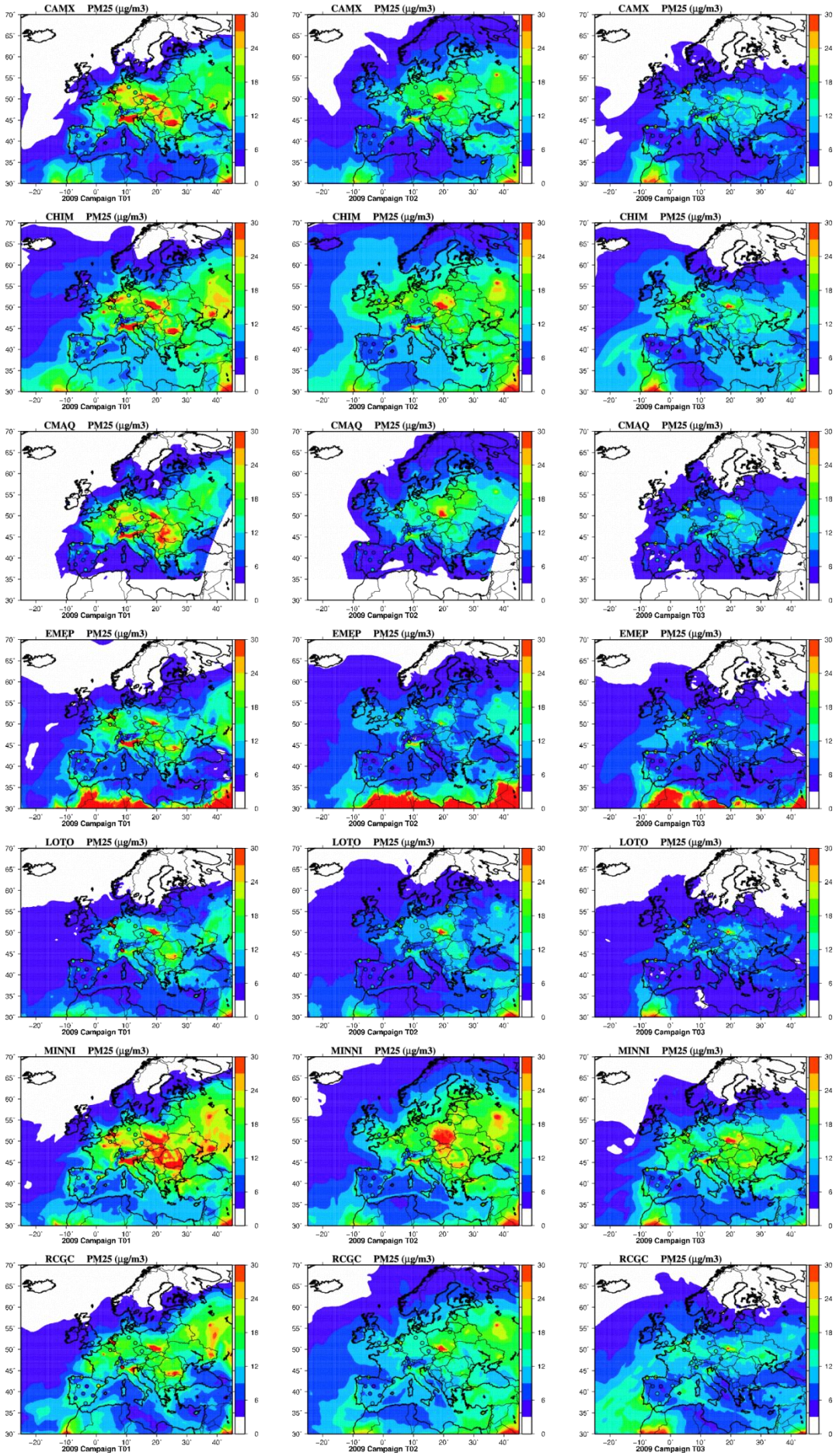
CAMX PM25 (µg/m3)
CHIM PM25 (µg/m3)
CMAQ PM25 (µg/m3)
EMEP PM25 (µg/m3)
LOTO PM25 (µg/m3)
MINNI PM25 (µg/m3)
RCGC PM25 (µg/m3)
2009 Campaign T01
2009 Campaign T02
2009 Campaign T03

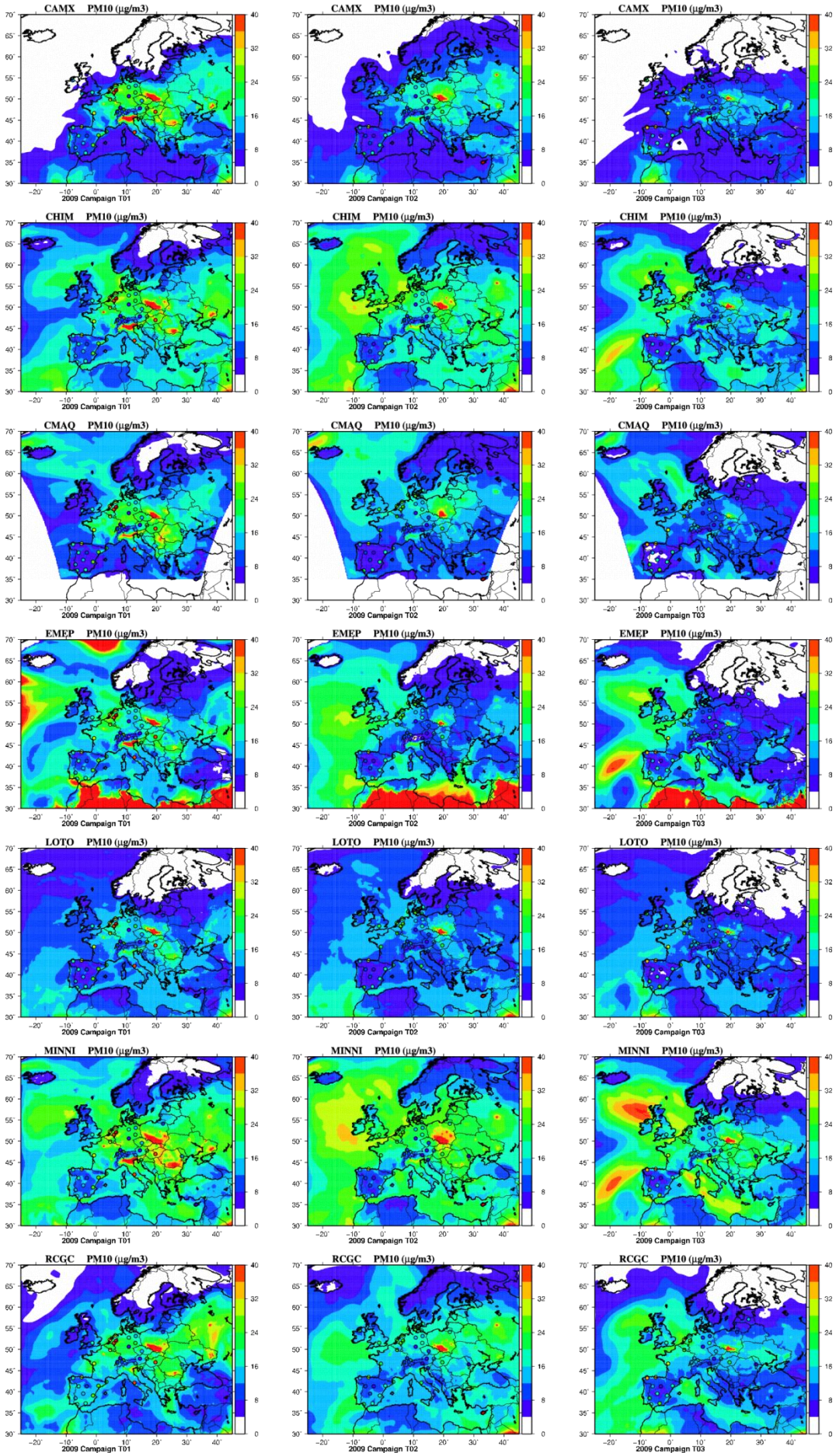
CAMX PM10 (µg/m3)
CHIM PM10 (µg/m3)
CMAQ PM10 (µg/m3)
EMEP PM10 (µg/m3)
LOTO PM10 (µg/m3)
MINNI PM10 (µg/m3)
RCGC PM10 (µg/m3)
2009 Campaign T01
2009 Campaign T02
2009 Campaign T03